The Influence of Dopants on Copper Chloride Catalysts for Ethylene Oxychlorination Reaction

Dissertation for the degree of "Philosophiae Doctor"

by

Naresh Babu Muddada

Department of Chemistry
Faculty of Mathematics and Natural Sciences
University of Oslo

November 2012

Series of dissertations submitted to the
Faculty of Mathematics and Natural Sciences, University of Oslo
No. 1317

ISSN 1501-7710

Cover: Inger Sandved Anfinsen.
Printed in Norway: AIT Oslo AS.

Produced in co-operation with Akademika publishing.
The thesis is produced by Akademika publishing merely in connection with the thesis defence. Kindly direct all inquiries regarding the thesis to the copyright holder or the unit which grants the doctorate.

Acknowledgements

One of the joys of completion is to look over the journey past and remember all the friends and family who have helped and supported me along this long but fulfilling road.

I would like to express my heartfelt gratitude to my principal supervisor, Prof. Unni Olsbye, whose encouragement, guidance, patience and the support with big smile on her face even in the odd times, taught me how to be keep calm, independent, stubborn and develop thought provoking process. Your ability to select and to approach compelling research problems, your high scientific standards, and your hard work set an example. I admire your ability to balance research interests and personal pursuits. Above all, you made me feel a friend, which I appreciate from my heart.

I owe tons and tons of gratitude to my second supervisor Prof. Carlo Lamberti, with whom I worked during my Master's thesis and first year of my PhD at University of Turin. Throughout those years, you acted me not only as my mentor, but also as caretaker, motivator and taught how to become a self-grown expert in one particular field and able to connect and apply to several other fields. He and his family especially Prof. Silvia Bordiga cared me so much, that I never felt like I was away from my home and miss my family. I think I am one of the luckiest persons was offered to have dinners at their home; we call it as "Philadelphia restaurant". Thank you so much for your guidance and wonderful times. You and Silvia taught me so much in my life. Stay in Italy is one of my best parts of life.

I would also thank my third mentor Mr. Terje Fuglerud. I must acknowledge that I learnt more about this catalytic system, once we both started gathering all the pieces of knowledge from both laboratory and industry. His simplicity, insightful and inspirational comments and motivating discussions provoked me to study and understand this system at more basic levels. And also thankful to Mr. Steinar Kvisle, head of the facility, allowed me to be part of their team and encouraged me to learnt business side of this process.

It is no easy task, reviewing a thesis. I am surprised the way they reviewed my thesis with patience, giving their constructive feedback, and I am grateful for their constant help, thoughtful and detailed comments. I would like to convey my heartfelt gratitude to all my

supervisors for teaching me scientific writing and gave the opportunity to interact with international community. One simply could not wish better or friendlier supervisors.

As I spent my PhD life at University of Turin, University of Oslo, wonderful colleagues have surrounded me: both communities have provided a rich and fertile environment to study and explore new ideas. At University of Turin, I would like to thank my maestro of FTIR Dr. Elena Groppo and EXAFS maestro Dr. Diego Gianolio for their wonderful support and contributions to my work and the lab activity. I also thank all my lab colleagues and ERASMUS friends, who made my life not only easier but also made much like a party life in Italy.

At University Oslo, I would like to thank Prof. Karl Petter Lillerud and Prof. Stain Svelle for their help and kind support. I would like to thank Sharmala Aravinthan and Gloria Bostick, for their kind and patience assistance. My office mates: Wegard Skistad and Shewa Teketel. I am very glad that I met you people and thank you, so much, for wonderful discussions in science and politics, fighting's, fun, what else more, it was such wonderful experience to work with you. I would also thank Dr. David Wragg for reviewing my thesis and his constructive feedback. I would like to thank all my colleagues for creating a kind, supportive and nice working atmosphere. To all my colleagues at the inGAP, thank you so much. To the colleagues at INEOS, I am grateful for the chance to visit and be a part of the lab. Thank you for welcoming me as a friend and helping to develop the ideas in this thesis. Norwegian Research council funded this thesis, and I would like to thank the organization for their generous support.

I would not have contemplated this road if not for my mom Parvathi, who instilled within me a love of creative pursuits, science and language, all of which finds a place in this thesis. To my mom, thank you. My siblings, Ramesh, Swathi, Uma and Venkat, have also been the best of friends and motivators along this journey: who encouraged me and always cherished me with their love and care. Though I am far away, their love made me stronger and happy smiley person. To my best friends Seyran Khalili, Anand Tatikonda and Roman Belousov, for your wonderful times, binding together and shared my personal life. Thanks for just being with me.

Kind Regards,

Naresh Babu Muddada

Table of Contents

List of Publications and Presentations

This thesis is based on the following manuscripts and unpublished results. The manuscripts of both published and unpublished results are collected in the Appendix. A summary of all published and unpublished results is given in Chapter 6.

Publication I: N. B. Muddada, U. Olsbye, G. Leofanti, D. Gianolio, F. Bonino, S. Bordiga, T. Fuglerud, S. Vidotto, A. Marsella, C. Lamberti, "Quantification of copper phases, their reducibility and dispersion in doped-$CuCl_2/Al_2O_3$ catalysts for ethylene oxychlorination" Dalton Transactions, **2010**, 39, 8437-8449.

Publication II: N. B. Muddada, U. Olsbye, L. Caccialupi, F. Cavani, G. Leofanti, D. Gianolio, S. Bordiga, C. Lamberti, **"**Influence of additives in defining the active phase of the ethylene oxychlorination catalyst" Physical Chemistry Chemical Physics, **2010**, 12, 5605-5618.

Publication III: D. Gianolio, N.B. Muddada, U. Olsbye, C. Lamberti, "Doped-$CuCl_2/Al_2O_3$ catalysts for ethylene oxychlorination: influence of additives on the nature of active phase and reducibility", Nuclear Instruments Methods Phys. Research B, **2012,** 284, 53-57.

Publication IV: N. B. Muddada , U. Olsbye, T. Fuglerud, S. Vidotto, A. Marsella, S. Bordiga, D. Gianolio, G. Leofanti and C. Lamberti, "The role of chlorine and additives on the density and strength of Lewis and Brønsted acidic sites of gamma-Al_2O_3 support used in oxychlorination catalysis: a FTIR study", Journal of Catalysis, **2011**, 284, 236–246.

Publications not listed in this thesis:

Publication V: Unni Olsbye, Ole Vaaland Saure, Naresh Babu Muddada, Silvia Bordiga, Carlo Lamberti, Merete Hellner Nilsen, Karl Petter Lillerud and Stian Svelle, "Methane conversion to light olefins - how does the methyl halide route differ from the methanol to olefins (MTO) route?", Catalysis Today, **2011**, 171(1), 211-220.

Publication VI: Elena Groppo, Giovanni Agostini, Andrea Piovano, Naresh B. Muddada, Giuseppe Leofanti, Riccardo Pellegrini, Giuseppe Portale, Alessandro Longo, Carlo Lamberti, "Effect of reduction in liquid phase on the properties and the catalytic activity of Pd/Al_2O_3 catalysts*",* Journal of Catalysis, **2012**, 287, 44–54.

Oral Presentations:

1. N.B. Muddada*, U. Olsbye, T. Fuglerud, C. Lamberti, "Ethylene Oxychlorination catalysis- Insight through combined spectroscopy and kinetic tests", EuropacatX International conference, Glasgow (S), Aug 2011.

2. N.B. Muddada*, U. Olsbye, T. Fuglerud, C. Lamberti, " Ethylene oxychlorination catalysis: role of metal promoters on activity and selectivity of the process", 2nd Trondheim Gas Technology conference, Trondheim (N), Oct 2011.

3. N.B. Muddada*, U. Olsbye, T. Fuglerud, C. Lamberti , "EXAFS, FTIR and Kinetic studies on $CuCl_2$ based catalysts for Oxychlorination of Ethylene", NKS catalysis Symposium, Lillestrøm (N), Sep 2011.

4. N. B. Muddada*, U. Olsbye, T. Fuglerud, E. Groppo, G. Agostini, D. Gianolio, A. Piovano, S. Bordiga, and C. Lamberti, "An in situ EXAFS investigation of the interaction with C_2H_4, O_2 and HCl for the MCl_xCuCl_2/γ-Al_2O_3 (M = Li, K, Cs, Mg, La) ethylene oxychlorination catalysts", XVII Italian Synchrothron Radiation Society (SILS) National Meeting, Camerino (I), 24-26 July 2009.

The Author's Contribution

Publication I: The author planned and performed the catalysts characterisation by FTIR. The author further contributed to the EXAFS data treatment and analysis. Author was strongly involved in the interpretation of the data and the preparation of the manuscript. Carlo Lamberti's group performed the EXAFS experiments in early 2000s and Fabrizio Cavani's group performed the series of pulse experiments.

Publication II: The author contributed to the data treatment and analysis. Author was strongly involved in the interpretation of the data and the preparation of the manuscript. Carlo Lamberti's group performed the XANES experiments in early 2000s'.

Publication III: The author contributed the data treatment and analysis. The author was strongly involved in the interpretation of the data and the preparation of the manuscript.

Publication IV: The author planned and performed all the experiments. Author performed treatment, analysis of the data and was strongly involved in the interpretation of the results. Author prepared the manuscript with the help of Carlo Lamberti and Unni Olsbye.

Unpublished results: The author planned and performed all the experiments. Author performed the treatment, analysis of the data and was strongly involved in the interpretation of the results. Author prepared the manuscript. The results were discussed with Unni Olsbye, Terje Fuglerud and Carlo Lamberti.

Preliminary Report: The author planned and performed all the XAS experiments along with the help of Unni Olsbye, Terje Fuglerud, Filippo Giordanino, Jia Yang and Carlo Lamberti at BM01B, ESRF facility. Author performed the processing, treatment and preliminary analysis of the XANES data. Author prepared the preliminary report.

Thesis Scope

The scope of this Ph.D. project was to study and understand the effect of the dopants on the properties of Cu-based catalysts for the conversion of ethylene-to-1,2-dichloroethane (oxychlorination), a crucial intermediate reaction in poly-vinyl chloride (PVC) chemistry.

Selection of an optimal catalyst for heavy industrial processes such as ethylene oxychlorination is an important practical problem. Oxychlorination of ethylene is a catalytic process performed over a copper chloride based heterogeneous catalyst. The main concerns of the catalyst are deactivation and product selectivity. Deactivation of the catalyst and production of undesirable chlorinated by-products increase the overall costs of the PVC process. It is also desirable, for economic and environmental reasons, for the oxychlorination catalyst composition to effect a high conversion of HCl used in the reaction. In commercial applications, a combination of high HCl conversion and high ethylene efficiency or selectivity of ethylene to EDC is most desirable.

Despite the commercial usage of oxychlorination catalysts (both base $CuCl_2/\gamma\text{-}Al_2O_3$ and doped catalysts ($MCl_x+CuCl_2/\gamma\text{-}Al_2O_3$)) for more than 50 years, the fundamental understanding of the catalyst and its mechanism are still under investigation. The available literature on catalytic oxidative chlorination reveals considerably uncertainty with respect to the actual mechanism of the reaction, the role of each of the components constituted in the catalyst and how they play together.

There is, therefore, a need to understand the system properly and thereby address some of the problems persisting in the commercial operation of oxychlorination process. The main challenges constrained in the economy and efficiency of the oxychlorination process, thereby in PVC industry, are summarized as:

- EDC selectivity
- EDC yield (Ethylene efficiency)
- HCl conversion
- Catalyst's lifetime.

Taking into consideration all of the above, the main aim of the thesis is:- ***"To gain fundamental understanding, at the atomic and molecular level, of the working catalytic system, particularly the role played by the additives and the carrier, and there-by optimize the performance of the catalyst."***

As our primary goal is to understand the system at the molecular level, the first part of the work was devoted to surface characterization of the various doped catalysts. In order to obtain deeper insight on the catalyst's performance during the reaction, fundamental advanced in-situ and operando X-ray absorption spectroscopy techniques were employed along with other complimentary-methods. It is wise to remind the reader at this point that doped copper chloride catalysts for oxidative chlorination of hydrocarbons are multi-component heterogeneous systems that consist of active species with varying compositions and co-presence of different solid phases/mixtures, beside that its performance is directly linked to the state of surface copper species. Hence, high emphasis is given to surface characterisation throughout the work. As a secondary goal is to understand the catalyst performance on atomic level, the reaction tests were performed by using a home-built test rig. Time and process obligations did not permit a full kinetic and mechanistic study on all the catalysts, but preliminary results are provided.

The following chapters will provide a detailed background for the present work with an emphasis on the oxychlorination process, technologies, general chemistry of the copper-chlorides and a detailed overview of the catalyst's literature up-to-date. The subsequent chapter presents the experimental methods employed in this work, and is followed by a chapter devoted to a summary of the results. A preliminary report on the XAS experiments performed in last July 2012 has been provided.

Chapter 1

INTRODUCTION

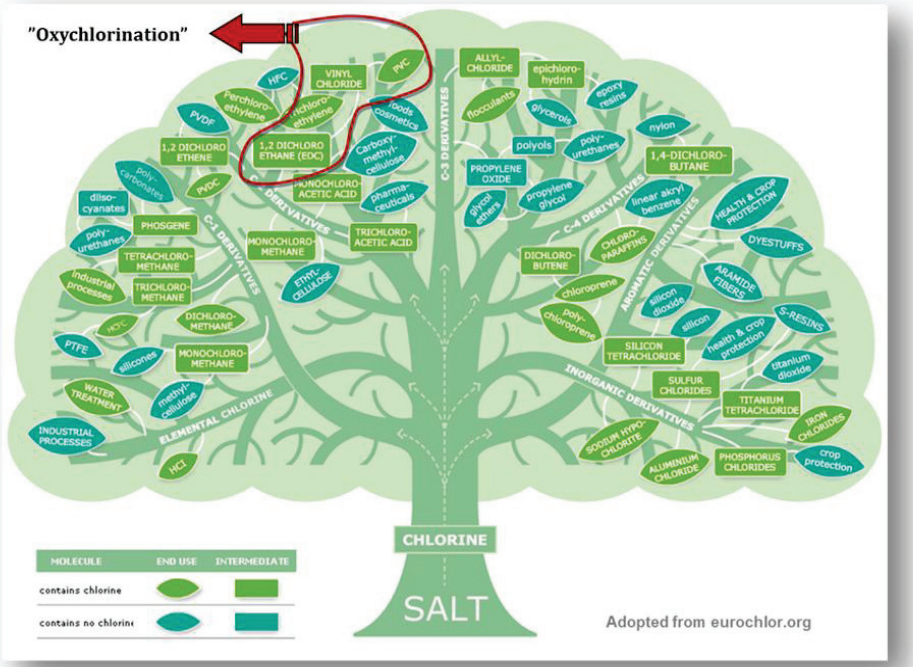

"Chemistry without catalysis, would be a sword without a handle, a light without brilliance, a bell without sound" — Alwin Mittasch

1.1. General Catalysis

Catalysts are the workhorses of the chemical industry. Catalysis changes how a chemical reaction happens. This process usually speeds up a reaction as illustrated in a simplified way in Figure 1, and can make new reactions possible that allow different starting materials to be used. The chemical that causes these changes simply is called a catalyst. A general simplified definition of a "Catalyst" is a substance that increases the rate of a chemical reaction by reducing the activation energy, but which is left unchanged by the reaction. It has been for more than a century at the center of our economy and is clearly one of the keys to sustainable development because it involves efficient conversion processes, both in terms of energy and atom economy. Approximately 85-90% of the processes of the chemical industry are catalytic processes. Development of new catalysts is critical for the development of more efficient, economic and greener technologies. It is thus obvious that catalysis will still play a central role in our future, and that catalyst development and technology will remain a very active research field [1].

Kinetically, catalytic reactions are typical chemical reactions; i.e. the reaction rate depends on the frequency of contact of the reactants in the rate-determining step. Usually, the catalyst participates in this slowest step, and rates are limited by the amount of catalyst and its "activity". However, the mechanistic explanation of catalysis is complex. Even more so when speaking about heterogeneous catalysts; which have highly complex, inhomogeneous and dynamic behaviour, their surfaces constantly changing with temperature and atmospheric composition. The active sites are generally integrated with the surface of materials or nanoparticles on top of materials or even at the interface between the two. In view of improving them, one strategy has been to develop catalysts that are more efficient, in a predictive way using molecular approaches without losing the advantages of heterogeneous systems.

One among the well-known and extensively studied complex systems is "Oxychlorination Catalyst". The following sections will outline the evolution of the oxychlorination process, the level of knowledge and developments achieved on oxychlorination catalysts. It also gives an idea on how multidisciplinary this field has become,

where many gaps still remain to be bridged, but where much progress has been achieved in the past decades.

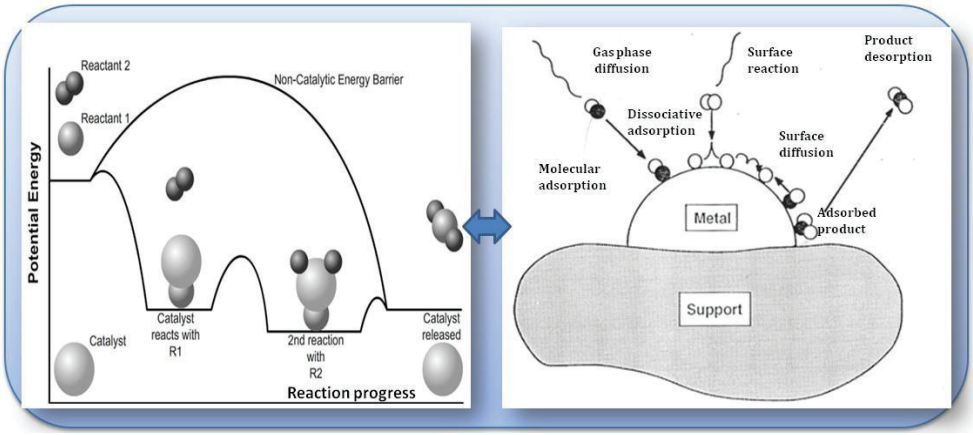

Figure 1: General illustration of heterogeneous catalysis - potential energy diagram for catalytic reaction and non-catalytic reaction (left); molecular view of catalysis on metal supported catalysts (right). Image adopted from "The Basis and Applications of Heterogeneous Catalysis by Michael Bowker" [2].

1.2. The Origin of Oxychlorination

1.2.1. Chlorine –potentially harmful yet an essential element

Chlorine (Cl) is the second most abundant halogen and 21st most abundant chemical element in Earth's crust. About 70% of all manufactured chemical products involve chlorine in one or more synthesis steps [3].

Millions of tons of chlorine are consumed annually in reactions that produce such everyday goods as plastics, paints, various drugs, insecticides, herbicides, dyestuffs, computer hardware, silicon chips, packaging materials and automotive parts etc.,. In the course of these reactions, most of the chlorine is incorporated into the products. Nevertheless, some of the chlorine frequently combines with hydrogen, becoming hydrogen chloride (HCl) - a corrosive and hazardous waste material. Most of these processes involve a saturated or unsaturated hydrocarbon, reacted with elemental chlorine. Such reactions can be additions to olefins, chlorination of aromatics, or homolytic cleavage of carbon-hydrogen bonds. In many cases, the final products constitute the chloride; however, in some processes (addition of an alcohol or amine to phosgene to produce, for example, polycarbonate and polyurethane plastics) no chloride is present in the final product. In addition, most of the processes produce the

hydrogen chloride "HCl" as a co-product, via dehydro halogenations or free radical reactions of chlorine with aliphatic hydrogen.

The amounts of chlorine and toxic hydrogen chloride waste involved are huge. The current world production of chlorine is approximately 42 million metric tonnes per year. Approximately 50% of the chlorine produced is reduced to HCl or chloride salts, resulting in production of HCl estimated at 20 million metric tonnes annually, mt/a, (expressed as 100 wt-% HCl). Figure 2 shows the compiled processes involving hydrogen chloride as co-product and emphasis the need to reuse or purify the waste hydrogen chloride [3]. Handling of this chemical poses a great challenge to scientists and engineers from centuries. In spite of numerous achievements made on processes, that can convert hydrogen chloride to Cl_2 and other useful products, these processes are still hindered by issues such as unbalanced demand –supply gap, expensive nature of the process, low yield and low process efficiency.

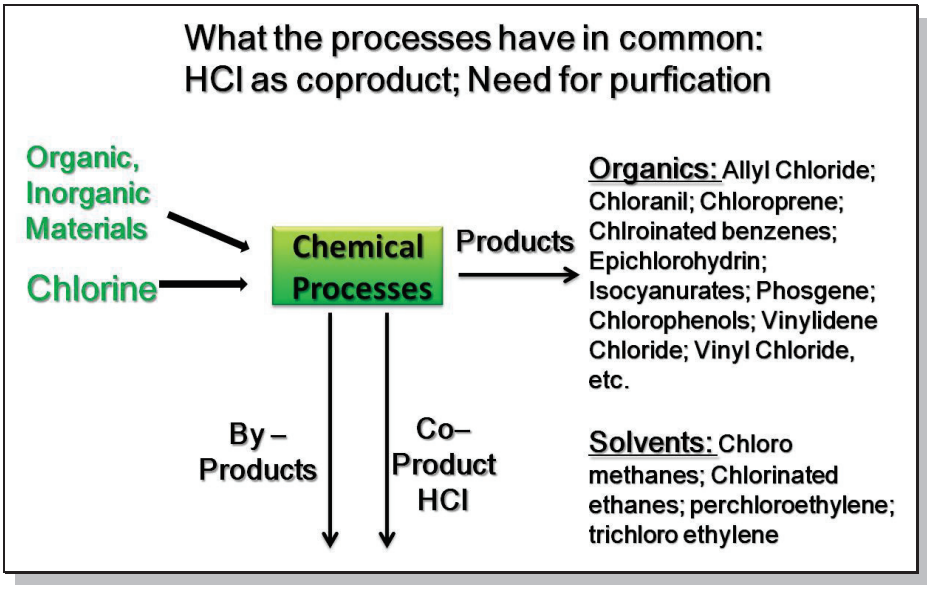

Figure 2: Chemical processes that produce hydrogen chloride (HCl) as a co-product. [3].

The various possible routes for recovering chlorine from hydrogen chloride or for using the latter directly in chlorination reactions are described below.

1.2.2. HCl to Cl_2 – the Deacon process

The direct oxidation of HCl to hydrogen and chlorine is thermodynamically unfavourable ($\Delta G>0$) at all practical temperatures. Therefore, thermo-chemical processing is possible only if the oxidation of HCl is coupled with a thermodynamically favourable reduction reaction. One of the most studied and successful process is the "Deacon Process", in which chlorine is produced through the reaction between hydrogen chloride and oxygen.

$$HCl\ (g) + \tfrac{1}{2}\ O_2\ (g) \rightarrow Cl_2\ (g) + H_2O\ (g) \quad ; \Delta H = -117\ kJ/mol \qquad (1)$$

The process is operated at high temperatures (673-723 K) in the presence of "*cupric chloride supported on porous carrier*" as catalyst and was developed as an efficient technical process for the recovery of chlorine by H. Deacon and F. Hurter in 1868 [4, 5] and further developed by Hasenclever in 1883. The overall reaction is exothermic and controlled by equilibrium [6].

There have been three commercial chlorine recycling processes based on reaction (1) but using different catalyst systems. The three commercial processes are Shell-Chlor (Shell company, Netherlands) using rare earth metals doped $CuCl_2$ supported on SiO_2 as catalyst [7], Kel-Chlor (M. W. Kellogg Company, Houston, USA) using nitrogen dioxide as catalyst [8]and MT-Chlor (Mitsui Toatsu Company, Tokyo, Japan) using Cr_2O_3/SiO_2 as catalyst [9]. Recently, a process developed by the Sumitomo chemical company (Japan) using RuO_2/TiO_2 as catalyst [10] has been commercialised.

In spite of numerous improvements, the process has inherent disadvantages: the sluggish reaction kinetics of the oxygen reduction reaction, a limit of 60 - 80% single pass conversions, low chlorine yield, progressive loss of catalytic activity, volatility of the active species, corrosion problems and high energy-costs.

1.2.3. HCl to Cl_2 – Direct electrolysis process

Electrochemically, HCl can be directly converted to chlorine and hydrogen. Compared to thermo-chemical processing, electrolysis is a low temperature operation (343-363 K) and the amount of water associated with the electrochemically produced chlorine is lower. In addition, the co-produced hydrogen has commercial value. The most commercialised process is the Uhde process [11] patented in 1965. In this process, anhydrous HCl is first absorbed in water and the resulting aqueous hydrochloric acid solution is electrolyzed in separated cells to

yield chlorine at the anode and hydrogen at the cathode. In later years, Uhde and DeNora jointly developed "De Nora Electrolytic Cell System technology", which performed successfully for many years. Another well-known commercial process is a HCl gas electrolysis developed by DuPont using a Nafion ion exchange membrane covered with a porous catalyst containing noble metals such as Pt and Ru [12].

Though, the above electrolytic processes with hydrogen chloride acid as electrolyte may prove to be economical if the recovered hydrogen has sufficient value, but this appears likely to be the case in only few circumstances. Moreover, these processes suffer huge energy costs, due to the large amount of electric power-required. However - these dual processes represent a viable option for reuse of the hydrogen chloride, their non-viable economics created a renewed interest in direct-use of the waste hydrogen chloride as a reagent.

1.2.4. HCl to Chlorocarbons – the Oxychlorination process

In the quest to fulfil the above requirement, derivatives of the Deacon catalyst paved the way for a new process called "***Oxychlorination***". Oxychlorination (OXCH- also referred to as oxidative chlorination), is the hydrocarbon chlorination reaction occurring with participation of an oxidising agent (usually oxygen) and a chlorination agent (as a rule hydrogen chloride). Oxychlorination is generally carried out in the gas phase in the presence of a heterogeneous catalyst. For example, in the case of C_1- hydrocarbons, the overall reaction is

$$CH_4\,(g) + HCl\,(g) + \tfrac{1}{2}\,O_2\,(g) \longrightarrow CH_3Cl\,(g) + H_2O\,(g) \qquad (2)$$

Many studies have been devoted on the oxidative chlorination of lower hydrocarbons - methane, ethane, ethylene, propylene, and their chlorine derivatives [13]. In the early 20th century, interest in the process revived with the essential aim being to develop a more active catalyst with lower volatility. Roka [14] in 1923 first achieved the oxychlorination of methane with chlorine in the presence of oxygen (Eq.2). At about the same time, Ernst and Wahl [15] used the Deacon system at 573-923 K to chlorinate methane, ethane, ethylene and benzene; Roka and Kraus [16] also pointed out the possibility of chlorinating methane in the Deacon reaction. Tizard and co-workers [17] patented a two-step chlorination method in which the second stage was the regeneration of the copper chloride mixture in the early 1920 's'-. Both Mares and Prahl studied the oxychlorination of benzene in the 1930's. Mares [18] patented a

process using elemental chlorine; the hydrogen chloride formed being converted to chlorine for recycling. Prahl [19] examined various Deacon catalytic systems for application to the commercially successful Raschig process for the production of phenol, in which benzene was chlorinated to chloro-benzene as an intermediate step. The proposed catalyst consisted of co-precipitated copper and aluminium hydroxides with promoters that allowed the chlorination of benzene to mono chloro-benzene at 508-518 K.

Since 1946, the petrochemical industries have boomed, these industries contributed several patents on the modification of the Deacon process using promoters, a decrease in volatility by double salt formation [20-22] and fluidized bed techniques [23] for the chlorination of aliphatic and aromatic hydrocarbons. During the same period, the formation of 1,2–dichloroethane (EDC) from ethylene (Eq.6) [24] and unsaturated higher chlorination products from partly chlorinated ethylene by oxychlorination process was examined. It was found, that the Deacon catalyst could chlorinate ethylene with a mixture of HCl and air. This reaction did not produce molecular chlorine but chlorinated ethylene directly with the chlorine species formed on the catalyst surface.

Oxychlorination has many advantages compared to the direct chlorination (discussed in section 0), such as complete utilization of chlorine atoms, use of cheap abundant reagent (oxygen), easy to handle chlorinating agents (HCl) rather than more expensive and toxic ones like chlorine. These reactions became especially attractive if di-oxygen, the most abundant and cheapest oxidant is used. The prospects of several other processes in recycling waste chlorine have been extensively reviewed and the conclusion has been drawn that the Deacon/oxychlorination route constitute the preferred approach to the joint problems of the unbalanced growth of chlorine demand and the vast availability of excess by-product hydrogen chloride.

Since 1950, the patent literature has been mainly concerned with variations of catalyst compositions and process improvements. The detailed aspects of oxychlorination have been reviewed [13, 25-29] [6] from the 1950 ’s’ to the - 90’s’. These articles have covered catalysts with varied compositions, processes and economics [30]. However, tremendous improvements and advances in catalyst characterisation and process development occurred in the late 20th century and early 21st century.

The work presented in this thesis is devoted to giving more insight specifically into the “ethylene oxychlorination catalysis and processes”. The following sections will provide a

brief overview on the oxychlorination catalysis and of the available technologies, the catalyst developments, its complexity, process concerns and improvements made during the last century.

Chapter 2

Oxychlorination in Poly -Vinyl Chloride Process

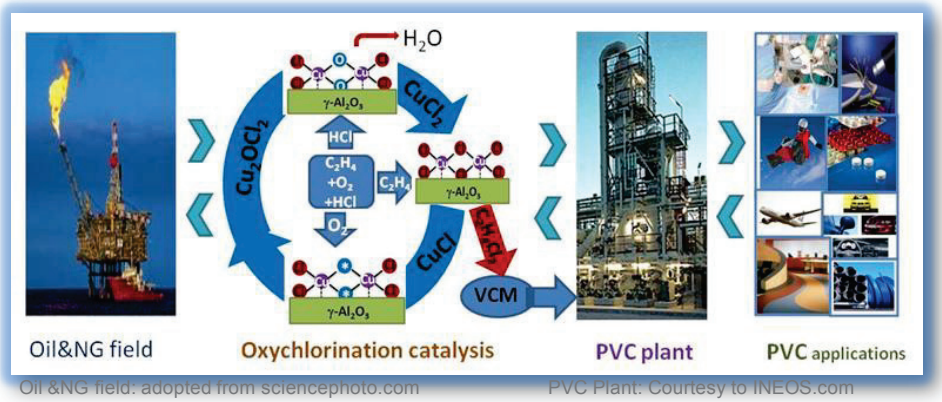

Oil &NG field: adopted from sciencephoto.com PVC Plant: Courtesy to INEOS.com

The main aim of this section is to give a brief overview of the ethylene oxychlorination process as a crucial intermediate step in the poly vinyl chloride (PVC) industry. It will also provide detailed information about geographical aspects and the technologies available for the production of the vinyl chloride monomer (VCM, CH_2=CHCl) and 1,2-dichloroethane (EDC, $C_2H_4Cl_2$).

2.1. PVC/ VCM – Global perspective

The vinyl chain (EDC/VCM/PVC) represents an important part of the petrochemical industry. An important monomer within the chain is vinyl chloride, which is used as a building block for the production of PVC, a versatile plastic material. PVC is a thermoplastic (it can be melted and frozen into desired shapes repeatedly), with range of applications across the construction, household, electronic, pharmaceutical and automotive industries. This makes PVC the second largest commodity plastic after polyethylene, growing at nearly 4% annually [30].

During the past few years, the VCM market has been growing annually at about 4-5% globally and is expected that the world production to exceed 42 million tons per year by 2020 [30]. The lower prices of vinyl plastics, combined with their useful properties and wide range of applications, helped the markets for PVC to grow in the housing and automobile industries and accelerated the growth of VCM production to its present large scale. Presently, VCM is among the top twenty largest petrochemicals in world production. However, growth rates in the developed world had been slipping as these markets matured while stronger demand growth has been seen in Asia, in particular China and India.

VCM was first prepared by Regnier in 1835 by direct chlorination of ethylene by producing 1,2-dichloroethane as an intermediate (Eq.4) [31]. Around 1900, when the industry began to take interest in acetylene chemistry, Fritz Klatte produced VCM from acetylene and hydrogen chloride in the presence of mercury chloride catalyst [31]. Over the following years, the manufacture of acetylene became a very expensive and energy intensive process. As demand for VCM increased, more economical feedstocks were sought. After ethylene became plentiful in the early 1950's, commercial processes were developed to produce VCM from ethylene via EDC route.

Since then, VCM manufacturing technology has been improved from the standpoint of safety, the environment, quality and scale of production. Currently, commercial VCM capacity can be categorized based on the feedstocks: acetylene and ethylene. Figure 3 below illustrates the VCM capacity share between these feed stocks derived from various sources and expected increase in the VCM demand over the period from 2000-2020. Ethylene is the dominant feedstock comprising an 82.7% share, which is derived from naphtha and natural gas.

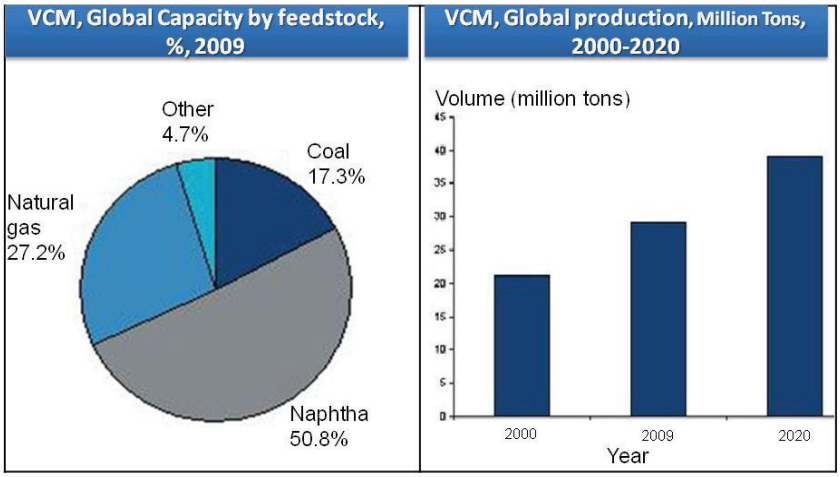

Source: Global Business Intelligent research

Figure 3: VCM global capacity by feedstock and production demand, reported by Global Business Intelligent, 2009 [30].

2.2. VCM process technologies

2.2.1. Conventional Technologies

2.2.1.1. Acetylene-Based VCM

The oldest and simplest commercial route to VCM is via the vapour phase addition to acetylene (C_2H_2) with anhydrous hydrogen chloride (HCl) over a mercuric chloride ($HgCl_2$) catalyst supported on activated carbon.

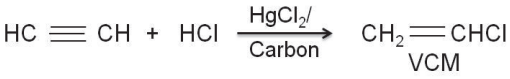

(3)

Acetylene and hydrogen chloride are used in a 1:1 molar ratio. This process little commercialised outside China, which has cheaper abundant coal reserves, substantial hydroelectric power generation and limited reserves of natural gas and crude oil (the main source of ethane from which ethylene is obtained by thermal cracking). The acetylene is produced from calcium carbide, itself produced from coked coal. In China, expansion of coal-based acetylene-based technology proceeded at nearly 20% per year during 2005–2010.

2.2.1.2. Ethylene-Based VCM

The majority of VCM processes are based on the so-called "balanced" ethylene process with ethylene as the hydrocarbon feedstock reacting with chlorine gas to produce the intermediate 1,2-dichloroethane (Eq. 4) . Hydrochloric acid generated in the EDC cracking section (Eq. 5) is completely recycled and used up in an oxychlorination reactor in the presence of oxygen (Eq.6). The process scheme is depicted in Figure 4. The main chemical steps involved are:

a) **Direct chlorination of ethylene to 1,2- dichloroethane (EDC):**

$$C_2H_4 + Cl_2 \rightarrow C_2H_4Cl_2 + 218\ kJ/mol \quad (FeCl_3\ catalysts) \qquad (4)$$

b) **Thermal cracking (pyrolysis) of EDC to VCM:**

$$C_2H_4Cl_2 \rightarrow C_2H_3Cl + HCl - 71kJ/mol \qquad (5)$$

c) **Oxychlorination of ethylene to EDC via recycles of HCl:**

$$\mathbf{C_2H_4 + 2HCl + \tfrac{1}{2}\ O_2 \rightarrow\ C_2H_4Cl_2 + H_2O + 238\ kJ/mol\ (CuCl_2\ catalysts)} \qquad (6)$$

Hence, an ideal balanced process has the overall equation:

$$\mathbf{C_2H_4 + 0.5\ Cl_2 + 0.25\ O_2 \rightarrow C_2H_3Cl + 0.5\ H_2O + 192.5\ kJ/mol} \qquad (7)$$

Therefore, half of the ethylene and all of the chlorine are fed to direct chlorination, while the other half of the ethylene goes to oxychlorination. Since the overall reaction is very exothermic, the VCM plant should be able to cover a large part of its energy needs. The first

oxychlorination plant was built by B.F. Goodrich in 1964 and produced 15000 tons/year of vinyl chloride in a fluid bed [32]. At about the same time the Stauffer chemical company built a unit using three tube-cooled-oxychlorination reactors in series [32]. This was the beginning of the end for routes based on acetylene atleast in the western countries.

The development and commercialization of oxychlorination technology paved the way for the "balanced ethylene process" combining direct chlorination, oxychlorination and EDC pyrolysis processes, as the most commercialized and efficient VCM technology.

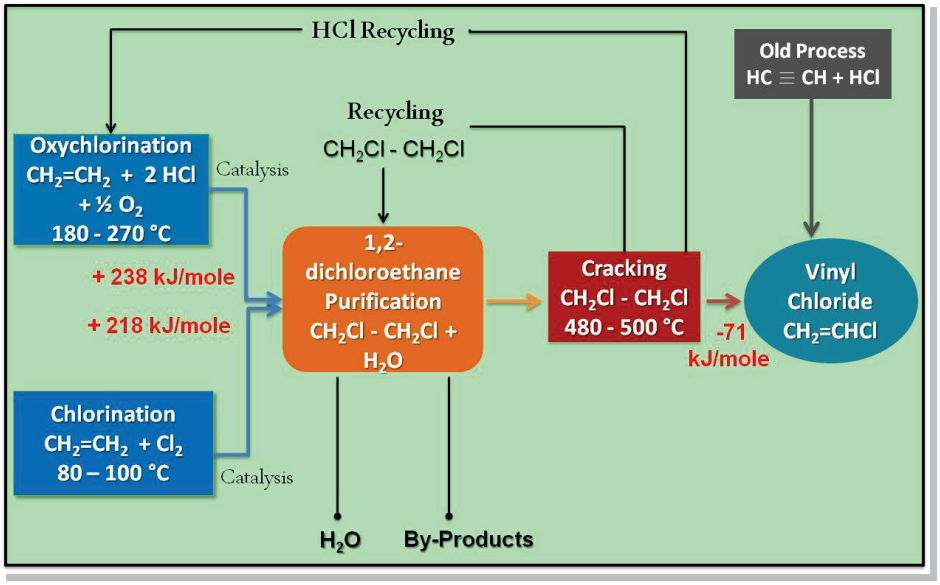

Figure 4: Balanced VCM (Vinyl Chloro Monomer) process flow sheet. (Unpublished figure)

This technology development is a prime example of how chemical process research and development efforts provided the means to utilize the best available feedstocks and lower manufacturing costs for VCM/PVC production.

2.2.2. Competing technologies

2.2.2.1. Ethane to VCM

In spite of the successful journey of the balanced VCM technology, the quest for more cost-effective and the advent of new technologies continued. With the incentives of lower cost feedstock and a simpler process scheme, the development of ethane-based technology

for the production of VCM has been a long identified, albeit difficult to realize, target of VCM process research. A number of companies have been involved in the attempted development of an ethane-based process, several have been patented, yet none has been commercialized.

The EVC Corporation has been very active in this research and demonstrated a catalyst derived from Ziegler-Natta chemistry. They reported [33] a copper-based catalyst promoted by lanthanum containing compounds with a stabilization package for the ethane-to-vinyl oxychlorination reaction (7), with a reaction temperature of 450-470 ^{0}C.

$$2\ C_2H_6 + Cl_2 + 3/2\ O_2 \rightarrow\ C_2H_3Cl + 3\ H_2O \qquad (8)$$

They have operated a 1000 m.t./year pilot plant in Germany with excellent results. Licensing efforts are underway. Since the operation temperature is in boundary limits, where the corrosion is uncontrollable, this might be the reason hindering for successful commercialisation. Another recent development in this process was outlined by Dow chemical [34] using copper-containing ZSM-5 catalysts for oxychlorination of ethane to VCM at 773 K. Although possible, this process has not progressed beyond the conceptual stage. This is because oxychlorination reactor design presents a severe challenge in terms of construction materials. The reaction temperature is as high as 773 K. At this temperature, chlorine becomes very aggressive to most construction materials.

2.3. Oxychlorination process technologies

Commercial oxychlorination processes differ with respect to catalysts (composition, morphology, and physical properties), catalyst contacting method (fluid or fixed bed reactor), and oxygen source (air or pure oxygen feed). Thus, the operating conditions, feed ratios, conversions and yields also vary, depending on the particular combination used and on the methods employed for secondary recovery of feedstock and products. For any particular combination of reactor type and oxygen source, however, good temperature control of this highly exothermic reaction is crucial in the choice of oxychlorination technology. The major variations offered by various licensors, are combination of these two processes.

(i) Air or Oxygen based oxychlorination.

(ii) Fixed bed or fluid bed oxychlorination.

A schematic flow diagram of a licensed oxychlorination process [by Vinnolet Technology] based on oxygen and fluidized bed oxychlorination technology, is shown in Figure 5.

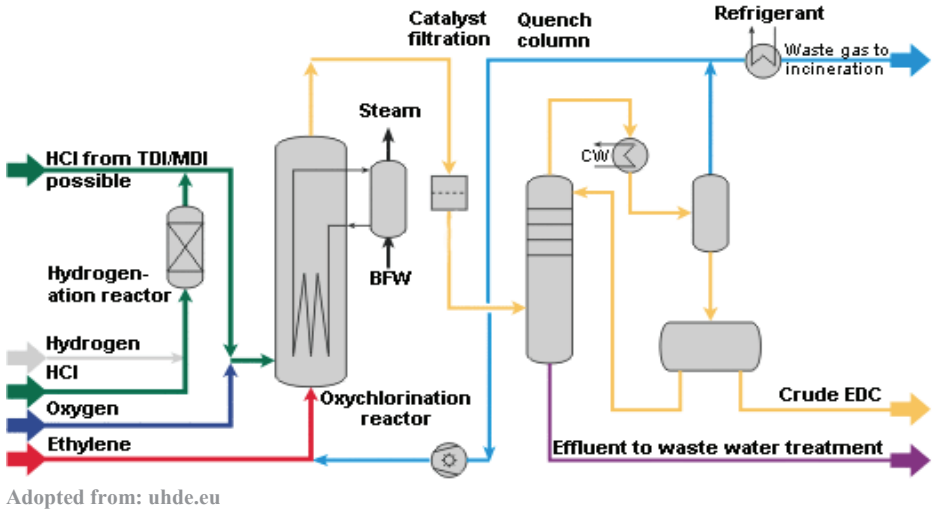

Figure 5 : Schematic representation of a typical oxychlorination process [licensed by Vinnolit technology] [35].

Typical fluid bed reactors are vertical cylindrical vessels supported on a grid, equipped with a feed spraying system for adequate feed distribution and fluidization, internal cooling coils for heat removal, and cyclones (either of external or internal) to minimize catalyst carry-over [36-38]. A schematic diagram [39] illustrating a typical catalytic fluidized bed reactor and the different phases of catalytic particles present during reaction is shown in Figure 6. In fluid bed oxychlorination processes, a fluidized catalyst is loaded into the reactor; the preheated gas mixture allowed entering at the base of the vessel at an operating temperature of 493- 518 K and reactor gauge pressures of 150-500 kPa. Generally, these fluidized bed oxychlorination reactors are well behaved and operate predictably, however, they can suffer from catalyst stickiness, which is characterized by declining the quality of fluidization and, in severe cases, result in a slumped or collapsed bed.

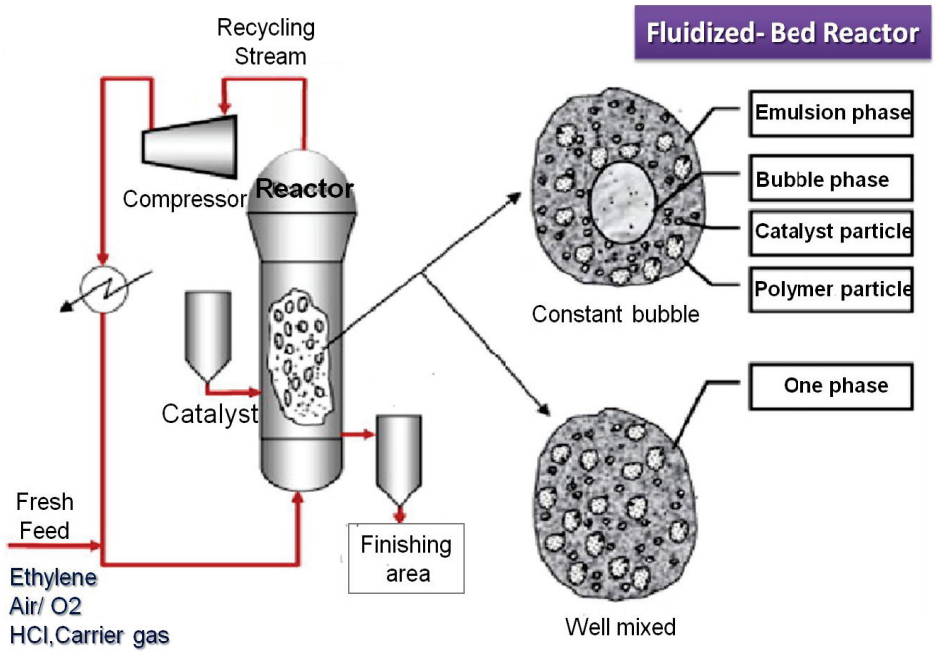

Figure 6: Typical illustration of general catalytic fluidized bed reactor system. Image courtesy to "Process Systems Enterprise Ltd" [39].

Oxychlorination catalyst stickiness mainly arises from adverse operating conditions that promote the formation of dendrite growths of cupric chloride on the individual catalyst particles' surface. This leads to increasing inter-particle interactions and agglomeration. The degree of particle agglomeration and severity of stickiness depends on the operating conditions and the catalyst characteristics [37, 38, 40, 41].

Fixed bed reactors are generally looking like multi-tube heat exchangers, with catalyst packed in vertical tubes held along the reactor with a supporting grid on the top and bottom. Figure 7 illustrates the typical catalytic fixed bed reactor and 2D-distribution of catalyst composition and temperature [39]. It is essential to pack the catalyst uniformly along the tubes, which further ensure a safe operation with uniform pressure drop, flow, and residence time throughout the each tube. Though it has many advantages such as easy scale-up, flexibility of process conditions, however, main disadvantage is difficulty in the temperature control compared to the fluidized bed reactors; because of localized hot spots tend to develop in the tubes [42]. This problem can be addressed in several ways: one is to pack the reactor tubes with the active catalyst and inert diluents mixtures in proportions that vary along the

tubes, so that there is low catalyst concentration at the inlet (where the catalyst activity is high due to the high reactant concentration), and steadily increases to maximum at the outlet. Another way of minimizing hot spots is to pack the tube with catalysts having progressively higher loading of $CuCl_2$ [42]. These methods of grading the catalyst activity tend to flatten the temperature profile thus improve the temperature control. Typical oxychlorination reactor systems contain multiple fixed bed reactors in either series or parallel.

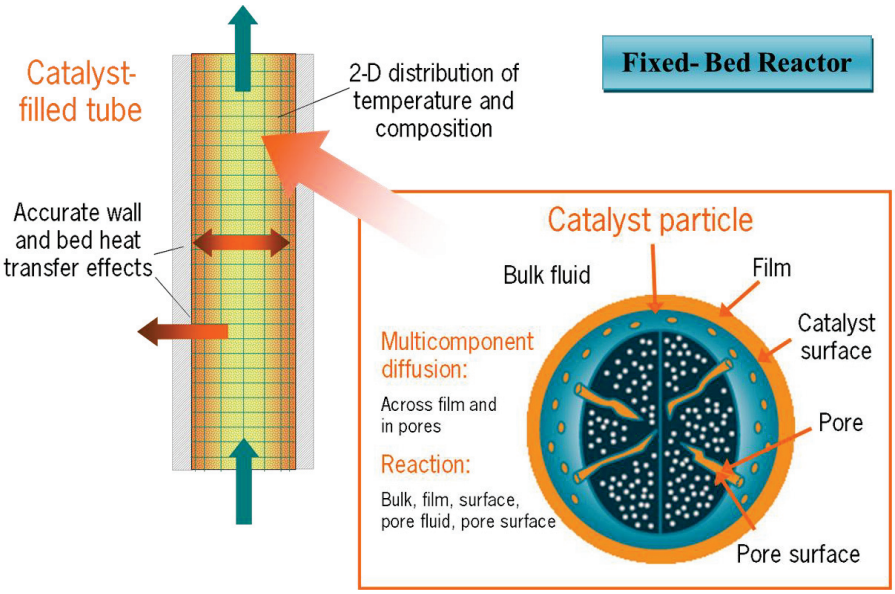

Figure 7: Cross sectional illustration of typical catalytic fixed bed reactor. Image curtsey to "Process Systems Enterprise Ltd" [39].

In the Air-based oxychlorination process with either fixed or fluidized bed reactor, ethylene and air are fed in slight excess of stochiometric requirements to ensure high conversion of HCl and to minimize the loss of excess ethylene. In Oxygen-based process, pure oxygen is fed insted of air, thus, resulting in a drastic reduction in volume of vent gas discharge, which is the main advantage over air-based process. There by avoidance of expensive facilities to recover ethylene, EDC, other chemicals from large vent gas stream and a reduction in nitrous oxide (NOx) and other nitrogen based by-products [43]. Problems can occur, however, if the ethylene / O_2 molar ratio approaches the explosion limits. Ethylene's lowest explosion limit is 2.7 vol % in air i.e 12.8 ethylene/O_2 molar ratio. However, this risk can be minimized/eliminated by operating- parallel reactors with various optimal ethylene/O_2 feed ratios.

The use of a liquid - phase oxychlorination process for the production of EDC was investigated [44-46] using promoted aqueous copper salt as a catalyst. The inventor's observations on increased selectivity at moderate temperatures (473-623 K) were constrained to pilot plant studies, but there is no information about its practical exploitation, which indicates difficulties in the industrial application of such processes.

Chapter 3

General Chemistry of Copper - Chlorides

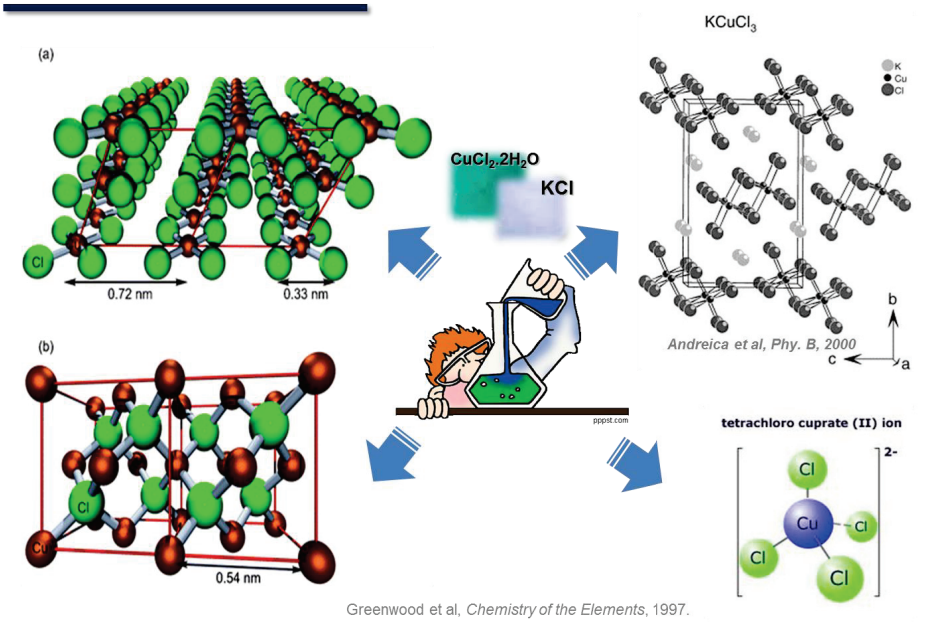

Greenwood et al, *Chemistry of the Elements*, 1997.

This chapter focuses on the general chemistry of the active species: the structure and properties of copper chlorides. It also further reviews some recent work done on the effect of dopants on the structure, properties and thermodynamics of copper chloride. The final section will give brief overview on possible formation of binary and ternary mixtures in doped catalyst systems.

3.1 General chemistry of Copper containing chlorides

Being the central component of an oxychlorination catalyst, a study of the general trends observed among relevant cuprous (Cu^{I}) and cupric (Cu^{II}) compounds may give valuable inputs to the understanding of the oxychlorination catalyst in terms of structural preferences and correlation to their reactivity.

Copper forms compounds in the oxidation states of +1 (cuprous) and +2 (cupric); trivalent copper survives no more than a few seconds in an aqueous solution. The relatively small change in electrochemical potential as shown in below equation (Eq.9) between the cuprous and cupric ions in solution leads to the usefulness of copper compounds in chemical reactions.

$$\mathbf{Cu^{2+} + e^{-} \rightleftharpoons Cu^{+}} \quad (E^{\emptyset}_{Cu2+/Cu+} = +0.15V) \qquad (9)$$

Copper compounds are used as catalysts in reactions, due to their reduction and oxidation capabilities.

3.1.1 Structure and Properties of Cupric Chloride

Cupric chloride ($Cu^{II}Cl_2$) is a very hygroscopic yellowish to brown deliquescent powder; soluble in water, alcohol, and ammonium chloride. It readily absorbs moisture from the air and turns into the greenish blue hydrate, $CuCl_2 \cdot 2H_2O$. The structure of solid dihydrate $CuCl_2$ consists of trans-square planar arrangement so that there is weak intermolecular Cu···Cl interactions [47]. Upon heating up to 393-423 K, the water leaves the crystal, forming anhydrous $CuCl_2$ [48]. The anhydrous salt can also be prepared by heating the dihydrate to a moderate temperature in a stream of hydrogen chloride. The blue cupric chloride dihydrate is converted to brown pseudo amorphous needles. The general structure of anhydrous $CuCl_2$ contains a polymeric chain formed by planar $CuCl_4$ units sharing opposite

edges, the chains are packed so that each Cu has two more chlorines bonded rather with longer Cu-Cl distances, forming the well-known octahedral environment around Cu, as shown in Figure 8a.

Divalent copper probably has the richest stereochemistry of all ions. Generally there is a tendency for $Cu^{(II)}$ to form structures derived from square planar substructures and exhibit distortions from idealized octahedral geometry due to the Jahn-Teller effect. The four bonds may also take on the geometry of a flattened tetrahedron; the degree of deviation from planar geometry seems to depend on the strength of additional bonds [49]. The structure of coordination compounds is a combination of the coordination number (CN) and the possible geometries of the attached ligands. For the compounds with CN = 2, the structure is always linear; for CN = 4, the geometry can be one of two structures: square planar or tetrahedral and for CN = 6, the structure is almost always octahedral. It is suggesting that copper can have various structural preferences depending on its coordination number and type of ligand, on the fresh catalyst and during the reaction. That means these changes of structural preferences during the oxychlorination reaction, may play an important role.

Since the length of the Cu^{II}-Cl bond (2.30 Å) in anhydrous $CuCl_2$ is the same as that of Pd^{II}-Cl, it was assumed that it follows the same structure as $PdCl_2$ [50]. However, lately it was shown to differ significantly [50]. Wells A.F [50] showed that the Cu and Cl atoms joined together to form square planar structures which in turn form infinite chains that are bonded together by weaker bonds, resulting in a distorted octahedral arrangement around Cu(II). In this octahedral geometry, each Cu is surrounded by 4 Cl ions (two at 2.30 Å and other two at 2.95± 0.05 Å) and each Cl is attached to two Cu ions as illustrated in Figure 8a . The crystallites of $CuCl_2$ were found to take the shape of thin needles or laths, which, by applying very little pressure, can be split into a bundle of fibres (Wells, 1947).

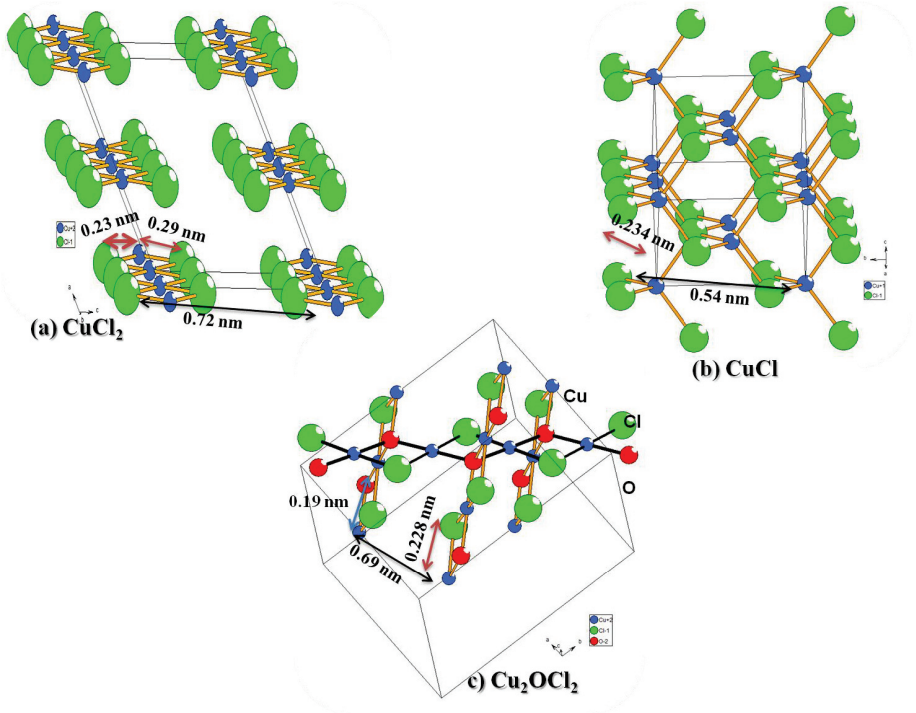

Figure 8: Schematic representations of the crystal structures of anhydrous: (a) $CuCl_2$, (b) CuCl, and (c) Cu_2OCl_2. (Unpublished figure)

It was also believed that $Cu^{(II)}$ compounds prefer to form mono $[CuCl_4]^{2-}$ or bi-nuclear complexes $[Cu_2Cl_6]^{2-}$. Desjardins *et al* [51] explained the polarization and electronic properties of binuclear $Cu^{(II)}$ complexes. Authors argued that the preferential formation of these two complexes depend on the attached ligands. This is vital important, to connect these structural preferences to the oxychlorination reaction mechanism, which is not yet resolved. For example: in mono layer anhydrous $CuCl_2$, when Cu^{2+} is coordinated to four Cl ligands in a square-planar arrangement, the crystal field will split the 3d-orbitals into the usual t_{2g} triplet and an excited e_g doublet, which in turn result in an increase in the energy of $d_{x^2-y^2}$ orbital [52]. This information might explain the specific site adsorption of an alkene molecule. In this case, $d_{x^2-y^2}$ position is preferable position for stronger adsorption of ethylene molecule. And also it was anticipated that, during the reaction, this infinite chain of $Cu^{(II)}Cl_2$ would break preferably into one of these complex forms. The general illustration of copper chloride complexes formed during the oxychlorination reaction is shown in Figure 9 (representing a square planar unit). These phenomena could explain the structural relationship to the reaction

mechanism presented in the section 4.5. However, the credential structural knowledge is vital for a better understanding of oxychlorination mechanism.

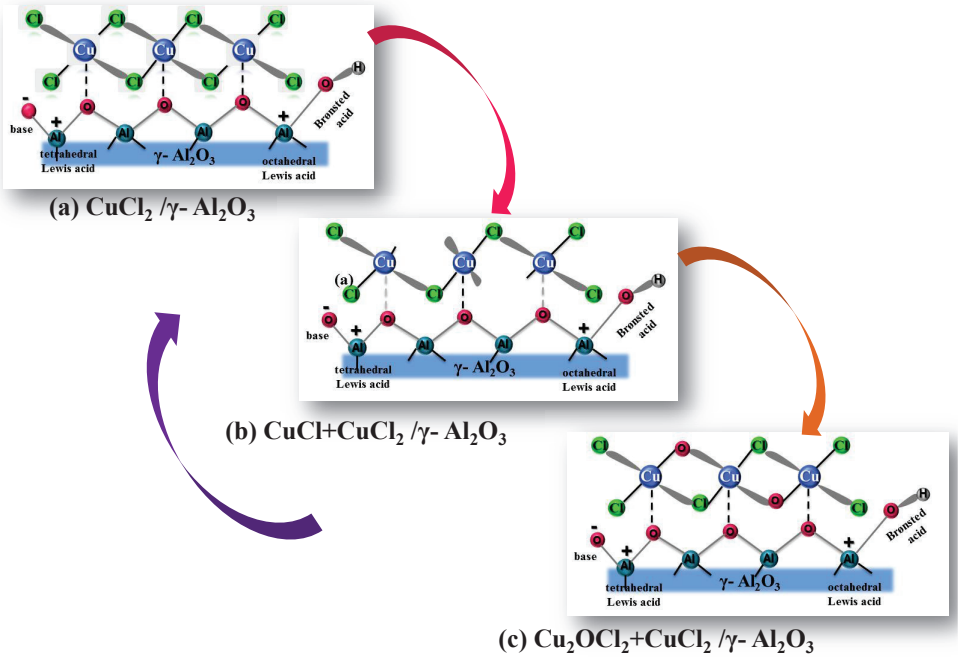

Figure 9: A general representation of three different species of copper formed during the oxychlorination reaction. a) Cu_2Cl_4/γ-Al_2O_3, b)Cu_2Cl_2/γ-Al_2O_3 and c) Cu_2OCl_2/γ-Al_2O_3. (Unpublished figure)

The structure of oxychloride Cu_2OCl_2 (Figure 9c), formed during the oxidation of the cuprous chloride (Eq.16), is still in debate. However, pure, unsupported reddish brown Cu_2OCl_2 has an orthorhombic crystal lattice structure, observed from the XRD [53] and NMR patterns [54] as shown in Figure 8. The structure is described as cross-linking chains of the edges of squares of Cu_2OCl_2, in which the Cu ions are located at the center of the distorted square plane formed by two Cl and two O ions being at the corners. The authors indicated that Cu_2OCl_2 is charge-transfer type materials with no crystal field exist to split 3d orbital, like in anhydrous $CuCl_2$.

Another interesting structure is the hydroxyl chloride $Cu_2(OH)_3Cl$, which is formed when γ-alumina is impregnated with an aqueous solution of $CuCl_2$ [55-57]. There are two crystal modifications atacamite and paratacamite. Atacamite is orthorhombic, in both Cu atoms display distorted octahedral geometry, where Cu is bonded to the four OH-groups at a

equatorial distance of 2.02 Å. While the chloride ions occupy the axial positions at a distance of 2.76 Å, indicating that chlorine is rather weakly bonded. However, paratacamite structure still in debate, and argued to be a rhombohedral, in which Cu atoms display three different types of octahedral arrangements. These crystal chains cannot break into single chains like $CuCl_2$. The Cu-O bonds are 0.07 Å longer than in Cu_2OCl_2 and CuO (2.02 vs. 1.95 Å), indicating that the Cu-O bonds are weaker in the hydroxyl chloride [56]. These copper hydroxyl chlorides, especially paratacamite, are observed [57] in the fresh oxychlorination catalyst and it has been shown [57] that they disappear upon heating above 473 K.

It is interesting to note that cupric ions appear to have a stronger affinity to oxygen atom than to chlorine: whenever both oxygen and chlorine are present in a structure, oxygen will always appear among the shorter equatorial bonds, displacing the chloride to the weaker bonds in the axial positions. This may be of importance for the mechanism of the oxychlorination process.

In a simple conclusion, copper chloride changes its structural preferences depending on its surrounding environment, coordination number and temperature.

3.1.2 Structure and Properties of Cuprous Chloride

Copper(I) chloride was first prepared by Robert Boyle in the mid-seventeenth century from mercury(II) chloride ("Venetian sublimate") and copper metal:

$$HgCl_2 + 2\ Cu \rightarrow 2\ CuCl + Hg \qquad (10)$$

Monovalent or so-called cuprous chloride often forms four bonds in a tetrahedral arrangement, as shown in Figure 8b. Compounds with three coplanar bonds are also common. Of interest in our case is the tendency to form infinite chains or rings with unsaturated hydrocarbons.

A well-known property of cuprous chloride is its high volatility, which causes problems for the lifetime of oxychlorination catalysts. The vapor pressures in the temperature range 503 - 673 K were determined from diffusion experiments done by Hammar and Gregory *et al* [6] and tri-meric structure, Cu_3Cl_3 has been reported to fit the below equation

$$\log P_{CuCl}\ (\text{mm Hg}) = -7574\ T^{-1} + 10.29 \qquad (11)$$

The composition of Cu_xClx in the gas phase has been determined by mass spectrometry, which revealed Cu_3Cl_3 molecules, Cu_4Cl_4 molecules have also been reported to exist (Well 1984). The exact structures of the gas phase species are not known, but ring structures are assumed. Such ring structures will probably have a tendency to bind unsaturated hydrocarbons present in the gas phase. Therefore, it is possible that an atmosphere containing unsaturated hydrocarbons will increase the evaporation of cuprous chloride, although this merely a hypothesis.

3.1.3 Structure and Properties of mixed chlorides

Generally $Cu^{(I)}$ and $Cu^{(II)}$ chlorides have a strong tendency to form mixed chlorides when they interact with other metal chlorides especially those of alkali- metals. Binary and ternary systems containing copper (II) halides are of interest in many fields of application. The catalytic activity of the solid halocuprates is strongly influenced by their compositions and structure and varies significantly for compounds formed with the different alkali metal cations. Investigation by Skripkin *et al* [58] of the solid-solution phase equilibrium in the systems CuX_2- MX-H_2O (X = Cl^-, Br^-: M = Li^+, K^+ and Cs^+) at 298 K showed that in the presence of excess halide ions, solid halocuprate (II) compounds formed in most systems, often with coordinated water. The compositions of the halocuprates (II) (double salts or mixed salts) were of the forms M_nCuX_{n+2} and $M_nCuX_{n+2}\bullet yH_2O$. Since, most of the commercialized oxychlorination catalysts contain one or more alkali metal cations, knowledge of the structure and bonding in the coordination compounds is needed in order to understand and control the catalytic properties [59].

The most commonly found double salts containing KCl and $CuCl_2\bullet 2H_2O$ are bluish $K_2CuCl_4\bullet 2H_2O$ and red brownish $KCuCl_3$ compounds. The octahedral arrangement repeats itself in these both mixed chlorides, contains features from both anhydrous and hydrous $CuCl_2$. The crystal structure of K_2CuCl_4 is only known in the hydrated form, since the anhydrous form is too unstable. Even the hydrated compound seems to be unstable, and is reported to decompose at 365-397 K by one of the following reactions:

$$K_2CuCl_4\bullet 2H_2O \rightarrow KCl + KCuCl_3 \quad (12)$$

$$K_2CuCl_4\bullet 2H_2O \rightarrow 2KCl + CuCl_2\bullet 2H_2O \quad (13)$$

However, in controlled atmosphere $KCuCl_3$ can exist, of further note, it readily hydrolyzes in the moist air:

$$2\ KCuCl_3(s) + 4\ H_2O(g) \rightarrow CuCl_2{\bullet}2H_2O(s) + K_2CuCl_4{\bullet}2H_2O(s) \qquad (14)$$

Both these compounds contain discrete, planar, $[Cu_2Cl_6]^{2-}$ ions forming an octahedral arrangement around Cu(II) ion and forms a double chain of octahedral $[Cu_2Cl_6]^{2-}$ held together by the positive K^+. These dimers are very similar to the dimers found in $LiCuCl_3{\bullet}2H_2O$. In $CsCuCl_3$ there are infinite chains of $[CuCl_3]_n^{n-}$, the chain anions are held together longitudinally by Cs^+ ions. The length of the Cu-Cl bond in $CsCuCl_3$, $K_2CuCl_4{\bullet}2H_2O$ is same (2.3Å) as that in anhydrous cupric chloride CuCl.

Several authors [60-63] presented the detailed structures and properties of several double salts. Our aim here is not to provide discrete analysis of the crystal structures of these double salts, however, a brief knowledge on the structure and properties of these salts will give further inputs to our understanding on the doped oxychlorination catalyst.

3.2. Thermodynamics of mixed chlorides

The thermodynamics of mixtures of CuCl, $CuCl_2$ and potassium chlorides have been studied by only a few authors [20, 21, 46, 63-67]. Table 1 shows the melting points of some relevant solids. It is clearly seen from these numbers that the double salts have significantly lower melting points than CuCl and $CuCl_2$, and this is believed to be an important feature affecting the oxychlorination catalysts.

Fontana [21] proposed a phase diagram for the ternary mixture of CuCl-KCl-$CuCl_2$ system using freezing point-solubility determination method as shown in Figure 10. The detailed experimental method was illustrated in the respective reference. It showed the clear evidence of the formation of double salts. In the case of cuprous chloride, K_2CuCl_3 was formed, whereas for cupric chloride, the two double salts formed were $KCuCl_3$ and K_2CuCl_4. The phase diagram showed that $KCuCl_3$ only was formed on a sample containing KCl+$CuCl_2$ compounds with 50 mol% KCl corresponding to K:Cu= 1 molar ratio. However, with increasing amounts of KCl, K_2CuCl_4, K_2CuCl_3 appeared, lowering the melting point of the mixtures further [63], which is of course the eutectic behaviour.

Table 1: Summary of compositions and melting points of various binary and ternary eutectic mixtures (depicted from [21]).

Type of points	Solid Phases	Melt composition, Mole %			Melting Point ° C
		KCl	CuCl	$CuCl_2$	
Compounds	CuCl	0	100	0	422
	$CuCl_2$	0	0	100	622
	KCl	100	0	0	760
	$KCuCl_3$	50	0	50	364
	K_2CuCl_4	66.7	0	33.3	380
	K_2CuCl_3	66.7	33.3	0	
Binary eutectics	CuCl-$CuCl_2$	0	87	13	378
	CuCl-K_2CuCl_4	34	66	0	150
	$CuCl_2$-$KCuCl_3$	46	0	54	360
	$KCuCl_3$-K_2CuCl_4	60	0	38	320
	K_2CuCl_4-KCl	70	0	30	325
Binary transition	K_2CuCl_4-KCl	47	53	0	245
Ternary transition	CuCl-$CuCl_3$-$KCuCl_3$	24	59.5	16.5	250
	K_2CuCl_4-KCl-$KCuCl_3$	51	38.5	10.5	225
	K_2CuCl_4-KCl-$KCuCl_3$	56	22	22	267

Further, Fontana [21] proposed that all the chlorine ion available from the potassium chloride was associated either with cuprous chloride to form $[Cu_2Cl_3]^-$ or with cupric chloride to form $[Cu_2Cl_6]^{2-}$, which is interesting in structural point of view to its connection to the reaction. Ruthven and Kenny [66] argued that Gibb's free energy (ΔG) for the reduction of $CuCl_2$ reaction (Eq. 18) decreased with increasing KCl content. The changes appears to be associated with the entropy term i.e the entropy change associated with the release of Cl_2 from $CuCl_2$ decreases significantly with increasing KCl content, thus shifting the equilibrium to the left side of eq.18. They further argued that weak copper-potassium interaction resulted in an increase in the partial entropy of $CuCl_2$. It was postulated that the reason for this increase in entropy, might be due to breakdown of long chains of $[CuCl_2]_n$ into complex copper species for example: $[CuCl_4]^{2-}$ or $[Cu_2Cl_6]^{2-}$. Also, Sachtler and Helle [67] suggested that increasing the KCl content will decreases the ΔG of the reduction reaction. They explained that it might be due to an increased complexation of cuprous species, reducing entropy of cuprous chloride in the melt. The effect of KCl presence on thermodynamics of the reaction involved $CuCl_2$ explained by the previous papers were quite analogy to each other, emphasizing the complex

behaviour of the present system. Though, the results of experiments conducted at high temperatures (673 - 973 K) with release of Cl_2, are perfect analogues for the oxychlorination reaction. The key data on the effect of KCl on the structural change around copper and influence (decrease/increase) on the entropy of copper chloride are very relevant.

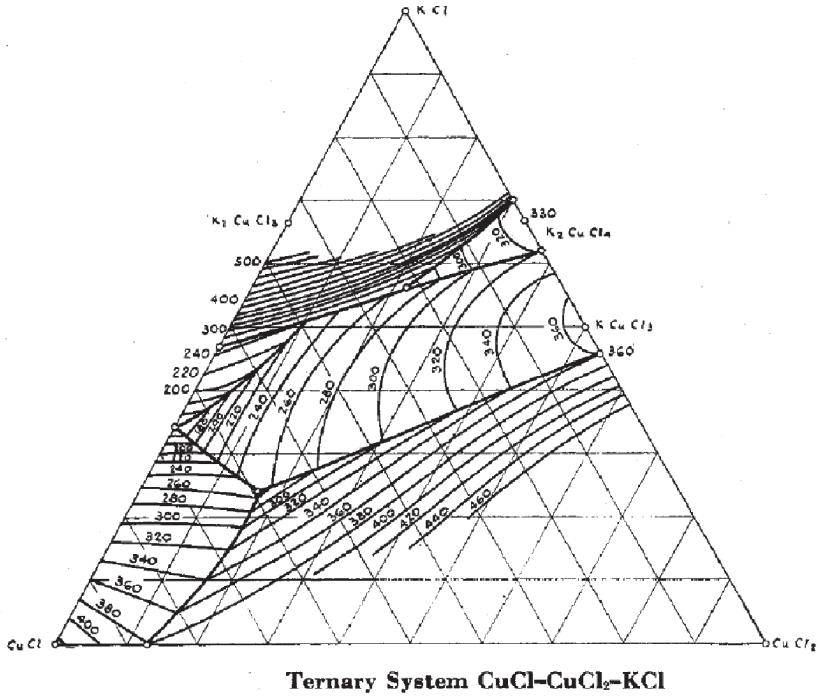

Figure 10: Ternary phase diagram for CuCl-$CuCl_2$-KCl system proposed by Fontana *et al*. [21]

Zurowski [68] has studied extensively the phase changes of the $CuCl_2$-KCl systems (molar ratio of Cu:K = 0.2 to 2.0) by differential thermal analysis (DTA). The author suggested that the fresh sample (unsupported) contains the double salt in the form of $K_2CuCl_4 \cdot 2H_2O$ which transforms into $KCuCl_3$ [68] at 365 – 398 K. This was the last phase change of the mixtures observed before melting. The later phase changes were observed at 573 - 583 K and 603 - 618 K, which were attributed to the formation of the Cu^{2+}, $[CuCl_4]^-$, $[Cu_2Cl_6]^{2-}$ ions from $[CuCl_3]^-$ ions (ions form the $KCuCl_3$ compound) or simply with the establishment of an equilibrium between them. The observations made by Zurowski were in agreement with the previous authors [21, 22, 65].

Unfortunately, the results so far reported do not say much about the nature of species of the double salts on ”the supported systems”. The only thing that is evident is that KCl has a

significant impact on the structure and properties of CuCl-$CuCl_2$ mixtures at oxychlorination temperatures. Very few [49, 63] studies were reported on other ternary systems containing, $LaCl_3$ or LiCl as co-dopant along with KCl. La is known to form strong chloride complexes [49, 69, 70] which further increased the rate of sublimation of CuCl by favouring the formation neutral CuCl species. Addition of $LaCl_3$ to $CuCl_2$-KCl-CuCl system was reported to have no effect on activation energy of the oxychlorination reaction [71, 72].

Chapter 4

Review of Ethylene Oxychlorination Catalysis

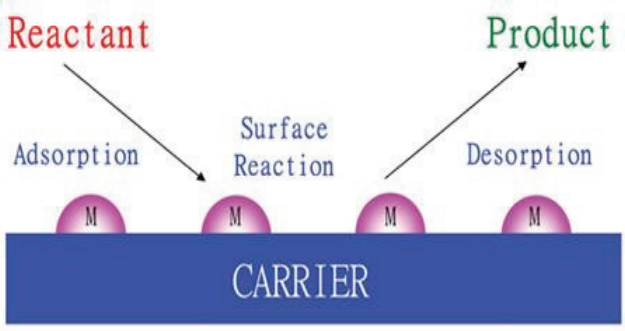

An important goal in catalytic research is the identification of the sites controlling activity and selectivity for a given reaction; elucidating the local structure of the active sites as well as their dispersion and oxidation state during operation. Various studies have been devoted to the search for improved or new catalysts for the oxychlorination reaction [6, 13, 25, 27, 48, 56, 57, 73-80]. The goal of these studies has been to develop less volatile, more active and selective catalytic compositions - by varying the supports, promoters and/or preparation methods. This chapter will provide a detailed review on the oxychlorination catalysis literature published so far.

4.1 Oxychlorination catalytic cycle

Oxychlorination of ethylene [48, 56, 78, 80-88] (Eq.6) is catalyzed by a highly dispersed $CuCl_2$ phase and follows a three- step redox mechanism: a) chlorination of ethylene by the reduction of $CuCl_2$ to CuCl [Eq.15], b) oxidation of CuCl to an oxychloride [Eq. (16)], and c) re-chlorination of this oxychloride with HCl to $CuCl_2$ [closure of the catalytic cycle, Eq.(17)]. The reaction steps are highlighted below and illustrated in a schematic triangle diagram in Figure 11.

Step1: $\mathbf{2CuCl_2 + C_2H_4 \rightarrow C_2H_4Cl_2 + 2CuCl}$ (15)

ΔG_{298K} =-89.4 kJ/mol ; ΔH_{298K} = -112 kJ/mol

Step 2: $\mathbf{2CuCl + \frac{1}{2} O_2 \rightarrow Cu_2OCl_2}$ (16)

ΔG_{298K} =-88.6 kJ/mol ; ΔH_{298K} = -83 kJ/mol

Step 3: $\mathbf{Cu_2OCl_2 + 2HCl \rightarrow 2CuCl_2 + H_2O}$ (17)

ΔG_{298K} = -4 kJ/mol ; ΔH_{298K} = +25 kJ/mol

The above mechanism is an illustration of classical catalysis. The mechanism involves the formation of intermediate compounds that are then converted into reaction products with regeneration of the initial catalyst state. This red-ox mechanism illustrates that the relative rate of the different steps will determine the relative amounts of the different species that are present on the surface, thereby the reaction rate, the selectivity and the stability of the catalysts.

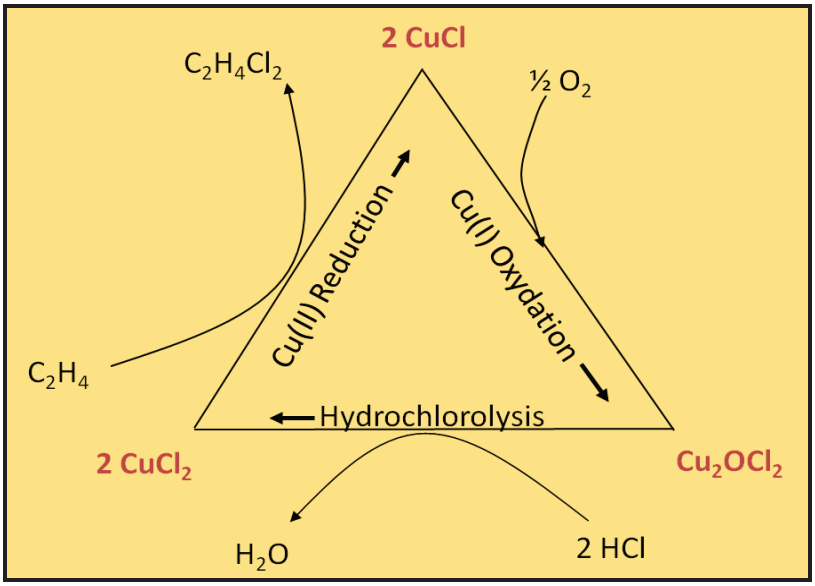

Figure 11 : Schematic diagram representing the reaction mechanism of ethylene oxychlorination on a $CuCl_2/\gamma$-Al_2O_3 catalyst at 473-573 K. (Unpublished figure)

4.2 Why is copper chloride a superior oxychlorination catalyst?

Copper (II) chloride, was identified as a superior catalyst for hydrogen chloride oxidation and – for oxychlorination of hydrocarbons as early as the 19th century. Despite of advances, it still remains the main constituent of the industrial catalysts for the oxychlorination of several hydrocarbons for example: methane, ethylene, benzene, alkyl benzenes, propene and butane and also of a non-hydrocarbon "CO" [6, 13, 27, 30, 74, 89-92].

Allen [6] presented an interesting hypothesis why this is so: i.e., that a good Deacon catalyst must have the property that the standard free energy changes associated with the individual reactions of the Deacon reaction (illustrated for copper chloride in Eq (19) and (20) below) must be small:

$2CuCl_{2\,(S)} \leftrightarrow 2CuCl\,(s) + Cl_2$; $\Delta G_{298\text{-}900\,K} = +142$ to 60 kJ/mol (18)

Adding Eqs (16) and Eqs (18)

$2CuCl_2\,(s) + 1/2\,O_2(g) \rightarrow CuO.CuCl_2(s) + Cl_2\,(g)$; $\Delta G_{298\text{-}900K} = +57$ to $+6$ kJ/mol (19)

$CuO.CuCl_2(s) + 2HCl \rightarrow 2CuCl_2\,(s) + H_2O(g)$; $\Delta G_{298\text{-}900K} = -84{,}4$ to $-5{,}4$ kJ/mol (20)

The author calculated [6] the standard free energies ($\Delta G°_T$) as a function of temperatures (298-900 K) for Eqs (19) and (20) using Eq (21) from the recorded standard enthalpy ($\Delta H°_{298K}$) and entropy data ($\Delta S°_{298K}$) for copper chloride catalysts along with a range of other monovalent, divalent, trivalent oxides/chloride pairs.

$$\Delta G°_T = \Delta H°_{298K} - T\,\Delta S°_{298K} \quad (21)$$

This property of having smallest $\Delta G°_T$ for each step followed in the order (shown:

Mg<**Cu**<Sn(II)<Ni<Zn<Rh<Fe(II)<V(II)<Mn<Co<Pd<Cd<Hg<Pb<Ca<Sr<Ba

It appears from this series that metals to the right of copper in above order are likely to be progressively less effective catalysts and that the only one more favourable than copper is magnesium. However, magnesium exists only in +2-oxidation state and has no red-ox properties, and therefore cannot perform the reaction of Eq. (18). Another group of elements fulfilling the intention of low Gibbs energy for the reaction steps (19) and (20) are rare earth elements [6]. However, like Mg, most lanthanides are not red-ox active. Therefore, the author merely evaluated the catalysts as Deacon catalysts. Their favourable properties for catalysing Eq. (19) and (20) may explain why rare earths and magnesium (Mg) have a promoting effect in combination with cupric chloride. Although oxychlorination catalysts are derivatives of the Deacon catalyst, Allen's model is not sufficient for making a prediction for oxychlorination catalysts, as the ethylene chlorination step is not included.

Palladium, Platinum and other noble metal chlorides were also reported [27] as catalyst ingredients for the ethylene oxychlorination. However, it is not possible to draw any conclusions regarding their effect on product distribution from his review. The author reported that vinyl chloride (VCM) was formed in most cases. Treger *et al* [74] reported in his review that palladium containing catalyst was more selective to VCM in the temperature range of 473-573 K and the remaining followed the order: $PdCl_2 > RhCl_2 > PtCl_2 > RuCl_2$. A disadvantage of these catalysts reported was the limited conversion of ethylene.

Todo, Kurita and Hagiwara [13] examined the relative catalytic activity of various metal chlorides for the ethylene oxychlorination reaction and found the following order:

$$CrCl_3 > CuCl_2 > FeCl_3 > MnCl_2 > NiCl_2$$

Further, they reported that $CuCl_2$ was more selective for formation of 1,2-dichloroethane than $CrCl_3$.

The above conclusions were further supported by Hall *et al* [93] with his experimental observations, who performed kinetics and simultaneous adsorption studies of ethylene in the temperature range 423-623 K using a micro-reactor coupled with gas adsorption chromatography (g.a.c). The authors examined various transition metal chloride systems: VCl_3, $CrCl_3$, $CrCl_2$, $MnCl_2$, $FeCl_2$, $CoCl_2$, $NiCl_2$, $CuCl_2$, CuCl, $PtCl_2$, $PtCl_4$ and $PdCl_2$. They reported that the reaction proceeded on $PtCl_2$, $PtCl_4$ and $PdCl_2$ - and HCl, Vinyl chloride, dichloroethane and polymers were identified as products. Among the remaining systems:

i. VCl_3 showed activity to vinyl chloride, but showed very rapid deactivation due to high volatility at 423 K,

ii. $CrCl_3$ formed VC, EDC and also other chlorinated ethanes and polymers at 423 K,

iii. $NiCl_2$ showed the chemisorption of C_2H_4 but no reaction at > 523 K,

iv. Physically adsorbed C_2H_4 with no activity on CuCl, $CrCl_2$, $MnCl_2$ and $CoCl_2$,

v. Only $CuCl_2$ system was selective for EDC with strong C_2H_4 chemisorption.

All reviews of the data [6, 13, 25, 27, 74] indicated that no catalyst rivals to $CuCl_2$ in the selective formation of 1,2-dichloroethane.

The results described above were further compared and correlated with the strengths of M-C_2H_4 bonds (M= Transition metal chloride) expressed as isosteric heats of adsorption versus the metal's electronic configuration (Figure 12a). Their correlation with d-electrons and ion-polarising effect in terms of the ratio of ionic charge/ (ionic radius)^2, is shown in Figure 12b. Figure 12a shows that bonding of C_2H_4 is not favoured by d^4, d^5 and d^{10} configurations, this can be explained by the molecular-orbital bonding approach. These configurations have no л-back bonding effect for d^4, d^5 and no σ-bonding for d^{10} configurations (though this configuration has complete л-back bonding). The C_2H_4 is strongly adsorbed on d^8 and d^9 configurations. Their ion-polarising effects can further help to understand the above explanation. Figure 12b shows that even though Mn^{2+}, Co^{2+} , Fe^{2+}, Ni^{2+} and Cu^{2+} have more or less same ion-polarization effect, for $FeCl_2$, $NiCl_2$ and $CuCl_2$ electron configurations are the one factor altering the q_o value for these compounds. Hall [93] further observed that $PdCl_2$, $PtCl_2$ and $PtCl_4$ gave higher adsorption strengths for C_2H_4 but were less active and selective in C_2H_4 oxychlorination reaction. These chlorides are known to have different crystal structures than copper chlorides, thus may have high adsorption strengths, so

that reaction/desorption becomes the rate-limiting steps, which suggest that structure may be a major factor here.

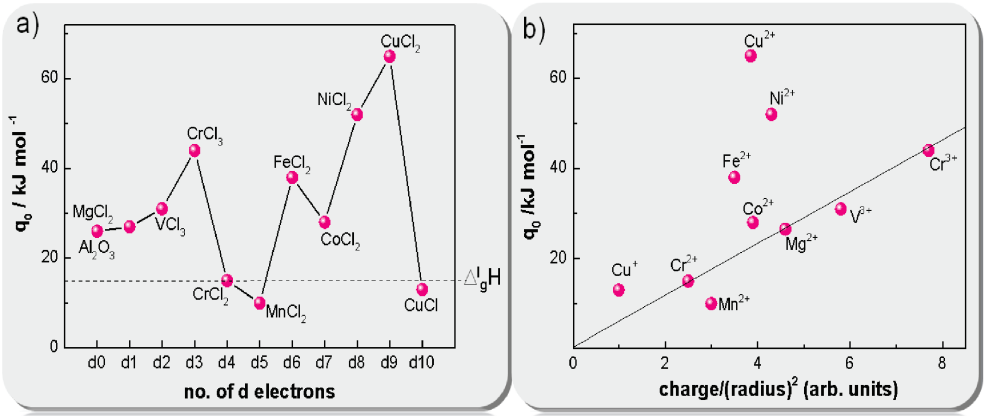

Figure 12: Isosteric heats of adsorption of C_2H_4 on transition metal chlorides: a) effect of d-electron configuration. (Δ^l_gH is the heat of liquefaction of C_2H_4), b) effect of charge/(radius)^2. Adopted from Hall et al. Publication [93].

Linear relations between the activation energies and heats of adsorption have long been assumed to be valid, such relations are called Brønsted-Evans-Polanyi relations [94]. Although no comparison between activation energies for each metal chloride and their adsorption energies of ethylene (provided by the authors), it is tempting to suggest that the activity and selectivity of ethylene oxychlorination somehow depend on the M-C_2H_4 adsorption strength. Which in turn, depend on the metal chloride's electron configuration, ion-polarising effect and its structure (i.e.: "Cu"structure preference ⇔ gas molecule adsorption strength and position ⇔ activity ⇔ selectivity). The main objective of explaining the above relationship in detail here is to emphasize the importance of copper chloride besides other metal chlorides [6, 13, 25, 74, 93] and their electronic configuration and structural preferences as the determining factors on the activity and selectivity for ethylene oxychlorination reaction.

There remain, however, some disadvantages in using the cupric chloride catalyst:- volatility of the active ingredient at the operating temperatures, non-negligible formation of side products, notably from the oxidation of hydrocarbon, progressive loss of the catalytic activity with time on stream. Since the high exothermicity of the reaction contributes to an acceleration of side reactions [6, 13, 74, 95-98] involving possible combustion of ethylene and the further conversion of EDC to produce higher poly hydrocarbon chlorides, dioxins and CO_x. The detailed by-product formation will be discussed in later section (4.5). Since then,

many authors investigated other options such as adding stabilizers, activity promoters, improving the process parameters and technologies.

The side reactions are believed to be a catalytic process [99] [100] and it was suggested that both the carrier surface free of salt melt and the different phases of copper chlorides are responsible. The experimental observations on the by-product formation will be discussed in a later section (4.5.2). Here, we will only mention that attempts have been made to bind copper in spinel structures' ($CuAlO_4$, $CuCrO_4$ etc.,) and, furthermore, suggested that copper could be used in the form of oxide, sulphate, nitrate, phosphate, stannate, plumbate, chromate, molybdate, vanadate etc., in mixture with the copper chlorides. However all these attempts were unsuccessful, since, under oxychlorination conditions, with an excess of hydrogen chloride and at elevated temperatures, all these compounds gradually converted into copper chlorides. In the end, the real system was not much different than traditional copper chloride based system [13, 74].

4.3 Catalyst Supports

The choice of support is very important for the activity of a catalyst. Porous materials with a wide range of specific surfaces (0.5-1 to 150-1000 $m^2\ g^{-1}$) are generally used as supports. Among them, γ-Al_2O_3 is the most commonly used support in petroleum refining, petrochemical industries and oxidation–reduction reactions. In the present case as well, γ-Al_2O_3 is the most studied and commercialised support for ethylene oxychlorination reaction [13, 27, 48, 73, 74, 85, 101]. A reasonable explanation might be its high specific surface area, porous structure, high thermal stability, high mechanical strength and acidity [102]. The surface acidity of γ-Al_2O_3 controls the dispersion and activity of supported catalysts [103-105]. Various natural and synthetic materials that differ in chemical nature and structural characteristics can also be used as supports such as activated charcoal, silica gel, alumina silicate, zeolites, and other carriers [13, 27, 74].

Allen *et al* [13] and Mallikarjuan *et al* [27] reviewed the available literature studies and patents on several variations of catalyst compositions for oxychlorination of ethylene, and depicted them generally in the following Table 2. However, the authors did not draw any conclusions on the effect of support on the reaction in terms of activity and selectivity. A few authors [85, 101, 106, 107] studied the influence of support explicitly on the reaction activity and selectivity and those studies will be discussed in the following paragraphs.

Zipelli *et al* [106] investigated the nature of copper species on γ-Al_2O_3, SiO_2 and α-Al_2O_3 impregnated with $CuCl_2$ aqueous solution and subjected to various treatments, by X-ray diffraction (XRD) and near-infrared reflectance spectroscopy (IR). They suggested that $CuCl_2$ was highly dispersed on γ-Al_2O_3 compared to the other supports and observed a strong metal-support interaction in case of γ-Al_2O_3 compared to other supports. Rouco *et al* [85] studied the mobility of copper on potassium and lanthanum doped copper catalysts supported on γ-Al_2O_3, SiO_2 and α-Al_2O_3 using XRD, temperature-programmed reduction (TPR) and solubility tests, and reported that a strong salt-support interaction occurs in γ-Al_2O_3-, compared to α-Al_2O_3- and SiO_2-supported copper chloride. The author observed that volatility of copper chloride was less on γ-Al_2O_3 support compared to other two. Allen and other authors [13, 27, 74] reported in their reviews that silica gel was eventually suggested by Engel *et al* and Fleurke *et al*, while Todo *et al* studied various supports with 15wt% of copper (II)chloride for the oxychlorination of ethylene and reported the preferred order

$$\gamma\text{-}Al_2O_3 >> SiO_2 >> \text{Celite}$$

Several reviews [13, 27, 74] have been written about the support influence on oxychlorination catalysts. Particularly one review [27] gave an overview of the support/metal combinations tested and depicted in Table 2. It concluded that γ- alumina support was the most commercialised support. It was further suggested that silica and α-Al_2O_3, used in combination with γ- alumina, led to increase the EDC selectivity considerably, but also led to a small change in stability of the catalyst. For further information, please refer to the mentioned review and refs given there in- [27].

Table 2 – Overview of catalysts for Oxychlorination of Ethylene [27]

Catalyst	**Carriers**	**Promoters**	
		Stabilizers	**Activators**
Oxides, Chlorides, Silicates of Cu, Fe, Cr, Mg, Mn, Ag, Au, Ni, Ca, V, Pd, Pt and W	Aluminas, bentonite, silica gel, activated carbon, zeolites, magnesia, zirconia, titania, celite, pumice and alundum	Chlorides, bisuplhates of Li, K, Na, NH_4, Zn, Cd, B, I, P, Ca, Sr	Oxides and Chlorides of La, Pt, Zr, U, Ce, Th, Ti, Ta, Rh, Mo, Ru and W.

Based on the analysis of available literature data so far, it has been concluded [13, 27, 48, 73, 74, 85, 101, 106, 108] that the best efficiency of the catalyst in the temperature range 473 - 533 K was shown by the copper chloride catalysts supported on γ-Alumina.

Treger *et al* [74] reported in their review article that the activity and selectivity of catalysts supported on γ-alumina depend to a great extent on the phase composition of the alumina. The use of n- or α-Al_2O_3 leads to almost 100% yield of 1,2-dichloroethane at 473-513 K. It was suggested that content of theta-phase of alumina plays as a major role, since, the copper chloride reacts with it to form copper aluminates with spinel structures. Since the cited article is from the 1980's and written in Russian, the supporting information for the above claims is not provided here.

The processes taking place during impregnation of γ-Al_2O_3 with $CuCl_2$ in aqueous solution have been studied by Fricke *et al* [55]. The authors observed that exposing γ-Al_2O_3 to an aqueous solution of $CuCl_2$ for a longer period, led to complete dissolution of the alumina, thus basic copper hydroxyl chloride ($Cu_2(OH)_3Cl$) was formed. If the process was allowed to continue for shorter periods, only partial formation of this compound could be observed, but in addition, another phase richer in chlorine was formed. Blanco *et al* [109, 110] first reported the co-existence of different compounds of copper chloride on γ-Al_2O_3 support. Author performed IR, EPR and XRD studies on $CuCl_2$/γ-Al_2O_3 catalysts containing increasing amounts of Cu, and concluded that $CuCl_2$ forms two different kinds of active complexes on the surface. The author attributed these active complexes to two square planar copper chloride complexes formed on the surface by bonding with oxygen from the alumina support as shown in Figure 13.

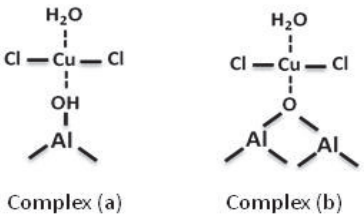

Figure 13 : Square planar complexes of copper chloride supported on gamma alumina support proposed by Blanco *et al*. [110]

A few authors, in papers devoted to aspects of this topic, such as effect of different carriers, have discussed briefly the nature of Cu-interacting species in a $CuCl_2$/γ-Al_2O_3:

(i) the two different complexes hypothesized as shown in Figure 13 by Blanco and Avila, [101, 109, 110] tentatively supported by Arcoya and Baiker [73, 81, 111],

(ii) a mono dispersed positive oxidation state of Cu suggested by Sermon *et al* [82],

(iii) the monolayer of interacting species proposed by Sai Prasad *et al* [83],

(iv) highly dispersed species interacting with support via oxygen bonds (Cu-O-Al surface species) as reported by Bond *et al* [112] and supported by other authors [84, 108],

(v) an attached bi-dimensional phase and strongly interacting with the support [85].

They investigated this system using techniques such as TPR, EPR, XRD, XPS and ESR. As far as species are concerned on the freshly prepared catalyst, with low Cu content: CuO, $CuAl_2O_4$ and with high Cu content: $CuAl_2O_4$, $CuCl_2$ and $Cu_2(OH)_3Cl$ (paratacamite) were hypothesised to be formed.

Recent studies by Leofanti and co-workers [56, 57, 76, 79, 80, 88], reported a clear picture about different compounds of Cu and its formation on variably Cu loaded $CuCl_2/\gamma$-Al_2O_3 catalysts (γ-Al_2O_3 specific area, 168 m^2/g; pore volume, 0.50 cm^3). They also investigated the stability of the catalyst upon aging and subjected to thermal treatments using several complementary characterisation techniques such as XRD, UV-vis-NIR DRS, FTIR, EPR XANES, EXAFS and solubility tests. It was shown [56, 88] that the copper formed two different kinds of species on the alumina surface during impregnation. For copper contents lower than 0.95 wt% Cu/100 m^2 of support, the formation of a surface aluminates species took place: copper occupied octahedral vacancies of the alumina surface and was surrounded (within experimental error) by five oxygen ligands at about 1.92 A°. This species were inactive during the oxychlorination reaction. The chlorine released by $CuCl_2$ during its interaction with alumina reacted with the support giving rise to >Al–Cl species as documented by the constant Cl/Cu ratio = 2, which was found by elemental analysis. After adsorptive capacity of the surface alumina is exhausted, up-on increasing the Cu loading, copper chloride starts to precipitate directly from the solution during drying. This leads to the formation of highly dispersed amorphous $CuCl_2$, on top of the surface aluminates, and gives the rise to active sites [79, 88] for the oxychlorination reaction. A contemporary slow hydrolysis reaction gives traces of insoluble copper hydro-oxychloride (paratacamite). Under heating, the alumina partially releases the chlorine fixed to the surface with the slow transformation of paratacamite into copper chloride. During a 6 month aging process, most of

the $CuCl_2$ is transformed in to the paratacamite phase and it was accelerated when the sample was exposed to air for more than an hour [57]. However, low-copper-concentration samples (0.25-1.4 wt %) are not involved in this process, reflecting high stability of the surface copper aluminates [79, 88]. But for high-copper content samples (2.3-9.0 wt %), the percentage of paratacamite increases with increasing copper content [57]. The $CuCl_2.2H_2O/Cu_2(OH)_3Cl$ ratio decreases with increasing aging time. This phenomenon of forming strong surface interacted copper complexes may also explain the copper chloride supported on alumina is highly active compared to other supports and less volatile during the reaction, compared to the bare $CuCl_2$ species or $CuCl_2$ supported on less acidic supports [73].

You-Chang Xie *et al* [113] observed the monolayer dispersion of copper chloride salt impregnated on γ-Al_2O_3 support by XRD and CO-chemisorption studies. They reported that monolayer dispersion is a spontaneous process. In the case of an ionic compound such as oxide or salt dispersed on the surface of porous oxides, the surface bond between the monolayer and the surface of support is usually strong enough to make the entropy effect a determining factor. This accounts for the widespread occurrence of monolayer or sub monolayer dispersion in these systems. They suggested that the threshold value for formation of monolayer is 0.13 g $CuCl_2$/g γ-Al_2O_3, corresponding to a dispersion capacity of 0.077 g $CuCl_2$/100 $m^2.g^{-1}$ γ-Al_2O_3 surface, which suggest that $CuCl_2$ forms a monolayer covering about 77% of the γ-Al_2O_3 surface [113]. Other authors [114-116] also reported a similar threshold value for $CuCl_2$ to form a monolayer, on around 18-98 % of the surface, depending on the surface area of alumina and drying procedure after impregnation.

4.4 Aspects of the active sites and their reactivity

Summarizing the earlier section, $CuCl_2/\gamma$-Al_2O_3 catalysts have two or more different kind of species: Cu-aluminate, highly dispersed dihydrated $CuCl_2$, and paratacamite (depending on hydration process). Among these three, it has been shown that Cu-aluminate is inert during the oxychlorination of ethylene and paratacamite might be turned into $CuCl_2$/CuCl during the thermal activation process. As quoted in sections 4.1-4.3, it has been shown [17, 25, 74, 78, 80-82, 93, 95, 97, 106, 108, 117, 118] that highly dispersed anhydrous $CuCl_2$ is the active species for the oxychlorination of ethylene. The generally accepted model proposed [48, 56, 57, 79, 84, 101, 113-115, 119] as the active complex involves $Cu^{II}Cl_2$ fixed

to the support via oxygen bridge sites on the Al_2O_3 surface. The nearby hydroxyl groups, oxygen and/or chlorine atoms that anchor the Cu_xCl_y clusters to the Al_2O_3 support, were thought to control the copper's activity. A generally accepted schematic structure model for alumina based copper chloride catalyst is illustrated in Figure 14.

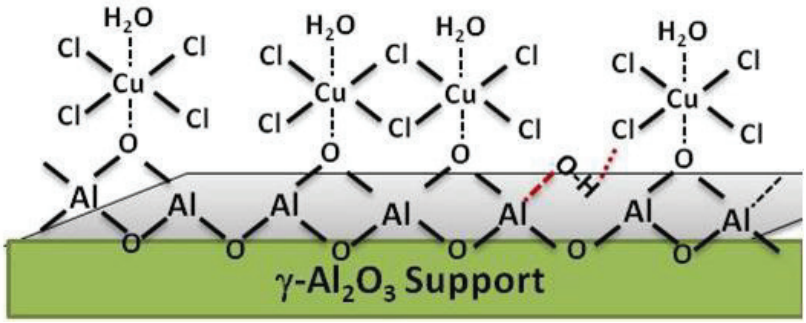

Figure 14 : Model structure of the proposed active Cu_xCl_y phase supported on γ-Al_2O_3 on a freshly prepared catalyst. (Unpublished figure)

4.4.1 Adsorption behaviour of the oxychlorination reactants

Hall *et al* and Xiaohai *et al* [120-122] studied the adsorption of oxychlorination reagents (C_2H_4, HCl and oxygen) on $CuCl_2/\gamma$-Al_2O_3 using gas-adsorption chromatography and surface area measurements (BET - Brunauer, Emmett and Teller). Hall *et al* [121] studied the unsupported $Cu^{(I)}Cl$ and $Cu^{(II)}Cl_2$, and γ-alumina supported $CuCl_2$ systems in the temperature range 298–421 K and measured isosteric heats of adsorption for several surface concentrations. The results obtained on the unsupported $Cu^{(II)}Cl_2$ for the reactants of oxychlorination are reported in Table 3 [150]. It was observed that isosteric heat of adsorption (q_0) at zero coverage (Γ=0) of ethylene is ca.65±5 kJ mol^{-1}, the magnitude suggests a chemisorption. A general trend of decreasing heat with increasing coverage was reported, as expected for a heterogeneous surface. Corresponding q_0 values for O_2 and HCl were 16±3 and 22±4 kJ mol^{-1} respectively. It is clearly indicated that C_2H_4 has the strongest interaction with $CuCl_2$ (unsupported). It was observed that in the presence of a mixture O_2 and HCl, neither of these reagents affected the adsorption of the other (when HCl was not in excess). However, an excess of HCl appeared to decrease the adsorption energy of C_2H_4. Comparing these values with reactants' q_0 values ($q_{0\ C2H4}$ =13 kJ mol^{-1}, $q_{0\ O2}$ = 7 kJ mol^{-1}) on unsupported copper (I)

chloride, it was showed that ethylene and oxygen are only physically adsorbed on CuCl. The adsorption behaviour of HCl was not studied further, owing to its corrosive behaviour. Hall *et al* also reported the adsorption behaviour of the products 1,2-dichloroethane (EDC) and H_2O on these samples. Experimental observations suggested that the EDC ($q_{0\ DCE}$ = 39.75 kJ mol^{-1}) [121] was physically adsorbed and water (similar heat of adsorption to that of ethylene) was more strongly adsorbed on both unsupported $Cu^{(I)}Cl$ and $Cu^{(II)}Cl_2$. However, on unsupported $Cu^{(I)}Cl$ samples, water was physically adsorbed owing to its value $q_{0\ H2O}$ =30±3 kJ mol^{-1} and therefore the Cu^{+}- H_2O interactions are unlikely to be of great importance. More importantly, γ-alumina supported $Cu^{(II)}Cl_2$ showed the same isosteric heat of adsorption (q_0) for ethylene (ca.65±5 kJ mol^{-1}). The same value was obtained for unsupported copper (II) chloride.

Hall and co-workers [93, 121], made another effort to elucidate the importance of presence of small amount of Cu^{+} on the copper surface for adsorption of ethylene. All adsorbents were heated to 523 K for 1h before using them for ethylene adsorption. The authors compared the observed values with the ones measured on pure samples (discussed in earlier paragraph), and concluded that $CuCl_2$ adsorbent contains some Cu^{+} upon heating above 423 K, and that is important for adsorption. The author suggested that, ethylene first physically adsorb on $Cu^{I}Cl$ with the heat of adsorption of 10 kJ mol^{-1} and provide enough time to diffuse on to the preferred chemisorption sites i.e $Cu^{II}Cl_2$ sites with a heat chemisorption of 43 kJ mol^{-1} (< 65 kJ mol^{-1} for pure $CuCl_2$). If oxygen or hydrogen chloride interfered with this Cu^{+}/Cu^{2+} matrix then the adsorption of C_2H_4 could be hindered. Oxygen was not observed to affect adversely the adsorption of C_2H_4, whereas hydrogen chloride when present in excess reduced it. The authors concluded that neither the additives to $CuCl_2$ nor the bonding of $CuCl_2$ to the alumina surface affected the ethylene adsorption mechanism and the interaction strength between copper (II) chloride and ethylene. It was postulated that ethylene adsorbed preferentially on Cu^{2+} rather than Al_2O_3. The Isosteric heats of adsorption of ethylene and other gases on copper chloride based systems were summarised from the available literature [121] and depicted in Table 3.

Table 3 - The Isosteric heat of adsorption (q_0) of ethylene, ethylene* and the other gases on copper-based systems [121]. (* = notation for co-presence of other gases with ethylene in adsorbate mixture).

Adsorbate	isosteric heats of adsorption; q_0 / *kJ/mol* at zero coverage			
	$CuCl_2$	CuCl	KCl+ $CuCl_2$ / γ-Al_2O_3	γ-Al_2O_3
C_2H_4	**65 ± 5**	**13**	65	26
O_2	16 ± 3	7	-	-
HCl	22 ± 4	-	-	-
1,2- $C_2H_4Cl_2$	~40	49	-	-
H_2O	~64	~30	-	-
CO_2	6		-	-
$C_2H_4^*$ (+ O_2)	~55	~69	-	-
$C_2H_4^*$(+ HCl)	~59	~ 58	-	-
$C_2H_4^*$(+ O_2+ HCl)	~58	~67	-	-
$C_2H_4^*$ *($CuCl_2$+CuCl)*	**43**	**10**	-	-

Recently Neurock *et al* [52] examined ethylene chemisorptions on model copper chloride (Cu_xCl_y, $Cu_xCl_y(OH)_z$) and supported copper chloride ($Cu_xCl_y(OH)_z$/γ-Al_2O_3) clusters using spin-polarized gradient corrected density functional theory (DFT). The DFT calculations indicated that hydroxyl ligands at the Cu centre act as trans-directing agents for ethylene adsorption. They increase the binding energy of ethylene if they sit trans- to ethylene; otherwise, they weaken the interaction. The most favourable adsorption site, with its C=C bond oriented perpendicular to the Cu_xCl_y plane with an energy of -79 kJ/mol, is consistent with the value reported by Hall *et al* [121]. The interaction between ethylene and copper (II) follows the classic Dewer-Chatt donation/back-donation model (Figure 15), where an alkene donates electrons from its filled π molecular orbital between the carbon atoms to unoccupied valence *d* orbitals of the metal (in other way metal σ-bonding to C_2H_4 by accepting of its π electrons). While, the metal donates electrons back from a (different) filled *d*-orbital into the empty π^*- antibonding orbital of the adsorbate double bond as illustrated in Figure 15. The π-donation and π^* back-donation tend to reduce the carbon-carbon bond order, leading to an elongated C-C distance. The very important conclusion they postulated was that the alumina support increases the negative charge on the bridging oxygen species, which in turn increases the positive charge on the Cu center. This leads to a stronger interaction with ethylene by 12-20 $kJ.mol^{-1}$. However, this speculation was slightly at odds with Hall *et al*. , the reason might be that Hall treated the $CuCl_2$ system as single entity particle dispersed on

support, however Neurock treated $CuCl_2$ as cluster or complex model. Nevertheless, the phenomenon of ethylene adsorption on Cu^{2+} was a main conclusion from both works.

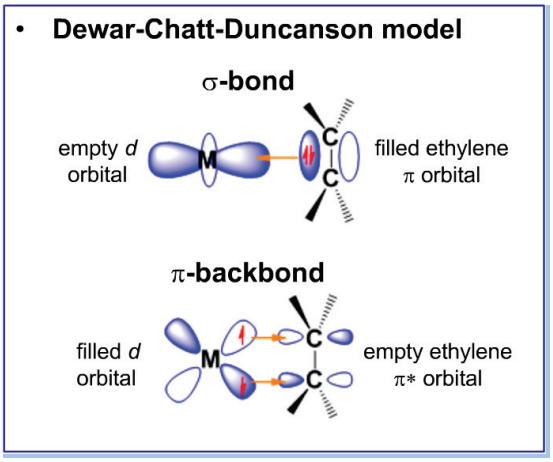

Figure 15 : Schematic representation of ethylene molecular orbital interaction with a transition metal illustrated by Dewar –Chatt –Duncanson model. (Unpublished figure)

To understand the mechanism of adsorption further, Hall and co-workers studied similar adsorbates such as ethane, acetylene, propene, buta-1,3-diene and 1,2-dichloroethane. The results are summarised in Table 3 [121]. The authors found that the importance of the double bond is very high and the conclusion is that a π–bond is essential for chemisorption on $CuCl_2$ based catalysts [123], further the presence of a δ-bond along with π^* back-donation as well is probably an important factor for increased reactivity. Studies have been carried out for a series of chloroalkenes on supported catalysts, with the conclusion that chlorine substitution decreases the strength of the $CuCl_2$- C_2H_4 bond [124]. Finocchio *et al* [114] also confirmed the above finding on the basis of an FTIR study of the oxychlorination reaction on the alumina supported catalyst and postulated the formation of surface copper chloride - ethylene pi-complex intermediates (which lead eventually to form EDC) and weakly adsorbed HCl during oxychlorination.

The adsorption studies performed by Xiaohai and co-workers [122] on γ-alumina-supported catalysts were in agreement with the above conclusions, except in the case of HCl. They reported that HCl strongly adsorbed on copper (II) chloride supported on γ-alumina and the adsorption amount decreased with increasing Cu content. It was postulated by comparing with Hall *et al* works, that adsorption sites for HCl on the catalyst might be the acid sites of γ-

Al_2O_3 support. The adsorption amount of C_2H_4 depended on Cu content, dryness of catalyst, and the adsorption ratio (mol C_2H_4/mol Cu) declined with the increase of Cu content on the catalyst. Several other authors [52, 78, 115, 123, 125-127] are in agreement with the above observations.

4.4.2 Desorption behaviour of oxychlorination reactants and products

Hall and co-workers extended their previous studies [93, 120, 121, 128-130] to desorption of the reactant and product species using temperature programmed desorption (TPD) and gas-adsorption chromatography on γ-alumina supported $CuCl_2$ catalysts. The authors concluded [130] that ethylene has two adsorption sites besides physisorbed site (postulated as Cu^+ site) [121] with activation energies for desorption (E_d) of 60 and 73 kJ mol^{-1} respectively. The former one is consistent with the value (65 kJ mol^{-1}) reported in adsorption experiments. The later high energy could be due to Cu sites at edges, dislocations and other surface defects. The desorption behaviour of O_2 showed that it was physically adsorbed [121]: no peaks were found in TPD. However, the authors did not attempt to study the adsorption or desorption behaviour of HCl, since it attacked the tungsten filament of the detector and was strongly adsorbed on tube walls in the process stream, left with difficulty to draw any firm conclusions on its behaviour. Concerning products, EDC was the only one physically adsorbed and it desorbed readily. Carbon dioxide (CO_2) had a high activation energy (ca 100 $kJ.mol^{-1}$) for desorption when pre-adsorbed on $CuCl_2$ below its sublimation temperature. When dosed at higher temperatures it readily desorbed [130].

4.4.3 Effect of Cu co-ordination number

Newrock *et al* [52] studied the influence of the number and type of ligands around the copper atom on its adsorption strength by DFT modelling. He observed that the coordination number of the cupric ion had a strong influence on the chemisorption of ethylene. It was found that the interaction strength between C=C or C-C or C-Cl or C-H/copper was dependant on the number of ligands [52, 124]. Newrock *et al* [52] observed that the mode and energy of ethylene adsorption are affected by the oxidation state, the coordination number (CN) and the ligand field at the Cu center. The authors reported that the degree of back-donation decreased as the number of ligands increased; this weakens the ethylene/copper interaction. The author concluded that the same trend observed for monomeric, dimeric and trimeric Cu_xCl_y

complexes, while only small perturbations in the chemisorption energies were observed as the size of complex increased from monomer to trimer. The results indicated that the active cupric reaction centres must have at least one vacancy at one of the four square-planar sites in order to chemisorb ethylene, Furthermore, ethylene chemisorption was favoured for "in-plane" sites over the "atop" sites for the square-planar sites. The difference in binding energy between the "atop" and in-plane" sites was a factor of two, which can be evident from the values reported in Figure 16b (in-plane adsorption) and Figure 16c (atop adsorption). The author reported a schematic diagram (Figure 16) illustrating the mode of ethylene chemisorption and energies on dimeric Cu_2Cl_y clusters. It can be seen from the below Figure 16 that ethylene chemisorption energies systematically decreased from -105 kJ/mol for dimeric Cu_2Cl_y cluster with CN= 1 to -18 kJ/mol (physisorption state) for CN=4; and decreased from -120 kJ/mol for monomeric cluster to -8 kJ/mol for trimeric Cu_3Cl_yclusters. From these values, it can be seen that that degree of back-donation decreased as the number of ligands increased, resulting in weak ethylene/cu interaction.

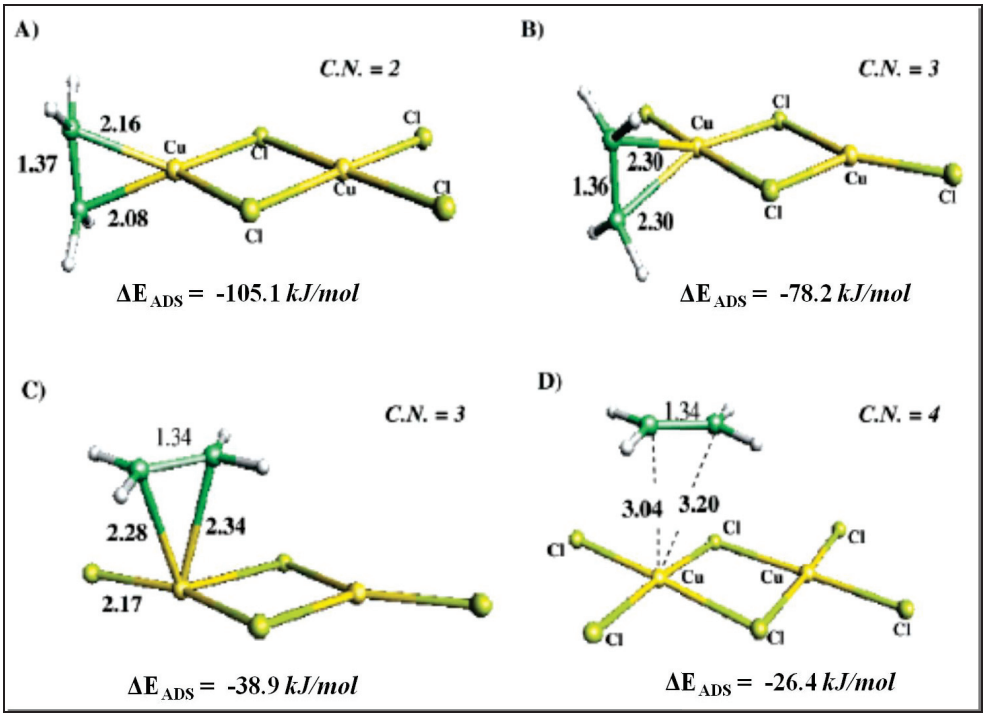

Figure 16 : Ethylene chemisorption energies on dimeric Cu_2Cl_y clusters. Part (A) and (B): Illustrate the effect of coordination number of Cu with Cl-ligands on the ethylene chemisorption energies (in-plane adsorption). Part (C) and (D): Illustrate the effect of coordination number of Cu on the ethylene chemisorption energies (atop adsorption). All the bond lengths are given in angstroms (Å). [52]

4.5 Reaction mechanisms and kinetics

$CuCl_2$ was widely recognized as the active chlorinating agent. However, there were speculation: 1) that the ethylene adsorption site was either $Cu^{(I)}Cl$ or $Cu^{(II)}Cl_2$, and 2) whether the ethene chlorination reaction proceeds according to the ethylene oxychlorination cycle (Eq.s 15-17) or whether it proceeds via gas phase chlorination, where Cl_2 is formed via the Deacon cycle. Nevertheless, it was concluded [48, 78, 79, 81-85, 88, 131] that $Cu(II)Cl_2$ is the active site and the whole reaction follows according to the cycle mentioned in Eq.s 15-17.

It was noticed [93] that ethylene was physically adsorbed on the freshly prepared copper (I) chloride and gave no detectable yield of any product with ethylene in the temperature range 423-523 K. Later, it was reported [48, 78, 79, 81-85, 88, 131] by feeding the three reagents separately that the oxychlorination reaction (Eq. 8) is catalyzed by a highly dispersed $CuCl_2$ species and follows a three- step redox mechanism as discussed in section 4.1.

Ruoco [85] refuted the above-proposed mechanism (Figure 11). The author studied the alumina and silica supported $CuCl_2$ catalysts by using TPR, XPS and EPR techniques to follow up the phase changes in copper chloride during sequential treatments with C_2H_4, air and HCl. He observed that the cycle $CuCl_2$-$CuCl$-Cu_2OCl_2-$CuCl_2$ did not occur with either support because HCl reduced the oxychloride to CuCl (as proposed in Deacon system). Author reported that TPR results showed the reduction of Cu^{II} to Cu^{I} occurred in the region 473-623 K dependent on the support; whereas the reduction of Cu^{I} to Cu^{0} occurred at temperatures higher than 623 K. However, the detailed mechanism of this behaviour was not discussed further.

The studies referred to above were based on ex-situ catalyst characterisation. Later, several in-situ characterisation studies have been published. Loos *et al* [131] [132] reported in-situ EXAFS studies which supported the mechanism described in Figure 11, but the author studied a non-standard catalyst: $CuCl_2$ supported on η- alumina. More recently, Lamberti *et al* [80, 88] provided an in situ, time resolved, XANES study of $CuCl_2/\gamma$-Al_2O_3 in ethylene oxychlorination environment (three reagents were co-fed) in the 373–623 K range. The results/spectra confirmed the presence of three different copper species following the reactions of Eq. (15) - (17). The XAS data, together with the simultaneous measurement of

the catalyst activity, led the authors to propose that $CuCl_2$ is the active site for the ethylene oxychlorination reaction and the rate-determining step is the oxidation of CuCl i.e Eq (16) under the reaction conditions employed. The use of synchrotron radiation facilities thus enabled Lamberti *et al* to confirm the generally accepted reaction mechanism as presented in section 4.1 (Figure 11).

4.5.1 Reaction kinetics

Coming to the detailed kinetics and mechanistic details, extensive studies on methane oxychlorination [6, 13, 20-22, 25, 28, 29, 64-66, 74] gave a starting point for the kinetic studies of ethylene oxychlorination, since the catalytic mechanism are similar. Fontana and co-workers [20] reported experimental evidence that chlorine was evolved from the cupric chloride (Eq.18) and chlorinated methane directly in the gas phase at temperatures of 673-873 K in the methane oxychlorination reaction. Other authors [28, 64] have also suggested that cupric chloride reacted directly with oxygen (Eq19), and produced Cl_2 in the similar temperature range. Allen [6] provided detailed thermo dynamical calculations, which supported the above observation. It was established that oxidation of HCl to Cl_2 by copper chloride catalysts requires temperatures higher than 623 K [20, 22, 64, 66] (well above ethylene oxychlorination temperatures) both thermodynamically and kinetically (Allen 1962, Table 1)[6] as indicated by Eq.(18) – (20).

In most of ethylene oxychlorination studies, a modified Deacon catalyst has been employed. A marked difference between the oxychlorination of ethylene and the Deacon process is the considerably lower reaction temperature (473-573 K) for the former reaction. Other process parameters such as partial pressures of reagents, contacting methods, reactor type can also have a great influence over the kinetics of the reaction. It was found [73] that below 573 K the evolution of free chlorine from the catalysts was almost negligible as compared with the rate of oxychlorination of ethylene, which was further support by XAS studies by Loos *et al*, [132] who did not observe any Cl-Cl peak contributions on the catalysts. In conclusion, there is now general consensus that the ethylene chlorination step proceeds on the catalyst surface, not in the gas phase, in the temperature range 473 – 573 K.

The first kinetic study [133] of the oxychlorination of ethylene was carried out on $CuCl_2/\gamma\text{-}Al_2O_3$ catalyst at 473 - 573 K. The authors observed that the rate of the ethylene conversion (Eq.15) is independent of partial pressure of the ethylene (p_{C2H4}) but does depend

on partial pressures of oxygen (p_{O2}) and also that the reaction is inhibited by 1,2-dichloroethane and HCl. In subsequent investigations, some of these conclusions were refuted. It was found [13, 27, 74, 95, 134] that the overall reaction rate depended in a complex manner on the partial pressures of the ethylene, HCl and oxygen and was described by a power equation of the type used to describe fixed bed reactor studies in the temperature range 473- 573K.

$$r = k\, p_{C2H4}{}^{m}\, p_{HCl}{}^{n}\, p_{O2}{}^{l}\, p_{H2O}{}^{x} \qquad (22)$$

In the presence of a $CuCl_2$-KCl/silica gel catalyst [13, 27, 74] in the region of limited ethylene conversion (<30%), the following parameters for Eq. (21) were reported: m = 0.6, n = 0.2, l = 0.5 and x = 0. For an activated charcoal based catalyst [74] in the temperature range 403-453 K the parameter values are: m = 1, n = 0.2, l = 0 and x = 0. For a $CuCl_2/\gamma$-Al_2O_3 catalyst at 503 K [13, 74], the parameters are: m = 1, n = 0.3, l = 1 and x = 0. In the region of low oxygen pressures with an overall activation energy of 63 kJ/mol were found; when $p_{O2} \geq$ 10 kPa, l = 0 was reported. However, an analogous picture was observed by Carrubba *et al* [134] on an alumina (not specified which type) supported catalyst. The Authors carried out the experiments in a differential fixed bed reactor in the temperature range of 454 – 469 K with limited ethylene conversion (<30%) , and suggested that the rate of reaction depend mainly on p_{C2H4}, p_{O2} and somewhat on p_{H2O}, but it was independent (or at most weakly dependent) on p_{HCl}, following the power law equation:

$$\text{Rate} = 2.49 \times 10^{-6}\, (C_2H_4)^{0.73}\, (O_2)^{0.34}\, (H_2O)^{-0.18} \qquad (23)$$

Increasing partial pressure of HCl decreased the side reactions to the other chlorocarbons; rather different interpretation of the reaction model was made based on the surface reaction of ethylene and oxygen to form an ethylene oxide as intermediate. Eichhron *et al* [96] studied kinetics of γ- alumina supported copper chloride catalysts (with and without of KCl dopant). The experiments were performed in a differential recycle reactor in the temperature range of 473-553K with a gas-hour-space-velocity (GHSV) of 670-4000 $m^3.m^3.h^{-1}$. The kinetics for 1,2-dichloroethane formation and well as for formation of other by-products were derived over a range of partial pressures of the reagents (p_{C2H4} = 0.05-0.25 bar; p_{HCl} = 0.10-0.50 bar and p_{O2} = 0.008-0.08 bar) with the molar composition of the feed was C_2H_4:HCl:O_2 = 1: 2: 0.5. The following kinetic equation was reported for the formation of EDC:

$$\text{rate} = k.\ E^{(-Ea/R\Delta T)}\ p_{C2H4}{}^{0.67} \quad ;\ \Delta T = (1/T+573)-(1/515) \tag{24}$$

Fengqiu *et al* [135] studied the γ-alumina supported catalysts in the temperature range 484-524 K and proposed that reaction proceeds though a coordination-reduction-oxidation catalytic mechanism [95]. They reported an activation energy of 95 kJ/mol with a power – law equation fitted to the observed experimental results for the formation of EDC: $r' = 1.21*10^{9}*e^{(-94671/RT)}$. The reported results and the experimental observations were in agreement with other works [95, 134, 136], that the reaction rate increased with an increase in partial pressures of ethylene and oxygen and was independent of HCl. They further reported that an excess of HCl would inhibit the side reactions including combustion reactions, and the rate was further depend on space velocity. A different rate expression was provided by Benhui *et al* [137] on the similar catalyst for the formation of EDC in the temperature range 483-523K and a pressure of 1.3 atm: $r = 1.21*10^{5}*e^{(-12300/RT)}*p_{C2H4}{}^{1.61}$.

The majority of the kinetic studies [95, 97, 134, 135, 137, 138] on this catalytic system reported analogous results, especially on the reaction rate expression and its dependence on partial pressure of HCl. There is also a general agreement among the published works, that the reaction rate is, to a great extent dependent on partial pressure of ethylene and follows the first-order kinetics.

Later, Wachi *et al* [97] studied the kinetics of oxychlorination of ethylene over $CuCl_2/Al_2O_3$ catalysts in a fixed bed reactor in the temperature range of 423-523 K. The experiments and kinetic studies show that the reaction was first order in the concentration of unreacted cupric chloride and that the dependency on ethylene concentration obeyed Langmuir – Hinshelwood – kinetics. This was in line with the assumptions made by other authors [13, 93, 108]. However, it was firmly shown [80] that the oxychlorination of ethylene proceeds via chlorination of ethylene by cupric chloride (Eq.15), then oxygen and HCl regenerate the copper salt (Eq. 16+17). From the reported experimental data, the rate equation for the earlier step (Eq.15) has the following form:

$$r = k_r\, K_a\, C_{C2H4}\, C_{CuClx} \,/\, (1+ K_a\, C_{C2H4}) \tag{25}$$

Where, $k_r = 269*e^{(-37.8/RT)}$, 1/s and $K_a = 0.63$, m^3/mol.

The authors reported activation energy of *37.8 kJ/mol* for the C_2H_4 chlorination (to EDC) and suggested that it is a fast process with the first-order kinetics. This was in good agreement with the values reported by *Hall et al* (1984) and *Kitamura et al* (1986). Allen and

other authors[13, 135, 139], however, reported a different values in the range of *67 to 125 kJ/mol* but as the over-all activation energies, which may mean that these values are combined activation energy for all three steps (Eq 15- 17). While the equilibrium constant of ethylene adsorption K_a (in Eq.24) is independent of temperature, the activity of the adsorption sites was enhanced by an increase in temperature. Wachi *et al* examined the reaction kinetics for the catalysts with varied amounts of cupric chloride and the reported results were shown in Figure 17. It was found that optimal performance in terms of both the rate constant and the yield of 1,2-dichloroethane was achieved at 5 wt% of copper impregnated on γ- alumina support.

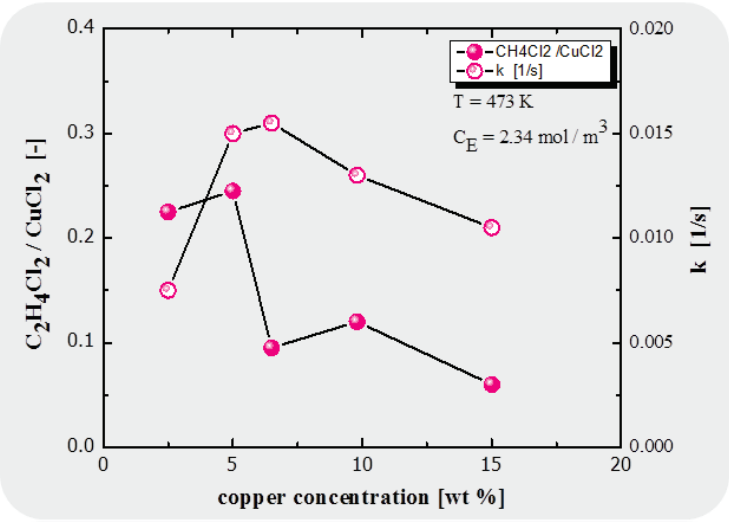

Figure 17 : Effect of copper concentration on the formation of 1,2-dichloro ethane ($C_2H_4Cl_2$). Rate constants, k (1/s) (y-axis on the right hand side), and concentration of $C_2H_4Cl_2/CuCl_2$ (y-axis on the left hand side) plotted vs copper concentration (wt%) on the catalyst surface (x-axis). [97]

Summarizing the above findings, one can conclude that the chlorinating agent is copper (II) chloride, and the rate of the reaction depends largely on the ethylene partial pressure irrespective of conditions applied. It was observed [140] that only 16% of the reaction proceeds by stereo specific trans-addition, while 84% was random. The authors noted that the rate of removal of chlorine from the copper (II) chloride was much less than that of formation of 1,2-dichloroethane. The ethylene chlorination reaction (Eq.15) follows the first-order kinetics [72, 78, 88, 98] with an activation energy of around 35 kJ.mol^{-1} [93] and an over-all activation energy is around 65-125 kJ.mol^{-1} [13, 27, 52, 74, 75, 134] depending on the catalyst compositions and process conditions. The rate dependency on oxygen and hydrogen chloride partial pressures was less clear [73, 74, 95] and discrepancy may be

attributed to their dependence on the employed reaction conditions and measuring routes [95]. There were no clear experimental observations consistent with the hypothesis that adsorption of the ethylene is the rate–determining step. The activity of the catalyst and rate of the reaction were very much dependent on temperature, partial pressures of the reactants, composition of the reaction mixture and of the catalysts.

4.5.2 By-product mechanism

The industrial oxychlorination of ethylene in a fixed bed reactor is usually carried out in the temperature range 453- 573 K. At these temperatures, however, a number of undesirable by-products are formed at rates that are dependent upon various factors such as temperature, the state of the catalyst surface, feed composition, and so on. Literature studies [13, 73, 74, 96, 115] suggested that the subsequent reactions proceed via a series of parallel/consecutive chlorination, dehydrochlorination, hydrodechlorination stages and accompanied by the oxidation of the starting materials to CO and CO_2. These reactions are believed to be catalytic [73, 95, 96, 141-143], since, the non-catalytic (gas-phase) dehalogenation or oxidation reactions of haloalkanes demand high temperatures and have high activation energies [144]. Allen *et al* [6] presented brief thermodynamical calculations and provided the standard Gibbs free energy changes data for the possible side reactions over copper chloride catalysts in the temperature range 450 - 900K.

The product distribution changes as temperature increases from high yields of 1,2-dichloroethane to a mixture of more highly chlorinated hydrocarbons such as vinyl chloride (C_2H_3Cl), 1,1,2-trichloroethane ($C_2H_3Cl_3$), ethylchloride (C_2H_5Cl), trichloroethylene (C_2HCl_3), 1,1-dichloroethane, 1,2-dichloroethylene, carbon tetrachloride (CCl_4), methyl chloride (CH_3Cl), 1,1,2,2-tetrachloroethane ($C_2H_2Cl_4$) and CO_x.

Eichhorn *et al* [96] studied copper chloride catalysts promoted with KCl supported on γ-Al_2O_3 in the temperature range 493-553 K in fixed bed reactor. They observed that at lower temperatures and low HCl conversions, the principal side reaction is the addition of HCl to ethylene to yield ethyl chloride (EC). As the temperature increases, HCl and ethylene conversion increases, but the selectivity of ethyl chloride formation decreased. He observed that the combustion of ethylene to CO and CO_2 become appreciable from 513 K, at the same time perchlorination reactions start to occur, principally the formation of 1,1,2-trichloroethane together with traces of $CHCl_3$, CCl_4 and other breakdown products. They also found that the

concentration of the active component influence the rate of side reactions and their selectivity. From the experimental observations, the authors concluded that the rate of combustion reactions fell and the rate of ethyl chloride formation increased with decrease in the copper levels, however, the rate of formation of 1,1,2-trichloroethane is not dependent on the copper content. They indicated from the experimental observations that the centers on the surface of the support might be responsible for ethyl chloride formation.

Mile *et al* [100] studied isotope labelled 1,2-dichloroethane conversion on copper chloride catalysts supported on alumina in the temperature range 473-623 K using a micro reactor, and reported that the conversion of EDC increased with increase in temperature and decreased with an increase in residence time from 0.2 s to1.0 s. From the experimental observations, the authors concluded that the primary dehydrochlorination reaction of EDC is a first order with a rate constant, $k_{EDC} = 0.168\ s^{-1}$ and an activation energy of 103 kJ/mol at 558 K. From isotope labelled experiments, a primary kinetic isotope ratio $k_{EDC}/k_{deutero\text{-}EDC}$ of 1.87 at 558 K was observed for per deutero 1,2-dichloroethane on the catalyst and suggesting that the C-H bond breaking occurs as the rate determining step.

Feijen *et al* [145] studied the mechanisms of C_2 -chlorinated hydrocarbons conversion on alumina and various metal oxide catalysts using FTIR spectroscopy and micro reactor studies. The FTIR experiments showed that conversion of 1,2-dichloroethane occurs on alumina via HCl elimination to vinyl chloride in the temperature range 423-723 K, attained almost complete conversion at 523 K, besides a small amounts of CO and CO_2. However, no activity in conversion of 1,1,2-trichloroethane was observed on alumina until 623 K, then they observed very little conversion to CO and CO_2 with rapid deactivation in the presence of O_2 and water. Youchang *et al* [95] extended his kinetics studies as discussed in earlier section 4.5.1 on $CuCl_2/\gamma\text{-}Al_2O_3$ base catalysts to evaluate the mechanisms in the by-product formation on the support, as well on the catalyst. They observed that CO_2 formation increased by an increase in the partial pressure of C_2H_4 and observed no activity on the support at 498K [146]. They concluded from the experimental observations that C_2H_4 oxidation to CO_x is a parallel reaction, which was catalyzed by $CuCl_2$, not by alumina. HCl reportedly inhibited this side reaction [95, 100, 115, 146, 147]. Their observations about VCM formation were in agreement with the observation of Feiejn *et al.*

Several other authors [73, 74, 124, 148] also studied the mechanisms in conversion of 1,2-dichloroethane and by-product mechanisms in oxychlorination of ethylene on copper

chloride catalysts and on alumina supports. Their findings were in agreement with Xie, Eichhorn and Feijen's observations. Their common argument is that at the oxychlorination temperature ranges, these side reactions are catalysed by either of the $CuCl_x$, surface acid sites of alumina or both together and their observations were reported in the general schematic diagram shown in Figure 18 below by Schirmerister *et al* [148].

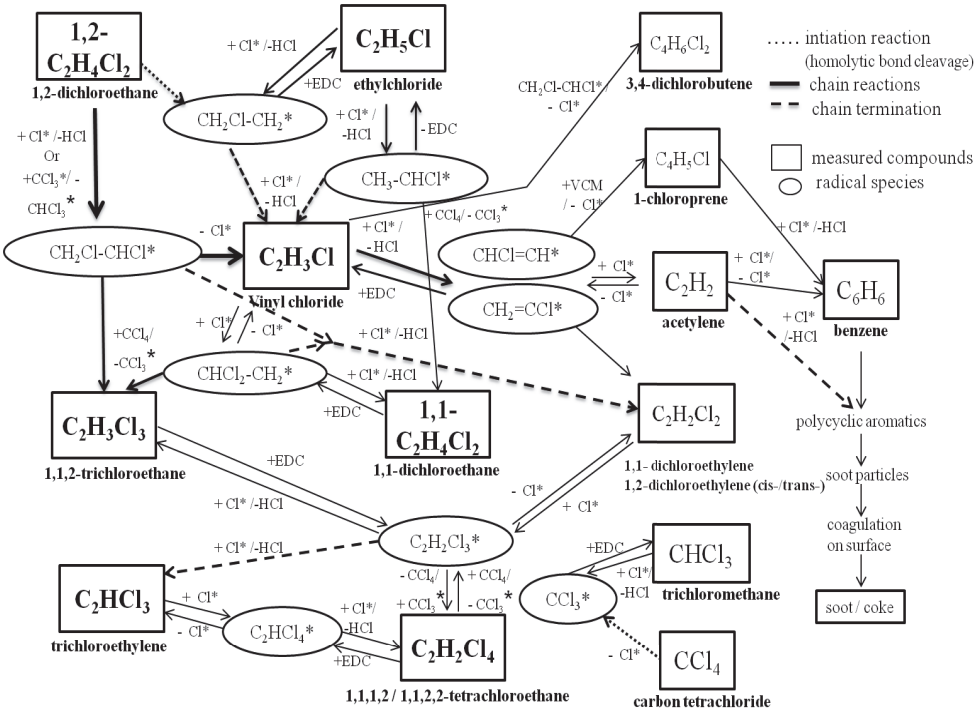

Figure 18: EDC cracking model (measured compounds from large-scale plant with a significant increase or decrease shown in bold) reported by Schirmerister *et al* [148].

However, the specific sites responsible for the side reactions illustrated in Figure 18 are still not clear. Some of the reactions contain more than one path making it a complex task to draw specific conclusions on active sites and mechanistic details. In the oxychlorination of hydrocarbons of the ethane-ethylene series, extensive formation of carbon oxides takes place. It has been reported that introduction of one chlorine atom into ethylene increases the observed CO_x formation rate constant by a factor of 7-8, while further increase in chlorine content in the molecule diminishes the degree of combustion of chloroalkenes [74].

To sum up, although numerous studies have targeted kinetic and mechanistic insight in the ethylene oxychlorination reaction over $CuCl_x$-based catalysts, many possible correlations remain open and have yet to be studied.

4.6 Role of the Dopants / Additives / Promoters

Despite its commercial use, copper chloride on alumina has disadvantages especially in stability, catalyst lifetime, long-term activity and selectivity. In order to address such problems, catalysts were modified with a variety of stabilizers and activators, simply known as "***dopants/additives/promoters***". They are usually oxides or chlorides of alkali metals and rare earth elements. These active ingredients are generally impregnated along with the copper chloride solution or pre impregnated on the porous support.

The most used and studied dopants in oxychlorination are chlorides of potassium (K), lanthanum (La), magnesium (Mg), lithium (Li), and caesium (Cs). Other dopants such as oxides and chlorides of for example: platinum, zirconium, silver, yttrium, cerium, neodymium and praseodymium which favourably influenced the pure Deacon reaction have been tested in a hope that they would influence ethylene oxychlorination in same way [13, 71]. However, the Deacon catalyst was in molten state [20, 22] upon dopants addition, especially potassium chloride (KCl). The catalyst state in low temperature oxychlorination of ethylene, however, is believed to be solid, which means the effect of dopants on catalyst properties will be different.

4.6.1 Influence on the support

Sergio R. de Miguel *et al* [149] studied the influence of alkali metals (Li^+ and K^+) on the Lewis acid sites of gamma-alumina with NMR and IR of adsorbed CO. The authors observed from the surface area measurements that the physical properties such as surface area and pore volume of the alumina are slightly changed by the addition of low alkali metal concentrations. NMR and IR results showed that Li^+ and K^+ adsorbed selectively on tetrahedral Lewis $A1^{3+}$ sites of the alumina surface. These effects on the tetrahedral cations are more marked with increasing molar concentration and ionic radius of the alkali metal added to alumina. Observed NMR results and shifts in the frequency of CO band in IR spectra indicated that the influence of the alkali metals was not only due to steric factors but also to

possible electronic modifications. Wang *et al* [150], who studied La_2O_3 doped γ-alumina using STEM and EXAFS concluded that La atoms anchor the bulk and adsorb strongly on γ-Al_2O_3 surfaces as isolated atoms, strongly pinning the surface and impeding sintering and phase transformation to avoid getting trapped in the bulk of γ-Al_2O_3. Burtin *et al* [151] reported kinetic data on the influence of additives on the surface area and thermal stability of the alumina support using differential thermal analysis (DTA) techniques and measured rate of transformation using X-ray diffraction (XRD) in the temperature range of 373 - 973 K. The author showed that Mg^{2+} acts as an accelerator for the transformation of alumina phase from γ (through ɵ) → α-Alumina, while La^{3+} acts as an inhibitor.

Summarising the above results, Li^+ and K^+ adsorbed selectively on tetrahedral Lewis sites, while La^{3+} adsorbed selectively on octahedral Lewis sites (>Al^{3+}) of the alumina surface. This effect became more pronounced with the increasing concentration and ionic radius of the metal. It is evident that either of the additives (single valence, di-, tri-valence dopants) will have an influence on the physical properties of the γ-Al_2O_3 and their occupied position were also determinable factors, that will be discussed later in the presented results section (paper III).

However, from the available literature (accessible so far), very few authors [27, 73, 152] devoted to the influence of additives on supports in the low temperature ethylene oxychlorination reaction. One exception is Arcoya *et al* [73] who examined the Li- , Na- and K-chloride doped copper catalysts supported on α-Alumina, γ- alumina and SiO_2 for the oxychlorination of ethylene in a fixed bed reactor at 573 K. They reported a substantial increase in ethylene conversion level and selectivity to EDC for the α-Alumina and SiO_2 series, due to the presence of KCl , NaCl and LiCl, while less pronounced effect was observed on γ- alumina. Marsella *et al* [152] studied the K- and Mg-chloride doped catalysts and γ-alumina supports for oxychlorination of ethylene using IR spectroscopy and the results suggested that both dopants efficiently killed most of alumina nucleophilic sites (exposed oxide anions) and observed a reduction in the activity for the dehydrochlorination of 1,2-dichloroethane.

4.6.2 Influence on the base catalyst

Potassium chloride (KCl) is the most commercialised [37, 59, 153-166] and most extensively studied [27, 59, 94, 114, 127, 145] additive for the oxychlorination catalyst

(especially for fixed bed operations). Previous studies on K doped catalyst for methane/ethane oxychlorination [74, 127] showed that doping improved the catalysts performance. The KCl doped catalysts were in molten state and facilitated the release of chlorine from $CuCl_2$ at the reaction temperature. The promoting effect of KCl for the low-temperature oxychlorination of ethylene, where the catalyst should be in solid state, has been subjected to further studies. So far all publications [21, 22, 46, 73, 83, 96, 98, 132] reported that the addition of KCl to the copper chloride catalyst had a positive impact on the process by increasing the efficiency of the catalyst and also decreasing the loss of the copper chloride under reaction conditions.

The introduction of alkali metal chlorides into copper chloride catalysts reduces the melting point of the salt mixture and results in formation of complexes or mixed salts with different chemical compositions [20, 21, 59, 75, 167, 168]– $KCuCl_3$, K_2CuCl_4, K_2CuCl_3 and K_2CuCl_6. The detailed chemistry and thermodynamics behind this phenomenon was discussed in earlier sections 3.1.3 and 3.2. It was even hypothesized that mixed double salt $KCuCl_3$ itself act as the active phase [59] and observed that ethylene burning was reduced on this catalyst by following reduction in CO_x formation. The author proposed that the burning of ethylene might be due to higher levels of free copper on the catalyst, though the author, even in later studies, did not provide a clear mechanism for the reaction.

Many authors reported quite analogous results concerning the activity versus K:Cu ratio. Prasad *et al* [75] reported that addition of KCl resulted in a decrease of ethylene uptake from 50 to 20 µmol/g. cat with K:Cu =0.5. The role of the KCl appears to be as a moderator, it increased the activation energy to 92 kJ/mol from 63 kJ/mol (in case of undoped catalyst) [13, 73] and also reduced the extent of dispersion by forming a double salt. This caused an increase in activation energy presumably due to changes in the reaction mechanism. Garcia and Resaco [84, 169] studied the doped catalyst at 523 K and concluded that undoped catalyst supported on γ-Al_2O_3 was more active than KCl containing one corresponding to K : Cu = 1.

In contrary to Garcia *et al* [84, 169], Rouco [85] studied a $CuCl_2/SiO_2$ catalyst at 498 K, and found that KCl enhanced the redox activity of copper. Arocya [73] studied KCl doped catalyst supported on SiO_2, α-Al_2O_3 and γ-Al_2O_3 at 573 K. A positive effect of KCl on the conversion and selectivity of ethylene was observed on all supports with the following order of improvement: $SiO_2 > \alpha$-$Al_2O_3 > \gamma$-Al_2O_3. The author measured an increase in the weight on both KCl doped and undoped catalysts supported on α-alumina, during the oxidation step (i.e during the Eq.16, step2). He found that the rate of oxidation increased by a factor of "2" upon

addition of KCl, thus suggested that there was a change in the oxychlorination rate-limiting step, from the oxidation of the reduced catalyst to the chlorination of the hydrocarbon, hence, KCl working as an electron promoter. Please note that this observation was made on a α-Al_2O_3 supported catalyst, the author did not report any effect of KCl on rate limiting step in the case of γ-Al_2O_3 supported catalysts. The Author also studied the influence of co-dopants especially cerium (Ce), neodymium (Nd) and praseodymium (Pr) chlorides on the KCl doped catalysts and reported that there was an extra increase in conversion, particularly for the case of Pr, with highest selectivity to 1,2-dichloroethane among other studied catalysts

To summarise the observations [13, 20, 21, 59, 73-75, 84, 85, 167-169] made so far:

- KCl forms a double salt ($KCuCl_3$) with copper chloride and its corresponding amount depends on potassium loading, support and preparation method.
- KCl may act as a promoter at temperature above 525 K and as a de-promoter at lower temperatures; this may depend on the KCl loading.
- The addition of KCl increases the activity and selectivity, but upon high loading, the activity deceases with no effect on selectivity.
- KCl reduces the volatility of CuCl and $CuCl_2$, thereby decreasing the deactivation rate.
- KCl affects the redox properties and it may change the rate-determining step from the oxidation of the catalyst to the chlorination of hydrocarbon.

The second most studied group of dopants are chlorides of rare earth metals, in particular lanthanum chloride $LaCl_3$. $LaCl_3$ is used in fluid–bed processes [161, 165, 170] in order to prevent agglomeration of catalyst particles. It has been suggested that La, because of its strong complex-forming tendency, removes chloride ions from copper chloride system, and increased the volatility of copper chloride. Xueju *et al* [171] studied the $LaCl_3$ doped catalyst for ethane oxychlorination at 498 K in fixed bed reactor, and the results suggested that the $LaCl_3$ acted as a promoter, made copper chloride more highly dispersed and prevented the catalyst effectively from sintering and agglomeration, which was observed by transmission electron microscopy (TEM) measurements. It was observed [71] that $LaCl_3$ promoted the activity of the catalyst (based only on an increase in the pre-exponential frequency factor in the Arrhenius equation), with no effect on the apparent activation energy, since it accelerated the rate-determining step in the undoped catalyst i.e re-oxidation of the Cu(I) species. Rouco [72] studied KCl and $LaCl_3$ co-doped catalysts supported on SiO_2, α-Al_2O_3 and γ-Al_2O_3 for

ethylene oxychlorination in the temperature range 458 - 513 K in a fluidized bed reactor. The reported results were in agreement with the Xueju's observations that were discussed in earlier paragraph. Author also made an effort on mobility studies on these catalysts using a micro reactor. The fraction of each element on the sieved spent particles was determined using acetone extraction method. The results suggested that copper chloride and KCl were mobile under reaction conditions, but not $LaCl_3$ [84] on γ-Al_2O_3 supported catalysts, while, this phenomenon was not observed on either of the supports observed on SiO_2, α-Al_2O_3. It was suggested that both dopants negatively influenced the salt-support interaction in case of γ-Al_2O_3 supported catalysts.

Chen Zhitao *et al* [172] reported that the addition of Ce in the form of $CeCl_3$ to copper chloride catalysts increased the activity by promoting the adsorption of oxygen on the surface. Little *et al* [46] reported that $CeCl_3$ promoter decreased agglomeration of copper chloride species supported on γ-alumina and TiO_2. Chao Li *et al* [173] recently studied the copper chloride based catalyst for ethane oxychlorination promoted by La_2O_3 and CeO_2 and supported on MgO-γ-Al_2O_3. They suggested [174] that a modified alumina support impregnated with La_2O_3 precursor enhanced the dispersion and the interaction strength of copper chloride and CeO_2 on the support. All of these authors observed that addition of Ce increased the activity of the catalyst. The promotional effects may originate from the surface capping oxygen species; these species further accelerate the oxidation of Cu^+ to Cu^{2+}, which was assumed as the rate- determining step in the Deacon process and the ethylene oxychlorination processes (see section 4.5.1). However, the deactivation of the catalyst is rapid compared to the undoped catalyst due to formation of inert phase $CeAlO_3$ and CeOCl. These also promoted side reactions.

There are patents on commercialised catalysts [155, 156, 159, 160, 162, 163, 165, 166] that mentioned other dopants such as $MgCl_2$, LiCl or CsCl, alone or mixed with KCl. However, the characteristics of the respective dopant's influence appeared to depend more on the preparation method, the support they used and temperature studied.

4.6.3 Influence of Ternary mixtures

Several patents [37, 160, 170, 175-179] reported the use of ternary or binary mixture of copper with other chlorides of Lithium, calcium, rubidium, caesium, magnesium, sodium, and potassium for oxychlorination of ethylene in fluidized bed reactors. All the above patents

suggested that ethylene and HCl conversions were greatly influenced by the addition of these dopant chlorides. The active phase is thought to be composed of binary and ternary mixtures of these mixed chlorides along with cupric chloride. Reported observations covered the existence of the binary mixtures of K + Cu, Cs + Cu and also the ternary mixtures of Cu + Mg + Li chlorides; Cu + Na + Mg chlorides; Cu + K + Mg chlorides on the oxychlorination catalyst, though no experimental evidence was provided to support their existence.

US patent 3624170 [179] reported the formation of a ternary mixture based on Cu + Na + Mg chlorides. Such catalysts seem to prevent the deactivation which could be caused by contamination due to FeCl3. EP-A-0255156 [178] also reported a ternary system based on Cu + Mg + Na or Li chlorides. Such systems are reported to achieve high EDC yields in fluidized bed operations, simultaneously reducing reactor corrosion, sticking and clumping of the catalyst particles. This patent suggested that the Na containing systems are more corrosive than Li containing systems. US 4849393 [177] also reported a ternary system composed of copper chloride with KCl or LiCl and $MgCl_2$. They reported > 99 % selectivity and > 98.6 % HCl conversion, high ethylene efficiency and low stickiness.

4.6.4 Summary of the dopant's effect

Most of the literature studies and patents [13, 27, 37, 46, 72-75, 83, 96, 127, 154, 155, 157, 158, 166, 170, 172-174, 180-182] agree that the addition of dopant meal chlorides influenced positively on the stability and the efficiency of the copper chloride based catalysts for the oxychlorination of ethylene. Different dopants had different effects on the activity, selectivity and thermal stability of the catalyst. Most of the dopants (K, Cs, Li) interacted with copper chloride and formed binary or ternary mixtures. In a summary, from the available literature data:

(i) KCl, enhanced the stability and the selectivity of catalysts.

(ii) $LaCl_3$, enhanced the dispersion on the catalysts, thereby, activity.

(iii) $MgCl_2$, increased the catalysts effectiveness on activity and fluidization capacity, thus suitable for fluid bed reactors.

(iv) Other dopants influences were in-between of those reported in (i)- (iii): LiCl had a moderate effect on activity and selectivity, CsCl had great effect on stabilising, but not on the activity, $CeCl_3$ influence seemed to be moderate as well.

However, the mechanisms behind the dopant's influence on metal supported catalysts are still unclear, thus needs further investigation. This is motivating not only for the oxychlorination process, but for other processes as well.

4.7 Starting point for thesis work

It is clear from the above review that many aspects of the oxy chlorination mechanism and oxychlorination catalysts are not fully understood at a molecular level.

In the present study, our aim was to progress further in the molecular understanding of the $CuCl_x/\gamma\text{-}Al_2O_3$ and doped catalyst systems for ethylene oxychlorination reaction. In particular, the effect of promoters was targeted. Our aim was quite ambitious because the effect of additives is potentially extremely complex, and can be summarized in the following five main points:

(i) Additive cations can compete with Cu^{2+} cations in the saturation of cationic vacancies at the alumina surface, thus altering the fraction of Cu^{2+} cations present in the active phase compared to that established for the bare $CuCl_2/\gamma\text{-}Al_2O_3$ system.

(ii) Additive cations can modify the Cu dispersion, favouring or inhibiting the clustering of the particles of the active phase on the support.

(iii) Additive cations can modify the acidity of the support, which are of both Lewis (surface Al^{3+} species) and Brønsted (surface Al–OH species) nature.

(iv) $CuCl_2$ could form a mixed chloride with the chloride of the corresponding additive cation, thus modifying (on the chemical ground) the active phase of the catalyst.

(v) Considering all the above- mentioned influences, hence thereby, result in an overall influence on the catalytic activity, selectivity and thus on kinetics and mechanisms involved.

In order to study and understand the above-mentioned possible phenomena and their influence on the efficiency of the catalyst, a "multi-technique characterization" strategy has been adopted as illustrated in Figure 19.

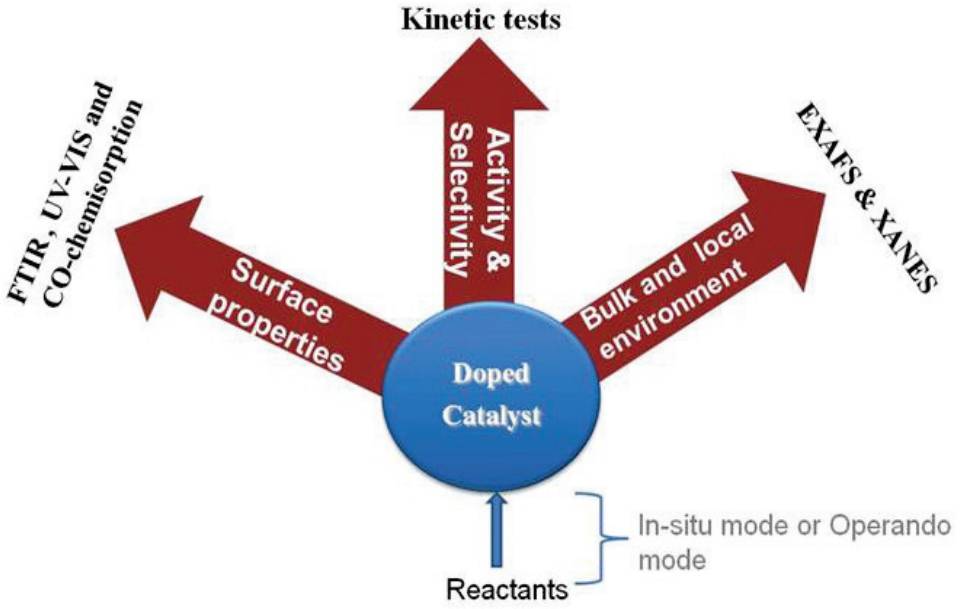

Figure 19: Illustration of the proposed **"multi - technique characterization"** approach used to study the catalyst both as prepared and during reaction.

As a final comment, it is important not only to give qualitative information on the catalyst characteristics but also quantitative information on the prospects of the proposed catalytic system for large-scale operations.

Chapter 5

Material Synthesis & Experimental methods

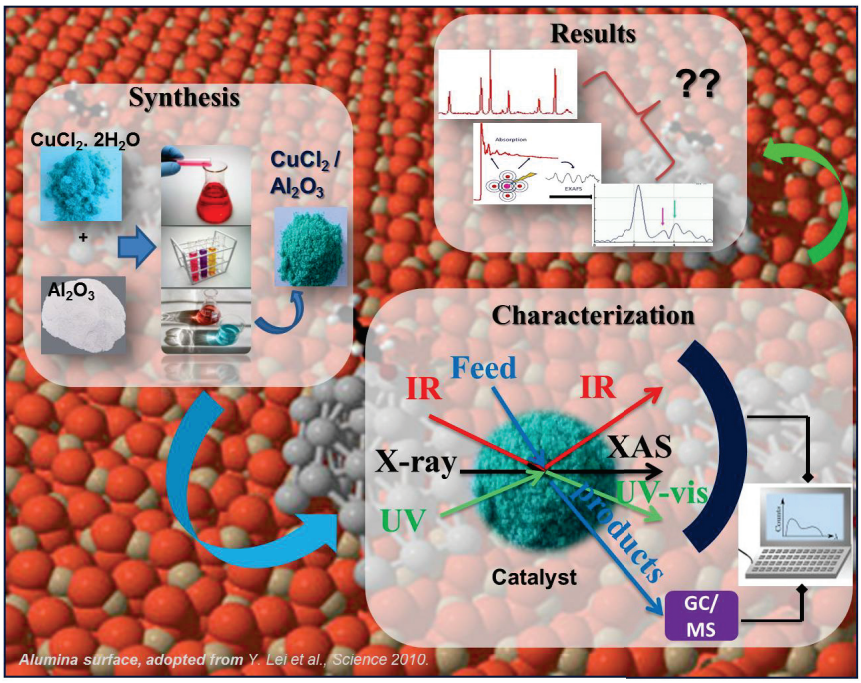

5.1 Catalyst preparation

All samples have been prepared by impregnation of a γ-alumina (Condea Puralox SCCa 30/170, surface area: 168 m^2g^{-1}, pore volume: 0.50 cm^3g^{-1}) with the aqueous solution of the corresponding chlorides following the incipient wetness impregnation method. After impregnation, the samples were dried at 373 K under the air flow for 3 h and then kept at RT. Owing to its air sensitiveness as discussed in earlier section 4.3; all samples were stored in airtight containers. Regarding the nomenclature, samples were labelled according to weight (wt%) content of the different metals (Cu and additive). As an example, sample Cu5.0 represents a 5.0 wt% Cu loaded sample without additives, while sample K3.6Cu5.0 represents a catalyst prepared with 5.0 wt% Cu plus 3.6 wt% K co-impregnated. In all catalysts used for the present studies the amount of copper has been fixed to 5 wt%, while for the doped samples, an atomic ratio of Cu to dopant metal equal to 1 : 1 has been adopted, resulting to K3.6Cu5.0, Mg1.9Cu5.0, Cs10.4Cu5.0, Li0.5Cu5.0, La10.9Cu5.0, Ce11.0Cu5.0, Ce5.5La5.45Cu5.0 and K1.55La5.45Cu5.0 catalysts. While, in the catalysts used for catalytic tests in pulse reactor the amount of copper was always 5 wt% but the atomic ratio of Cu to dopant metal was equal to 2:1, resulting in K1.55Cu5.0, Mg0.95Cu5.0, Li0.26Cu5.0 and Cs5.21Cu5.0 samples.

Another set of chlorinated γ-alumina samples have been prepared by impregnating the γ-Al_2O_3 support with aqueous solution of HCl following the incipient wetness method with 1.4 and 2.8 Cl wt%, here after the samples were labelled as Cl1.4 and Cl2.8 respectively. The higher concentration (2.8 wt%) corresponding to the amount of Cl^- ions available for the Cu5.0 sample. The combined effect of dopant cations (M^+) and Cl^- anions on the support has been investigated by preparing samples, again with the incipient wetness method on γ-alumina, with LiCl, KCl, CsCl, $MgCl_2$, $CaCl_2$, and $LaCl_3$ chlorides characterized by the same dopant atomic concentration used for the preparation of the catalysts (D^{n+}:Cu^{2+} = 1:1). Such samples were be labelled in the following as Li0.5, K3.1, Cs10.4, Mg1.9, Ca3.2, La10.9 and K1.55La5.45, with obvious nomenclature.

5.2 Characterisation Methods

5.2.1 Fourier Transform Infrared (FTIR) Spectroscopy

Infrared (IR) spectroscopy undoubtedly represents one of the most important tools in characterization of the surface species on the oxychlorination catalyst [183, 184]. IR spectroscopy is used here to investigate the influence of dopants on the nature, population and strength of the acid sites on the support, as well as on the active copper species.

Simply speaking, an IR spectrum measures the fraction of photos absorbed by the sample as a function of the wavenumber in the MID-IR region (typically 800–4000 cm^{-1} range). The absorptions occur at well-defined wavenumbers that corresponds to the transition from the fundamental to the first excited vibrational state of the chemical groups present in the sample that can so be detected. The fundamental requirement for infrared activity, leading to absorption of infrared radiation, is a change in dipole moment of the molecule during its vibrational transitions within the molecule. As an example, when IR light is hit on the alumina surface, >OH groups on the surface are active for IR adsorption and rise their vibrational bands in the stretching region of ν(O-H) i.e 3750-3600 cm^{-1} range able to provide information about their presence, nature and population.

In addition, the technique can be more informative and identify the surface accessible species (which are not active to IR, or which are not directly detected as result of absorption in the far-IR region). This occurs by dosing on the sample an ad hoc chosen probe molecules (like e.g. CO, CO_2, NO, NH_3, pyridine and so on), and by analyzing the vibrational region of probe molecule. The perturbations undergone by the vibrational modes of the probe upon adsorption are informative on the adsorption site [183, 185, 186]. In present work CO was used owing to its advantages: 1) it is very simple molecule with only one vibration (at 2143 cm^{-1} for the unperturbed molecule), ii) it interacts with most surface sites with well measurable shift of the vibrational frequency and iii) it has been used since long time and its interaction with different surfaces are rather known.

The interaction between CO and surface sites can be separated into an electrostatic, a covalent σ-dative and a π-back donation contributions, the first two causing a blue shift of the ν(CO), while the last causes a red shift [187-190], with respect to the unperturbed molecule: $\nu_0(CO)$ = 2143 cm^{-1}. CO interacts strongly with Brønsted acid sites, Lewis acid sites of the alumina surface and with the Cu^+ acid sites on the catalyst surface. Thus, the molecular

approach of using CO as probe to investigate the surface of the catalyst support can be highly informative on the species formed, or covered, or leaving the surface during the catalyst preparation steps represented by the impregnation of the active phase or the dopant phase and the thermal activation.

FTIR spectra measurements performed at University of Turin, Italy. The spectra have been recorded at 2 cm^{-1} resolution on a BRUKER FTIR 66 spectrometer equipped with a mercury cadmium telluride (MCT) cryo detector. For FTIR measurements, performed at liquid nitrogen temperature (Publication IV) as well as at room temperature (Publication I & II), a thin self-supporting wafer of the catalyst has been prepared and activated under dynamic vacuum at 503 K for 1 h inside an IR cell designed to allow in situ temperature treatments, reagents dosage and evacuation, and CO dosage. For the experiments presented in publications II, and I before CO dosage, the sample was reduced in ethylene at 503 K and then cooled down to RT. More precisely, once the catalyst has been activated *in vacuum* at 503 K, a C_2H_4-equilibrium pressure of 200 Torr Torr (1 Torr = 133.3 Pa) has been dosed on the sample. The ethylene/catalyst interaction was kept under static condition for 5 min, $C_2H_4Cl_2$ products and unreacted C_2H_4 molecules were evacuated down to 10^{-3} Torr and a second dose of 200 Torr of C_2H_4 was send with the same procedure. After 5 min of contact the pressure inside the cell was decreased down to 10^{-3} Torr, the sample was cooled down to RT.

In all the presented set of experiments, a CO equilibrium pressure of P_{CO} = 40 is dosed, representing the maximum surface covering; successive expansions down to $P_{CO} = 10^{-3}$ Torr are then performed to investigate the lower coverage. This allows us to discriminate among species characterized by different adsorption enthalpies. All spectra reported in the present work were background subtracted, using the spectrum obtained before CO dosage as background. The intensity of the reported spectra has been normalized by the pellet weight.

5.2.2 X-ray Absorption Spectroscopy (XAS)

The aim of this section is to provide the reader with a concise review of the basic physical principles on which the interpretation XAS data is based. For a more detailed description of the theoretical background and experimental aspects of XAS, the reader was advised to refer the extensive specialized literature (e.g. [191-196]).

XAS theoretical background. XAS measures the variations of the X-ray absorption coefficient μ as a function of the incident X-ray energy E. According to the Fermi Golden Rule, the XAS signal is proportional to the electron transition probability from the core-state |i> of energy E_i to the unoccupied state |f> of energy E_f, as expressed by Eq. (26), where the product $\mathbf{e}\cdot\mathbf{r}$ indicates the electronic transition dipole operator[197], where $\rho_{i\ (occ)}$ and $\rho_{f\ (unocc)}$ are the densities of initial occupied and final unoccupied states, respectively, and where $\delta(E_f - E_i - E)$ is a Dirac delta function [197].

$$\mu(E) \propto |< i|\mathbf{e}\cdot\mathbf{r}|f >|^2 \delta(E_f - E_i - E)\rho_i(occ)\rho_f(unocc) \qquad (26)$$

The behavior of the $\mu(E)$ function is represented in Figure 20b. A general decrease of the absorption with increasing incident energy can be noticed, following approximately the law:

$$\mu(E)/\rho \approx Z^4/AE^3, \qquad (27)$$

where ρ is the sample density, Z the atomic number and A the atomic mass. This equation holds for a sample containing a unique chemical species like a metal foil, but can be easily generalized for any sample of known composition. In Figure 20b also evident is the presence of the characteristic saw-tooth like edges, whose energy position is a distinctive features of each kind of absorbing atom. These absorption edges correspond to transitions where a core-orbital electron is excited to (i) the free continuum (i.e. when the incident energy is above the ionization energy of the absorber atom) or (ii) unoccupied bond states lying just below the ionization energy. The nomenclature adopted for the edges recalls the atomic orbital from which the electron is extracted, as shown in Figure 20a: K-edges are related to transitions from orbitals with the principal quantum number n = 1 ($1s_{1/2}$), L-edges refers to electron from the n = 2 orbitals (L_I to $2s_{1/2}$, L_{II} to $2p_{1/2}$, and L_{III} to $2p_{3/2}$orbital), and so on for M, N, … edges.

When the energy of the X-ray photon exceeds the ionization limit (case (i) mentioned above), the excited electron (generally named "photoelectron") has a kinetic energy E_K given by $E_K = h\upsilon - E_B$, where E_B indicates the electron binding energy, that is typical of the absorption edge (K, L_I, L_{II} or L_{III}) of the selected atomic species [196]. Once ejected, the photoelectron propagates thorough the sample as a spherical wave diffusing from the absorber atom, with a wave vector of modulus k defined by Eq.(28) [196]:

$$k = \frac{2\pi}{\hbar}\sqrt{2m_e E_K} \tag{28}$$

A close zoom on the energy region in proximity of an absorption edge shows a well-defined fine-structure. In particular, only when the absorber is surrounded by neighboring atoms (molecules or crystals) a structure of oscillatory nature modulates the smooth *μ(E)* profile at energies above the edge. Figure 20c provides an example for a Cr containing material. Such modulation in the absorption coefficient derives from the interference between the outgoing photoelectron wave diffusing from the absorber and the wavefronts back-scattered by the neighboring atoms [198]. In a typical XAS experiment, the energy range probed around the edge is conventionally divided into two different regions (Figure 20c):

(i) X-Ray Absorption Near Edge Structure (XANES) region: portions of the XAS spectrum just below and above the edge energy;

(ii) Extended X-ray Absorption Fine Structure (EXAFS) region: portion at higher energies in respect to the edge (from tens to hundreds of eV), characterized by the oscillatory modulation in the absorption coefficient.

Hereby, we will briefly discuss the main information that can be extracted from the analysis of each of the two regions listed above.

The XANES region. XANES spectroscopies promote into unoccupied states core electrons. According to the Fermi Golden rule, see Eq. (26), K- and L_1-edge XANES, promoting an *s*-electron, probes mainly unoccupied *p* states. Consequently, L_2- and L_3-edge XANES, promoting a *p*-electron, probe mainly unoccupied *s* and *d* states. So, the XANES part of the XAS spectrum reflects the unoccupied electronic levels of the selected atomic species. The investigation of these levels provides information on oxidation and coordination state of the absorber atom.

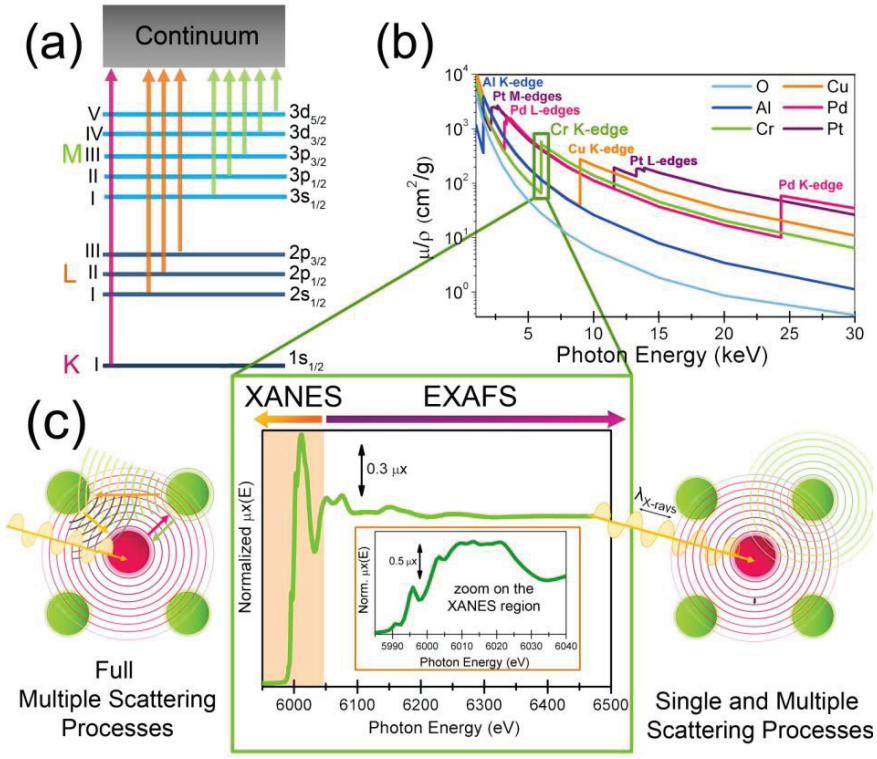

Figure 20: Part (a): X-ray absorption edges nomenclature and representation of their relation with the atomic orbitals from which the electron is excited. Part (b): General behaviour of the X-ray absorption coefficient μ/ρ, see Eq. (27), as a function of the incident X-ray energy E for O (Z = 8), typically contained in MOFs organic ligands, and for some selected metals present in the MOFs cornerstones, i.e.Al (Z = 13), Cr (Z = 24), Cu (Z = 29), Pd (Z=46), and Pt (Z=78). Data obtained from NIST web site http://physics.nist.gov/PhysRefData/XrayMassCoef/tab3.html. Part (c): Cr K-edge XAFS of activated $Cr_3(BTC)_2$ MOF [199] (data collected at BM01B beamline of the ESRF). The conventional division between XANES and EXAFS region and the schematic models of full multiple and single scattering processes, dominating respectively the XANES and EXAFS region, are indicated (color code: absorber atom in magenta; neighbor atoms that back-scatter the photoelectron wave outgoing from the absorber in green). (Unpublished figure)

The EXAFS region. The EXAFS region of the spectrum is located at higher energies and is characterized by the modulation of the absorption coefficient $\mu(E)$. Such feature is caused by the interference between the X-ray waves diffused by the absorber atom and back-scattered by its neighbors. Hence, EXAFS oscillations can be related via Fourier transform to a specific spatial arrangement of the atoms in the local environment of the absorber, bridging the energy space to the real distances r-space.

The higher photoelectron kinetic energy in the EXAFS region implies that the phenomenon is no more dominated by the full multiple scattering regime, that instead

dominate in the XANES region [200]; consequently data analysis can be performed using the simpler Fourier transform operation[198].

The EXAFS signal χ(E) is generally expressed as the oscillatory part of the $\mu(E)$ function, normalized to the edge-jump, i.e. $\chi(E) = [\mu(E) - \mu_0(E)]/\Delta\mu_0(E)$, where $\mu_0(E)$ is the atomic-like background absorption and $\Delta\mu_0(E)$ the normalization factor. Above the absorption edge, the energy E can be substituted with the photoelectron wave-vector k using Eq.(28), therefore obtaining the EXAFS function $\chi(k)$. The relation between the modulation of the $\chi(k)$ signal and the structural parameters is provided by the EXAFS formula that, in the single scattering approximation, is reported in Eq. (29).

$$\chi(k) = S_0^2 \sum_i N_i F_i(k) e^{-2\sigma_i^2 k^2} e^{-\frac{2r_i}{\lambda(k)}} \frac{\sin\left[2kr_i + 2\delta_l(k) + \theta_i(k)\right]}{kr_i^2} \qquad (29)$$

S_0^2 is the overall amplitude reduction factor; the index i runs over all the different shells of neighboring atoms around the absorber, $F_i(k)$ is the back-scattering amplitude as a function of k for each shell, in N_i is the coordination number (number of equivalent scatterers), σ_i is the Debye-Waller factor accounting for thermal and static disorder. The parameter r_i indicates the interatomic distance of the i-th shell from the central absorber. The phase shift of the photoelectron is distinguished in two contributions, related to the absorber ($2\delta_l$) and to the scatterer (θ_i).

In Eq. (29) the electron back-scattering amplitude $F_i(k)$ is measured in Å [197], because the cross section, that's is an area, is the modulus squared of the back-scattering amplitude. As it is the case for XRD, EXAFS will be less efficient in the detection of low Z neighbors and the discrimination among neighbors having similar Z will be critical. When the difference in Z is sufficiently large, then both back-scattering amplitude $F_i(k)$ and phase shift functions are markedly different to allow an easy discrimination between the different neighbors.

The term $\lambda(k)$ is the energy-dependent photoelectron mean free path, typically few Å, determining the local nature of the technique that can investigate only up to ≈ 5–8 Å around the photo-excited atom. The standard EXAFS formula, Eq. (29), provides a convenient parameterization for fitting the local atomic structure around the absorbing atom to the experimental EXAFS data [197]. The dependence of the oscillatory structure of the EXAFS signal on interatomic distance and energy is clearly reflected in the $\sin(2kr_i)$ term. The

strength of the interfering waves depends on the type and number of neighboring atoms through the backscattering amplitude $F_i(k)$ and the coordination number N_i, and hence is primarily responsible of the magnitude of the EXAFS signal. Once the phase and amplitude functions have been independently measured on model compounds or *ab initio* computed, the structural parameters N_i, r_i, and σ^2_i, can be determined in a least square approach where the difference between the experimental and the modeled $k^n\chi(k_j)$ function is minimized along all the sampled experimental points k_j. The minimization routine can be done either in *k*-space, directly on the measured $k^n\chi(k_j)$ function, or in *r*-space, working on the Fourier-transformed functions. So, for each coordination shell, the coordination number, the atomic distance and the thermal factor can be extracted from an accurate EXAFS study.

Since, oxychlorination is a red-ox reaction, thus the key factors influence the reaction: are the relative fraction of copper with different oxidation states, their local geometry and structures, of course by careful analysis and using reliable reference materials. Besides, addition of the dopant may influence on some of these factors. So, valuable information (on both qualitative and quantitative grounds) on these microscopic factors can be obtained from the XAS experiments. Therefore, a great emphasize was given to the XAS spectroscopy in this thesis. Below, detailed experimental procedures and adopted methods were given.

Operando XANES (Publication I & Publication IV): Time resolved X-ray absorption near edge spectroscopy (XANES) in operando conditions have been performed in transmission mode at the ID24 dispersive EXAFS beamline [80] of the ESRF facility by the Carlo Lamberti's group. For each experiment, the dispersive set-up allows the collection of a large number of XANES spectra. The experiments have been performed by feeding a cell [80] containing a self-supported thin pellet of the catalyst with a diluted mixture of the three reagents (C_2H_4 : HCl :O_2:N_2 = 100 : 36.1 : 7.6 : 180), representative of the fixed bed process. In the course of the experiment, the temperature was increased from 373 to 623 K, was kept constant at 623 K for 10 min, and then decreased again to 373 K. In both ramps, a heating (cooling) speed of 12 K min^{-1} has been adopted, while each XANES spectrum has been obtained by integrating for 30 s. Both values resulted in a good compromise between signal/noise ratio of the spectra and temperature resolution of the experiment: one spectrum each 6 K. The gas output was analyzed by a Balzers Quadstar 422 quadrupole mass spectrometer. Details on the X-ray absorption cell allowing measurements in operando conditions to be made have been reported elsewhere [80].

In situ X-ray Absorption Spectroscopy (Publication II & IV): X-ray absorption measurements were carried out using synchrotron radiation of the EXAFS13 station at LURE (Orsay, France) by Carlo Lamberti's group. Both Extended X-ray absorption fine structure (EXAFS) and X-ray absorption near edge spectroscopy (XANES) measurements were carried out in transmission mode using air filled ionization chambers for both incident and transmitted beams, the pressure inside the second ionization chamber was ad hoc optimized for each sample. The beam was monochromatized using a Si(111) or a Si(331) channel-cut monochromator for EXAFS and XANES spectra respectively. Four EXAFS spectra have been collected in the same experimental conditions with a sampling step of 2.0 eV/point and an integration time of 2 s/point. A single XANES spectrum was acquired for each sample, with a sampling step of 0.5 eV/point and an integration time of 2 s/point. EXAFS data analysis has been performed using the Artemis software [201]. Catalyst preparation for *in situ* X-ray absorption experiments has been performed by introducing a self-supported pellet of the sample with optimized thickness inside an ad hoc conceived cell [202]allowing activation *in vacuum* at the desired temperature (503 K) and successive interaction with C_2H_4, again at 503 K, performed as described for IR spectroscopy of adsorbed CO.

Operando X-ray Absorption Spectroscopy (Preliminary report): Operando X-ray absorption measurements were carried out using synchrotron radiation of the BM01B station at ESRF facility (Grenoble, France). Both Extended X-ray absorption fine structure (EXAFS) and X-ray absorption near edge spectroscopy (XANES) measurements were carried out in transmission mode, for Cu K (8979 eV), using air-filled ionization chambers for both incident and transmitted beams. The beam was monochromatized using a water –cooled monochromator equipped with a double-crystal (a flat Si(111) pair) for both EXAFS and XANES spectra.

The same experimental set up has been used as explained in section 5.3.2, except by replacing the quartz reactor with an insitu-cell [80] equipped with provision to hold the self-supported thin pellet of the catalyst and continuous feeding of the reaction mixture. In these present experiments, feed and effluent gas composition was analysed with an on-line Quadruple Mass Spectrometer (MS). The gas stream passed through a water bath and was further diluted with Ar before reaching the MS, in order to keep the HCl concentration below 2 %. The experiments have been performed in the temperature range 293-563 K with variable feed mixture concentrations reagents (C_2H_4: HCl : O_2: He = 1: 2: 0.6: 16.4 and 1: 0.38: 0.08:

11.04 molar ratio). Quick XANES spectra have been collected with a sampling step of 0.2 eV/point over the 8900-9500 eV energy range in an overall integration time of 300 s per spectra. Once the catalyst reached the steady state under the same reaction mixture at constant temperature, four EXAFS spectra have been collected under the He gas purging with a sampling step of 0.2 eV/point over the 8700 – 10400 eV energy range in an integration time of 200 ms/point. XANES data analysis has been performed using the Athena software [201]. The detailed experimental procedure was explained in the preliminary report provided in the chapter 6.

5.2.3 UV- Vis-NIR Spectroscopy

UV-Vis-NIR spectra have been performed in diffuse reflectance mode on a Cary 5 spectrophotometer equipped with a reflectance sphere, available at the University of Turin. The UV-Vis technique had been used due to its high sensitivity towards d-d transitions and charge transitions. It has been suggested that the oxychlorination catalyst contains more than one type of copper chloride phases. UV-Vis in diffuse reflectance mode can selectively identify Cu(II) ions in octahedral complexes, due to its characteristic d–d $^2E_g \rightarrow {}^2T_{2g}$ transitions. Hence, UV-Vis technique can distinguish between these different types of copper species and their structural geometry, especially Cu(II) compounds vs paratacamite or other mixed compounds. Before UV-Vis-NIR experiments, samples were activated under a dynamic vacuum at 500 K for 2 h.

5.2.4 CO – Chemisorption

Static-volumetric CO adsorption measurements were acquired on a Micromeritics ASAP 2010C device equipped with a turbo molecular pump. Experiments were performed by Andrea Marsella's group at European Vinyls Corporation, Inovyl technology centre, Porto Marghera (Italy). CO was chosen as the best probe molecule to calculate the number of sites, their dispersion and surface area of the dispersed species. Because, CO adsorb strongly with only Cu^+ sites, characterized by an adsorption enthalpy in the 120 kJ $mol^{-1} < \Delta H_{ads} <$ 80 kJ mol^{-1} range [184]. This fact justify the use of CO as a probe molecule to detect the number of surface Cu(I) sites by usual static volumetric adsorption measurements. Since, the fresh

catalysts will contain mostly $Cu(II)Cl_2$ sites, all the catalysts were reduced to Cu(I)Cl sites by interaction with ethylene. Thus, CO can act as the excellent probe molecule for the objective of this work. All the treatments, including adsorption were performed with sufficient time to reach equilibrium. The pre-treatment consisted in an evacuation at 308 K for 5 min, an evacuation at 503K for 0.5 h, five cycles of reduction with ethylene at 200 Torr at 503K for 15 min followed by evacuation at the same temperature for 15 min and, at last, an evacuation at 308 K for 30 min. The adsorption measurements were made with CO at 308 K. They consisted of the determination of the isotherms in the 10^{-4}–600 Torr range (about 20 min per point). The volume of adsorbed CO correspondent to the full coverage has been evaluated by linearizing the adsorption isotherm with the Langmuir equation in the 100–600 Torr range. The knowledge of *V*m allows to calculate the number of Cu(I) ions exposed to the surface (Cu(I)s). Further, the dispersion (D) and the surface area of dispersed CuCl (S_{CuCl}) are estimated by using Eqs (30):

$$D = Cu(I)_s / Cu(I)_{total} \text{ and } S_{CuCl} = Cu(I)_s * a_{CuCl}, \quad (30)$$

where a_{CuCl} (11.64 $Å^2$ as estimated from the density (ρ_{CuCl}) of CuCl) is the average area per Cu(I) at the surface of CuCl [78].

5.3 Catalytic tests and Experimental set-up

From the reactor catalytic testing and gas chromatograph (GC) and gas chromatograph coupled with mass spectrometer (GC-MS) analysis of the effluent stream, detailed information about the average properties of the catalysts can be gained. The gas chromatograph utilizes a capillary column to separate the molecules. The difference in the vapour pressures between different molecules in a mixture will separate the molecules as the sample travels the length of the column. The molecules are retained by the column and then elute from the column at different times (called the retention time), which further can be identified by a detector at the downstream of GC. However, these separation and retention times were depend on the column dimensions and choice of the column i.e. property of the column phase. The ethylene conversion and the selectivities towards the main product and other by-products that are formed on the catalysts surface can be quantified from GC-data. Relevant changes in the selectivities, product distribution and the conversion levels on various

catalysts (doped and undoped), can also give a valuable information on the mechanistic details of the reaction and the each dopant's influence.

However, drawbacks of the method are that the GC analyses are not taken in continuously, but in certain intervals. In addition, information of the conversion of HCl was not obtained, owing to its corrosive nature to the electronic equipments and to the sensors. Owing to the wide range of product distribution and some of them having very close proximity in their nearer boiling points *i.e.* have the same retention times in GC column, hence GC alone cannot differentiate between them. However, GC coupled with MS allows the mass spectrometer downstream to capture, ionize, accelerate, deflect, and detect the ionized molecules separately. The mass spectrometer does this by breaking each molecule into ionized fragments and detecting these fragments using their mass to charge ratio. Though some of the products have similar pattern of ionized fragments in mass spectrum, however, combining these two processes reduces the possibility of the error.

5.3.1 Pulse reactor tests

Activity tests of the oxychlorination reaction have been made by using a conventional pulse reactor with the following procedure. The activity of the catalyst in conversion of C_2H_4 to $C_2H_4Cl_2$ has been determined by a gas chromatograph (Carlo Erba Fractovap 4200). The outlet of the reactor is directly fed to a gas chromatograph equipped with a column, packed with 1% SP-1000-carbopack 60/80; the column is maintained at 423 K. A flame-ionization detector (T = 493 K) and an integrator (Shimadzu C-R3A Chromatopac) is used to determine the concentration of unconverted ethylene and of produced 1,2-DCE. Two methods adopted in the this reaction tests procedure according to the objective. One is "Non- Depletive mode" and other one is "Depletive mode".

Non-Depletive mode (Publication II) consists in alternating a pulse of air (0.25 cm^3), with one of HCl (0.20 cm^3) and one of ethylene (0.10 cm^3) (corresponding to the stoichiometric ratio for ethylene oxychlorination to dichloroethane), and repeating the sequence until a constant ethylene conversion is asymptotically obtained, which corresponds to a pseudo steady-state situation. At these conditions, the catalyst can be considered as representative of the steady state reached under flow conditions, with the exception of a lower surface coverage by adsorbed reactants. Once the steady state conditions have been reached, the experiment continues under depletive mode dosing ethylene pulses until the consumption

of half of the total chlorine available on the sample, as predicted by eqn (15) is reached. In order to better evidence variations of catalytic performance with pulse number, a high catalyst volume/gas volume was used: 0.30 g catalyst, was pre-activated at 493K under carrier gas flow (N_2) 30 cm^3 min^{-1}.

In Depletive mode (Publication I), in order to ensure a complete and stable re-chlorination of the catalyst, the sample was then treated with alternate pulses of air (0.75 cm^3) and HCl (0.60 cm^3) for five times; a series of C_2H_4 pulses (0.30 cm^3) was then sent to the sample. In this tests, the reactor loaded with 0.15 g of sample employed, was pre-activated at 500 K in nitrogen stream (30 cm^3 min^{-1}), corresponding to a contact time of 1 s.

5.3.2 Fixed bed reactor tests

Experimental Set-up:

A second focus of this PhD work has been to study the effect of dopants on the kinetics and mechanisms of the oxychlorination reaction. The experimental set-up in the presented publications and in the unpublished work were quite different, especially in the case of pulse reactor experiments (Publication I and II), and slightly different in case of publication IV and unpublished work which were performed by using a fixed bed reactor. In this section, the experimental set-up and the description for catalytic tests performed on a fixed bed reactor was provided. After several modifications, respective to the object of the work, the final form of the experimental set –up was presented here.

The schematic representation of detailed experimental set-up is shown in Figure 21. The reactor was made up of quartz with an inner diameter of 10 mm. The reaction temperature was measured by a thermocouple (K-type) placed in a quartz thermocouple well with outer diameter 3 mm, which was centred axially in the reactor and temperature of the oven was controlled by a temperature controller (Eurotherm 3100). All feed lines were made of Teflon. The reactor was loaded with a mixture of the catalyst (250-450 μm) and graphite granules (250-450 μm). Dilutant (graphite) was added in order to keep control the temperature of the catalyst bed within the error of ±1 °C. The effluent stream (after the reactor) was further divided in two streams. One stream diluted with helium, in order to avoid the corrosion and condensation problems in the downstream analytical equipments. Other stream was let pass through the separation units, where first diluted the effluent stream with water in the water bath and then pass though caustic bath to absorb all chlorinated and CO_x

compounds, before escape to ventilation system. The chlorinated products in the helium diluted effluent stream were analyzed using on-line GC-MS (Agilent HP 6950) and online MS.

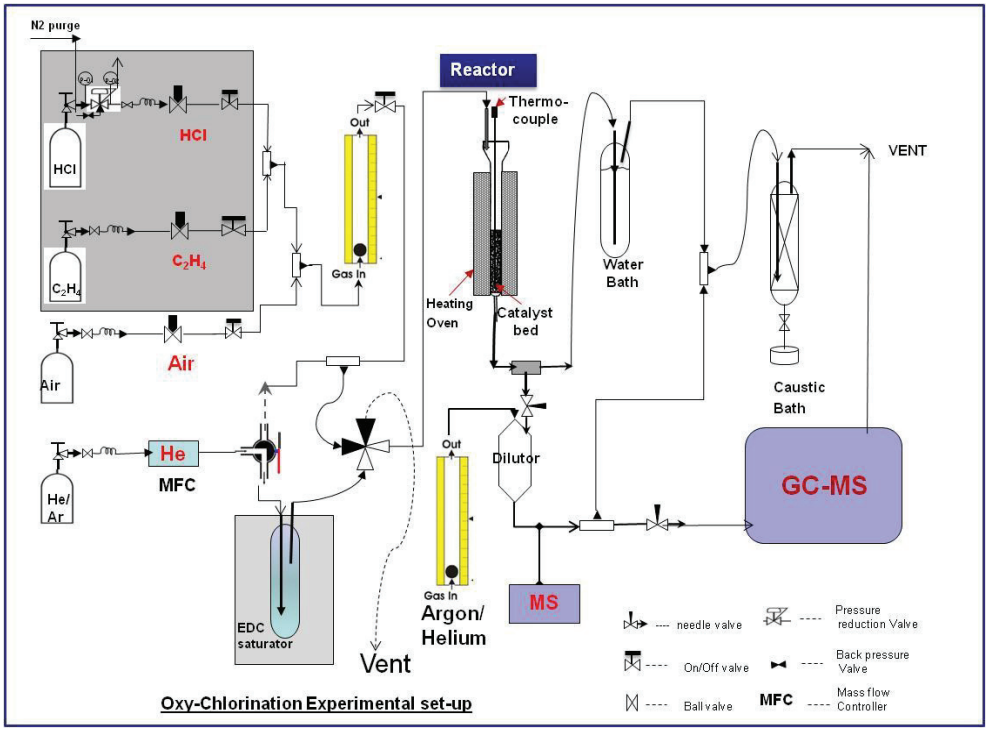

Figure 21: Schematic diagram of experimental-set up for 1,2-dichloroethane conversion tests.

Catalytic Tests (Publication III and Unpublished work): Catalytic testing was performed in a fixed bed quartz reactor with inner diameter of 10 mm in the temperature range 503 to 623 K. In order to avoid temperature run-off, the ethylene conversion was kept low, not exceeding 40% at 623 K. The catalyst (200 mg, 250–450 µm) was diluted with graphite (400 mg, 250–450 µm). The feed gas composition was C_2H_4:HCl:O_2:He = 1:1.10:0.38:14.4 M ratio with total feed rate of 45 N ml/min. The effluent gas was analyzed by offline GC–MS (Agilent HP 5973 equipped with Gaspro column). GC–MS analysis was made after 60 min of isotherm at each temperature under reaction mixture. Reaction selectivity toward chlorinated by-products was estimated by dividing the sum of by-product areas by the EDC (ethylene dichloride) area at each temperature.

Catalytic Tests (Unpublished work):

The catalytic activity in conversion of ethylene dichloride (EDC) was measured in a fixed-bed reactor in the temperature range 503-543 K at WHSV of 1.5 g of EDC *$g.cat^{-1}$ * h^{-1}. The reactor was loaded with 0.4g of catalyst and 0.2 g of graphite granules (170-450 μm). The catalyst were pre activated at 503 K for 1h under argon (Ar) gas flow, before exposing to reactant mixtures. In mean time, Ar gas flow was let pass through EDC saturator bath, and kept by-pass to ventilation, to ensure a stable EDC/Ar mole ratio in the feed stream (EDC + Ar) to the reactor. The reaction of EDC was studied in the kinetic regime with low conversions ranging from 0-5%. The effluent stream was analyzed with an on-line Quadruple mass spectrometer (MS) and with a GC-MS (Agilent HP 6950). The responses of reactants and products were directly measured by MS with a selected ion mode. However, MS alone cannot able to differentiate between certain products (e.g. EDC vs vinyl chloride). Hence, the chlorinated products in effluent stream were analyzed using on-line GC-MS equipped with DB-1 column and a quadrupole mass spectrometer. HCl and Cl_2 were not analyzed.

Chapter 6

Summary of the results

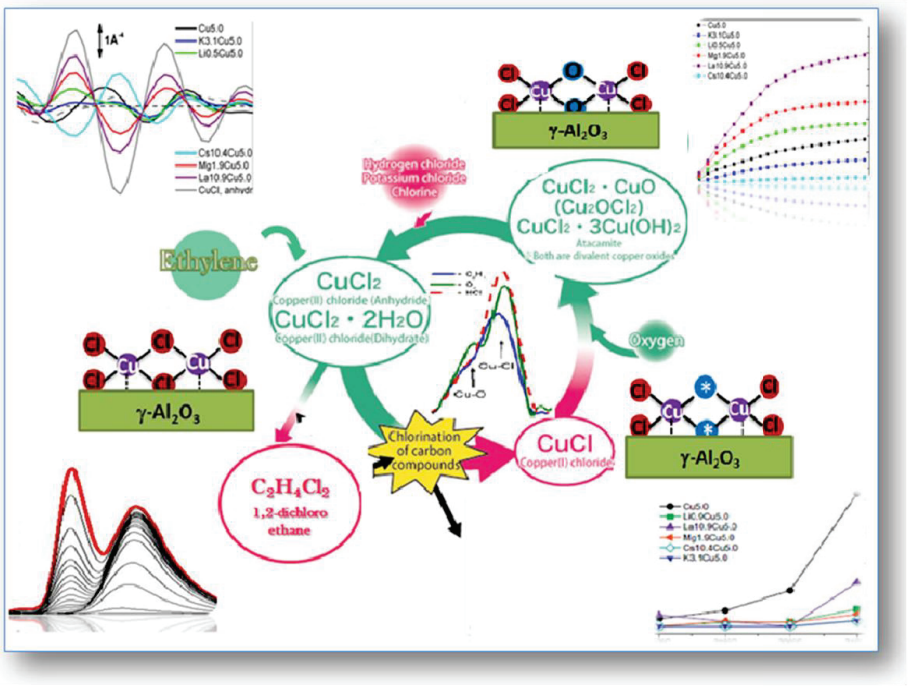

Publication I: **"Quantification of copper phases, their reducibility and dispersion in doped-$CuCl_2/Al_2O_3$ catalysts for ethylene oxychlorination"**

Scope of the study

The present contribution aimed to study and understand the role of the dopants have at molecular level on: (i) the nature, (ii) the relative fraction, (iii) the reducibility and (iv) the dispersion of the $CuCl_2$ active phase, addressing the first two points and partially the last point listed in the objectives of the present work.

Materials studied and methods used

In the present work Cu5.0, K3.1Cu5.0, Mg1.9Cu5.0, Cs10.4Cu5.0, Li0.5Cu5.0, La10.9Cu5.0, and Ce11.0Cu5.0 catalytic systems were studied. The multi-technique approach as explained in section 4.7 was used to study these catalytic systems. Combined *in situ* XANES/EXAFS, FTIR, CO chemisorption techniques were used to characterize the catalytic systems. Along with these techniques, catalytic tests performed using a pulse reactor in depletive mode.

Main findings and conclusions

The k^3-weighted, phase uncorrected FT (Fourier Transform) of the different catalysts activated in vacuum at 503 K are reported in Figure 22a. The two model compounds i.e. Cu1.4 and anhydrous $CuCl_2$ samples were used. These model compounds exhibit a markedly different first coordination shell: the Cu-aluminate phase (sample Cu1.4, dashed gray curve) exhibits a first Cu-O shell contribution at 1.5 Å while the $CuCl_2$ shows a much more intense Cu-Cl signal at 1.87 Å (both phase uncorrected values). It has been proved [56, 126] that two different copper species are present on the activated Cu5.0 catalyst (dried at 500 K in N_2 flux): a surface aluminate where the copper ions are hosted in the octahedral vacancies of γ-Al_2O_3, and a highly dispersed copper chloride on the surface. While studying parent and doped $CuCl_2$ catalysts, it was observed from Figure 22a, that Cu-Cl peak intensity increased, and that intensity rise is linked to the dopant added. EXAFS and XANES results presented in this work confirmed that all the dopant ions compete with Cu^{2+} ions in occupying the vacancy sites of γ-Al_2O_3 support. La and Mg metals were very efficient in doing that so, preferentially occupy octahedral vacancies, thereby allowing all the available copper to form surface copper

chloride species of 100% by fraction. While the alkali metal cations are able to react with both cationic vacancies, thus being less competitive for the occupation of octahedral ones.

By using a linear combination method and accurate analysis of XANES spectra, we were successfully able to quantify the fraction of Cu-aluminate and copper chloride species presented on the doped catalysts, The $CuCl_2$ fraction is shown in Table 4, 5th column. A successful investigation of the doped catalysts using an in-situ X-ray absorption spectroscopy enables us to highlight that all dopants contributed more or less efficiently in increasing the fraction of the active copper species on the surface. The following trend in the ability of the dopant cation to compete with Cu^{2+} in the aluminate phase formation has been found: $Cs^+ \leq K^+ << Li^+ > Mg^{2+} << La^{3+}$.

EXAFS directly (Figure 23a), and IR indirectly, proved that the addition of KCl or CsCl (and less efficiently of LiCl) results in the formation of mixed CuK_xCl_{2+x} or $CuCs_xCl_{2+x}$ phases. To the best of our knowledge, the signal observed for the Cs10.4Cu5.0 catalyst (cyan curve)in Figure 23a is the first direct structural evidence of the presence of Cs^+ cations in the second coordination shell of copper, thus proving the formation of a mixed $CuCs_xCl_{2+x}$ salt. The cases of Li0.5Cu5.0, and K3.1Cu5.0 are less straightforward to be assigned because of the significantly smaller scattering power of Li (Z=3) and K (Z=19) with respect to Cs (Z=55), the presence of mixed $CuLi_xCl_{2+x}$ and CuK_xCl_{2+x} salts can only be hypothesized but not proven at this point.

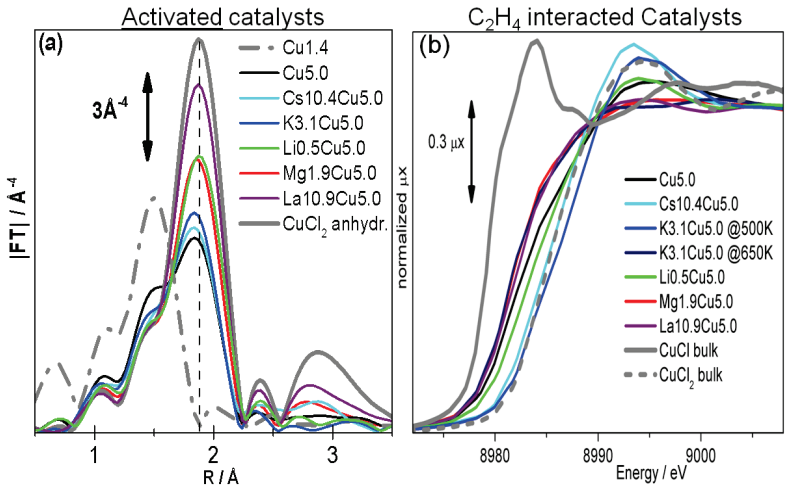

Figure 22: Part (a) EXAFS spectra , k^3-weighted, phase uncorrected |FT| of the different catalysts activated *in vacuum* at 503 K; Part (b) Normalized XANES spectra of the whole set of catalysts after interaction with C_2H_4 at 503 K.

The effect of the additives on the reactivity of the catalysts towards ethylene at 503 K, was examined by an in situ EXAFS/XANES spectroscopy under static conditions and by catalytic activity measured in a depletive mode by a pulse reactor. The results obtained by in situ EXAFS/XANES experiments (Figure 22b), showed that K3.1Cu5.0 and Cs10.4Cu5.0 catalysts, show a negligible reduction fraction at 500 K, suggesting that these two dopants K^+ and Cs^+ dopants influence the reduction step (Eq.15). The fact that the thermodynamic properties of the active phase have been changed is proven by the fact that when ethylene is dosed on K3.1Cu5.0 catalyst at 650 K, the catalyst exhibits a significant reduction.

To understand the dispersion of the active phase with different additives presence, measured by CO chemisorptions (Table 4): it has been found that addition of LiCl increases enormously the dispersion of the active phase, $LaCl_3$ significantly and $MgCl_2$ barely, while addition of both KCl and CsCl results in a decrease of the surface area of the active phase.

Being the pulse reactor experiments (Figure 23b) performed in a depletive mode that the C_2H_4 can be converted to $C_2H_4Cl_2$ only at the expense of the Cl coming from the reduction of $CuCl_2$ to CuCl, so the determination of C_2H_4 conversion allow the direct determination of Cu available for reduction. For the same reason the conversion per pulse is higher at the beginning and decreases progressively as the source of Cl is consumed. These results gave more detailed picture of dopants effect on catalysts, reactivity towards ethylene resulted in the following order:

La10.9Cu5.0 > Mg1.9Cu5.0 > Li0.9Cu5.0 > Cu5.0 > K3.1Cu5.0 ≈ Cs10.4Cu5.0.

Summarizing the use of a multidisciplinary approach has been the unavoidable to understand the complex role that the different additives have on the active phase of the $CuCl_2$/ γ -Al_2O_3 catalysts for ethylene oxychlorination.

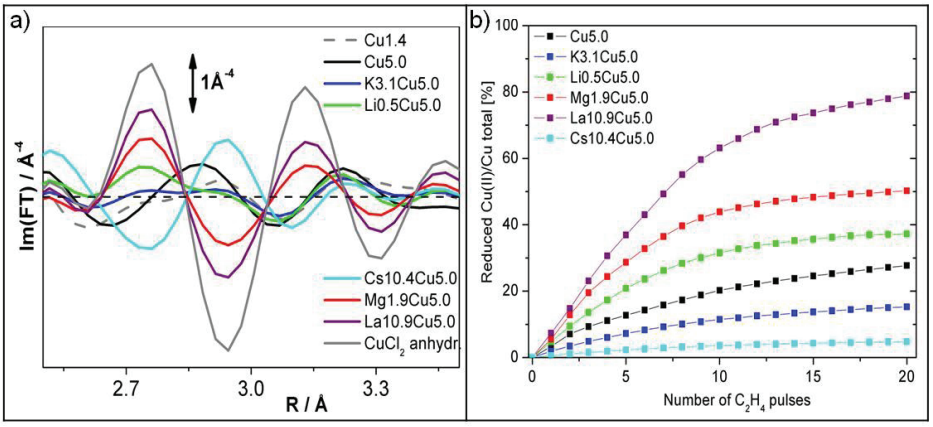

Figure 23: Part (a) reports moduli of the FT in the first and second shell region; Part (b) Fraction of reduced Cu(II) *vs.* the number of ethylene pulses dosed on all catalysts as obtained from the measured ethylene conversion to 1,2-dichloroethane by depletive mode catalytic tests.

Table 4: Raw results of static-volumetric measurements of CO adsorption (columns 2–4): Volume of adsorbed CO (V_m), ratio between adsorbed CO molecules and total number of Cu atoms (D'), and estimation of the surface area of CuCl (S'_{CuCl}). Average fraction of the active $CuCl_2$ phase, in % from XANES and EXAFS analyses ($<x_{cl}>$ Column 5). Dispersion corrected by $<x_{cl}>$ and referred to the active $CuCl_2$ phase (D, Column 6). Raw and renormalized data from the catalytic experiments in pulse reactor (Fig. 1): % of the total Cu reduced after 20 ethylene pluses (R', Column 7);% of Cu reduced in the active phase ($R = R'/<x_{cl}>$, Column 8); % of reduction of the first monolayer of the active phase (R/D Column 9).

Technique	CO chemisorption raw data			EXAFS/XANES		Activity in pulse reactor		
Sample	V_m (cm^3g^{-1})	D'	S_{CuCl} (m^2g^{-1})	100 $<x_{cl}>$	D = D'/$<x_{cl}>$	R'	R= R'/$<x_{cl}>$	R/D
Cu5.0	8.3	0.45	25.1	66	0.68	28	42	62
K3.1Cu5.0	8.4	0.46	25.4	78	0.59	15	24	41
Cs10.4Cu5.0	8.3	0.45	25.1	82	0.55	5	7	12
Li0.5Cu5.0	14.2	0.78	43.0	82	0.94	37	54	58
Mg1.9Cu5.0	12.6	0.69	38.1	94	0.74	50	56	76
La10.9Cu5.0	14.4	0.79	43.6	98	0.80	79	82	102

***Publication II*: "Influence of additives in defining the active phase of the ethylene oxychlorination catalyst"**

Scope of the study

Present work focused on the influence of promoters on the active sites presented on $CuCl_2$/ γ -Al_2O_3 catalyst system, improved our knowledge of the role that dopants addition has on the chemistry and red-ox behaviour of the active phase. The effect that these chemical modifications have on the increase or decrease of catalytic activity at pseudo steady state observed as a consequence of catalyst doping, addressing the (iv) and (v) points of the objective list. The results from this publication gave comprehended evidence on the characteristic influence of each dopant on the catalyst, first of its kind.

Materials studied and method used

In this work, we studied undoped and doped $CuCl_2$/γ -Al_2O_3 catalysts with varied loadings: Cu5.0, K3.6Cu5.0, Mg1.9Cu5.0, Cs10.4Cu5.0, Li0.5Cu5.0, La10.9Cu5.0, and Ce11.0Cu5.0 catalyst systems by using complimentary characterization techniques such as operando XANES, FTIR and UV- Vis spectroscopy. And the catalytic activity at pseudo steady state was measured on K1.55Cu5.0, Mg0.95Cu5.0, Li0.26Cu5.0 and Cs5.21Cu5.0 samples by testing them in pulse reactor.

Main findings and conclusions

Among the most used additives for both fluid and fixed beds technologies (LiCl, KCl, CsCl, $MgCl_2$, $LaCl_3$, $CeCl_4$), most highlighted result is that we have been able to show that KCl, and CsCl, are able to displace the rate determining step from the CuCl oxidation (undoped catalyst) to the $CuCl_2$ reduction (Figure 24B&D). For all remaining additives the rate determining step remains the CuCl oxidation, as for the undoped catalyst [80]. In the presence of reagent flux, the stable form of the active phase observed on Cu5.0 catalyst is CuCl (Figure 24A), while for K3.1Cu5.0, it was mixture of $CuCl_2$ and CuCl phases (Figure 24C). These results have been obtained coupling the catalyst activity monitored with a pulse reactor working in both non-depletive and depletive modes with time resolved XANES spectroscopy performed under in operando conditions. Present operando XANES results showed that for La10.9Cu5.0, Mg1.9Cu5.0 and Ce11.0Cu5.0 samples the Cu(II) reduction and O_2 conversion started at the same temperature (≈ 480 K) as observed for Cu5.0 sample

and was able to reduce CuII species completely at the end of ramp up temperature. While for K3.1Cu5.0, Li0.9Cu5.0 and Cs10.4Cu5.0 samples, the reduction and oxidation started at much higher temperatures, and at the end of ramp up, partial reduction has been observed (Table 5). Summarizing the XANES results, Cu5.0, La10.9Cu5.0, Mg1.9Cu5.0 and Li0.9Cu5.0 samples behaves similarly to what is observed for highly dispersed CuCl nanoparticles, where surface Cu^{+} sites are separated just by one Cl^{-} anion. While a much larger distance must be inferred for copper species hosted on K3.1Cu5.0 and Cs10.4Cu5.0 samples because Cu^{+} sites are separated also by dopant cations and by unreduced Cu^{2+} cations. Formation of CuK_xCl_{2+x} and $CuCs_xCl_{2+x}$ mixed phases [21, 75] has been proved by monitoring the Cu(II) d–d transitions with UV-Vis spectrometer and the CO stretching frequency of carbon monoxide adsorbed on reduced catalyst by in situ IR spectroscopy (Figure 25 b & c). These results were in good agreement with the observations and giving further the support to the hypothesis made in earlier contribution i.e. formation of mixed phase.

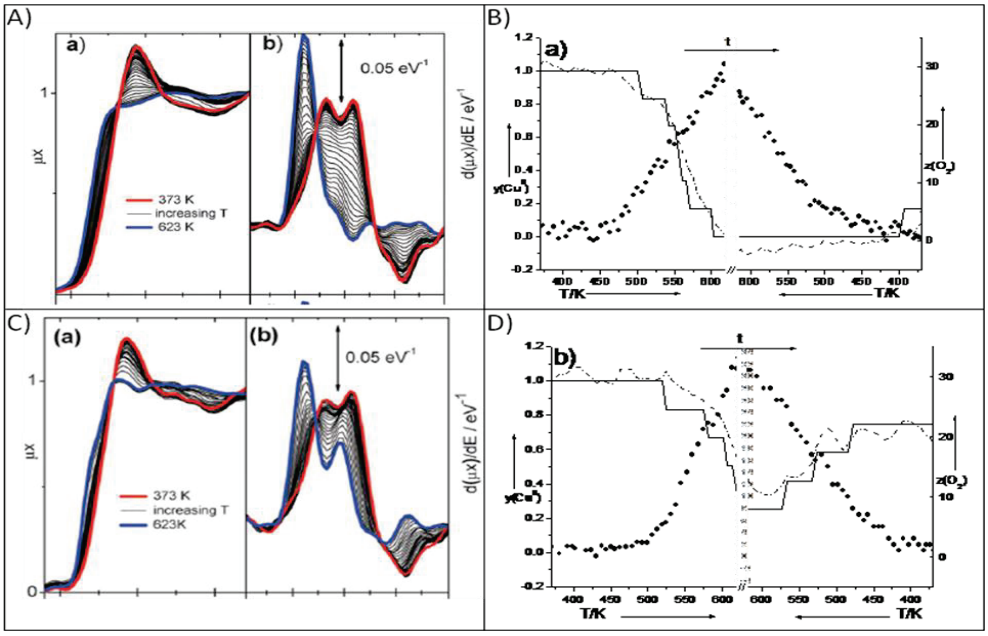

Figure 24: Part (A&C): XANES spectra and its derivative of Cu5.0 and K3.1Cu5.0 catalysts during the heating part of the experiment: from 373 (red curve) up to 623 K (blue curve) by 12 K min^{-1}. Part (B&D) : Summary of the XANES experiments of Cu5.0 and K3.1Cu5.0 catalysts in operando conditions. O_2 conversion (scattered dots right axis: z) and Cu(II) fraction (left axis: y).

Table 5: Summary of the main results obtained from the analysis of the operando XANES spectra. For the ramp up experiments we report the starting (at 373 K) and the final (at 623 K) fraction of Cu(II) and the temperature when a valuable fraction of Cu(I) and a valuable amount of O_2 consumption have been detected. For the ramp down experiments we just report the starting (at 623 K) and the final (at 373 K) fraction of Cu(II).

Catalyst	ramp up				ramp down	
	Cu(II) [%]		T start [K]		Cu(II) [%]	
	initial	final	Cu(II) reduction	O_2 conversion	initial	final
Cu5.0	100	0	480	480	0	0-20
Li0.5Cu5.0	95	25	550	500	0	0-10
K3.1Cu5.0	100	35	520	480	30	70
Cs10.4Cu5.0	90	45	580	560	35	100
Mg1.9Cu5.0	95	0	490	480	0	10
La10.9Cu5.0	100	0-10	510	520	0-10	0-10
Ce11.0Cu5.0	100	0-10	475	470	0-10	0-10
Cu/α-Al_2O_3	100	50	505	525	30	30

Pulse tests (Figure 25a) demonstrate that the average oxidation state of Cu at the pseudo steady state is affected by the presence of the promoters. Finally, of high relevance is the observation that the fully oxidized catalyst is inactive. This unexpected evidence highlight the role of coordinative unsaturated Cu(I) species in adsorbing ethylene on the catalyst surface indicating that copper, in the working catalyst, exhibits a (I)/(II) mixed valence state. This implies that, for all samples, the active phase is a valence mixed $CuCl_2$/CuCl phase, in agreement with XANES measurements in operando conditions.

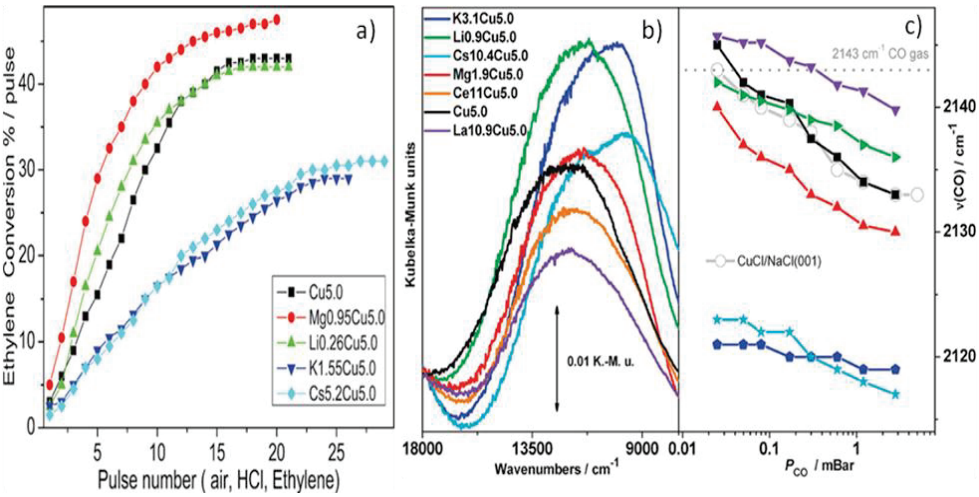

Figure 25: Part(a) Percentage of ethylene conversion per pulse in non-depletive mode at the temperature of 493 K. Pulse number refer to the subsequent dosage of three different pulses of air, HCl and ethylene. Part (b) UV-Vis DRS spectra, in the d–d transitions region for the different catalysts. Part (c) Evolution of the C–O stretching frequency, ν_{CO}, as a function of the CO equilibrium pressure (logarithmic scale) in IR experiments of CO dosed at 300 K on the different catalysts.

The experimental evidence reported in this work highlight the important role of dopants in red-ox catalysis. Selected alkali dopants, specifically Cs and K, have a profound effect on red-ox properties of the catalyst and hence on catalytic performance. This implies a long-range effect, which corresponds to a modification of the electronic properties of the active phase, rather than a localized interaction between the active site and the dopant atom. These results along with spectroscopy results (both from the above contributions publication I and II), highlighted that there were two families of catalysts among the investigated samples. Family I catalysts: being Cu5.0, La10.9Cu5.0 and Mg1.9Cu5.0, while, Family II catalysts: being K3.1Cu5.0 and Cs10.4Cu5.0 and Li0.9Cu5.0 being in the middle.

Publication III: **"Doped-$CuCl_2/Al_2O_3$ catalysts for ethylene oxychlorination: Influence of additives on the nature of active phase and reducibility"**

Scope of the study

The present contribution is complementary from the above two contributions, where we understood the role that dopants have in nature, relative fraction, reducibility and dispersion of Cu-phases on $CuCl_2/\gamma$-Al_2O_3 catalysts for ethylene oxychlorination reaction. In the present contribution, we summarized some important conclusions by comparing the evidences obtained from the spectroscopy results and catalytic tests.

Main Conclusions

From XANES results (Figure 22b) presented in publication I, using the edge shift as rough approximation of the fraction of reduced Cu(II), Mg1.9Cu5.0 and La10.9Cu5.0 catalysts exhibit a reduction of 55% and 50%, Cu5.0 of 35% and Li0.5Cu5.0 25% , while K and Cs-doped catalysts showed no reduction. These results were become supportive to the results obtained by depletive mode pulse reactor test. The integration of the area below the experimental curves (see inset) provides a direct estimate of the fraction of Cu(II) sites available for the reduction by ethylene at the pseudo-steady-state condition reached in the previous part of the experiment. In good agreement with the XANES results, catalysts having the lowest amount of Cu(II) were Cu5.0 and Mg0.95Cu5.0, those having the greater amount of Cu(II) were Li0.26Cu5.0, K1.55Cu5.0 and Cs5.21Cu5.0.

Operando XANES (Publication II) results showed that K and Cs-doped catalysts displace the rate-determining step under the oxychlorination reaction mixture, while remaining catalyst followed the same as of that for undoped Cu5.0 catalyst i.e "oxidation of CuCl". Non-depletive pulse tests support XANES experiments, both experiments underline that the composition of the active phase changes upon exposure to reactants.

The results from the both these contributions indicates that we are dealing with two different families of catalysts. Family I: refers to Cu5.0, Mg1.9Cu5.0, Ce11.0Cu5.0 and La10.9Cu5.0 catalysts, under the adopted conditions. Family II: refers to K3.1Cu5.0 and Cs10.4Cu5.0, while Li0.5Cu5.0 being the intermediate. The qualitative results of this in situ, static, XANES experiment fully mirrors the quantitative results obtained in the operando XANES experiments.

***Publication IV*: "The role of additives determining density and strength of Lewis and Brønsted acidic sites on the γ-Al_2O_3 support used in oxychlorination catalysis: a FTIR study"**

Scope of the study

In the present work, we have investigated individual contributions and elucidated the effect of alkali, alkaline earth, lanthanide metal and chlorine, respectively, the dopants and chlorine have on the nature, population and strength of the surface Lewis (>Al^{3+}) and Brønsted (>Al-OH) sites of the γ-Al_2O_3 support and also $CuCl_2$/γ-Al_2O_3 catalyst over a wider temperature range (393-623K). Further, to correlate the modified surface properties of the doped catalysts to their selectivity in oxychlorination of ethylene reaction, catalytic tests were performed. The observed results gave a molecular level understanding on the influence of these dopants on the catalysts properties, there by addressing the point (iii) and partially point (v) in the objective's list.

Materials studied and methods used

To understand both the effect of Cl^- anions and dopant cations a set of dopant free, HCl-impregnated and of Cu-free dopant-impregnated supports have been prepared and investigated. In the series of supports: bare-Al_2O_3, Li0.5, K3.1, Cs10.4, Mg1.9, Ca3.2, La10.9, Cl1.4A and Cl2.8A samples; and in the series of catalysts: Cu5.0, Li0.9Cu5.0, La10.9Cu5.0, Mg1.9Cu5.0, K3.1Cu5.0 and Cs10.4Cu5.0 samples were studied. The best credible way to get the information on the nature of the surface sites is by applying FTIR spectroscopy of CO adsorbed at liquid nitrogen temperature. In addition, the selectivity tests were performed in the fixed-bed reactor in the temperature range 503-623 K. The products in the effluent stream were analysed by an off-line GC-MS and their corresponding selectivities were measured.

Main findings and conclusions

Table 6 summarizes those results from FTIR with CO as probe molecule on the chlorinated samples (Cl1.4 and Cl2.8) and on all doped catalysts, reporting the ν(CO) frequencies of CO adsorbed on both the sites at the low and maximum coverage on the surface. The impregnation of alumina with HCl reduces the amount and acidic strength of the Lewis sites, saturating the coordinative vacancies of >Al sites with the formation of >Al-Cl

species. Chlorination of the surface results in an increase of the acidity of the Brønsted sites, moving the ν(C-O) in Al-OH···CO adducts from 2154 to 2158-2159 cm^{-1}. Upon increasing the loading, these phenomena are prevailed more. However, by increasing the temperature, the effect of HCl addition on the Lewis sites strength and population is almost negligible, owing to the fact that chlorine leaves the surface of γ-Al_2O_3 at that temperature. However that the influence on the increased acidity of the Brønsted sites still holds.

For the copper-free samples, all dopants significantly reduce the fraction of available $>Al^{3+}$ Lewis sites, mainly due to the formation of surface >Al-Cl species, resulting in a similar effect as that obtained with HCl. In Li0.5, Mg1.9, Ca3.2 and La10.9 case the absence is replaced by a new acidity of Lewis nature due to the appearance of D^{n+} surface sites. No Lewis sites are available to CO after impregnation with CsCl, and very few and weak remain after KCl impregnation. With respect to chlorinated alumina, the Brønsted acidity is completely (almost completely) quenched by CsCl (KCl) impregnated, almost changed by LiCl and $CaCl_2$ doping, and enhanced by $MgCl_2$ and $LaCl_2$ impregnation.

Coming to the doped catalysts (Figure 26), comparing doped supports and doped catalysts, the higher overall amount of chlorine deposited on the catalysts implies an increase of the Brønsted acidity in both ν(CO) and adduct stability. When comparison is made with the bare support, the increase of the strength of the Brønsted sites is remarkable in all cases except the CsCl doped one. Moreover, the surface Lewis acidity is totally suppressed for CsCl and KCl doped-catalysts, being strongly suppressed in the remaining cases.

This work has high importance for the ethylene oxychlorination catalysis, as surface acidic sites of alumina have been reported as the main origin of undesired side products [145]. Besides this specific goal, our study has a much broader goal, as it deals with one of the fundamental open questions in heterogeneous catalysis: determining the actual role that the support has in the structure and reactivity of the supported active phase. The huge number of experimental results reported in this work results in an empirical correlation (Figure 27a) between the strength of the Brønsted acid sites of the support and the ν(CO) of CO adsorbed on the reduced fraction of the active copper chloride phase.

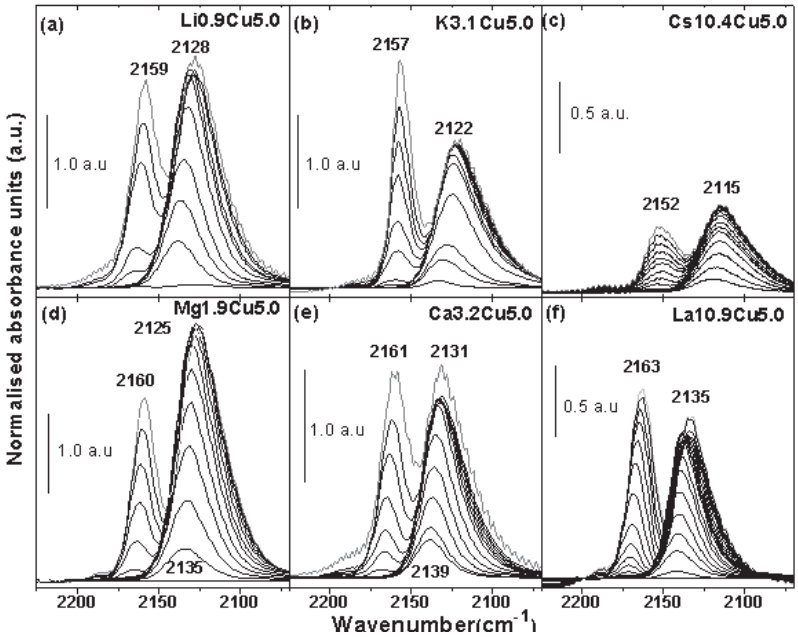

Figure 26: IR spectra of CO adsorbed at liquid nitrogen temperature on: Li0.5Cu5.0, K3.6Cu5.0, Cs10.4Cu5.0, Mg1.9Cu5.0, Ca1.9Cu5.0 and La10.9Cu5.0, catalysts. In all cases, before CO dosage samples where activated in dynamic vacuum at 503 K for 1 h.

Table 6: Summary of the CO stretching frequencies observed on the doped catalysts at low ($\theta \rightarrow 0$) and high ($\theta \rightarrow \theta_{max}$) coverages for adducts formed on both Lewis (>Al^{3+}) and Brønsted (>Al-OH) sites. For comparison, also the data of the bare (Al_2O_3) and chlorinated (Cl1.4 and Cl2.8) supports and of the undoped catalyst (Cu5.0) are reported. All samples were activated at 503 K.

Sample	ν(CO) for adducts formed on Lewis sites		ν(CO) for adducts formed on Brønsted sites		ν(CO) for adducts formed on Cu^+ sites	
	$\theta \rightarrow 0$ (cm^{-1})	$\theta \rightarrow \theta_{max}$ (cm^{-1})	$\theta \rightarrow 0$ (cm^{-1})	$\theta \rightarrow \theta_{max}$ (cm^{-1})	$\theta \rightarrow 0$ (cm^{-1})	$\theta \rightarrow \theta_{max}$ (cm^{-1})
Li0.5Cu5.0	2190	~ 2180	2164	2159	2139	2128
K3.6Cu5.0	notobserved	not observed	2159	2157	2132	2122
Cs10.4Cu5.0	notobserved	not observed	2153	2152	2119	2115
Mg1.9Cu5.0	~ 2190	~ 2185	2165	2160	2134	2125
Ca3.2Cu5.0	~ 2200	~ 2190	2166	2160	2138	2131
La10.9Cu5.0	~ 2200	~ 2190	2170	2163	2139	2131
Al_2O_3	2195	~ 2185	2155	2154	–	–
Cl1.4	2196	~ 2180	2159	2155	–	–
Cl2.8	2202	~ 2185	2163	2158	–	–
Cu5.0	2187	~ 2180	2160	2158	2137	2127

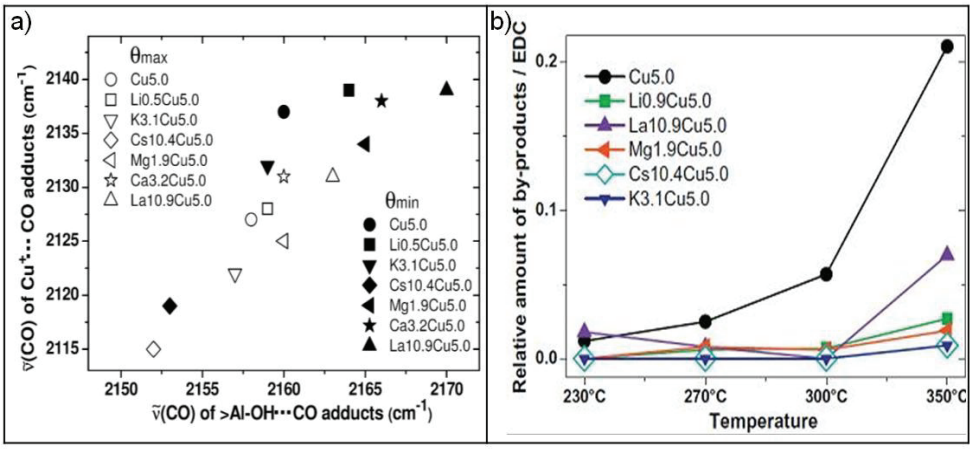

Figure 27: Part (a): Empirical correlation between the ν(CO) of $Cu^{+}\cdots CO$ adducts and that of >Al-OH···CO adducts formed on Cu5.0 and on doped catalysts at low (full symbols) and high (open symbols) coverage Θ_{CO}; Part (b): Selectivity toward chlorinated by-products over the target product 1,2-dichloroethane (EDC) for all the catalysts over the temperature range 503-623 K.

The results (Figure 27b) indicated that the selectivity towards chlorinated by-products correlates directly with the density of Lewis acid sites and strength of Brønsted acid sites (as reported in Figure 26), in the following order:

Cu5.0 > La10.9Cu5.0 > Li0.9Cu5.0 > Mg1.9Cu5.0 > K3.1Cu5.0 ≈ Cs10.4Cu5.0

***Unpublished Work*: "Influence of dopants in controlling the by-products formation in ethylene oxychlorination reaction: site selective mechanistic details"**

Scope of the study

In the present work, attempts were made to tune the base catalysts by co-doping, based on the understating from our previous publications. In addition, further, to elucidate the influence of the selective dopants and co-dopants in controlling the formation of by-products during ethylene oxychlorination reaction at 503 K. For this purpose, conversion of 1,2-dichloroethane (EDC) was studied on both the supports and also on the catalysts. The possible active sites on the oxychlorination catalyst system are: Brønsted acid sites (>Al-OH), Lewis sites (> Al^{3+}) of the carrier and $CuCl_2$, Cu_2OCl_2, CuCl on the catalysts surface along with dopant metals. Our initial efforts were focused towards identifying the active sites responsible for different reactions involved in further chlorination of EDC and to understand the existing complexity in the reaction mechanism involved on copper chloride supported catalysts. Efforts were made on deducing the mechanisms in the by-product formation from the experimental observations. Finally, an efficient catalyst was proposed for ethylene oxychlorination reaction.

Materials studied and methods used

New catalysts were prepared by co-doping with KCl, CeO_2 and $LaCl_3$ and prepared Ce5.5La5.45Cu5.0 and K1.55La5.45Cu5.0 by incipient wetness impregnation method, and for activity and selectivity tests, we screened other catalytic systems (Cu5.0, K3.1Cu5.0, Li0.9Cu5.0, Cs10.4Cu5.0, Mg1.9Cu5.0 and La10.9Cu5.0) along with the new catalysts. Catalytic tests were performed in the fixed bed reactor under steady state conditions, in the temperature at 503-573K.

For EDC reactivity and selectivity studies, the most studied dopants KCl and $LaCl_3$were chosen. In the present work, bare Al_2O_3, K3.1A, La10.9A, K1.55La5.45A supports and Cu5.0, K3.1Cu5.0, La10.9Cu5.0 and K1.55La5.45Cu5.0 the catalytic systems were studied. The catalytic tests were performed in a fixed-bed reactor at temperature 503 K. The reactants and products were analysed by an on-line mass spectrometer (MS) and by an on-line GC-MS. The selectivities of the products were calculated from the GC-MS analysis.

Main findings and Conclusions

Figure 29 shows the activity and selectivity of various catalysts at 573K. From part (a) and part (b), it can be seen that K1.55La5.45Cu5.0 catalyst showed the maximum activity for ethylene and oxygen and maximum selectivity to EDC at steady state conditions. Other catalyst CeO_2 doped catalyst also showed the significant conversion and selectivity increase compared to the single doped catalysts. From this observation, it showed that co-doping with K and La chlorides i.e. K1.55La5.45Cu5.0 catalyst increased the efficiency of the catalyst, when compared with single doped catalysts.

Figure 29 shows the conversion of EDC and selectivities of the chlorinated products over the bare and doped alumina supports. The results on the non-chlorinated supports, highlighted that the formation of vinyl chloride (VCM), 1,1-dichloroethane (1,1-EDC) and ethyl chloride (EC) occurred on the support, most precisely on the active acid sites of the carrier. The freshly activated samples at 503 K showed a remarkable conversion of EDC to VCM in larger abundance, followed by other ethyl chloride and 1,1-EDC. From the experimental results, it has been suggested that dehydrochlorination of 1,2-EDC to VCM is the primary reaction on the support surface. The mechanisms for these reactions were proposed based on the experimental results and depicted in Figure 31(a) and (b). It has been proposed that, the dehydrochlorination reaction occurred on a closely spaced Lewis acid-base pair (Figure 31a), while hydro-chlorination to ethyl chloride is occurred on closely spaced Brønsted acid- Lewis acid pair (Figure 31b). Besides, HCl- addition reaction seems to proceeds on the [Al-Cl +Al-OH] pair (Figure 31b), which are formed from dehydrochlorination. Alumina support is also active for polymerization of the chlorinated compounds, and forming toluene in a non-negligible fraction, which might be by the strong Brønsted acid sites of the surface.

Upon adding dopants K and La-chlorides, vinyl chloride formation was enhanced in case of La-doped support, while K dopant decreased the dehydrochlorination activity. It has been suggested [150, 151] that K^+ and La^{3+} ions selectively adsorb on tetrahedral and octahedral Lewis sites of alumina respectively. That means, in spite of the blockage of these Lewis sites, dehydrochlorination was still active. However, these experimental results were in agreement with the fact that La^{3+} may itself a Lewis acid site and can active for this reaction, if it is closely spaced to basic site [= Al-O^-]. However, co-doping with these cations on

alumina surface, seemed to be very efficient in killing the all active sites not only for dehydrochlorination reaction, but also for hydro-dechlorination and HCl-addition reactions.

Upon chlorination of the supports by interaction with gaseous HCl flux for 30 minutes, a 20 fold increase in the conversion of EDC to VCM and to 1,1-EDC was observed. Abundance of VCM was increased atleast by 30 times on chlorinated alumina. Nevertheless, chlorination of alumina completely hindered the formation of EC and other products. The same trend appears on the La doped support, but in less extent, when compared with bare alumina. On the other hand, K and K + La co-doped supports completely hindered the conversion of EDC. It seems likely that HCl neutralized the remaining active sites at the surface of K and K + La doped supports, thus hindered the dehydrochlorination and other reactions; while on bare and La doped supports, HCl increased the fraction and strength of active sites for dehydrochlorination, with simultaneous killing of the active sites for hydro-dechlorination reactions. These results strongly support the well- known reaction of the HCl on the alumina.

- Al-OH + HCl → Al-Cl + H_2O

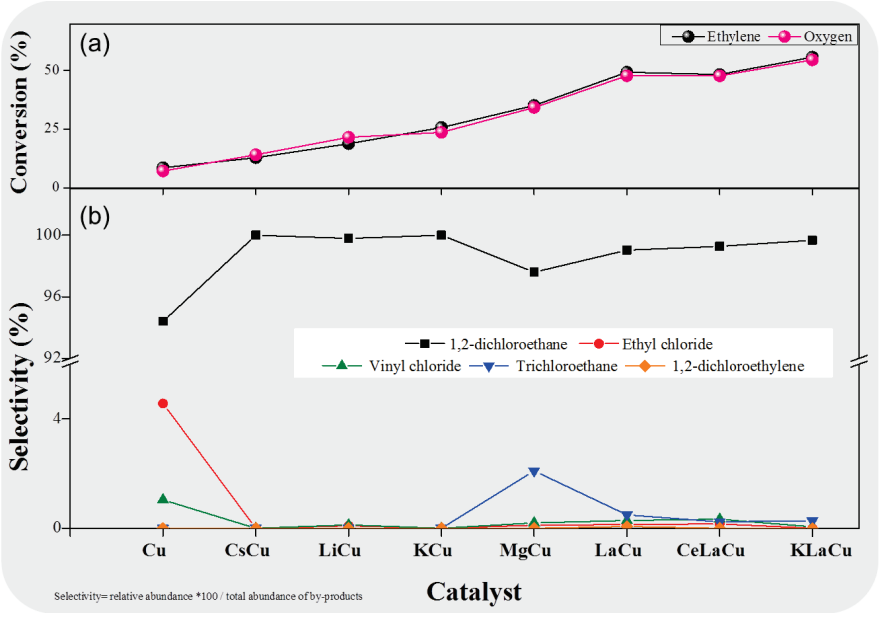

Figure 28: Conversion and Selectivities of copper-based catalysts in fixed bed reactor at 573K. (a): Ethylene and oxygen conversions (%) and (b): selectivities (%) of various products. The catalysts studied are Cu = Cu5.0, CsCu = Cs10.4Cu5.0, LiCu = Li0.9Cu5.0, KCu = K3.1Cu5.0, MgCu = Mg1.9Cu5.0, LaCu = La10.9Cu5.0, CeLaCu = Ce5.5La5.45Cu5.0 and KLaCu = K1.55La5.45Cu5.0

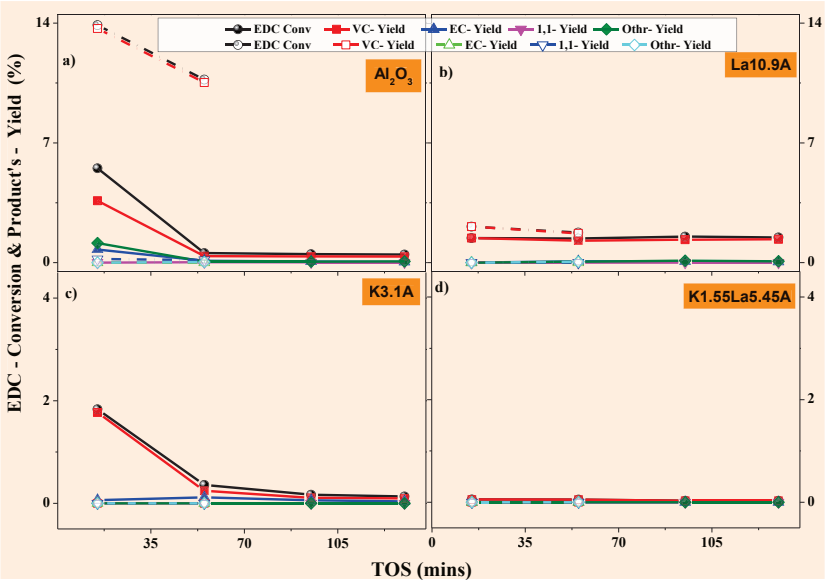

Figure 29: Conversion of 1,2-dichloroethane (EDC) and the product's selectivities at 503K over the both non-chlorinated and chlorinated supports: a) γ-Al_2O_3, b) La10.9A, c) K3.1A and d) K1.55La5.45A. (Values with closed symbols represent for non-chlorinated supports and values with open symbols represent for chlorinated supports). Please note that parts a) and b) are scaled on the same conversion levels, while part c) and d) are scaled on same level.

Figure 30 shows the conversion of EDC on each of the three copper species, which are existing on the real oxychlorination catalyst systems at given point of time during the reaction. The results showing that, the EDC conversion on individual copper species was not straightforward. However, conversion of EDC on the undoped and doped catalysts is remarkable and indicating that La doped catalyst and undoped catalyst were active for EDC conversion, especially to vinyl chloride, 1,1,2-trichloroethane (TCE), CO_2 irrespective of the different copper species. However, as remarkable, as we observed in case of supports, K and KLa doped catalyst showed the least activity for the conversion of EDC. Further, from Figure 30, it can be conclude that $CuCl_2$- species are the most active for EDC conversion, compared to the other two species Cu_2OCl_2 and CuCl. If we consider the fact that the catalyst surface was chlorinated with the gaseous HCl, in order to regenerate the $CuCl_2$ species, the increased activity of EDC conversion is justified on all the catalysts. By comparing Figure 30 and Figure 29, the products: VCM , 1,1-EDC and EC were most likely formed on the support, than on the copper species. However, from Figure 30c, it was quite clear that formation of

TCE is favourable on $CuCl_2$ sites and it has been proposed that it formed by chlorination of vinyl chloride to TCE, as shown in Figure 32c.

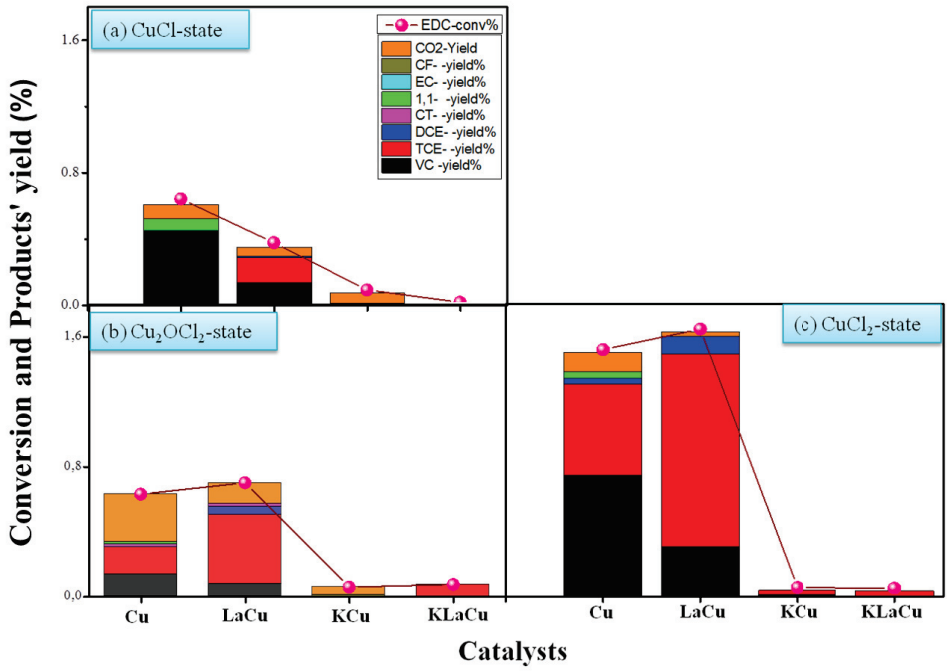

Figure 30: Conversion of 1,2-dichloroethane (EDC) and the product's selectivities at 503K over the undoped and doped supports containing: a) CuCl-rich sites, b) Cu_2OCl_2 –rich sites, c) $CuCl_2$-rich sites.

Further, it was suggested that, formation of 1,2-dichloroethylene proceeds through dehydrochlorination of TCE, which is believed to occur on the Lewis acid-base pair of support as shown in Figure 32a. The experimental results shown in Figure 30c, strongly supporting the above claim, since the chlorination enhance the dehydrochlorination activity, as discussed earlier with simultaneous enhanced activity of EDC chlorination to TCE on active Cu^{II} sites. However, the mechanism behind the CO_2 formation is not straightforward. From the experimental results, it can be suggested that Cu_2OCl_2/CuCl species along with the help of Brønsted acid sites enhance the formation of CO_2. In Figure 30, it can be seen that the formation of C_1- compounds were not observed in a considerable fraction to elucidate their mechanisms.

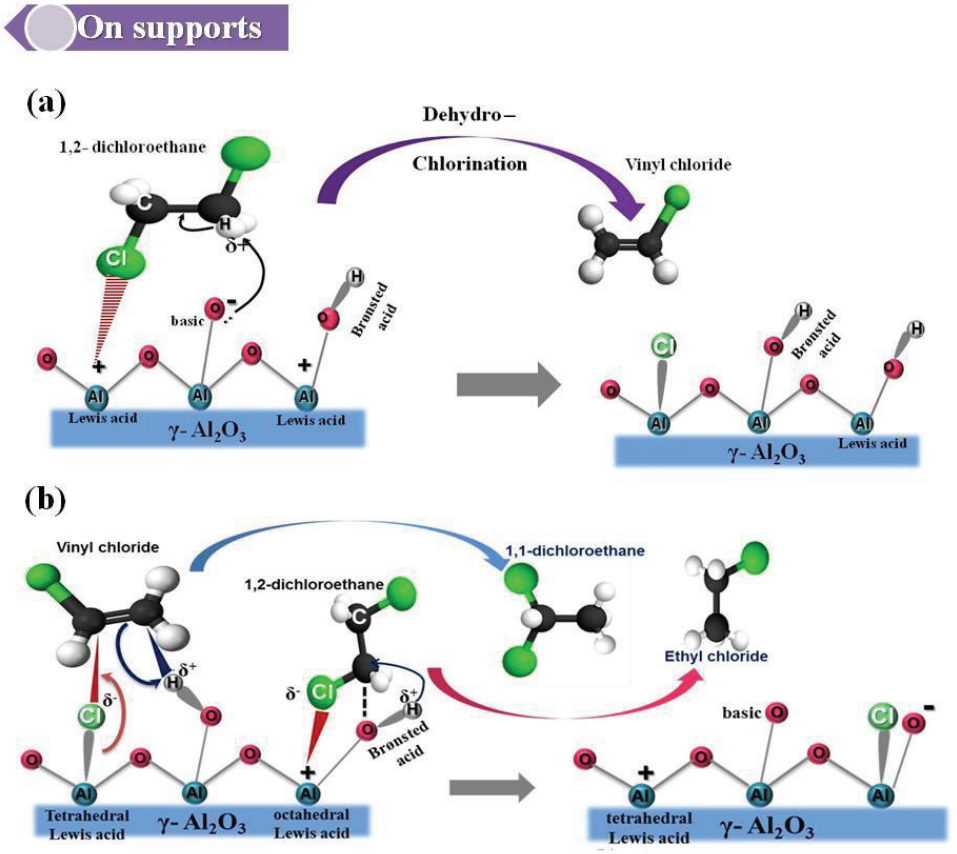

Figure 31: Proposed reaction mechanisms involved in the conversion of EDC via: (a) dehydrochlorination to VCM; (b) hydrochlorination to EC and HCl- addition reaction to form 1,1-EDC

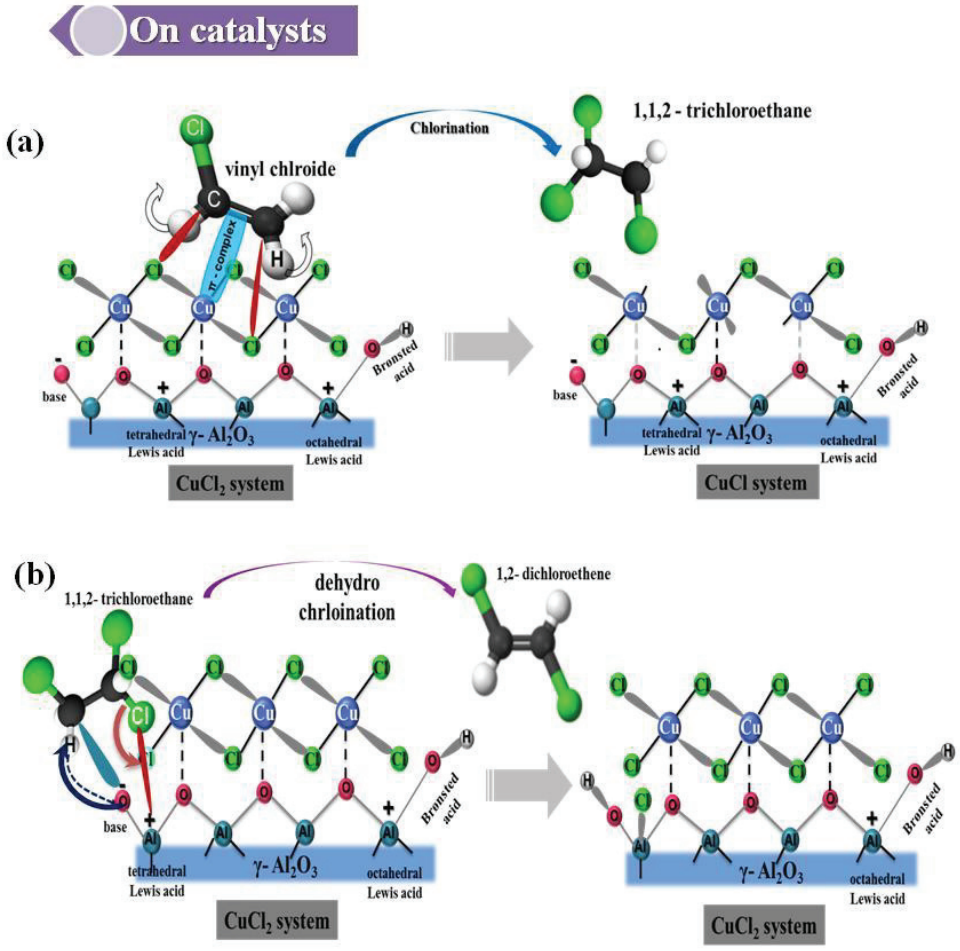

Figure 32: Proposed reaction mechanisms involved in the conversion of EDC via: (a) dehydrochlorination to VCM; (b) hydrochlorination to EC and HCl- addition reaction to form 1,1-EDC

In summary, these experimental results provided valuable information on the site selective mechanism for formation of different by-products from 1,2-dichloro ethane and correlation between the product distribution vs respective dopant added. Besides, that, a very important and eye striking finding is that co-impregnation with both K and La chlorides along with copper chloride on γ- alumina support, very efficiently killed/controlled the by-product formation in the oxychlorination reaction.

Preliminary Report: Operando XAS investigation of the doped copper chloride catalysts for ethylene oxychlorination reaction

N.B. Muddada, F. Giordanino, Y. Jia, T. Fuglerud, U.Olsbye and C. Lamberti

Objective and scope of the work

So, many efforts have been made on the study of the doped copper chloride materials, their catalytic behaviour, the reaction mechanisms in which they are involved and discussed briefly in publications I-IV and unpublished manuscripts. The main aim of the present work is to elucidate how the selective promoters affect $CuCl_x/Al_2O_3$ catalyst during the oxychlorination reaction under various reaction conditions. The study of the catalysts during working conditions would allow for improved understanding on how reactions kinetics changing, structure –relative activity and selectivity relationship (SAR) and, in turn, it will allow for the rational design of better catalytic materials for ethylene oxychlorination reaction. In that respects, the following objectives are intend to study:

1. Effect of temperature on Cu(I)/Cu(II) ratio with respect to the promoter added to make an effort to understand the transient reaction kinetics.
2. Study the surface dynamics under different reaction conditions and correlate the physical characteristics with by-product formation.
3. Effect of K/Cu ratio on the Cu(II)/Cu(I) ratio and also on the formation of K-Cu mixed compound.
4. Effect of different supports for the oxychlorination reaction, here: “UIO-66” was used.

Materials and experimental techniques:

Cu5.0, K3.1Cu5.0, La10.9Cu5.0 and K1.55La5.45Cu5.0 catalysts were subjected to investigation in this present set of experiments. K1.55Cu5.0, K0.75Cu5.0 and $CuCl_2$ containing Zr-MOF (UIO-66) were also studied. Operando XAS technique was used combining with online MS analysis of the product stream.

The three different set of experiments were performed on these materials under varying reaction conditions. In one set of experiments, oxychlorination reaction was studied using an in-situ cell [80] equipped with a provison to hold self supported thin pellet of catalyst, in the temperature range 503- 563 K under varying feed composition. In another set of experiments, ethylene dichloride conversion was studied on K1.55La5.45Cu5.0 catalyst, in

order complement the results provided in the unpublished manuscript, and for the improved understanding on the selectivity. The experimental procedure for the first set of experiments was as follows:

1. The fresh catalyst was subjected to quick XANES at room temperature.
2. The catalyst was heated to 503 K (dT/dt = 10 K/min) under He flow (20 Nml/min). Quick XANES scans were acquired during the ramp up (one spectrum for each 16.6 K) and then kept in an isotherm for an hour; simultaneously four EXAFS scans were collected.
3. The gas feed was switched to the reaction mixture (Oxy_1 = C_2H_4 : HCl : O_2: He = 1: 2: 0.6: 16.4 Nml/min). Qucik XANES scans were performed until a stable Cu (II)/Cu(I) ratio was observed i.e reaction reached the steady state conditions, then flushed the cell with He gas and four EXAFS scans were acquired.
4. Then switched back to feed mixture with simultaneous acquiring of quick XANES scans and after 15minutes, temperature was ramped up to 563 K (dT/dt = 10 K/min) while acquiring quick XANES spectra. Once the steady temperature reached, same set of acquisitions were performed as mentioned in point 3.
5. After acquired the four EXAFS scans under He gas flow, a reaction $mixture_2$ containing excess ethylene (Oxy_2 = C_2H_4 : HCl : O/He : He = 1.6: 0.6: 0.13: 17.6 Nml/min) was introduced. Quick XANES scans were performed until a stable Cu (II)/Cu(I) ratio was observed.
6. The temperature was ramped down to 503 K under the reaction $mixture_2$, while acquiring simultaneous quick XANES spectra. Once the temperature was stable, 4 EXAFS scans were acquired and then further ramped down to room temperature with simultaneous quick XANES spectra collection.

In the second set of experiments, same insitu cell [80] was used and same experimental procedure was followed as explained in unpublished manuscript (provided as an attachment). In course of sequential interaction of the reaction gases, quick XANES spectra were acquired, once it reached the steady state conditions (approx. 30 mins of time on stream), EXAFS spectra were acquired.

Results and Discussions:

An Operando XAS study in transmission mode, for Cu K (8979 eV), was performed. The sequential shots XANES spectra of Cu5.0, K3.1Cu5.0 and K1.55La5.45Cu5.0, during the

oxychlorination reactions at various reaction conditions, at the onset of the measurement with a time resolution of 100s are shown in Figure 33 (a), (b) and (c) respectively. The normalized absorption coefficient $\chi_\mu(E)$ at the onset of the measurement, the selected absorption spectra and their corresponding smoothened first derivative spectra at various reaction stages are shown in Figure 33 (a-c) and (e-g) respectively to illustrate the signal changes during the course of the reaction. The corresponding the activity data calculated from the MS analysis are shown Figure 33 (d).

From Figure 33, the fingerprint evidence is that various spectra changes observed with respective to the dopant added and the conversion of ethylene is increased upon increasing the temperature in case of doped catalysts and K1.55La5.45Cu5.0 catalyst is shown the higher activity. The vertical purple dotted line (in inset part (e)) evidences the huge peak in the first derivative spectrum of the Cu(I) phase at 8981 eV [80]. As the derivative of the spectrum of the Cu(II) phase is negligible at that energy, for any spectrum collected in operando conditions, the intensity of the signal at 8981 eV in its derivative is proportional to the amount of Cu(I) in the sample. However, the intensity of the peaks at later energies (8984.6, 8988, 8991 and 8995 eV) is proportional to the corresponding combined amount of Cu(II) and Cu(I) in the sample. Further careful analysis of the XANES spectra, the discrete transitions corresponding to 1s → 3d, 4s, 4p, 5s and 5p transitions can be assigned to the respective energy peaks. That information can be give further information about he corresponding shake up process for Cu atom, their nearby ligand -metal shake down, which are primarily important in understanding the copper chloride complexes and their structural behavior (as discussed in Chapter 3).

By comparing the derivative XANES spectra of each catalyst, suggesting that a visible dopant effect on Cu(II)/Cu(I) ratio at each stage of the reaction and also the spectra features are quite differentiable which may be due to the modified structural changes have been occurred during each reaction. By a careful analysis of the experimental data using linear combination fitting (LCF) and EXAFS spectra analysis with reference spectra, will provide valuable inputs to obtain the structural dynamics of the copper, and mapping of Cu(II)/Cu(I) ratio during the course of reaction. The information from this XANES and EXAFS data, that structural dynamics and the Cu(II) to Cu(I) ratio during the reaction at different temperatures and at different feed composition is vital to understand the shifting of rate determining step and also the stability of $CuCl_2$, that in turn influence on activity and selectivity of the catalyst, which we are aiming to get the information by further analysis.

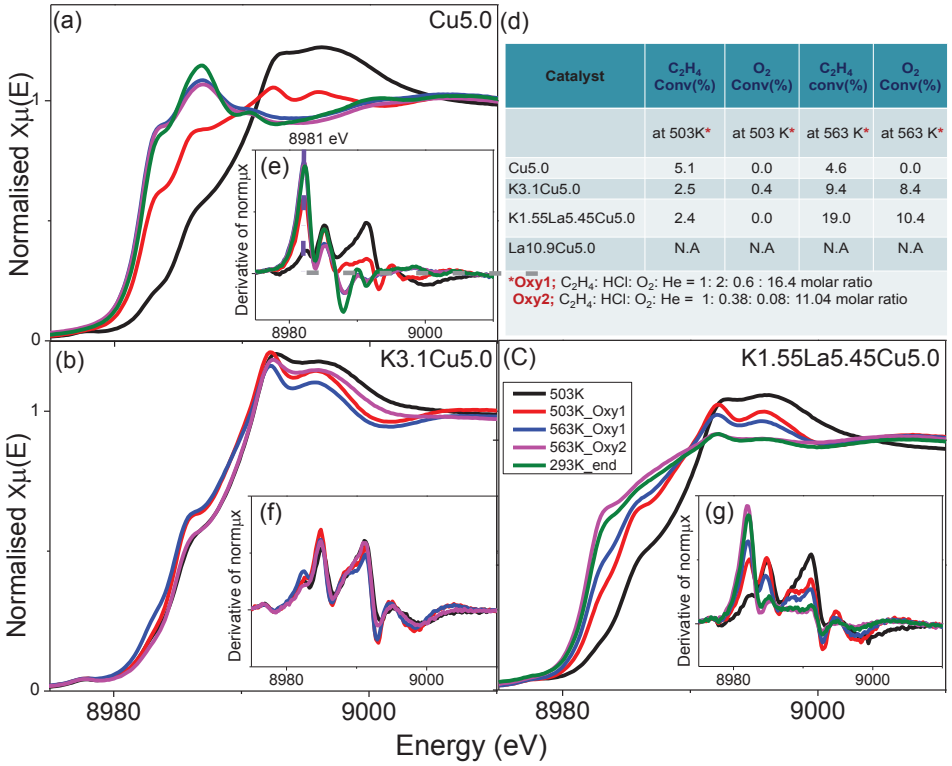

(d)

Catalyst	C_2H_4 Conv(%)	O_2 Conv(%)	C_2H_4 conv(%)	O_2 Conv(%)
	at 503K*	at 503 K*	at 563 K*	at 563 K*
Cu5.0	5.1	0.0	4.6	0.0
K3.1Cu5.0	2.5	0.4	9.4	8.4
K1.55La5.45Cu5.0	2.4	0.0	19.0	10.4
La10.9Cu5.0	N.A	N.A	N.A	N.A

*Oxy1; C_2H_4: HCl: O_2: He = 1: 2: 0.6 : 16.4 molar ratio
Oxy2; C_2H_4: HCl: O_2: He = 1: 0.38: 0.08: 11.04 molar ratio

Figure 33: XANES spectra, collected in transmission mode with the standard step scan acquisition mode, at various reaction stages of the catalysts: (a) Cu5.0, (b) K3.1Cu5.0 and (c) K1.55La5.45Cu5.0 and their corresponding smooth first derivative spectra reported in the insets (e), (f) and (g) respectively. Part (d): Respective catalytic activity measured during the reaction at various stages. ------ black spectra corresponding to the catalysts activated at 503 K, ----- red spectra collected after 30 mins under Oxy1 reaction feed at 503 K, ----- blue spectra collected after 30 mins under Oxy1 reaction feed at 563 K , ---- magenta coloured spectra collected after 30 mins under Oxy2 reaction feed at 563 K, and ---- green spectra collected at the end of experiment under Oxy2 reaction feed at 293 K. The vertical purple dotted line (in inset part (e)) evidences the huge peak in the first derivative spectrum of the Cu(I) phase.

The normalized absorption coefficient $\chi_\mu(E)$ of the selected XANES spectra and their corresponding smoothened first derivative spectra collected at the end of each cycle of interaction of the reactant gas are shown in Figure 34. In Figure 34, part (a) and (d) illustrate the XANES spectra changes during the ethylene interaction (resembling the reduced catalyst i.e CuCl) and the EDC interaction on the reduced catalyst. Part (b) and (e) illustrate the XANES spectra changes during the oxygen interaction (resembling the oxidized catalyst i.e Cu_2OCl_2) and the EDC interaction on the oxidized catalyst. Part (c) and (f) illustrate the XANES spectra changes during the HCl interaction (resembling the re-chlorinated catalyst i.e $CuCl_2$) and the EDC interaction on the re-chlorinated catalyst.

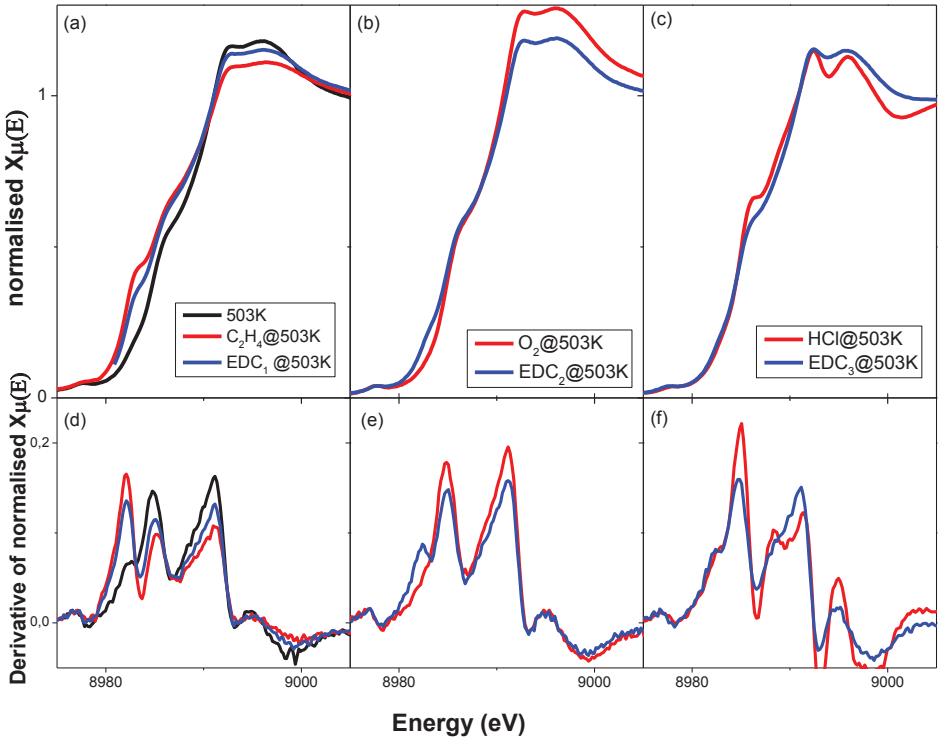

Figure 34: normalised XANES spectra, collected in transmission mode with the standard step scan acquisition mode of K1.55La5.45Cu5.0 catalyst acquired during at the end of each cycle, a) cycle1: interaction with ethylene (---) followed by interaction with EDC (---), b) cycle2: interaction with oxygen (---) followed by interaction with EDC (---), C) cycle3: interaction with HCl (---) followed by interaction with EDC (---) at 503 K. Their corresponding smoothened first derivative spectra are reported in (d), (e) and (f) respectively.

From normalised XANES spectra features and it's derivative spectra, at first instance, ethylene dichloride interacted with the modified catalysts and resulted in considerable changes in the Cu(II)/Cu(I) ratio as well as may on their structural changes, pronouncing on each of the CuCl containing, Cu_2OCl_2 containing and $CuCl_2$ state catalysts. By careful further analysis of the obtained XANES and EXAFS data would reveal important information and would further improve our understanding obtained from the earlier EDC experiments at home laboratory. The comparison of the spectral changes and the corresponding by-product distribution will provide a way to tune the unwanted by-product formation, which is very crucial to improve industrial oxychlorination reactor performance, in turn the VCM process itself.

As a curiosity, $CuCl_2$ containing Zr- MOF was also studied for the ethylene oxychlorination reaction. This material surprisingly showed the redox behaviour upon

interaction with reaction mixture (Ethylene, O_2 and HCl). EXAFS region of the spectra (spectra is not reported for the sake of brevity) for the sample interacted with reaction mixture, we started to loose the Cu signal, it signalling that Cu is leaving the structure, and it confirmed from the in-situ XRD experiments done back in home laboratory at University of Oslo. In summary, this MOF is not stable under acidic environments at higher temperatures (> 393 K), still it is an interesting material for other red-ox reactions.

Conclusions

The present work gave a molecular level insight on the influence of various dopant metals (K, La, Mg, Li, Cs and Ce chlorides) have on the chemical and physical properties of copper chloride based catalysts for/during ethylene oxychlorination reaction. The main conclusion from the reported results and observations can be summarized as:

- All dopant cations compete with the copper ions to occupy the octahedral vacancy sites of γ- alumina support, they consequently contribute to an increase of the available fraction of copper chloride species on the surface, with the following order:

$$La^{3+} > Mg^{2+} > Li^{+} > K^{+} \geq Cs^{+} > Cu^{2+}$$

- The activity of the catalysts for ethylene chlorination (Eq.15) was enhanced with addition of some dopants, in the following order:

$$La10.9Cu5.0 > Mg1.9Cu5.0 > Li0.9Cu5.0 > Cu5.0 > K3.1Cu5.0 \approx Cs10.4Cu5.0$$

- KCl and CsCl dopants interacted with copper and strong indications were found that they formed mixed salts, which might be the reason that these doped catalysts, showed low activity compared to the undoped one.

- All dopants were found to modify the support by influencing the surface acidic properties: La, Mg, and Li dopants increased the strength and population of Brønsted acid sites and increased the Lewis acid strength, but not the population. On the other hand K almost and Cs completely killed the Lewis acid sites, and decreased the Brønsted acid strength.

- Operando XANES experiments suggested that, K and Cs doped catalysts, modified the rate-determining step from the oxidation step (in case of undoped catalyst) either to reduction or to re-chlorination steps. On other hand, La and Mg doped catalysts followed the undoped catalysts, with oxidation as the rate-determining step.

- Steady state fixed bed kinetic tests showed that the promoters increased the activity of the catalysts and selectivity to the target product i.e. EDC, when compared to the base copper chloride catalyst. The following order was observed:

  Activity (C_2H_4 and O_2 conversions): ***K1.55La5.45Cu5.0 > Ce5.5La5.45Cu5.0 >> La10.9Cu5.0 > Mg1.9Cu5.0 > K3.1Cu5.0 > Li0.9Cu5.0 > Cs10.4Cu5.0 >> Cu5.0***

  Selectivity: ***K1.55La5.45Cu5.0 ~ Cs10.4Cu5.0 ~ K3.1Cu5.0 > Ce5.5La5.45Cu5.0 > Mg1.9Cu5.0 > Li0.9Cu5.0 > La10.9Cu5.0 >> Cu5.0***

- The preparation of a co-doped catalyst, K1.55La5.45Cu5.0, with superior activity and selectivity for EDC in the commercial oxychlorination temperature range (503 – 573 K), was based on the insight gained about individual dopants' influence on the Cu/γ-Al_2O_3 oxychlorination catalyst, notably:

  - The ability of lanthanum to compete favourably with copper for the vacancies on the γ-alumina surface, thus enhancing the fraction of available Cu surface sites

  - The ability of potassium to suppress Lewis acid sites and reduce the strength of Brønsted acid sites on the γ-alumina surface, thereby reducing its activity for by-product formation.

- By summarizing the above findings, the studied dopants can be divided into two types of families according to their influence on the catalyst's properties.

  - Family I: K3.1Cu5.0 and Cs10.4Cu5.0

  - Family II: Cu5.0, La10.9Cu5.0, Mg1.9Cu5.0 and Li0.9Cu5.0.

The catalysts belonging to Family I are characterised by an enhanced preference for the Cu(I) state over the Cu(II) state; by suppression/weakening of acid sites on the support surface; and finally, by a lower oxychlorination activity and higher EDC selectivity compared to the undoped catalyst.

The catalysts belonging to Family II are characterised by the competition between the dopants and copper for vacancies on the support surface, leading to an enhanced fraction of exposed Cu surface sites, and hence, to an improved activity for the oxychlorination reaction

compared to the undoped catalyst. Furthermore, these dopants were found to enhance the strength (and population) of acid sites on the support surface, but even so, to improve the EDC selectivity compared to the undoped catalyst. The above findings and observations led to a better fundamental understanding on the effect of promoters on the catalytic properties at molecular level, and implies that together with pure geometrical effects, dopants also have an electronic and steric effect on the catalyst's active species.

Impact of the present results on industrial catalysis:

As stated in the Introduction, current oxychlorination plants are already performing well, with $C_2H_4Cl_2$ selectivities >95 %. However, further improvement of the product yield is desirable, as it influences directly the competitiveness of each plant, as well as the environmental impact of the process. Another important parameter, which has not been targeted here, is catalyst stability, which affects the total productivity of each plant.

Disregarding the catalyst stability issue, the two main activity/selectivity issues of the industrial process for $C_2H_4Cl_2$ production are total hydrogen chloride conversion and minimal combustion. In general the higher the HCl/C_2H_4 ratio, the lower the selectivity to CO_x, and the higher the amount of unconverted HCl. On the other hand, higher activity means higher production of $C_2H_4Cl_2$, but also an increase in the amount of by-products. Therefore, it is necessary to search for a compromise in the industrial operation.

When discussing the industrial implications of the findings of this thesis, it is important to note that the findings are limited to the conditions studied, and that most studies were performed under non-industrial conditions. However, fixed bed reactor tests, Operando XANES and in-situ EXAFS studies along with other complementary techniques have provided better knowledge about the specific dopants effects in that regard, that K and Cs dopants influenced the rate-determining step of reaction, and controlled the activity and selectivity of the reaction. On the other hand, La, Mg dopants increased the activity, and only modestly increased the selectivity. FTIR and reactions tests provided further in-depth knowledge about the influence of HCl, acidity of the support and their influence on activity and selectivity of the reaction. With this knowledge, one possibility to improve the performance of the industrial reactor is to load the reactor with various dopants at different stages,. For example: Loading the top reactor with K or Cs doped catalysts with optimized atomic loading, so that the activity and selectivity will be controlled to avoid the hotspots. In

the subsequent part of the reactor, where the ethene conversion is higher, it can be loaded with more active catalyst, since less by-product formation will take place due to shorter residence time of the end product. The second possibility is to further optimize the so called “better catalyst”, K1.55La5.45Cu5.0, by varying the loading of each dopant under varying reactant feed compositions.

In a short conclusion, the present results can help in tuning the reactor performance and catalyst loadings to optimize the process, and also give leads to further catalyst optimization.

Limitations:

Though, the present set of results (Publication I, II and III) provided the finger print evidence to the presence of the mixed phase containing Cu and K/Cs chlorides, the possibility to treat the second shell contribution of the respective EXAFS data was hindered by the lack of the reference compound of CuK_XCl_{x+2} and $CuCs_xCl_{2+x}$ mixed compounds. The information obtained from further analysis of EXAFS data could have provided the crucial information or the direct evidence of the existence of mixed chloride phase.

The numerical values obtained in the present results could not be used directly to obtain quantitative data for a given industrial reactor. However, reported results have a general value from the chemical point of view, regardless of the type of reactor (fluid or fixed bed), of the type of oxidant used in the feed (air or oxygen), of the feed composition and they can consequently be used to construct useful qualitative trends. The present results cannot able to provide the scientific explanation, why $LaCl_3$ dopants is enhanced the activity of the catalyst than other catalysts, while potassium is inhibiting the by-product formation.

Future Work

In summary, our conclusion is that there is a vital correlation between structure of the active species to their activity, selectivity and stability. However, the dopant's effect needs further investigation. In order to elucidate the most relevant features on this correlation and to elucidate the presence of co-dopants effects on wider prospects of oxychlorination, my suggestions are:

(i) Extend the careful analysis of our recent Operando XAS studies in order to develop a micro kinetic model based on Cu (II)/Cu (I) ratio vs temperature vs dopant vs feed composition.

(ii) Extended analysis of EXAFS data may provide information on the structural changes to the dynamics of the reaction, thus providing a very important base knowledge about structure-relative activity and selectivity relationship (SAR).

(iii) Key complimentary techniques such as FTIR, X-ray photoelectron spectroscopy (electronic features of the influential species) on K1.55La5.45Cu5.0 catalyst will give valuable information on why this catalyst shows the best activity and selectivity.

(iv) Further characterisation of the proposed co-doped catalyst by varying each dopant's loading will give added information.

(v) From all the above-suggested points, information that is more constructive can be provided to tune further the K1.55La5.45Cu5.0 catalyst.

(vi) Stability issues are very important to scale-up the improved catalyst to industrial scale. Therefore, I suggest performing scanning transmission electron microscopy (STEM) studies to have a microscopic point of view on the interaction of dopants with surface and active species, and mobility of these dopants during reaction.

(vii) Detailed mechanistic studies are necessary in order to differentiate the intrinsic and extrinsic effect of dopants.

References

[1] G. Ertl, H. Knözinger, F. Schüth, and, J. Weitkamp (Eds.), Handbook of Heterogeneous Catalysis, 8 volumes, 2nd Edition, Wiley -VCH, , 2008, p. 4270.

[2] M. Bowker, "The Basics and Applications of Heterogenous Catalysis", Oxford University Press, 1998, p. 90.

[3] United Nations, *"Best Available Techniques-Best Environmental Practices (BAT-BEP) for Chemical Processes Involving Chlorine",*, in: *UN Environmentla Programme.,* , 2003.

[4] H. Deacon, Brit. Pat. 1403, (1868).

[5] F.J. Hurter, *J. Soc. Chem. Ind.,* 2 (1868) 106.

[6] J.A. Allen, *J. Appl. Chem.,* 12 (1962) 406-412.

[7] Shell Oil Corporation Ltd, "Shell-Chlor process", in: 1965, pp. US 3,210,158.

[8] A.G. Oblad, *Ind. Eng. Chem.,* 61 (1969) 23-26.

[9] T. Kiyoura, K. Yoshida, H. Nishida, , Shokubai, 33 (1991) 15.

[10] Sumitomo Chemical company Ltd, in: vol JP 4,182,608, 2008.

[11] Uhde brochure, "Chlorine and hydrogen from hydrochloric acid by electrolysis" (1965).

[12] E. I. Dupont de Nermours and Company, HCl electrolysis process using a Nafion exchange membrane, in: US 5,411,641, 1995.

[13] J.A. Allen, A.J. Clark, *Rev. Pure and Appl. Chem.,* 21 (1971) 145.

[14] K. Roka, Brit. Pat. 186,270 (1923).

[15] O. Ernst, H. Wahl, U.S. pat. 1,654,821; German. Pat. 486,952.

[16] K. Roka, E. Kraus, US pat. 1,654,821 (1920).

[17] H.T. Tizard, D.L. Chapman, R. Taylor, Brit.Pat 214,293 (1930).

[18] J.R. Mares, U.S. pat. 1,935, 648 (1920).

[19] W.H. Prahl, U.S.Pat. 1,963,761 and 2,305, 917 (1930).

[20] C.M. Fontana, E. Gorin, G.A. Kidder, R.E. Kinney, *Ind. Eng. Chem.,* 44 (1952) 369–373.

[21] C.M. Fontana, E. Gorin, G.A. Kidder, C.S. Meredith, *Ind. Eng. Chem.,* 44 (1952) 363–368.

[22] C.M. Fontana, E. Gorin, C.S. Meredith, *Ind. Eng. Chem.,* 44 (1952) 373–378.

[23] Socony- Vacuum Oil Co, Brit. Pat. 587,969.

[24] O. Ernst, H. Wahl, German Pat. 430539 (1923).

[25] Y.A. Treger, V.N. Rozanov, *Russ. Chem. Rev.,* 58 (1989) 84-99.

[26] R.M. Crawford, *Chem. Eng. Progr.,* 46 (1950) 483.

[27] M.M. Mallikarjunan, Z.S. Hussain, *J.Sci. and Ind. Res.,* 42 (1983) 209 - 229.

[28] J.A. Allen, *J. Appl. Chem.,* 16 (1966) 327-332.

[29] F. Bruke, R. Muller, *Chem Week,* 95 (1964) 93.

[30] Nexant Chem systems, ICIS, Global Business Reports, *"VCM gloabl report",* (2009-2012).

[31] M. Rossberg, et al, "*Chlorinated Hydrocarbons*" in Ullmann's Encyclopedia of Industrial Chemistry" Wiley-VCH (2006) Weinheim.*doi:10.1002/14356007.a14356006 14356233.pub14356002*.

[32] Charles E. Wilkes, James W. Summers, Charles A. Daniels, (Eds). "PVC Handbook", Hanser Gardner Publications, Inc., Munich, 2005.

[33] Ray Harmann, Ian Michael Clegg, in: vol US. Pat. 667845 (1998); US. Pat. 5,278,905 (1998); US. Pat. 5,763,710 (1998)

[34] E.J. Mark, M.O. Michael, A.H. Daniel, in: vol US. Pat. 6,797,845 (2000).

[35] Uhde brochure, "Vinnolit Technology", in: http://www.uhde.eu/competence/technologies/organic-chemicals/264/268/edc-oxychlorination.html.

[36] J.S. Eden, J.A. Cowfer, in: US Pat. 4849393, 1989.

[37] G.H. Young, J.A. Cowfer, V.J. Johnston, US.Pat. 5292703 (1994).

[38] J.S. Eden, US. Pat. 4,446,249 (1984).

[39] PSE, "PSE enterprises Ltd", in: www.pseenterprise.com.

[40] J.C.S. Moreira, C.A.M. Pires, *Cand.J.Chem.Eng.,* 88 (2001) 350 - 358.

[41] P. Trambouze, J. Euzen, "Chemical Reactors: From Design to Operation", (2004).

[42] R.W. McPherson, C.W. Starks, and, G.J. Fryar, *J. Hydrocarbon proc.,* 58 (1979) 75.

[43] Jeremey dry et al., "VCM production"- Capstone design project , (2003).

[44] H.M. Stanley, *Proc. Roy. Soc.,* A303 (1968) 259.

[45] M.L. Sepctoe, H. Heinemann, and, K.D. Miller, *Ind, Eng, Chem., Process design Develop.,* 6 (1967) 327.

[46] J.A. Little, and, C.N. Kenny, *J. Catal.,* 93 (1985) 23.

[47] E.H. Catherine, G.S. Alan, "Inorganic Chemistry", 3rd Edition, Pearson Prentice Hall, 2008.

[48] E.M. Fortini, C.L. Garcia, and, D.E. Resasco, *J. Catal.,* 99 (1986) 12-18.

[49] A.F. Wells, *" Structral Inorganic Chemistry"*, in: Oxford University press, London, 1984.

[50] A.F. Wells, " The crystal Structure of anhydrous cupric chloride, and the Sterochemistry of the Cupric Atom", J.of the Chem. Soc., (1947) 1670-1675.

[51] S.R. Desjardins, D.E. Wilcox, R.L. Musselamn, E.I. Solomon, *Inorg. Chem.,* 26 (1987) 288-310.

[52] M. Newurock, X. Zhang, M. Olken, M.E. Jones, D. Hickman, T. Calverley, R. Gulotty, *J. Phys. Chem. B,* 105 (2001) 1562-1572.

[53] H. Okabe, K. Suzuki, K. Kawashima, T. Muranka, J. Akimitsu, *J. Phys. Soc. Jpn.,* 75 (2006) 123705-123701 to 123704.

[54] M. Nishiyama, A. Oyamada, T. Itou, S. Megawa, H. Okabe, J. Akimitsu, *J. Phys. : Conference series,* 320 (2011) 012030 (012031-012036).

[55] R. Fricke, W. Neugebauer, and, H. Sachafer, "Uber die Einwirkung wassriger Kupferchlorid - Losungen auf gamma- Aluminiumoxyd", *Z.Anorg. Allg. Chem.,* 273 (1953) 215 - 226.

[56] G. Leofanti, M. Padovan, M. Garilli, D. Carmello, A. Zecchina, G. Spoto, S. Bordiga, G.T. Palomino, C. Lamberti, *J. Catal.,* 189 (2000) 91-104.

[57] G. Leofanti, M. Padovan, M. Garilli, D. Carmello, G.L. Marra, A. Zecchina, G. Spoto, S. Bordiga, C. Lamberti, *J. Catal.,* 189 (2000) 105-116.

[58] M.Y. Skripkin, and, L.V. CheryKh, *Russ. J. Inorg. Chem. ,* 39 (1994) 1747.

[59] Kearley, and, A. Robert, PPG Industries. Inc, EP. Pat. 0041330, (1981).

[60] L.V et al., *J. Raman Spectrosc.,* 39 (2008) 16 -31.

[61] Roger. D.W et al., *J. Chem.phy.,* 38 (1963) 2429.

[62] J.J. de Boer, D. Bright, and, J.N. Helle, *Acta. Cryst.,* (1972) 3436 -3438.

[63] L.V. Stepakova, M.Y. Skripkin, L.V. CheryKh, I.M. Gusev, *Russ. J. Gen. Chem.,* 76 (2006) 512-516.

[64] D.M. Rutheven, and, C.N. Kenny, *Chem. Eng. Sci.,* 22 (1967) 1561-1570.

[65] D.M. Rutheven, and, C.N. Kenny, *J. Inorg. Nucl. Chem.,* 30 (1968) 931-944.

[66] D.M. Rutheven, and, C.N. Kenny, *Chem. Eng. Sci.,* 23 (1968) 981-990.

[67] W.M.H. Sachtler, and, J.N. Helle, *Chemisorption and Catalysis:* "Thermodynamic Investigation of Deacon-Type Catalysts", in: Institute of Petroleum, London, 1970.

[68] K. Zurowski, *J. Thermal Anal.,* a) 36 (1990) 947; b) 36 (1990) 545; c) 37 (1991) 721-726; d) 37 (1991) 835-840; e) 38 (1992) 2369-2375; f) 44 (1995) 197-204; g) 45 (1995) 447-455; h) 47 (1996) 775-790.

[69] R.L. Dotson, *J. Catal.,* 33 (1974) 210-218.

[70] Å. Berg, *Z.anorg. allg. Chem.,* 583 (1990) 145-151.

[71] Muller et al., US. Pat. 5,986,152 (1999).

[72] A.J. Rouco, *J. Catal.,* 157 (1995) 380-387.

[73] A. Arcoya, A. Cortes, X.L. Seoane, *Can. J. Chem. Eng.* 60 (1982) 55-60.

[74] Y.A. Treger, V.N. Rozanov, M.R. Fild, and, L.M. Kartashov, *Russ. Chem. Rev.,* 57 (1988) 326-335.

[75] P.S.S. Prasad, K.B.S. Prasad, P.K. Rao, V.K. Kaushik, *J. Mater. Sci.,* 32 (1997) 1479-1482.

[76] C. Lamberti, S. Bordiga, M. Salvalaggio, G. Spoto, A. Zecchina, F. Geobaldo, G. Vlaic, M. Bellatreccia, *J. Phys. Chem. B,* 101 (1997) 344-360.

[77] V. Bolis, S. Maggiorini, L. Meda, F. D'Acapito, G. Turnes Palomino, S. Bordiga, C. Lamberti, *J. Chem. Phys.,* 113 (2000) 9248-9261.

[78] G. Leofanti, A. Marsella, B. Cremaschi, M. Garilli, A. Zecchina, G. Spoto, S. Bordiga, P. Fisicaro, G. Berlier, C. Prestipino, G. Casali, C. Lamberti, *J. Catal.,* 202 (2001) 279-295.

[79] G. Leofanti, A. Marsella, B. Cremaschi, M. Garilli, A. Zecchina, G. Spoto, S. Bordiga, P. Fisicaro, C. Prestipino, F. Villain, C. Lamberti, *J. Catal.,* 205 (2002) 375-381.

[80] C. Lamberti, C. Prestipino, F. Bonino, L. Capello, S. Bordiga, G. Spoto, A. Zecchina, S.D. Moreno, B. Cremaschi, M. Garilli, A. Marsella, D. Carmello, S. Vidotto, G. Leofanti, *Angew. Chem. Int. Edit.,* 41 (2002) 2341-2344.

[81] A. Baiker, W.L. Holstein, *J. Catal.,* 84 (1983) 178-188.

[82] P.A. Sermon, K. Rollins, P.N. Reyes, S.A. Lawrence, M.A. Martin Luengo, M.J. Davies, *J. Chem. Soc. Farad. Trans. 1,* 83 (1987) 1347-1353.

[83] P.S. Sai Prasad, P. Kanta Rao, *J. Chem. Soc. Chem. Commun.,* (1987) 951-952.

[84] C.L. Garcia, D.E. Resasco, *J. Catal.,* 122 (1990) 151-165.

[85] A.J. Rouco, *Appl. Catal. A: General,* 117 (1994) 139-149.

[86] C. Prestipino, G. Berlier, F.X. Llabres i Xamena, G. Spoto, S. Bordiga, A. Zecchina, G. Turnes Palomino, T. Yamamoto, C. Lamberti, *Chem. Phys. Lett.,* 363 (2002) 389-396.

[87] A.J.A.a.C.A. J, *Rev. Pure and Appl. Chem.,* 21| (1971).

[88] C. Lamberti, C. Prestipino, L. Capello, S. Bordiga, A. Zecchina, G. Spoto, S.D. Moreno, A. Marsella, B. Cremaschi, M. Garilli, S. Vidotto, G. Leofanti, *Int. J. Mol. Sci.,* 2 (2001) 230-245.

[89] S.e. Penner, A.L. Malone III, US 3148222 (1964).

[90] S. Altuglu, R.W. Roberts, *Ind. Eng. Chem. Process Des. Dev.,* 12 (1973) 160-164.

[91] T.Z. Zhang, C. Troll, B. Rierger, J. Kintrup, O.F.K. Schluter, R. Weber, *J. Catal.,* 270 (2010) 76-85.

[92] M. Strebelle, A. Petritjean, Solvay, US 7807604 (2010).

[93] P.G. Hall, P. Heaton, D.R. Rosseinsky, *J. Chem. Soc., Faraday Trans. 1,* 80 (1984) 3059-3070.

[94] I. Chorkendroff, J.W. Niemantsverdriet (Eds.), "Concepts of Modern Catalysis and Kinetics", Wiley - VCH.,, 2007, p. 267.

[95] X. Youchang, Z. Huixin, and, W. Ronghua, *Scientia Sinica,* 23 (1980) 979-991.

[96] H.D. Eichhron, J. Jackh, W.D. Mross, H. Schuler, BASF, "Activity and Selectivity relationships in the oxychlorination of ethylene on $CuCl_2$-KCl / g -Al_2O_3 catalysts", in: *8th International Congression on Catalysis,* , vol IV-647, 1985.

[97] S. Wachi, and, Y. Asai, *Ind. Eng. Chem. Res.,* 33 (1994) 259-264.

[98] P.S. Sai Prasad, K.B.S. Prasad, and, M.S. Ananth, *Ind. Eng.Chem. Res.,* 40 (2001) 5487-5495.

[99] EPA, "Locating and estimating air emissions from sources of ethylene dichloride", in: EPA-450/4-84-007d, *United States Environmental protection Agency,*, 1984.

[100] B. Mile, T.A. Ryan, T.D. Tribbeck, M.A. Zammitt, G.A. Hughes, *Topics in Catal.,* 1 (1994) 153-162.

[101] P. Avila, J. Blanco, J.L. Garcia-Fierro, S. Mendiroz, and, J. Soria, *New Horizons in Catalysis,* 78 (1982).

[102] A.B. Stiles, "Catalyst supports and supported catalysts: theroretical and applied concepts", in: Butterworths, Boston 1987.

[103] C. Morterra, G. Cerrato, V. Bolis, *Catal. Today,* 17 (1993) 505-515.

[104] M. Trueba, S.P. Trasatti, *Eur. J. Inorg. Chem.,* (2005) 3393-3403.

[105] E. santacesaria, D. Gelosa, *Ind, Eng, Chem., Prod. Res. Dev.,* 16 (1977) 45-46.

[106] C. Zipelli, J.C.J. Bart, G. Petrini, S. Galvagno, and, C. Cimino, *Z.anorg. allg. Chem.,* 502 (1983) 199.

[107] N. Todo, M. Kurita, and, J. Hugiwana, *Chem. Soc. Japan, Industr. Chem. Soc. ,* 8 (1966) 69 *(I couldn't able to access)*.

[108] J. Valle, A. Vargas, J.M. Ferreira, A. Flores, and, O. Novaro, *Stud. Surf. Sci. Catal.,* (1981) 1040-1046.

[109] J. Blanco, J. Fayos, B. Garcia, and, J. Soria, *J. Catal.,* 31 (1973) 257.

[110] J. Blanco, R. Blanco, A. Cortes, J. Soria, *Nat. Phys. Sci.,* 22 (1971) 155-156.

[111] A. Baiker, D. Monti, and, A. Wokaun, *Appl. Catal.,* 23 (1986) 425-436.

[112] G.C. Bond, S.N. Namijo, and, J.S. Wakeman, *J. Mol. Catal.,* 64 (1991) 305.

[113] Y.-C. Xie, Y.-Q. Tang, "Spotaneous of monolayer dispersion of oxides and salts on to the surface of supports: Applications to Heterogenous Catalysis", in: *Academic Press Inc.*, , 1990.

[114] E. Finocchio, N. Rossi, G. Busca, M. Padovan, G. Leofanti, B. Cermaschi, A. Marsella, D. Carmello, *J. Catal.,* 179 (1998) 60-618.

[115] D. Carmello, E. Finocchio, A. Marsella, B. Cremaschi, G. Leofanti, M. Padovan, G. Busca, *J. Catal.,* 191 (2000) 354-363.

[116] C.G. Timothy, C.K. Wilbur, C.W. Frederick, US Pat., 5,126,310 (1990).

[117] C. Xiaohai, X. Youchang, G. Linlin, T. Youqi, *Petrochemical Tech.,* 04 (1992).

[118] C. Lamberti, S. Bordiga, F. Bonino, C. Prestipino, G. Berlier, L. Capello, F. D'Acapito, F.X. Llabres i Xamena, A. Zecchina, *Phys. Chem. Chem. Phys.,* 5 (2003) 4502-4509.

[119] M. Fernández-García, I. Rodríguez-Ramos, P. Ferreira-Aparicio, A. Guerrero-Ruiz, *J. Catal.,* 178 (1998) 253-263.

[120] P.G. Hall, M. Parsley, D.R. Rosseinsky, R.A. Hann, K.C. Waugh, *J. Chem. Soc., Faraday Trans. 1,* 79 (1983) 343-361.

[121] P.G. Hall, P. Heaton, D.R. Rosseinsky, *J. Chem. Soc., Faraday Trans. 1,* 80 (1984) 2785-2802.

[122] C. Xiaohai, X. Youchang, G. Linlin, T. Youqi, *Petrochemical Tech.,* 02 (1992).

[123] H.Y. Huang, J. Padin, R.T. Yang, *Ind. Eng. Chem. Res.,* 38 (1999) 2720-2725.

[124] V.I. Avdeev, V.I. Kovalchuk, G.M. Zhidomirov, J.L. d'Itri, *J. Struct. Chem.,* 48 (2007) S160-S170.

[125] X. Youchang, C. Xiaohai, G. Linlin, T. Youqi, *Acta Physico-chemica Sinica,* 06 (1986).

[126] C. Prestipino, S. Bordiga, C. Lamberti, S. Vidotto, M. Garilli, B. Cremaschi, A. Marsella, G. Leofanti, P. Fisicaro, G. Spoto, A. Zecchina, *J. Phys. Chem. B,* 107 (2003) 5022-5030.

[127] L. Jie, L. Xueju, Z. Guangdong, Z. Kaiji, Z. Wenxiang, C. Tiexin, *React. Kinet, Catal. Lett.,* 88 (2006) 315-323.

[128] P.G. Hall, P. Heaton, D.R. Rosseinsky, *J. Chem. Soc., Faraday Trans. 1,* 80 (1984) 2777-2783.

[129] P.G. Hall, P. Heaton, D.R. Rosseinsky, *J. Chem. Soc., Faraday Trans. 1,* 81 (1985) 69-82.

[130] P.G. Hall, P. Heaton, D.R. Rosseinsky, *J. Chem. Soc., Faraday Trans. 1,* 81 (1985) 83-89.

[131] M. loos, J. Goulon, M. Bertucci, R. Bachelard, *Journa de Physique,* C8 (1986) 285-288.

[132] M. loos, J. Goulon, M. Bertucci, R. Bachelard, *Physica B,* 158 (1989) 188-190.

[133] K. Naumberg, G. Schwedler, *Chem. Ind. Techn.,* 39 (1967) 505.

[134] R.V. Carruba, J.V. Spenser, *Ind. Eng. Chem. Process Des. Develop.,* 9 (1970) 414-419.

[135] C. Fengqiu, Y. Yongrong, R. Shaunxi, C. Cantang, *Petrochemical Tech.,* 07 (1994).

[136] C. Wirotsakul, J. Panpranot, P. Praserthdam, TIChE International Conference, Thailand, cr018 (2011) 1-4.

[137] Z. Benhui, Z. Jingquan, *Petrochemical Tech.,* 01 (1985).

[138] M.P. Dmitrieva, Y.M. Bakshi, A.I. Gel'bshtein, *Kinet. and Catal.,* 37 (1996) 85.

[139] Z. Benhui, and, Z. Jingquan, *Petrochemical Tech.,* 01 (1985).

[140] P.P. Nicholas, R.T. Carroll, *J. Org. Chem.,* 33 (1968) 2345.

[141] K.E. Nelson, D.T. Sawyer, A.E. Martell (Eds.), "Industrial Environmental Chemistry", *Plenum*, Newyork, 1992, p.

[142] NASA, "Oxidation of chlorinated hydrocarbons", in: USA, 1995.

[143] G.R. Lester, *Catal. Today.,* 53 (1999) 407.

[144] A. Maccol, *Chem. Rev.,* 69 (1969) 33-60.

[145] M.M.R. Feijen-Jeurissen, J.J. Jorna, B.E. Neiuwenhuys, G. Sinquin, C. Petit, J.P. Hindermann, *Catal. Today.,* 54 (1999) 65-79.

[146] S.A. Kurta, *Catalysis in Industry,* 3 (2011) 136-143.

[147] A.G. Aglulin, *Kinet. and Catal.,* 50 (2009) 427-434.

[148] r. Schirmeister, J. Kashsnitz, M. Trager, *Ind. Eng. Chem. Res.,* 48 (2009) 2801-2809.

[149] S.R. de Miguel, O.A. Scelza, A.A. Castro, J. Soria, *Topics in Catal.,* 1 (1994) 87-94.

[150] S. Wang, A.Y. Borisevich, S.N. Rashkeev, M.V. Glazoff, K. Sohlberg, S.J. Pennycook, S.T. Pantelides, *Nature Materials,* 3 (2004) 143-146.

[151] P. Burtin, J.P. Brunelle, P. Pijolat, M. Soustelle, *Appl. Catal.,* 34 (1987) 225-238.

[152] A. Marsella, D. Carmello, E. Finocchio, B. Cremaschi, G. Leofanti, M. Padovan, G. Busca, *Stud. Surf. Sci. Catal.,* 130 (2000) 1823-1828.

[153] F. Casagrande, O. Carlo, Sud Chemie; US7687429(2010); US0129008 A1 (2006).

[154] F. Casagrande, M. Marinella, US6452059 (2002).

[155] L. Cavalli, F. Casagrande, US 6759365 (2002).

[156] J.S. Eden, J.A. Cowfer, US 4446249 (1984); US 4849393 (1989).

[157] Eichhron et al., BASF, US 4,740, 644 (1988).

[158] EVC Technologies AG, US6465701 (2002); US 6777373 (2004); US6180841 (2001); US5841009 (1998); US 5763710 (1998).

[159] D. Helmut, M. Strebelle, Solvay, EP 0494474B1 (1991); US8049047 (2011); US8058490 (2011) ; US8071827 (2011); US7807604 (2010).

[160] R.P. Hirschmann, J.W.O. Beard, E.L. Mainz, E.B. Smith, B.M. Little, US5098878 (1992).

[161] Ineos Vinyls UK Ltd, US7141708 (2006); .

[162] E.L. Mainz, J. Beard, W.Q., R.P. Hirschmann, B.M. Little, E.B. Smith, US 5192733 (1993); US5113027 (1992); US5098878 (1992); US5004849 (1991).

[163] Produits Chimiques Pechiney-Saint Gobain, US3983181 (1976); US3992463 (1976); .

[164] I. Schussler, W. Henry, US 6174834 (2001).

[165] SUED-CHEMIE CATALYSTS ITALIA S.R.L., US 20100152505 (2010); US 20100160697 (2010); US8216960 (2012).

[166] H. Urtel, H. Junicke, BASF, *U.S. Pat. Appl.,* 0274061 (2010).

[167] I.I. Kurlyandskaya, V.Y. Danyushevskii, I.G. Solomonik, T.F. Kudryavtseva, V.I. Yakerson, *Physical Chemistry (translated fromSeriya Khimicheskaya),* 6 (1987) 1220-1225; 44 (1970) 2931; (1979) 271; .

[168] I.I. Kurlyandskaya, I.G. Solomonik, E.D. Glazunova, Y.A. Treger, M.R. Flid, *Kinet. and Catal.,* 42 (2001) 381-389.

[169] C.L. Garcia, D.E. Resasco, *Appl. Catal.,* 29 (1989) 55-66.

[170] Montepollmeri, EP119933.

[171] L. Xueju, L. Jie, Z. Guangdong, Z. Kaiji, L. Wenxing, C. Tiexin, *Catal. Lett.,* 100 (2005) 153-159.

[172] Z. Chen, M. Han, D. Wang, F. Wei, *Chin. J.Catal.,* 29 (2008) 951-953.

[173] L. Chao, Z. Guangdong, W. Liping, D. Shuli, L. Jing, C. Tiexin, *Appl. Catal. A. General,* 400 (2011) 104-110.

[174] L. Chao, Z. Guangdong, W. Liping, L. Zhe, X. Yingxue, C. Tiexin, *Catal. Comm.,* 13 (2011) 22-25.

[175] EVC Technologies AG, US6,777,373.

[176] Enichem, EP 0278922.

[177] GEON, US 4,446,249; US 4,849,393.

[178] Solvay, EP-A-0255156; US 5,260,247.

[179] Toyo Soda, US 3,624,170.

[180] P.S. Sai Prasad, R.V. Nageshwar, K.B.S. Prasad, P. Kanta Rao, *Solid State Ionics,* 42 (1990) 117-119.

[181] Christian. K et al, US7126035 (2006).

[182] BASF Catalysts LLC, US7,902,411 (2011).

[183] C. Lamberti, E. Groppo, G. Spoto, S. Bordiga, A. Zecchina, *Adv. Catal.,* 51 (2007) 1-74.

[184] C. Lamberti, A. Zecchina, E. Groppo, S. bordiga, *Chem. Soc. Rev.,* 39 (2010) 4951-5001.

[185] A. Zecchina, D. Scarano, S. Bordiga, G. Spoto, C. Lamberti, *Adv. Catal.,* 46 (2001) 265-397.

[186] A. Zecchina, S. Bordiga, M. Salvalaggio, G. Spoto, D. Scarano, C. Lamberti, *J. Catal.,* 173 (1998) 540-542.

[187] S.H. Strauss, *J. Chem. Soc.-Dalton Trans.,* (2000) 1-6.

[188] A.J. Lupinetti, S.H. Strauss, G. Frenking, *Prog. Inorg. Chem.,* 49 (2001) 1-112.

[189] V. Bolis, A. Barbaglia, S. Bordiga, C. Lamberti, A. Zecchina, *J. Phys. Chem. B,* 108 (2004) 9970-9983.

[190] R. Wischert, C. Coperet, F. Delbecq, P. Sautet, *ChemCatChem.,* 2 (2010) 812.

[191] E.A. Stern, in: vol 3, Koningsberger, D. C. and Prins, R. (Ed.;) http://www-ssrl.slac.stanford.edu/mes/xafs/xas_intro.html., *Willey & Sons: New York*, 1988.

[192] P.A. Lee, P.H. Citrin, P. Eisenberger, B.M. Kincaid, *Rev. Mod. Phys.,* 53 (1981) 769-806.

[193] G. Bunker, S. Hasnain, D. Ayers, "In X-ray Absorption Fine Structure":Hasnain, S. S. Ed., Ellis Horwood: , New York, 1991.

[194] A. Filipponi, A. DiCicco, C.R. Natoli, *Phys. Rev. B,* 52 (1995) 15122–15134.

[195] A. Filipponi, A. DiCicco, a)*Phys. Rev. A,* 52 (1995) 1072–1078; b) *Phys. Rev. B,* 52 (1995) 15135–15149.

[196] S. Bordiga, F. Bonino, K.P. Lillerud, C. Lamberti, *Chem. Soc. Rev.,* 39 (2010) 4885-4927.

[197] F. Boscherini, *"X-ray absorption fine structure in the study of semiconductor heterostructures and nanostructures, in Characterization of Semiconductor Heterostructures and Nanostructures":* ed. C. Lamberti,, Elsevier, Amsterdam, 2008.

[198] D.E.S. Sayers, E. A.; Lytle, F. W., *Phys. Rev. Lett.* 27 (1971) 1204.

[199] L.J. Murray, M. Dinc, J.R. Long, *Chem. Soc. Rev. ,* 38 (2009) 1294.

[200] E.A. Stern, *Phys. Rev. B: Solid State,* 10 3027.

[201] B.R. Quote, M. Newville, *J. Synchrot. Radiat.,* 12 (2005) 537.

[202] C. Lamberti, C. Prestipino, S. Bordiga, G. Berlier, G. Spoto, A. Zecchina, A. Laloni, F. La Manna, F. D'Anca, R. Felici, F. D'Acapito, P. Roy, *Nucl. Instrum. Meth. B.* 200 (2003) 196-201.

Appendix

Publications I –IV and Unpublished Manuscript

Naresh Babu Muddada

Publication I

Dalton Transactions 2010

Quantification of copper phases, their reducibility and dispersion in doped-$CuCl_2/Al_2O_3$ catalysts for ethylene oxychlorination

N. B. Muddada, U. Olsbye, G. Leofanti, D. Gianolio, F. Bonino, S. Bordiga, T. Fuglerud, S. Vidotto, A. Marsella, C. Lamberti

This article is published as part of the *Dalton Transactions* themed issue entitled:

Bridging the gap in catalysis *via* multidisciplinary approaches

Guest Editors: Christophe Coperet and Rutger van Santen
Université de Lyon, France and Eindhoven University of Technology, The Netherlands

Published in issue 36, 2010 of *Dalton Transactions*

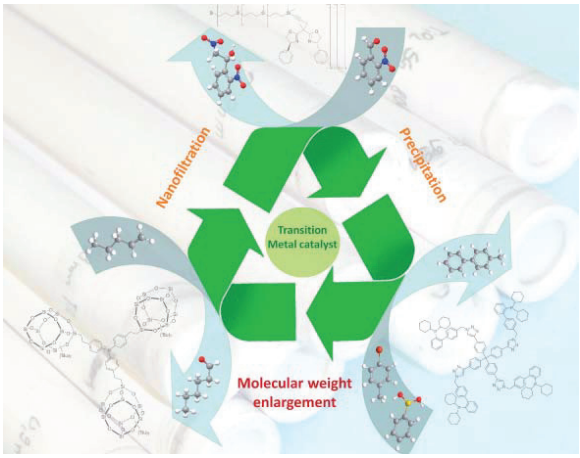

Image reproduced with the permission of Dieter Vogt

Articles in the issue include:

Quantification of copper phases, their reducibility and dispersion in doped-$CuCl_2/Al_2O_3$ catalysts for ethylene oxychlorination

N. B. Muddada,[a] U. Olsbye,[a] G. Leofanti,[b] D. Gianolio,[c] F. Bonino,[c] S. Bordiga,[c] T. Fuglerud,[d] S. Vidotto,[e] A. Marsella[e] and C. Lamberti*[c]

Received 17th May 2010, Accepted 3rd August 2010
DOI: 10.1039/c0dt00488j

The comprehensive understanding of the composition, behaviour and reactivity of a catalyst used inside industrial plants is an extremely hard task that is rarely achieved. It requires the use of different spectroscopic techniques, applied under *in situ* or in operando conditions, and combined with the investigation of the catalyst activity. Often the operating experimental conditions are different from technique to technique and the different results must be compared with care. In the present contribution, we combined *in situ* XANES/EXAFS, IR spectroscopy of adsorbed CO, CO chemisorption and catalytic tests performed using a pulse reactor in depletive mode. This multitechnical approach resulted in the understanding of the role that dopants (LiCl, KCl, CsCl, $MgCl_2$ $LaCl_3$) have in the nature, relative fraction, reducibility and dispersion of Cu-phases on $CuCl_2/\gamma$-Al_2O_3 catalysts for oxychlorination reaction, a key step of the PVC chemistry. In the undoped catalyst two Cu phases coexist: Cu-aluminate and supported $CuCl_2$, being the latter the only active one [*J. Catal*., 2000, **189**, 91]. EXAFS and XANES highlighted that all dopants contribute more or less efficiently in increasing the fraction of the active copper species, that reaches a value of almost 100% in the case of $MgCl_2$ or $LaCl_3$. EXAFS directly, and IR indirectly, proved that the addition of KCl or CsCl (and less efficiently of LiCl) results in the formation of mixed CuK_xCl_{2+x} or $CuCs_xCl_{2+x}$ phases, so altering the chemical nature of the active phase. XANES spectroscopy indicates that addition of $MgCl_2$ or $LaCl_3$ does not affect the reducibility by ethylene (under static conditions) of the active $CuCl_2$ phase and that the reducibility of the new copper-dopant mixed chloride are in the order $CuCl_2 > CuLi_xCl_{2+x} > CuK_xCl_{2+x} > CuCs_xCl_{2+x}$. However, when reduction is done inside a pulse reactor, a more informative picture comes out. The last technique is able to differentiate all samples, and their ability to be reduced by ethylene resulted in the order: La- > Mg- > Li-doped > undoped > K- > Cs-doped catalyst. To understand this apparent discrepancy the dispersion of the active phase, measured by CO chemisorption, was needed: it has been found that addition of LiCl increases enormously the dispersion of the active phase, $LaCl_3$ significantly and $MgCl_2$ barely, while addition of both KCl and CsCl results in a decrease of the surface area of the active phase. The mechanism of the enhancing effect of La and Mg on catalytic activity is still not clear, but it could be associated to the modification that they induce to the support surface: the Cu is so highly dispersed that almost all is in direct contact with support surface. It is finally worth noticing that the previous EXAFS and XANES study allowed us to refer the chemisorption data to the active phase only, while the IR study allowed us to fix the Cu^+/CO surface stoichiometry. Summarizing the use of a multidisciplinary approach has been the *conditio sine qua non* (mandatory condition) to understand the complex role that the different additives have on the active phase of the $CuCl_2/\gamma$-Al_2O_3 catalysts for ethylene oxychlorination.

1. Introduction

Oxychlorination of ethylene is by far the most important route to produce 1,2-dichloroethane (EDC), which is the main intermediate to produce poly-vinyl chloride (PVC). It offers a significant economic benefit in two ways: firstly it uses cheap and abundant feedstock and secondly it incorporates the recycling of waste hydrogen chloride produced in cracking EDC (1). Hence it is in agreement with the modern requests of chemical industry[1–3] that need more environmental friendly reactions. It is evident that oxychlorination is a key-process in the modern chemical industry, playing a relevant role for chlorine atom incorporation in hydrocarbons, both saturated and unsaturated, *e.g.*, in methane, ethylene and benzene.[4,5]

Almost all the world production of PVC is nowadays produced by the polymerization of vinyl chloride monomer (VCM). Production of VCM is based on cracking of 1,2-dichloroethane (EDC) following reaction (1),

[a]*inGAP centre of Research-based Innovation, Department of Chemistry, University of Oslo, Sem Saerlandsvei 26, N-0315, Oslo, Norway*
[b]*Consultant, Via Firenze 43, 20010, Canegrate, Milano, Italy*
[c]*Department of Inorganic, Physical and Materials Chemistry and NIS centre of excellence, University of Torino, Via P. Giuria 7, I-0125, Torino, Italy. E-mail: carlo.lamberti@unito.it; Fax: +39 011-6707855; Tel: +39 011-6707841*
[d]*Technology and Projects, INEOS ChlorVinyls, Heroya Industrial Park, N-3936, Porsgrunn, Norway*
[e]*Vinyls R&D team, INEOS Technologies, Via dell'Elettricità 39, I-30175, Venezia - Marghera, Italy*

$$C_2H_4Cl_2 \rightarrow C_2H_3Cl + HCl \quad (1)$$

this in its turn is produced by two parallel processes, *viz*. direct chlorination (2) and oxychlorination (3):

$$C_2H_4 + Cl_2 \rightarrow C_2H_4Cl_2 \quad (2)$$

$$C_2H_4 + 2HCl + 1/2O_2 \rightarrow C_2H_4Cl_2 + H_2O \quad (3)$$

Besides the economical and environmental aspects discussed above,[1–3] of these two processes, the oxychlorination step offers the greatest potentiality for improving selectivity and overall yield of the complete ethylene-to-vinyl chloride process, particularly acting on the catalyst formulation, that still offers space for in-depth examination.

The oxychlorination reaction (3) is performed at 490–530 K and 5–6 atm using both air and oxygen in fluid or fixed bed reactors. The Al_2O_3 supported $CuCl_2$ catalysts are effective in the oxychlorination of hydrocarbons (here ethylene) since $CuCl_2$ can catalyze the conversion of hydrogen chloride to chlorine. $CuCl_2$ is a highly volatile species at the reaction temperature, so other chlorides (dopants or promoters), (mainly alkaline or alkaline earth chlorides) in a variable concentration, are also incorporated in order to improve the catalytic performances making the catalyst more suitable for use in industrial reactors.[1–3,6–9] In particular, KCl is always present in the catalysts used in fixed bed technologies, sometimes together with other alkali-metal chlorides such as CsCl, NaCl or LiCl.[10–13] Rare-earth-metal chlorides such as $LaCl_3$, added to $CuCl_2$ and KCl, are also claimed in the patent literature.[12] $MgCl_2$ is the base additive in the catalysts used in fluid bed processes, which can also be added by other chlorides too.

Despite more than 30 years of great research and commercial practice, the mechanism of oxychlorination is still not fully understood;[1–3,6,7,13–26] but a significant improvement on the knowledge of the system has been done only recently,[22–27] even if limited to the base catalyst (containing only $CuCl_2$ without additives). It is generally agreed that oxychlorination involves a redox process in which copper cycles between Cu^{2+} and Cu^{+} states. It has been proved[22,23,26] that two different copper species are present on the activated catalyst (dried at 500 K in N_2 flux): a surface aluminate where the copper ions are hosted in the octahedral vacancies of γ-Al_2O_3, and a highly dispersed copper chloride which does not interact with support. The former phase is the only one present at the lowest Cu loadings, till the surface octahedral cationic vacancies of γ-Al_2O_3 are saturated, *i.e.* up to a copper content lower of 0.95 wt% Cu per 100 m^2 support. At higher Cu loading, the remaining fraction of copper precipitates directly from the solution in form of highly dispersed hydrated $CuCl_2$.

In the same set of works by Leofanti *et al.* it has been shown that the surface Cu-aluminate phase is totally inactive[23] and that the overall ethylene oxychlorination reaction (3) is catalyzed only by the $CuCl_2$ phase following a three steps redox mechanism: chlorination of ethylene by reduction of $CuCl_2$ to CuCl (4); oxidation of CuCl to an oxychloride (5) and re-chlorination with HCl (6), closure of the catalytic cycle:[24,25]

$$2CuCl_2 + C_2H_4 \rightarrow C_2H_4Cl_2 + 2CuCl \quad (4)$$

$$2CuCl + 1/2O_2 \rightarrow Cu_2OCl_2 \quad (5)$$

$$Cu_2OCl_2 + 2HCl \rightarrow 2CuCl_2 + H_2O \quad (6)$$

Successively,[28] an operando XANES study, coupled with mass spectrometry, has monitored the Cu(II) ↔ Cu(I) transformation occurring in ethylene oxychlorination environment along the 373–623 K range on the $CuCl_2$/γ-Al_2O_3, finding that the rate determining step of the overall process (3) is the CuCl oxidation (5). Only this year[29] this operando XANES study has been extended to a larger class of dopants used for both fluid and fixed beds technologies (LiCl, KCl, CsCl, $MgCl_2$, $LaCl_3$, $CeCl_4$) and supported by parallel determination of the catalyst activity with a pulse reactor working in non-depletive mode. In this last study it has been highlighted that KCl, and CsCl strongly modify the catalyst behaviour, being able to displace the rate determining step from the CuCl oxidation (5), to the $CuCl_2$ reduction (4). The change of rate determining step results from the decrease of the rate of reaction (4), thus the overall activity of the K- or Cs-doped system is lower than that of the undoped one.[29] For all remaining additives ($MgCl_2$, $LaCl_3$, $CeCl_4$) the rate determining step remains the CuCl oxidation (5), as for the undoped catalyst. The behaviour of Li-doped catalyst was intermediate between the two cases. Observed results have been interpreted hypothesizing that the co-impregnation with $CuCl_2$ and KCl or CsCl salts results in the precipitation in the support of mixed CuK_xCl_{2+x} and $CuCs_xCl_{2+x}$ phases,[30–33] that are less easily reduced by C_2H_4, that requires the presence of two adjacent Cu(II) surface sites. This hypothesis has been supported by indirect spectroscopic evidences related to the shape of the Cu(II) *d*-*d* transition in UV-Vis-NIR spectra and to the CO stretching frequency of carbon monoxide adsorbed on reduced catalyst measured by *in situ* IR spectroscopy.[29]

In this work we present a complete *in situ* Cu K-edge XANES/EXAFS study on LiCl-, KCl-, CsCl-, $MgCl_2$- and $LaCl_3$-doped $CuCl_2$/γ-Al_2O_3 catalysts after thermal activation at 500 K (aimed to transform hydrated $CuCl_2$ to anhydrous $CuCl_2$) and after interaction with C_2H_4 at 500 K, representing the natural extension of our previous works performed on the undoped catalyst.[22–25,34] The effect of additives is potentially extremely complex, and can be summarized in the following four main points. (i) $CuCl_2$ could form a mixed chloride with the chloride of the corresponding additive cation,[28,30–33] thus modifying (on the chemical ground) the active phase of the catalyst and modifying its red-ox properties.[29] (ii) Additive cations can compete with Cu^{2+} in the saturation of cationic vacancies of the alumina surface, thus altering the fraction of Cu^{2+} present in the active phase, that has been established for the bare $CuCl_2$/γ-Al_2O_3 in Ref. [22,23] to be a known function of the alumina surface area and of the copper loading. (iii) Additive cations can modify the acidity of the support, which has been proved to be of both Lewis (surface Al^{3+} species) and Brønsted (surface Al–OH species) nature [24] (iv) Additive cations can modify the Cu dispersion, favoring or inhibiting the clustering of the particles of the active phase on the support. In this work, we focus on points (i), (ii) and (iv). We have obtained the first direct structural proof by EXAFS that mixed CuK_xCl_{2+x} or $CuCs_xCl_{2+x}$ phases are formed upon doping with KCl or CsCl salts. Phase determination, performed with both EXAFS and XANES[28,34–36] allowed us to quantify the fraction of active coppers species in all cases. This values, combined with CO chemisorption experiments allowed to obtain quantitative values for the dispersion of the active phase, The qualitative evaluation of the fraction of cupric and cuprous chloride present on the catalyst after interaction with C_2H_4 at 500 K has given an independent set of data confirming the

trend observed in the recent operando XANES results.[29] Finally, the catalyst activity probed in depletive mode by dosing successive C_2H_4 pulses will quantify the fraction of copper available for ethylene conversion at 500 K and its relationship with $CuCl_2$ dispersion and double salt formation, as determined by additive effect.

2. Activated catalysts

On the basis of previous results[22–26] it is known that only two copper phases are present at the surface of undoped $CuCl_2/Al_2O_3$ catalysts activated *in vacuo* (or in inert gas) up to the minimum oxychlorination temperature (500 K): (i) a surface Cu-aluminate, where Cu^{2+} cations occupies the cationic octahedral vacancies of the γ-Al_2O_3 surface and (ii) an amorphous, highly dispersed, $CuCl_2$ anhydrous phase. In fact other phases such as hydrated amorphous $CuCl_2$ and crystalline paratacamite ($Cu_2(OH)_3Cl$) are transformed into anhydrous $CuCl_2$ during the thermal treatment by release of H_2O and HCl this last adsorbed on alumina surface during paratacamite formation.[22,23]

When doped samples are prepared both Cu^{2+} and dopant cations will be present in the solution, so both cations will compete for the saturation of the surface aluminate phase. In case the dopant cation will have a higher chemical affinity for the surface cationic vacancies, the doping will significantly affect the ratio between the two Cu species, increasing the fraction of the active $CuCl_2$ phase. Once the surface cationic vacancies are saturated, the cations remaining in solution may precipitate into the support either as two separate phases or as a mixed chloride phase. In the former case the active phase will still be $CuCl_2$, while in the latter one the doping process will modify the chemical nature of the active phase, and thus the catalyst performances. With the aim to clarify these points, Cu5.0, K3.1Cu5.0, Li0.5Cu5.0, Mg1.9Cu5.0, Cs10.4Cu5.0 and La10.9Cu5.0 catalysts have been activated at 500 K for one hour under dynamical vacuum and subjected to an *in situ* XANES/EXAFS investigation.

Both XANES and EXAFS parts can quantitatively determinate the fraction of different phases present in a given sample.[28,29,34–36] The method can be very accurate, according that a proper reference spectrum for each independent phase is available. Cu1.4 sample and anhydrous $CuCl_2$ will be used as model compounds of surface Cu-aluminate and of dispersed anhydrous $CuCl_2$ phases, respectively.

2.1. Qualitative consideration from the FT of doped catalysts

The k^3-weighted, phase uncorrected FT of the different catalysts activated *in vacuo* at 500 K are reported in Fig. 1. The two model compound exhibits a markedly different first coordination shell: the Cu-aluminate phase (sample Cu1.4, dashed gray curve) exhibits a first Cu–O shell contribution at 1.5 Å while the $CuCl_2$ anhydrous (full gray curve) shows a much more intense Cu–Cl signal at 1.87 Å (both phase uncorrected values). The difference in position and intensity reflect the difference in distance of the Cu–O and Cu–Cl and the difference in scattering amplitude of the anion. Of relevance is the fact that in the 1.5–1.9 Å region the Cu–O and Cu–Cl signals are almost out of phase, see the imaginary parts reported in Fig. 1b.

Cu5.0 is the sample having the higher fraction of the Cu-aluminate phase, because all cationic vacancies of alumina are saturated by Cu^{2+} cations during the precipitation, owing to the absence of other competitors. Solubility tests on Cu5.0 samples supported on 168 $m^2\ g^{-1}$ γ-Al_2O_3 results in 68% of $CuCl_2$, and thus in 32% of Cu-aluminate.[22] The co-presence of a significant fraction of both phases causes a destructive interference between Cu–O and Cu–Cl signals and explains why Cu5.0 sample (black curve) exhibits a first shell peak of lower intensity. Both Cs10.4Cu5.0 (cyan curve) and K3.1Cu5.0 (blue curve) samples have a first shell signal very similar to that of Cu5.0 (in both modulus and imaginary part), suggesting that both Cs^+ and K^+ are scarcely competitive with Cu^{2+} cations in occupying the octahedral surface vacancies. Conversely, the significant higher intensity of the first shell in both Li0.5Cu5.0 and Mg1.9Cu5.0 samples indicates that Li^+ and Mg^{2+} cations can compete with Cu^{2+} in the surface aluminate phase formation, leaving much more copper for the supported chloride phase. In the La10.9Cu5.0 sample (violet curve in Fig. 1) this effect is even more evident, suggesting that the La^{3+} cations are able to saturate almost all cationic surface vacancies of alumina, leaving almost all copper in the supported $CuCl_2$ phase. The difference in intensity, about 10%, between the La10.9Cu5.0 catalyst and $CuCl_2$ model compound (full gray curve) can be easily ascribed to a higher Debye–Waller factor, of static origin, due to the higher disorder of copper chloride supported on alumina with respect to the bulk. As expected this difference is higher in the second shell contribution, that loses 40% of intensity. Note that it has been proved by chemisorption experiments that the dispersion of supported copper chloride is as high as 70%;[24] so small particles are supposed to have a significantly lower second shell signal.

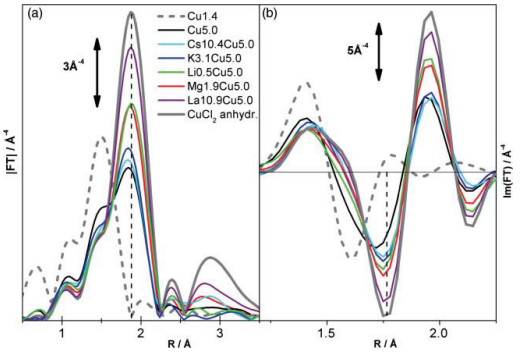

Fig. 1 k^3-weighted, phase uncorrected FT of the different catalysts activated *in vacuo* at 500 K and of Cu1.4 (dotted gray curve) and $CuCl_2$ (full gray curve) samples, used as model compounds for the Cu-aluminate and for anhydrous $CuCl_2$, respectively. Part (a) reports moduli of the FT in the first and second shell region, while part (b) reports a zoom on the first shell distance of the imaginary parts. Vertical dashed line evidences a small shift of the first shell contribution.

Summarizing, from a qualitative look on the bare FT-transformed data (Fig. 1), the following trend in the ability of the dopant cation to compete with Cu^{2+} in the aluminate phase formation has been found: $Cs^+ \leq K^+ \ll Li^+ \approx Mg^{2+} \ll La^{3+}$. This trend will be validated successively when a quantitative data analysis of both XANES and EXAFS parts of the X-ray absorption spectrum will be performed (*vide infra* Table 1). Along this trend, the progressive increase of the $CuCl_2$ phase to the detriment of the Cu-aluminate phase causes a small elongation

(about 0.03 Å) and a significant intensity increase of the first shell signal, the latter due to the decrease of the destructive interference between the two phases.

2.2. Determination of the formation of $CuCs_xCl_{2+x}$ mixed phase in Cs10.4Cu5.0 catalysts

In the investigated samples, the second shell contributions contains signals coming from Cu-cation scattering of the supported copper chloride phase and, if present, from the Cu-aluminate phase. In particular the imaginary parts, which phase is sensitive to the chemical nature of the second shell cation (Cu or dopant element in the supported phase and Al in the aluminate phase), can be informative on the possible presence of dopant atoms in the Cu second shell environment and thus can directly highlight the formation of mixed salts.

Anhydrous $CuCl_2$ has a layered structure, where Cu^{2+} lie in a high distorted octahedral geometry exhibiting four equivalent in plane Cl atoms at 2.26 Å (forming the first shell 1.2–2.2 Å region of Fig. 1, not corrected in phase) and two equivalent axial Cl atoms at 2.96 Å contributing to the complex higher shell signal (extending from 2.6–3.6 Å region, in the phase uncorrected FT reported in Fig. 1 and Fig. 2, full gray curve) together with two in plane Cu at 3.30 Å and four out of plane Cu at 3.83 Å. This peculiar combination of in plane and out of plane arrangement of Cl and Cu atoms results in a very specific phase, generating an imaginary part of the FT characterized by maxima at 2.75, 3.13 and 3.46 Å; nodes at 2.84, 3.04, 3.23 and 3.39 Å and minima at 2.94 and 3.30 Å, see gray curve in Fig. 2. In any case an unknown sample will result in such a peculiar FT we can conclude straightforwardly that we are dealing with anhydrous $CuCl_2$.

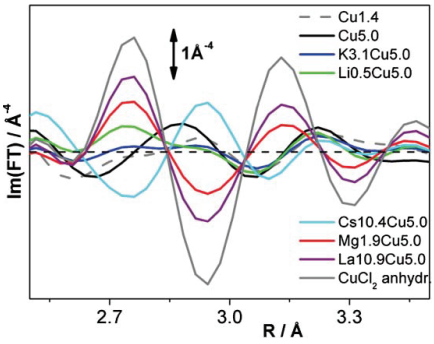

Fig. 2 Magnification of the second shell contribution k^3-weighted, phase uncorrected imaginary part of the FT of the different catalysts activated *in vacuo* at 500 K and of Cu1.4 (dotted gray curve) and $CuCl_2$ (full gray curve) model compounds (same data as in Fig. 1b).

The fact that the copper present in the La10.9Cu5.0 (violet curve) and Mg1.9Cu5.0 (red curve) samples is almost only highly dispersed $CuCl_2$ is confirmed by a better inspection of the imaginary part of the second shell contribution reported in Fig. 2. In both cases the imaginary part of the FT is perfectly in phase with that of $CuCl_2$ model compound. The lower intensity of the signal measured on the catalysts with respect to that of model $CuCl_2$ is due to a higher Debye–Waller factor of static origin and, in the Mg1.9Cu5.0 case, to the co-presence of a small fraction of Cu-aluminate phase.

As expected, the imaginary part of Cu5.0 catalyst can be obtained as linear combination of the signals of Cu1.4 and $CuCl_2$ model compounds (gray dotted and full curves, respectively), testifying hat only dispersed $CuCl_2$ and Cu-aluminate phases are present on the catalyst.

The signal observed for the Cs10.4Cu5.0 catalyst (cyan curve) can be in no way explained in terms of a combination of the $CuCl_2$ and Cu-aluminate phases, as it is strong and almost fully out of phase with respect to $CuCl_2$ bulk. To the best of our knowledge, this is the first direct structural evidence of the presence of Cs^+ cations in the second coordination shell of copper, thus proving the formation of a mixed $CuCs_xCl_{2+x}$ salt. Note that Muddada *et al.*[29] have recently reported indirect UV-Vis and IR evidences supporting this hypothesis. The cases of Li0.5Cu5.0, and K3.1Cu5.0 are less straightforward to be assigned because of the significantly smaller scattering power of Li ($Z = 3$) and K ($Z = 19$) with respect to Cs ($Z = 55$), the presence of mixed $CuLi_xCl_{2+x}$ and CuK_xCl_{2+x} salts can only be hypothesized but not really proven.

2.3. Quantitative determination of Cu-aluminate and supported $CuCl_2$ phases from XANES

One of the possible ways to verify the nature of a species is an accurate analysis of its XANES spectrum.[37–39] Starting from a cluster of atoms simulating the local environment of the absorber, the XANES spectrum could be reproduced theoretically by mean of apposite codes (FEFF-8,[40] or FDMNES,[41]) and compared with the experimental one to validate (or to discard) the tested phase. However, in our case, this approach cannot be used because of the co-presence of different phases and because, for each phase, it is very difficult to build a realistic cluster owing to the amorphous nature of the highly dispersed system.

An alternative way to reproduce the experimental spectrum of a complex sample, composed by different phases, is using a linear combination of experimental signals for each separate phase weighted by its own percentage.[28,29,34–36] For this reason we used as references the spectra of Cu1.4 sample and of anhydrous $CuCl_2$ ($\mu_{exp,al}(E_i)$ and $\mu_{exp,cl}(E_i)$, representative for the pure Cu-aluminate and supported $CuCl_2$ phases respectively) to compute a simulated spectrum $\mu_{sim}(x_{al},x_{cl},E_i)$ defined as linear combination of the experimental spectra of the two model compounds:

$$\mu_{sim}(E_i,x_{al},x_{cl}) = x_{al}\cdot\mu_{exp,al}(E_i) + x_{cl}\cdot\mu_{exp,cl}(E_i) \quad (7)$$

Then we optimized the weights x_{al} and x_{cl} for the two phases in order to minimize the difference between the experimental datum and the simulation, Searching, in the (x_{al}, x_{cl}) space, the minimum of the function R_{factor} defined as follows:

$$R_{factor}(x_{al},x_{cl}) = \sqrt{\frac{\sum_i(\mu_{exp}(E_i)-\mu_{sim}(E_i,x_{al},x_{cl}))^2}{\sum_i(\mu_{exp}(E_i))^2}} \quad (8)$$

Note that in the present case the sum of x_{al} and x_{cl} fractions has not been forced do be 1, so that the discrepancy between $x_{al} + x_{cl}$ and unit can be considered as an simple estimation on the validity of the adopted method, see 4th column in Table 1.

The effectiveness of the method reported in Eqs. (7–8) strongly depends on the presence of significant different features in the two

Table 1 Relative fractions of the Cu-aluminate (x_{al}) and supported $CuCl_2$ (x_{cl}) phases present in the different catalysts and reported in percentage. Columns 2–3: as determined by the linear combination of the XANES spectra of Cu1.4 and $CuCl_2$ model compounds according to Eqs (7,8) with x_{al} and x_{cl} used as independent free parameters. Columns 6,7: as determined *via* a standard two-phases Cu–O and Cu–Cl EXAFS fit of the first shell in the 1.0–2.3 Å range, fixing the sum to unit. Also reported are: the deviation of $x_{al} + x_{cl}$ from unit, representing an estimation of the error (column 4) and the $(R_{factor})^2$ of the best fit from eqn (8), (column 5), reported squared to allow a comparison with the R factor obtained from the output of the FEFF code (column 9). Catalysts are ordered by decreasing fraction of the aluminate phase

	Linear combination of XANES spectra				1st shell EXAFS fit		
Samples	100 x_{al}	100 x_{cl}	100 (1– x_{al} – x_{cl})	$(R_{factor})^2$	100 x_{al}	100 x_{cl}	R_{FEFF}
Cu5.0	35.8	63.8	0.4	0.13	32 ± 3	68 ± 7	0.003
K3.1Cu5.0	24.2	75.9	0.1	0.06	20 ± 1	80 ± 5	0.033
Cs10.4Cu5.0	22.3	78.2	0.5	0.05	14 ± 1	86 ± 5	0.038
Li0.5Cu5.0	19.7	79.7	0.6	0.04	15 ± 1	85 ± 5	0.014
Mg1.9Cu5.0	4.0	96.4	0.4	0.002	9 ± 1	91 ± 5	0.012
La10.9Cu5.0	1.7	98.9	0.6	0.001	3 ± 0.3	97 ± 8	0.005

experimental curves $\mu_{exp,al}(E_i)$ and $\mu_{exp,cl}(E_i)$, used to construct the simulated spectrum. In the present case, see Fig. 3, although almost indistinguishable in the edge region, the differences between $\mu_{exp,al}(E_i)$ and $\mu_{exp,cl}(E_i)$, are quite relevant in the white line (first resonance after the edge) and in the post edge region. In fact: (i) the white line of the Cu-aluminate phase is more than 20% more intense than that of the $CuCl_2$ phase; (ii) in the two cases, the minima after the white line are significantly separated (4 eV); (iii) in the whole 9005–9025 the $\mu_{exp,cl}(E_i)$ lies significantly above $\mu_{exp,al}(E_i)$. These relevant differences guarantee that in samples showing both phases, the relative fraction can be quantitatively determined with a good degree of confidence.

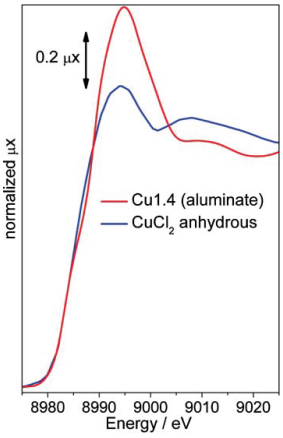

Fig. 3 Normalized XANES spectra of Cu1.4 (red curve) and $CuCl_2$ (blue curve) samples (both activated at 500 K), used as model compounds for the Cu-aluminate and for anhydrous $CuCl_2$, respectively.

The results of this approach, applied to all catalysts, can be graphically appreciated in Fig. 4 while the corresponding quantitative determination of x_{al} and x_{cl} fractions are listed in the columns 2 and 3 of Table 1.

The analysis of the XANES spectrum of the undoped Cu5.0 sample resulted in $x_{al} = 0.358$ and $x_{cl} = 0.638$, values that are in quantitative agreement with the fractions of 0.32 and 0.68 determined by chemical analysis on the soluble copper fraction present on a freshly prepared Cu5.0 sample.[22] This agreement

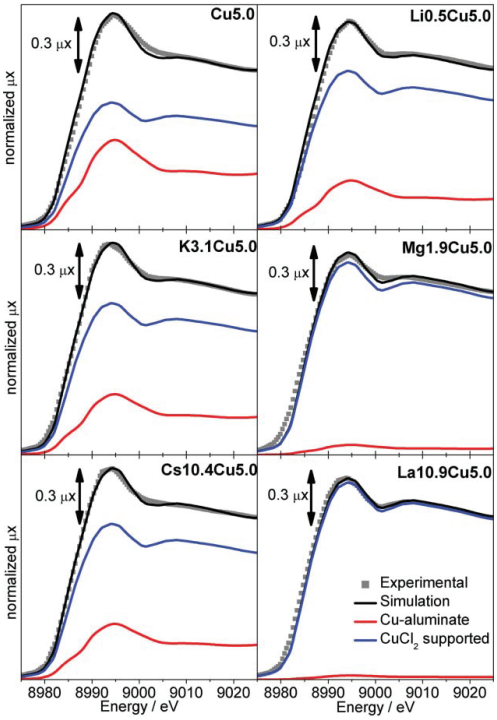

Fig. 4 Normalized XANES spectra of the different catalysts activated *in vacuo* at 500 K (scattered gray squares). Also reported are the best fit $\mu_{sim}(x_{al},x_{cl},Ei)$ (black curve), see eqn (7), together with the fraction of the two model phases Cu1.4 (red curve) and $CuCl_2$ (blue curve) weighted by the corresponding optimized x_{al} and x_{cl} fractions.

implies that the adopted experimental curves, $\mu_{exp,al}(E_i)$ and $\mu_{exp,cl}(E_i)$, are well representative of the two copper species present on the Cu5.0 catalyst and represent an important guarantee on the validity of the method applied to this set of data, with this choice of model compounds. Additional guarantees comes by the fact that the sum $x_{al} + x_{cl}$, done on the unrestricted parameters is very close to unit in all cases (column 4 of Table 1) and by the relatively low R_{factor} values (column 5 of Table 1).

Summarizing, from the quantitative analysis of the XANES spectra, the following trend in the ability of the dopant cation to compete with Cu^{2+} in the aluminate phase formation has been found: $K^+ \leq Cs^+ \leq Li^+ \ll Mg^{2+} < La^{3+}$.

The present ranking makes quantitative the previous qualitative one obtained at the end of Section 2.1 based on a simply observation of the bare FT of the EXAFS spectra collected on the different catalysts (Fig. 1a). Both methods agrees in finding both Mg^{2+} and La^{3+} cations much more efficient in saturating the cationic vacancies of alumina than the alkaline ones. The results of the XANES analysis will be further confirmed by an independent two phases analysis of the EXAFS part of the spectrum.

2.4. Quantitative determination of Cu-aluminate and supported $CuCl_2$ phases from EXAFS

To support the quantitative results obtained in the XANES analysis, a detailed EXAFS study has been done on undoped and doped samples using two-phase fit.[26,35] Since for all doped catalysts two phases are present, a reliable EXAFS data analysis must be done using two different models: the Cu1.4 model compound for the copper aluminate phase (Cu–O) and the anhydrous $CuCl_2$ for the active phase (Cu–Cl). The following parameters have been optimized during the fit: the energy shift (ΔE), the Cu–Cl bond length distance and Debye–Waller factor (R and σ^2), for the supported $CuCl_2$ phase, as well as its relative fraction x_{cl}. To limit the number of optimized parameters, and thus their relative correlation, the energy shift, the Cu–O bond length distance and Debye–Waller factor of the Cu-aluminate phase have been fixed to the values optimized in the one-phase fit performed on sample Cu1.4 (see Section 4.4. and Table 3), while the relative fraction x_{al} has been constrained to the optimized parameter *via* the equation: $x_{al} = 1 - x_{cl}$. For all catalysts, the results of the fits are summarized in columns 6 and 7 of Table 1, while the quality of the fits can be appreciated in Fig. 5.

The disagreement in the determination of the fraction x_{cl} of the active $CuCl_2$ phase estimated with the two quantitative methods (EXAFS and XANES) is always below 10%. It reaches a value of 9% in the Cs10.4Cu5.0 case, being close to 5% for Cu5.0, K3.1Cu5.0, Li0.5Cu5.0 and Mg1.9Cu5.0, while it is as low as 2% for the La10.9Cu5.0 catalyst. We note that for four catalysts XANES results in a higher estimation of x_{cl} than EXAFS, while for the remaining two the opposite holds. As both positive and negative discrepancies are observed, we can conclude that the two methods are equivalent in estimating the fractions of the two phases, so that there is no systematic over-estimation/under-estimation obtained with the XANES approach *vs.* the EXAFS one. As a consequence, the final estimation of the fractions can be considered as the average value obtained with the two techniques (vide infra the 5th column in Table 2). Considering now the quantitative evaluation obtained from both XANES and EXAFS techniques, the following trend of the dopant cations in the ability to compete with Cu^{2+} in the aluminate formation has been obtained: $K^+ < Cs^+ \approx Li^+ \ll Mg^{2+} < La^{3+}$.

Summarizing, all the additives cause a decrease of fraction of copper forming aluminate. A cross evaluation of data obtained by XANES and EXAFS evidences that the effect of alkali metal cations is moderate, while the effect of Mg and La is high. The different behaviour could be originated by the fact that the sites of alumina surface involved in surface aluminate formation are different. Potentially, the surface of γ-Al_2O_3 exhibits both tetrahedral and octahedral cationic vacancies, however cupric ions are able to occupy the latter ones only.[22,26] The results obtained in this paragraph suggest that Mg^{2+} and La^{3+} preferentially occupy octahedral vacancies, in a more efficient way than Cu^{2+}, while the alkali metal cations are able to react with both cationic vacancies, thus being less competitive for the occupation of octahedral ones. Probably also the charge of the cation plays a role: surface cationic vacancies in γ-Al_2O_3 are used to host trivalent Al^{3+} cations, this is probably the reason why cations with higher charge like Cu^{2+}, Mg^{2+} and La^{3+} are more efficient than monovalent Li^+, K^+ and Cs^+ ones.

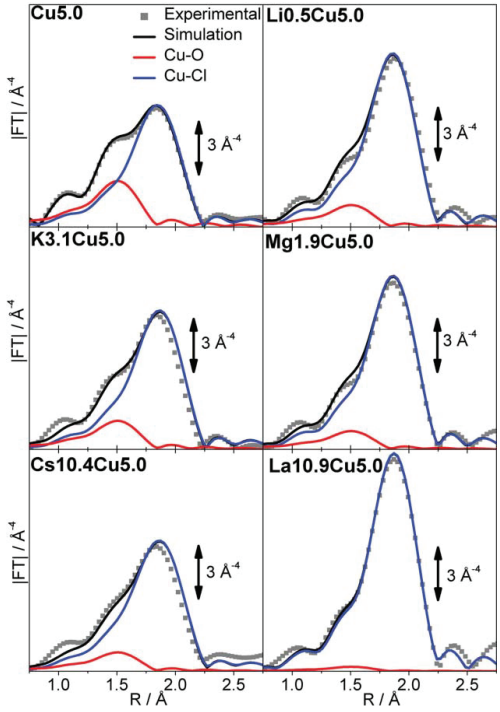

Fig. 5 k³-weighted, phase uncorrected, FT of the EXAFS spectra of the different catalysts activated *in vacuo* at 500 K (scattered gray squares). Also reported are the best fit obtained with a two-phases first shell analysis, together with the fraction of the two model phases Cu1.4 (red curve) and $CuCl_2$ (blue curve) weighted by the corresponding optimized x_{al} and x_{cl} fractions.

3. Catalyst reduction by C_2H_4

In this paragraph we will discuss the effect of the additives on the reactivity of Cu5.0, K3.1Cu5.0, Mg1.9Cu5.0, Cs10.4Cu5.0, Li0.5Cu5.0 and La10.9Cu5.0 catalysts towards ethylene at 500 K, comparing *in situ* EXAFS/XANES spectra and catalytic activity measured in a pulse reactor with the XANES spectra collected in operando mode and reported elsewhere.[29] For experimental

reasons intrinsic to each technique, the reactions have been performed in three significantly different conditions.

In the operando XANES experiments[29] the catalyst is submitted to a continuous flow of all three reagents, while temperature linearly increases with time. While the flow conditions would allow the reaching of the equilibrium between reactants and reaction products, thus of the copper reduction degree, the continuous change of temperature makes the system not close to the changing equilibrium, *i.e.* slightly under-reduced during ramp-up experiments, where the equilibrium tends toward Cu(I). In the *in situ* EXAFS/XANES, see experimental, an equilibrium pressure of C_2H_4 of 200 Torr is dosed twice on the catalysts at 500 K for 5 min, with an intermediate evacuation: the reaction (4) is the only possible. However, the static conditions make difficult to complete the reaction and a fraction of Cu(II) potentially reducible can be still present. Copper reduction is the only possible reaction also in pulse reactor experiments (ethylene in He). The temperature is kept at 500 K as in EXAFS/XANES experiments and the catalyst exposure to ethylene is shorter, but the flow conditions and the cleaning effect of He flow between pulses can make the system more efficient than the static one.

Summarizing, the results obtained with the three experimental set-ups can not be directly compared each other on a quantitative way, but the trends observed will result in an homogeneous picture.

3.1. XANES and EXAFS study of ethylene-reduced catalysts

The reduction process performed for the *in situ* EXAFS/XANES, has been performed at 500 K, a temperature sufficiently high to be observed in industrial reactors, but low enough to avoid the complete reduction of all samples, in order to obtain direct information on the capability of additives to affect the reducibility of copper active phase. This is evidenced by XANES spectra of the whole set of ethylene-reduced catalysts compared with those of $CuCl_2$ and CuCl model compounds, see Fig. 6.

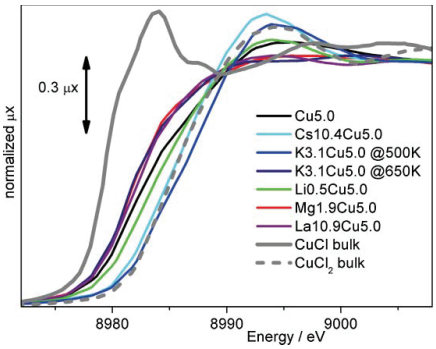

Fig. 6 Normalized XANES spectra of the whole set of catalysts after interaction with C_2H_4 at 500 K. For comparison, also the spectra of bulk $CuCl_2$ (dashed gray curve) and CuCl (solid gray curve).

K3.1Cu5.0 and Cs10.4Cu5.0 catalysts, show a negligible reduction fraction. This behaviour is agrees with the previous XANES study in operando conditions,[29] where it has been shown that K^+ and Cs^+ dopants slows down the speed of the reduction step (4), that starts at 520 and 580 K, respectively. The temperature of 500 K, adopted in the present study, is insufficient to activate the process. The fact that the temperature is the thermodynamic parameter preventing the reduction of the active phase is proven by the fact that when ethylene is dosed on K3.1Cu5.0 catalyst at 650 K, the catalyst exhibits a significant reduction. In all the other cases, 500 K is sufficiently high to ensure the reduction, however all edges lie far away from that of CuCl model compound. Using the edge shift as rough approximation of the fraction of reduced Cu(II),[28,29,42] Mg1.9Cu5.0 and La10.9Cu5.0 catalysts exhibit a reduction of 55% and 50%, Cu5.0 of 35% (that corresponds to 55% of the supported $CuCl_2$ phase) and Li0.5Cu5.0 25%. Once the fraction of uncreative Cu-aluminate[24] is taken into account, the data reported in Fig. 6 indicates that we are dealing with two different families of catalysts. Family I, including, Cu5.0, Mg1.9Cu5.0 and La10.9Cu5.0, shows under the adopted conditions about 50% of reduction of the active $CuCl_2$ phase. Family II, including K3.1Cu5.0 and Cs10.4Cu5.0, exhibit no reduction. Li0.5Cu5.0 is intermediate between the two cases. The qualitative results of this *in situ*, static, XANES experiment fully mirrors the quantitative results obtained in the operando XANES experiment.[29]

The incomplete reduction of the samples makes the quantitative phase speciation by XANES more delicate than in the case of the activated catalysts discussed so far. Difficulties came from the simultaneous presence of three different copper phases: unreactive Cu-aluminate, unreacted $CuCl_2$ and reduced CuCl. The situation is further worsen by the fact that bulk CuCl is not a good model compound for highly dispersed CuCl nanoparticles.[24]

The k^3-weighted, phase uncorrected, EXAFS spectra of the different catalysts after activation *in vacuo* at 500 K (blue curves) and after subsequent interaction with ethylene at 500 K (green curves) are reported in Fig. 7. As was the case for XANES spectra, also the EXAFS spectra of both K3.1Cu5.0 and Cs10.4Cu5.0 catalysts are almost unaffected by interaction with ethylene at 500 K. Remaining catalysts exhibit a significant decrease of the first shell EXAFS signal intensity. This is due to an increase of the heterogeneity of the first shell Cu–Cl distances: Cu^{2+} in anhydrous $CuCl_2$ exhibits 4 equivalent in plane Cl atoms at 2.26 Å,[43] while Cu^+ in CuCl has a distorted tetrahedral geometry with four Cu–Cl distances in the 2.29–2.42 Å.[44] It is remarkable to note that in the imaginary parts the maxima and the minima of the two signals of the activated and reduced catalysts occurs exactly in the same positions. Under such circumstances, it is evident that, EXAFS will not be able to discriminate between $CuCl_2$ and CuCl and that we must rely on the qualitative information extracted from the XANES data only.

3.2. Catalytic activity probed by dosing C_2H_4 pulses

The EXAFS and XANES experiments in ethylene performed under static conditions, and discussed in Section 3.1, have shown that the presence of potassium and cesium lowers the reducibility of Cu, further supporting the recent time/temperature resolved XANES experiments in operando conditions.[29] In order to make possible a more precise comparison among different catalysts, the Cu5.0, Li0.5Cu5.0, K3.1Cu5.0, Cs10.4Cu5.0, Mg1.9Cu5.0 and La10.9Cu5.0 catalysts have been submitted to a series of C_2H_4 pulses at the same temperature as static XANES/EXAFS

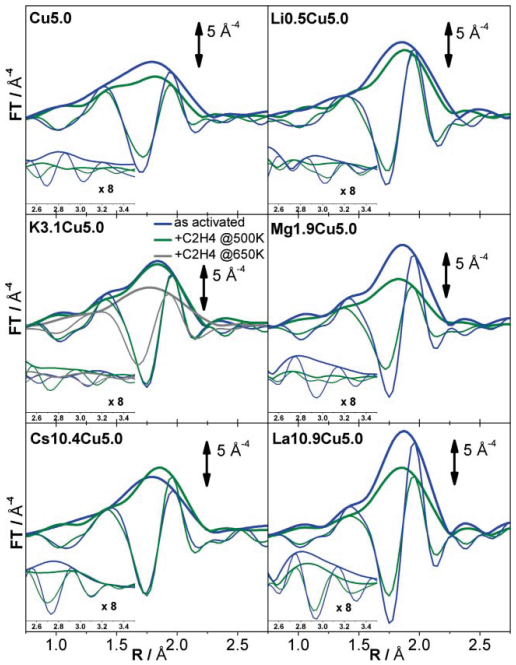

Fig. 7 Modulus and imaginary part of the k^3-weighted, phase uncorrected, FT of the EXAFS spectra, in the first shell region, of the different catalysts after activation *in vacuo* at 500 K (blue curves) and after subsequent interaction with C_2H_4 at 500 K (green curves). For K3.1Cu5.0 catalyst also the spectrum obtained after interaction with ethylene at 650 K (dark gray curve) is reported. The insets report the second shell signals magnified by a factor 8.

experiments (500 K) even necessarily in different fluid-dynamic conditions. The results are reported in Fig. 8.

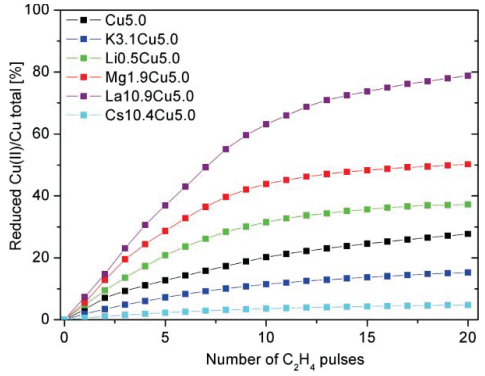

Fig. 8 Fraction of reduced Cu(II) *vs.* the number of ethylene pulses dosed on Cu5.0, Li0.5Cu5.0, K3.1Cu5.0, Cs10.4Cu5.0, Mg1.9Cu5.0 and La10.9Cu5.0 catalysts as obtained from the measured ethylene conversion to 1,2-dichloroethane. Quantitative data after 20 pulses have been reported and analyzed in Table 2.

Being the experiments performed in a depletive mode the C_2H_4 can be converted to $C_2H_4Cl_2$ only at the expense of the Cl coming from the reduction of $CuCl_2$ to CuCl, so the determination of C_2H_4 conversion allow the direct determination of Cu available for reduction. For the same reason the conversion per pulse is higher at the beginning and decreases progressively as the source of Cl is consumed (Fig. 8).

As expected, after 20 pulses Cu5.0 catalyst is more reduced than K3.1Cu5.0 and Cs10.4Cu5.0 one. However all the other tested catalysts show a higher reduction degree than Cu5.0, included Li0.5Cu5.0 and the differences are relevant. The different capability to convert C_2H_4 can be roughly attributed to three characteristics: (i) the chemical nature of the active phase; (ii) fraction of active Cu(II), that depends on the ability of the dopant cation in competing with Cu(II) for the formation of the surface aluminate phase,[22,23,26] (iii) the area of the active phase surface.

Point (i) explains why the data of catalyst K3.1Cu5.0 and Cs10.4Cu5.0 lies below all the other curves in Fig. 8. It is now proved that KCl- and CsCl-doping results in the formation of CuK_xCl_{2+x} and $CuCs_xCl_{2+x}$ mixed phases supported on alumina. Indirect evidences came from the Cu(II) *d-d* transitions and from the CO stretching frequency of carbon monoxide adsorbed on reduced catalyst by *in situ* IR spectroscopy.[29] Direct structural evidences have been reported in Section 2.2 of the present work from the inspection of the Cu second shell environment. Family I and II significantly differs by the fact that they exhibit a different active phase: $CuCl_2$ in the former case and CuM_xCl_{2+x} (M = K, Cs) in the latter one. The lower activity of Family II catalyst in ethylene conversion at 500 K is so fully justified.

The combined *in situ* EXAFS and XANES study summarized in Table 1 allowed us to quantify the fraction of active copper phase, so to be able to take into account point (ii). The higher activity of Mg1.9Cu5.0 and La10.9Cu5.0 catalysts is clearly due to the fact that they exhibits almost all copper in the active phase: 94 and 98%, respectively. The case of Li0.5Cu5.0 catalyst is more difficult to be discussed. The formation of a $CuLi_xCl_{2+x}$ mixed phase, at least for a fraction of copper has not been really proven, but suggested by the intermediate behaviour of this catalyst with respect to the clear responses of catalysts classified in Family I and II, see *e.g.* Fig. 6 and Fig. 7. This would result in an expected lower activity. The fact the Li0.5Cu5.0 catalyst has a higher activity than the undoped Cu5.0 can be justified by its higher fraction of active phase: 82% *vs.* 66%, see Table 1. It is evident that in order to go deeper detail into this topic it is necessary to know the exposed surface of the active phase: point (iii).

4. Interaction of CO on C_2H_4-reduced catalysts: IR spectroscopy and chemisorption

4.1. IR spectroscopy of adsorbed CO

CO is an excellent probe molecule for Cu(I) sites,[24,37,45–51] because its interaction is normally rather strong. The interaction can be separated into an electrostatic, a covalent σ-dative and a π-back donation contributions, the first two causing a blue shift of the ν-$_{CO}$, while the last causes a red shift.[52–54] From a measurement of the ν-$_{CO}$ of a given Cu(I) carbonyl complex, information are so obtained on the nature of the Cu(I)–CO bond. On the contrary, the interaction of CO with Cu(II) is very week and has been

Table 2 Raw results of static-volumetric measurements of CO adsorption (columns 2–4): Volume of adsorbed CO (V_m), ratio between adsorbed CO molecules and total number of Cu atoms (D'), and estimation of the surface area of CuCl (S'_{CuCl}). Average fraction of the active $CuCl_2$ phase, in % from XANES and EXAFS analyses ($<x_{cl}>$ Column 5). Dispersion corrected by $<x_{cl}>$ and referred to the active $CuCl_2$ phase (D, Column 6). Raw and renormalized data from the catalytic experiments in pulse reactor (Fig. 8): % of the total Cu reduced after 20 ethylene pluses (R', Column 7);% of Cu reduced in the active phase ($R = R'/<x_{cl}>$, Column 8); % of reduction of the first monolayer of the active phase (R/D Column 9)

Technique	CO chemisorption raw data			EXAFS/XANES		Activity in pulse reactor		
Sample	V_m/cm^3g^{-1}	D'	S_{CuCl}/m^2g^{-1}	$100 <x_{cl}>$	$D = D'/<x_{cl}>$	R'	$R = R'/<x_{cl}>$	R/D
Cu5.0	8.3	0.45	25.1	66	0.68	28	42	62
K3.1Cu5.0	8.4	0.46	25.4	78	0.59	15	24	41
Cs10.4Cu5.0	8.3	0.45	25.1	82	0.55	5	7	12
Li0.5Cu5.0	14.2	0.78	43.0	82	0.94	37	54	58
Mg1.9Cu5.0	12.6	0.69	38.1	94	0.74	50	56	76
La10.9Cu5.0	14.4	0.79	43.6	98	0.80	79	82	102

only very rarely observed,[55,56] and in the present case it can be considered, in first approximation, negligible at all. In order to allow a direct comparison with reduced samples investigated by *in situ* XANES/EXAFS experiments the catalysts were reduced in ethylene at 500 K before CO dosage to allow the molecule to probe the surface of the active phase.[24,25,28] The experiment has so been performed on partially reduced catalysts, see Fig. 6 and related discussion.

Parts (a) and (b) of Fig. 9 report the IR spectra of CO dosed at room temperature on the whole set of catalysts pre-reduced in ethylene at 500 K collected at low and high CO equilibrium pressure (P_{CO}), respectively. In all cases we are dealing with a single and well defined band due to the formation of $Cu^+ \cdots CO$ adducts. We can so conclude that, at room temperature, (i) CO is not absorbed on the γ-Al_2O_3 surface activated at 500 K (neither on Al–OH nor on Al^{3+} sites); (ii) only mono-carbonyl complexes are formed (di-carbonyls are characterized by two IR bands). This IR experiment testifies that the surface CO : Cu(I) stoichiometry is 1 : 1, a point of fundamental importance for the CO chemisorption experiments described in Section 4.2.

Family I samples exhibit ν-$_{CO}$ stretching frequencies very close to that of the unperturbed CO molecule (ν^0_{CO} = 2143 cm^{-1}), see vertical dotted gray line in Fig. 9ab, while for samples belonging to Family II we have ν-$_{CO} \ll \nu^0_{CO}$. In the former case we are dealing with non-classical carbonyls, while in the latter with classical ones.[52–54] Looking to the evolution of the spectra with P_{CO}, it is worth of note that the C–O stretching frequency ν-$_{CO}$ undergoes a significant red shift upon moving from low to high P_{CO}, for catalysts belonging to Family I, see vertical colored dashed lines in Fig. 9aFig. 9b. Conversely only a negligible shift is observed for catalysts belonging to Family II. This evolution is better shown in Fig. 9c reporting, for all catalysts, the ν-$_{CO}$ at intermediate P_{CO}. Even if the static arrangement of experiments and the temperature control in IR sample holder have caused some reproducibility difficulties, the difference between Family I and Family II is even more marked. The fact that the ν-$_{CO}$ of $Cu^+ \cdots CO$ adducts formed by Family I catalysts are P_{CO} dependent, is well known in surface science and is due to the mutual perturbation of adjacent carbonyls[57] that, in turns, testifies of Cu(I) adsorbing sites are adjacent each-other.[24] Conversely, for both K3.1Cu5.0 and Cs10.4Cu5.0 samples the ν-$_{CO}$ value is almost pressure independent, suggesting that Cu(I) adsorbing sites are sufficiently isolated from each other and that the interaction between two $Cu^+ \cdots CO$ adducts is negligible. Note again that the non complete reduction of K3.1Cu5.0 and Cs10.4Cu5.0 catalysts may be also responsible for this behaviour. Basically Cu5.0, La10.9Cu5.0, Mg1.9Cu5.0 and Li0.9Cu5.0 samples behaves similarly to what observed for highly dispersed CuCl nanoparticles supported on NaCl(001),[47] see open gray circles in Fig. 9c, where surface Cu^+ sites are separated just by one Cl^- anion, while a much larger distance must be inferred for copper species hosted on K3.1Cu5.0 and Cs10.4Cu5.0 samples.

The whole set of pressure dependent IR experiments has been duplicated in order to check the reproducibility and reported in Fig. 9d. Inspections of parts (c) and (d) of Fig. 9 results in the conclusion that the reproducibility of the experiments holds on a qualitative ground but not on a quantitative one. In fact, the presence of two distinct families of catalysts is fully confirmed but the exact ν-$_{CO}$ values observed at low and high P_{CO} differ in the two set of experiments by some cm^{-1}. On the basis of our experience we conclude that the critical point in the reproducibility lies in the reduction under static conditions, that can yield slightly different results depending on: (i) the actual reduction temperature; (ii) the actual ethylene equilibrium pressure dosed on the sample; (iii) the exact exposure time; (iv) the final vacuum reached between the two ethylene dosages.

4.2. Dispersion measurements by CO chemisorption

Dispersion measurements require that the phase under investigation is completely reduced. In order to safely reach 100% of the reduction of the active phase samples avoiding the use of too high temperature (modification of copper dispersion and possibility of heavy by-products deposition) number and time of exposure to ethylene – evacuation cycles before CO dosage have been substantially increased, see experimental (Section 6.3.1). Notice that the apparatus used allow a better control of operating conditions than IR experiments. The IR study on adsorbed CO leads to the conclusion that, for $CuCl_2/Al_2O_3$ samples reduced in ethylene, CO adsorbs only on Cu(I) sites at RT to form $Cu^+ \cdots CO$ adducts.[24,29] This fact justify the use of CO as a probe molecule to detect the number of surface Cu(I) sites by usual static-volumetric adsorption measurements.[58,59] The volume of adsorbed CO correspondent to the full coverage (hereinafter V_m) has been evaluated by linearizing the adsorption isotherm (not reported for brevity) with the Langmuir equation in the 100–600 Torr range. The knowledge of V_m allows to calculate the number of Cu(I) ions exposed to the surface ($Cu(I)_s$), then the dispersion (D'):

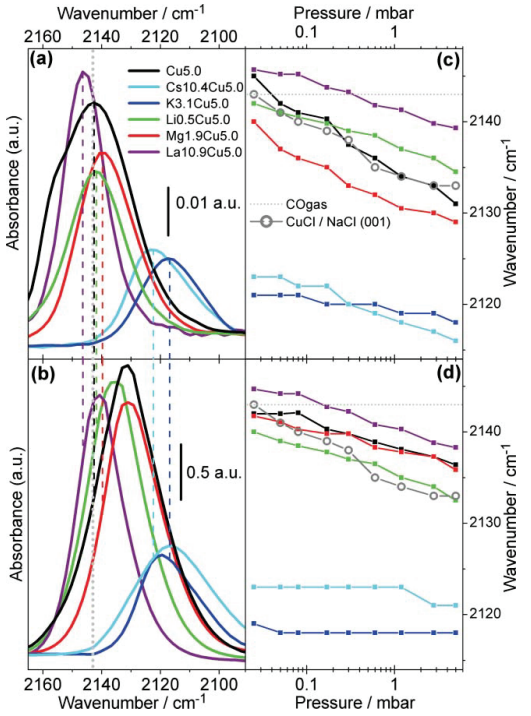

Fig. 9 Part (a): IR spectra of CO dosed on Cu5.0, Li0.5Cu5.0, K3.1Cu5.0, Cs10.4Cu5.0, Mg1.9Cu5.0 and La10.9Cu5.0 catalysts previously reduced in ethylene at 500 K under static conditions. P_{CO} = 2.5 10^{-2} mbar. Part (b): as Part (a) for P_{CO} = 5 mbar. The vertical dotted gray line refers to the stretching frequency of the unperturbed CO molecule: ν^0_{CO} = 2143 cm^{-1}, while the remaining vertical dashed lines highlight the frequency shift undergone by the $Cu^+ \cdots CO$ adducts in the investigated P_{CO} range. Part (c) Evolution of ν-$_{CO}$, as a function of P_{CO} (logarithmic scale) in IR experiments of CO dosed at 300 K on the different catalysts. The corresponding set of low and high P_{CO} spectra are reported in parts (a) and (b) respectively. The gray open circles refer to the data collected by Scarano *et al.*[47] on CuCl nano-crystals grown by vapor phase deposition on a NaCl(001) and represent a reference for the pure CuCl phase. The horizontal dotted line refers to ν^0_{CO}. Part (d) as part (c) for an independent second set of IR experiments performed to test the reproducibility.

$$D' = Cu(I)_s / Cu(I)_{tot}, \quad (9)$$

where $Cu(I)_{tot}$ represents the number of the Cu(I) ions in the sample. A further evaluation leads to the estimation of the surface area of CuCl (S_{CuCl}):

$$S_{CuCl} = Cu(I)_s \, a_{CuCl}, \quad (10)$$

where a_{CuCl} (11.64 Å^2 as estimated from the chemical density ρ_{CuCl}) is the average area per Cu(I) at the surface of CuCl. Table 2 summarizes the results obtained on the whole set of samples. A high dispersion is reached for all samples ($0.45 < D' < 0.79$). Addition of potassium leaves D' nearly unchanged, while the presence of Li, Mg and La strongly increase the dispersion of copper. Reported D' values refer to the whole amount of copper, but the interesting values are those related to the supported active phase. The combined EXAFS/XANES study performed in Sections 2.3 and 2.4 allowed us to know, for each catalyst, the fraction of inactive Cu-aluminate and of active Cu phase. In column 5 of Table 2 we report the average values $<x_{cl}>$ obtained with EXAFS and XANES technique (Table 1). So, the dispersion of the supported active phase can be obtained as:

$$D = D' / <x_{cl}> \quad (11)$$

and is reported in the sixths column of Table 2. From the reported data, it emerges that K and Cs dopants decrease the dispersion of the active phase, while Li, Mg and La increases the dispersion, resulting in an active phase showing almost only Cu(I) surface ions (absence of bulk atoms). The very high dispersion of the active phase can also be appreciated in the second shell signal of the EXAFS data, see insets in Fig. 7, that exhibits a dramatic decrease upon interaction with ethylene.

Summarizing the results, the double salts formed by CsCl and KCl with copper chloride tend to reach a lower dispersion than undoped copper chloride. Conversely, the dispersion of copper chloride is increased by the presence of $MgCl_2$ and $LaCl_3$. This mean that these additives, that do not form double salts with copper chloride, decrease its tendency to agglomerate. However, they are able to modify also the intrinsic reactivity of Cu chloride. In fact, by comparing the reduction degree R of the catalysts after 20 pulses (*i.e.* the total ethylene conversion, see Fig. 8) with the fraction of surface Cu atoms in the active phase (D in Table 2), we can calculate the fraction of the first monolayer that has been reduced (R/D, last column in Table 2). We notice that the fraction corresponds to 60% for undoped Cu and that it is increased by the addition of Mg (75%) and even more (100%) for La. This means that each Cu ion of the surface of Mg- and La-doped catalysts is more reactive than Cu ion of the undoped one. Accordingly to this approach, the specific reactivity of Cu is lowered by the addition of K (40%) and even more of Cs (10%), because of double salt formation. The effect of Li is more difficult to rationalize because it acts as Mg and La enhancing the dispersion of active phase, but the fraction of the first monolayer reduced after 20 pulses is lower than the corresponding fraction of undoped Cu, even if much less than K and Cs. The mechanism of the enhancing effect of Mg and La on catalytic activity is not clear, but it could be associated to the modification that they induce to the support surface: the Cu is so highly dispersed that almost all is in direct contact with support surface. A systematic set of IR experiment performed dosing CO at liquid nitrogen temperature, so probing both the alumina surface and the copper phase, is planned in the next future to better clarify this important aspect.

5. Conclusions and perspectives

As proved from a previous study, in the undoped $CuCl_2/\gamma$-Al_2O_3 catalysts for oxychlorination reaction, two Cu-phases coexist: Cu-aluminate and supported $CuCl_2$, the only active one.[22] In the present contribution, we investigated the role played by dopants on: (i) the nature, (ii) the relative fraction, (iii) the reducibility and (iv) the dispersion of the active phase. The study was extended to the mostly used dopants in both fixed and fluid bed technologies: LiCl, KCl, CsCl, $MgCl_2$ $LaCl_3$, added in a Cu/dopant atomic ratio of 1 : 1. Due to the complexity of the topic a multitechnical approach was unavoidable. We combined *in situ* XANES/EXAFS,

IR spectroscopy of adsorbed CO, CO chemisorption and catalytic tests performed using a pulse reactor in depletive mode. When needed, reference to results obtained in a XANES study performed in operando conditions was made.[29]

EXAFS and XANES highlighted that all dopants contribute more or less efficiently in increasing the fraction of the active copper species, that reaches a value of almost 100% in the case of $MgCl_2$ or $LaCl_3$. differences among dopants reflect the different ability of the corresponding cations to compete with Cu^{2+} in the occupancy of octahedral surface vacancies of alumina. EXAFS directly, and IR indirectly, proved that the addition of KCl or CsCl (and less efficiently of LiCl) results in the formation of mixed CuK_xCl_{2+x} or $CuCs_xCl_{2+x}$ phases, so altering the chemical nature of the active phase. XANES spectroscopy indicates that addition of $MgCl_2$or $LaCl_3$ does not affect the reducibility by ethylene (under static conditions) of the active $CuCl_2$ phase (eqn (4)) and that the reducibility of the new copper-dopant mixed chloride is in the order $CuCl_2 > CuLi_xCl_{2+x} > CuK_xCl_{2+x} > CuCs_xCl_{2+x}$. When the ethylene is dosed on the catalysts in a pulse reactor, the following trend in the overall reducibility is observed: La- > Mg- > Li-doped > undoped > K- > Cs-doped catalyst. Reducibility is thus affected by the adopted experimental conditions (static or flow). To understand this apparent discrepancy we used CO chemisorption, to determine the dispersion of the active phase. It is worth noticing that quantitative data could be extracted from the CO chemisorption experiments only thanks to the support of independent EXAFS/XANES and IR experiments: EXAFS/XANES study allowed us to refer the chemisorption data to the active phase only (Table 1), while the IR study allowed us to fix the Cu^+/CO surface stoichiometry to be 1 : 1 (Fig. 9). XAFS/XANES/IR-supported chemisorption data found that: addition of LiCl increases enormously the dispersion of the active phase, $LaCl_3$ significantly and $MgCl_2$ barely, while addition of both KCl and CsCl results in a decrease of the surface area of the active phase. The mechanism of the enhancing effect of La and Mg on catalytic activity is still not clear, but it could be associated to the modification that they induce to the support surface: the Cu is so highly dispersed that almost all is in direct contact with support surface. Summarizing the use of a multidisciplinary approach has been the unavoidable to understand the complex role that the different additives have on the active phase of the $CuCl_2/\gamma$-Al_2O_3 catalysts for ethylene oxychlorination.

This study has been focused on investigation of the effects that additives have on the active copper phase of the catalyst. From this study, it emerges that a comprehensive understanding of the effects that additives have in the chemistry of the oxychlorination reaction will be reached only once also the modification undergone by the alumina support will be investigated and rationalized. Obviously dopants also modify the support, by formation of dopant-aluminate phase and by precipitation of dopant-chloride. The data summarized in Table 2 clearly shows that, owing to the high dispersion of the active phase, the ability to convert ethylene into dichloroethane is influenced by the dopant-modified support.

6. Synthesis, Experimental and Methods

6.1. Synthesis and sample nomenclature

All samples have been prepared by impregnation of a γ-alumina (Condea Puralox SCCa 30/170, surface area: 168 m^2g^{-1}, pore volume: 0.50 cm^3g^{-1}) with the aqueous solution of the corresponding chlorides following the incipient wetness method as described elsewhere.[22] After impregnation, the samples were dried at 373 K under a dry air flow for 3 h and then kept at RT. To minimize aging effects,[23] characterizations of samples (also at the synchrotron) have been performed 1 h after impregnation. Following the nomenclature already used in the previous papers,[22–26,28,29,42,60] samples will be labelled according to wt.% content of the different metals (Cu and additive). As an example, sample Cu5.0 represents a 5.0 wt% Cu loaded sample without additives, while sample K3.1Cu5.0 represents a catalyst prepared with 5.0 wt% Cu plus 3.1 wt% K. In all catalysts the amount of copper has been fixed to 5 wt.%, while for the doped samples, an amount additives atoms equal to the copper ones has been added, resulting to K3.1Cu5.0, Mg1.9Cu5.0, Cs10.4Cu5.0, Li0.5Cu5.0 and La10.9Cu5.0 catalysts.

6.2. Ethylene conversion tests in pulse reactor

Activity tests of the oxychlorination reaction have been made by using a conventional pulse reactor with the following procedure.[23] The reactor, containing 0.15 g of sample was heated to 500 K in nitrogen stream (30 cm^3 min^{-1}), corresponding to a contact time of 1 s. In order to ensure a complete and stable re-chlorination of the catalyst, the sample was then treated with alternate pulses of air (0.75 cm^3) and HCl (0.60 cm^3) for five times; a series of C_2H_4 pulses (0.30 cm^3) was then sent to the sample and the C_2H_4 to $C_2H_4Cl_2$ conversion has been determined by a gascromatograph (Carlo Erba Fractovap 4200) equipped with a packed column, a flame detector and an integrator (Shimadzu C-R3A Chromatopac). The side products usually found in tests on oxychlorination reaction (for example ethyl chloride and vinyl chloride) have been not detected in our experiments, probably because of adopted depletion procedure.

6.3. Sample characterization

6.3.1. CO chemisorption. Static-volumetric CO adsorption measurements were made by a Micromeritics ASAP 2010C device equipped with a turbomolecular pump, which allowed to obtain a vacuum better than 10^{-5} Torr (1 Torr 133.3 Pa) in the sample holder. All the treatments, including adsorption were performed with sufficient time to reach equilibrium. The pretreatment consisted in an evacuation at 308 K for 5 min, an evacuation at 500 K for 0.5 h, five cycles of reduction with ethylene at 200 Torr at 500 K for 15 min followed by evacuation at the same temperature for 15 min (the last time for 60 min) and, at last, an evacuation at 308 K for 30 min. The adsorption measurements were made with CO at 308 K. They consisted of the determination of the isotherms in the 10^{-4}–600 Torr range (about 20 min per point).

6.3.2. IR spectroscopy of adsorbed CO. For IR measurements, performed at room temperature, a thin self-supporting wafer of the catalyst has been prepared and activated under dynamic vacuum at 500 K for 2 h, inside an IR cell designed to allow *in situ* temperature treatments, reagents dosage and evacuation.[29] Before CO dosage, the sample was reduced at 500 K in ethylene and then cooled down to RT. More precisely, once the catalyst has been activated *in vacuo* at 500 K, keeping constant the temperature, a C_2H_4-equilibrium pressure of 200 Torr has been

Table 3 First shell, single phase, EXAFS data analysis performed on samples Cu1.4 and $CuCl_2$ (both activated *in vacuo* at 500 K) were used as models for the Cu-aluminate phase and for the supported $CuCl_2$ phase, respectively

Sample	Treatment	Shell	ΔE/eV	$N^*S_0^2$	R/Å	σ^2 (10^{-3}·Å^2)	R_{FEFF}
Cu1.4	vacuo @500 K	Cu–O	−1 ± 1	3.2 ± 0.3	1.96 ± 0.01	5.0 ± 0.9	0.013
$CuCl_2$ (anhydrous)	vacuo @500 K	Cu–Cl	−1 ± 1	3.6 ± 0.2	2.28 ± 0.02	5.4 ± 0.4	0.004

dosed on the sample and the ethylene/catalyst interaction was kept under static condition for 5 min, $C_2H_4Cl_2$ products and unreacted C_2H_4 molecules were evacuated down to 10^{-3} Torr and a second dose of 200 Torr of C_2H_4 was send with the same procedure. After 5 min of contact the pressure inside the cell was decreased down to 10^{-3} Torr, the sample was cooled down to RT. The IR spectra have been recorded at 2 cm^{-1} resolution on a BRUKER FTIR 66 spectrometer equipped with a HgCdTe cryodetector.

6.3.3. ***In situ*** **X-ray adsorption spectroscopy.** X-ray absorption measurements were carried out using synchrotron radiation of the EXAFS13 station at LURE (Orsay, France). Both Extended X-ray absorption fine structure (EXAFS) and X-ray absorption near edge spectroscopy (XANES) measurements were carried out in transmission mode using air filled ionization chambers for both incident and transmitted beams, the pressure inside the second ionization chamber was ad hoc optimized for each sample. The beam was monochromatized using a Si(111) or a Si(331) channel-cut monochromator for EXAFS and XANES spectra respectively. Four EXAFS spectra have been collected in the same experimental conditions with a sampling step of 2.0 eV/point and an integration time of 2 s/point. A single XANES spectrum was acquired for each sample, with a sampling step of 0.5 eV/point and an integration time of 2 s/point. Extracted $\chi(k)$ have been averaged before the EXAFS data analysis as detailed elsewhere.[61] EXAFS data analysis has been performed using the Arthemis software.[62] For each sample, the averaged $k^3\chi(k)$ function was Fourier transformed in the Δk = 2.0–13.0 $Å^{-1}$ interval.

Catalyst preparation for *in situ* X-ray absorption experiments has been performed by introducing a self supported pellet of the sample with optimized thickness inside an ad hoc conceived cell[60] allowing activation *in vacuo* at the desired temperature (500 K) and successive interaction with C_2H_4, again at 500 K, performed as described for IR spectroscopy of adsorbed CO.

6.4. Strategies adopted in the 2-phases EXAFS data analysis

Phases and amplitudes generated by FEFF6.0 code.[63] have first been checked on model compounds. Samples Cu1.4 and $CuCl_2$ (both activated *in vacuo* at 500 K) were used as models for the Cu-aluminate phase and for the supported, $CuCl_2$ phase, respectively.

The EXAFS data analysis on sample Cu1.4 can be performed in a straightforward manner, since only the copper aluminate phase is present on it.[22,26] We performed a 1st shell fit in the 1–2.3 Å R-range, based on 4 parameters: $N^*S_0^2$, ΔE, R_{Cu-O}, σ^2_{Cu-O} obtaining a distance R_{Cu-O} of 1.96 ± 0.01 Å. According to our pervious experience[22,23,26] we know that bulk anhydrous $CuCl_2$ is a good reference compound for the dispersed $CuCl_2$ obtained on alumina surface upon activation at 500 K, because the smaller nature of the $CuCl_2$ supported clusters can be well simulated just increasing the σ^2_{Cu-Cl} disorder factor. Table 3 summarized the results of the EXAFS fit on the model compounds.

Acknowledgements

This collaborative work has been developed in the frame of the Network of Excellence IDECAT (FP6 of the EU). C. Prestipino, G. Spoto, L. Capello, G. Casali, E. Groppo, A Zecchina, B. Cremaschi, and M. Garilli, are gratefully acknowledged for the stimulating discussions that we had on this subject over the years. N. Muddada thanks the Erasmus Mundus MaMaSELF program (http://etudes.univ-rennes1.fr/mamaself) that allowed him to come to Europe for his Master and the Norwegian Research Council for his Ph.D.

References

1 J. S. Naworski and E. S. Evil, in: *Applied Industrial Catalysis;* B. E. Leach, Ed.; Accademic Press: New York, 1983; Vol. 1, p. 239.
2 M. N. Newmann, *Encyclopedia of Polymer Science and Engineering*Wiley: New York, 1985; Vol. 17.
3 M. Garilli, P. L. Fatutto and F. Piga, *La Chimica e l'Industria, Milan*, 1998, **80**, 333.
4 F. Cavani and J. H. Teles, *ChemSusChem*, 2009, **2**, 508.
5 F. Cavani, G. Centi, S. Perathoner and F. Trifiro, *Sustainable Industrial Chemistry*, Wiley-VCH: Wenheim, 2009.
6 A. Arcoya, A. Cortes and X. L. Seoane, *Can. J. Chem. Eng.*, 1982, **60**, 55.
7 W. D. Mross, *Catal. Rev. Sci. Eng.*, 1983, **25**, 591.
8 X. J. Lu, J. Liu, G. D. Zhou, Y. N. Li, K. J. Xhen, W. X. Li and T. X. Cheng, *Chin. J. Catal.*, 2005, **26**, 587.
9 L. Xueju, L. Jie, Z. Guangdong, Z. Kaiji, L. Wenxing and C. Tiexin, *Catal. Lett.*, 2005, **100**, 153.
10 P. R. Laurer, G. Krome, L. Cordemans, R. Seifert and E. Danz, *Euro Pat. 54674*, 1981.
11 K. Shiozaki and A. Onischi, *Euro Pat. 62320*, 1982.
12 I. Fatutto, D. Carmello and A. Marsella, *Euro Pat. 1053789*, 2000.
13 P. S. S. Prasad, K. B. S. Prasad, P. K. Rao and V. K. Kaushik, *J. Mater. Sci.*, 1997, **32**, 1479.
14 A. Baiker and W. L. Holstein, *J. Catal.*, 1983, **84**, 178.
15 K. Rollins and P. A. Sermon, *J. Chem. Soc., Chem. Commun.*, 1986, 1171.
16 E. M. Fortini, C. L. Garcia and D. E. Resasco, *J. Catal.*, 1986, **99**, 12.
17 P. A. Sermon, K. Rollins, P. N. Reyes, S. A. Lawrence, M. A. Martin Luengo and M. J. Davies, *J. Chem. Soc., Faraday Trans. 1*, 1987, **83**, 1347.
18 P. S. Sai Prasad and P. Kanta Rao, *J. Chem. Soc., Chem. Commun.*, 1987, 951.
19 C. L. Garcia and D. E. Resasco, *J. Catal.*, 1990, **122**, 151.
20 A. J. Rouco, *Appl. Catal., A*, 1994, **117**, 139.
21 S. Wachi and Y. Asai, *Ind. Eng. Chem. Res.*, 1994, **33**, 259.
22 G. Leofanti, M. Padovan, M. Garilli, D. Carmello, A. Zecchina, G. Spoto, S. Bordiga, G. T. Palomino and C. Lamberti, *J. Catal.*, 2000, **189**, 91.
23 G. Leofanti, M. Padovan, M. Garilli, D. Carmello, G. L. Marra, A. Zecchina, G. Spoto, S. Bordiga and C. Lamberti, *J. Catal.*, 2000, **189**, 105.
24 G. Leofanti, A. Marsella, B. Cremaschi, M. Garilli, A. Zecchina, G. Spoto, S. Bordiga, P. Fisicaro, G. Berlier, C. Prestipino, G. Casali and C. Lamberti, *J. Catal.*, 2001, **202**, 279.
25 G. Leofanti, A. Marsella, B. Cremaschi, M. Garilli, A. Zecchina, G. Spoto, S. Bordiga, P. Fisicaro, C. Prestipino, F. Villain and C. Lamberti, *J. Catal.*, 2002, **205**, 375.

26 C. Prestipino, S. Bordiga, C. Lamberti, S. Vidotto, M. Garilli, B. Cremaschi, A. Marsella, G. Leofanti, P. Fisicaro, G. Spoto and A. Zecchina, *J. Phys. Chem. B*, 2003, **107**, 5022.
27 K. S. Go, Y. Kim, S. R. Son and S. D. Kim, *Chem. Eng. Sci.*, 2010, **65**, 499.
28 C. Lamberti, C. Prestipino, F. Bonino, L. Capello, S. Bordiga, G. Spoto, A. Zecchina, S. D. Moreno, B. Cremaschi, M. Garilli, A. Marsella, D. Carmello, S. Vidotto and G. Leofanti, *Angew. Chem., Int. Ed.*, 2002, **41**, 2341.
29 N. B. Muddada, U. Olsbye, L. Caccialupi, F. Cavani, G. Leofanti, D. Gianolio, S. Bordiga and C. Lamberti, *Phys. Chem. Chem. Phys.*, 2010, **12**, 5605.
30 C. M. Fontana, E. Gorin, G. A. Kidder and C. S. Meredith, *Ind. Eng. Chem.*, 1952, **44**, 363–368.
31 C. M. Fontana, E. Gorin, G. A. Kidder and R. E. Kinney, *Ind. Eng. Chem.*, 1952, **44**, 369–373.
32 C. M. Fontana, E. Gorin and C. S. Meredith, *Ind. Eng. Chem.*, 1952, **44**, 373–378.
33 T. Z. Zhang, C. Troll, B. Rieger, J. Kintrup, O. F. K. Schluter and R. Weber, *Appl. Catal., A*, 2009, **365**, 20.
34 C. Prestipino, G. Berlier, F. X. Llabres i Xamena, G. Spoto, S. Bordiga, A. Zecchina, G. Turnes Palomino, T. Yamamoto and C. Lamberti, *Chem. Phys. Lett.*, 2002, **363**, 389.
35 E. Groppo, C. Prestipino, F. Cesano, F. Bonino, S. Bordiga, C. Lamberti, P. C. Thune, J. W. Niemantsverdriet and A. Zecchina, *J. Catal.*, 2005, **230**, 98.
36 R. Le Toquin, W. Paulus, A. Cousson, C. Prestipino and C. Lamberti, *J. Am. Chem. Soc.*, 2006, **128**, 13161.
37 C. Lamberti, G. T. Palomino, S. Bordiga, G. Berlier, F. D'Acapito and A. Zecchina, *Angew. Chem., Int. Ed.*, 2000, **39**, 2138.
38 L. Regli, S. Bordiga, C. Busco, C. Prestipino, P. Ugliengo, A. Zecchina and C. Lamberti, *J. Am. Chem. Soc.*, 2007, **129**, 12131.
39 D. Gianolio, E. Groppo, J. G. Vitillo, A. Damin, S. Bordiga, A. Zecchina and C. Lamberti, *Chem. Commun.*, 2010, **46**, 976.
40 A. L. Ankudinov, B. Ravel, J. J. Rehr and S. D. Conradson, *Phys. Rev. B: Condens. Matter Mater. Phys.*, 1998, **58**, 7565.
41 Y. Joly, *Phys. Rev. B: Condens. Matter Mater. Phys.*, 2001, **63**, 125120 art. no. 125120.
42 C. Lamberti, S. Bordiga, F. Bonino, C. Prestipino, G. Berlier, L. Capello, F. D'Acapito, F. X. Llabres i Xamena and A. Zecchina, *Phys. Chem. Chem. Phys.*, 2003, **5**, 4502.
43 P. C. Burns and F. C. Hawthorne, *Am. Mineral.*, 1993, **78**, 187.
44 S. Hull and D. A. Keen, *Phys. Rev. B: Condens. Matter*, 1994, **50**, 5868.
45 E. Giamello, D. Murphy, G. Magnacca, C. Morterra, Y. Shioya, T. Nomura and M. Anpo, *J. Catal.*, 1992, **136**, 510.
46 C. Lamberti, S. Bordiga, M. Salvalaggio, G. Spoto, A. Zecchina, F. Geobaldo, G. Vlaic and M. Bellatreccia, *J. Phys. Chem. B*, 1997, **101**, 344.
47 D. Scarano, P. Galletto, C. Lamberti, R. DeFranceschi and A. Zecchina, *Surf. Sci.*, 1997, **387**, 236.
48 A. Zecchina, S. Bordiga, M. Salvalaggio, G. Spoto, D. Scarano and C. Lamberti, *J. Catal.*, 1998, **173**, 540.
49 D. Scarano, S. Bordiga, C. Lamberti, G. Spoto, G. Ricchiardi, A. Zecchina and C. O. Arean, *Surf. Sci.*, 1998, **411**, 272.
50 A. Zecchina, S. Bordiga, G. T. Palomino, D. Scarano, C. Lamberti and M. Salvalaggio, *J. Phys. Chem. B*, 1999, **103**, 3833.
51 C. Prestipino, L. Capello, F. D'Acapito and C. Lamberti, *Phys. Chem. Chem. Phys.*, 2005, **7**, 1743.
52 S. H. Strauss, *J. Chem. Soc., Dalton Trans.*, 2000, 1.
53 A. J. Lupinetti, S. H. Strauss and G. Frenking, *Prog. Inorg. Chem.*, 2001, **49**, 1.
54 V. Bolis, A. Barbaglia, S. Bordiga, C. Lamberti and A. Zecchina, *J. Phys. Chem. B*, 2004, **108**, 9970.
55 K. Hadjiivanov and H. Knozinger, *J. Catal.*, 2000, **191**, 480.
56 C. Prestipino, L. Regli, J. G. Vitillo, F. Bonino, A. Damin, C. Lamberti, A. Zecchina, P. L. Solari, K. O. Kongshaug and S. Bordiga, *Chem. Mater.*, 2006, **18**, 1337.
57 A. Zecchina, D. Scarano, S. Bordiga, G. Spoto and C. Lamberti, *Adv. Catal.*, 2001, **46**, 265.
58 N. K. Nag, *Catal. Lett.*, 1994, **24**, 37.
59 V. Labalme, N. Benhamou, N. Guilhaume, E. Garbowski and M. Primet, *Appl. Catal., A*, 1995, **133**, 351.
60 C. Lamberti, C. Prestipino, S. Bordiga, G. Berlier, G. Spoto, A. Zecchina, A. Laloni, F. La Manna, F. D'Anca, R. Felici, F. D'Acapito and P. Roy, *Nucl. Instrum. Methods Phys. Res., Sect. B*, 2003, **200**, 196.
61 C. Lamberti, S. Bordiga, D. Arduino, A. Zecchina, F. Geobaldo, G. Spanò, F. Genoni, G. Petrini, A. Carati, F. Villain and G. J. Vlaic, *J. Phys. Chem. B*, 1998, **102**, 6382.
62 B. Ravel and M. Newville, *J. Synchrotron Radiat.*, 2005, **12**, 537.
63 S. I. Zabinsky, J. J. Rehr, A. Ankudinov, R. C. Albers and M. J. Eller, *Phys. Rev. B: Condens. Matter*, 1995, **52**, 2995.

Publication II

Physical Chemistry Chemical Physics 2010

"Influence of additives in defining the active phase of the ethylene oxychlorination catalyst"

N. B. Muddada, U. Olsbye, L. Caccialupi, F. Cavani, G. Leofanti, D. Gianolio, S. Bordiga, C. Lamberti

This paper is published as part of a *PCCP* themed issue on recent developments in X-ray absorption spectroscopy

Guest Editor: Jeroen Anton van Bokhoven

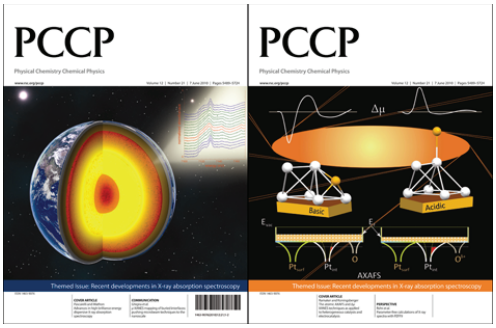

Editorial

Recent developments in X-ray absorption spectroscopy
J. A. van Bokhoven, *Phys. Chem. Chem. Phys.*, 2010
DOI: 10.1039/c0cp90010a

Perspectives

Parameter-free calculations of X-ray spectra with FEFF9
John J. Rehr, Joshua J. Kas, Fernando D. Vila, Micah P. Prange and Kevin Jorissen, *Phys. Chem. Chem. Phys.*, 2010
DOI: 10.1039/b926434e

The atomic AXAFS and Δ*μ* XANES techniques as applied to heterogeneous catalysis and electrocatalysis
D. E. Ramaker and D. C. Koningsberger, *Phys. Chem. Chem. Phys.*, 2010
DOI: 10.1039/b927120c

Advances in high brilliance energy dispersive X-ray absorption spectroscopy
Sakura Pascarelli and Olivier Mathon, *Phys. Chem. Chem. Phys.*, 2010
DOI: 10.1039/b926509k

Communication

***μ*-XANES mapping of buried interfaces: pushing microbeam techniques to the nanoscale**
Paolo Ghigna, Sonia Pin, Giorgio Spinolo, Mark A. Newton, Michele Zema, Serena C. Tarantino, Giancarlo Capitani and Francesco Tatti, *Phys. Chem. Chem. Phys.*, 2010
DOI: 10.1039/c000195c

Papers

L-edge XANES analysis of photoexcited metal complexes in solution
Renske M. van der Veen, Joshua J. Kas, Christopher J. Milne, Van-Thai Pham, Amal El Nahhas, Frederico A. Lima, Dimali A. Vithanage, John J. Rehr, Rafael Abela and Majed Chergui, *Phys. Chem. Chem. Phys.*, 2010
DOI: 10.1039/b927033g

EXAFS as a tool to interrogate the size and shape of mono and bimetallic catalyst nanoparticles
Andrew M. Beale and Bert M. Weckhuysen, *Phys. Chem. Chem. Phys.*, 2010
DOI: 10.1039/b925206a

X-Ray absorption in homogeneous catalysis research: the iron-catalyzed Michael addition reaction by XAS, RIXS and multi-dimensional spectroscopy
Matthias Bauer and Christoph Gastl, *Phys. Chem. Chem. Phys.*, 2010
DOI: 10.1039/b926385c

Combined TPRx, *in situ* GISAXS and GIXAS studies of model semiconductor-supported platinum catalysts in the hydrogenation of ethene
Sonja A. Wyrzgol, Susanne Schäfer, Sungsik Lee, Byeongdu Lee, Marcel Di Vece, Xuebing Li, Sönke Seifert, Randall E. Winans, Martin Stutzmann, Johannes A. Lercher and Stefan Vajda, *Phys. Chem. Chem. Phys.*, 2010
DOI: 10.1039/b926493k

Near sulfur *L*-edge X-ray absorption spectra of methanethiol in isolation and adsorbed on a Au(111) surface: a theoretical study using the four-component static exchange approximation
Sebastien Villaume, Ulf Ekström, Henrik Ottosson and Patrick Norman, *Phys. Chem. Chem. Phys.*, 2010
DOI: 10.1039/b926109e

Influence of additives in defining the active phase of the ethylene oxychlorination catalyst
N. B. Muddada, U. Olsbye, L. Caccialupi, F. Cavani, G. Leofanti, D. Gianolio, S. Bordiga and C. Lamberti, *Phys. Chem. Chem. Phys.*, 2010
DOI: 10.1039/b926502n

First-principles calculations of X-ray absorption spectra at the *K*-edge of 3*d* transition metals: an electronic structure analysis of the pre-edge
Delphine Cabaret, Amélie Bordage, Amélie Juhin, Mounir Arfaoui and Emilie Gaudry, *Phys. Chem. Chem. Phys.*, 2010
DOI: 10.1039/b926499j

First steps in combining modulation excitation spectroscopy with synchronous dispersive EXAFS/DRIFTS/mass spectrometry for *in situ* time resolved study of heterogeneous catalysts
Davide Ferri, M. Santosh Kumar, Ronny Wirz, Arnim Eyssler, Oxana Korsak, Paul Hug, Anke Weidenkaff and Mark A. Newton, *Phys. Chem. Chem. Phys.*, 2010
DOI: 10.1039/b926886c

Novel opportunities for time-resolved absorption spectroscopy at the X-ray free electron laser
B. D. Patterson and R. Abela, *Phys. Chem. Chem. Phys.*, 2010
DOI: 10.1039/c003406a

Spatially resolved 3D micro-XANES by a confocal detection scheme
Geert Silversmit, Bart Vekemans, Sergey Nikitenko, Sylvia Schmitz, Tom Schoonjans, Frank E. Brenker and Laszlo Vincze, *Phys. Chem. Chem. Phys.*, 2010
DOI: 10.1039/c004103n

Wavelet transform EXAFS analysis of mono- and dimolybdate model compounds and a Mo/HZSM-5 dehydroaromatization catalyst
Robert O. Savinelli and Susannah L. Scott, *Phys. Chem. Chem. Phys.*, 2010
DOI: 10.1039/b926474d

Electronic structure of alumina-supported monometallic Pt and bimetallic PtSn catalysts under hydrogen and carbon monoxide environment
Jagdeep Singh, Ryan C. Nelson, Brian C. Vicente, Susannah L. Scott and Jeroen A. van Bokhoven, *Phys. Chem. Chem. Phys.*, 2010
DOI: 10.1039/c000403k

Determination of CO, H_2O and H_2 coverage by XANES and EXAFS on Pt and Au during water gas shift reaction
Neng Guo, Bradley R. Fingland, W. Damion Williams, Vincent F. Kispersky, Jelena Jelic, W. Nicholas Delgass, Fabio H. Ribeiro, Randall J. Meyer and Jeffrey T. Miller, *Phys. Chem. Chem. Phys.*, 2010
DOI: 10.1039/c000240m

Complementarity between high-energy photoelectron and L-edge spectroscopy for probing the electronic structure of 5d transition metal catalysts
Toyli Anniyev, Hirohito Ogasawara, Mathias P. Ljungberg, Kjartan T. Wikfeldt, Janay B. MacNaughton, Lars-Åke Näslund, Uwe Bergmann, Shirlaine Koh, Peter Strasser, Lars G.M. Pettersson and Anders Nilsson, *Phys. Chem. Chem. Phys.*, 2010
DOI: 10.1039/b926414k

***In situ* time-resolved DXAFS for the determination of kinetics of structural changes of H-ZSM-5-supported active Re-cluster catalyst in the direct phenol synthesis from benzene and O_2**
Mizuki Tada, Yohei Uemura, Rajaram Bal, Yasuhiro Inada, Masaharu Nomura and Yasuhiro Iwasawa, *Phys. Chem. Chem. Phys.*, 2010
DOI: 10.1039/c000843p

Sulfur poisoning mechanism of steam reforming catalysts: an X-ray absorption near edge structure (XANES) spectroscopic study
Yongsheng Chen, Chao Xie, Yan Li, Chunshan Song and Trudy B. Bolin, *Phys. Chem. Chem. Phys.*, 2010
DOI: 10.1039/b925910b

Peroxide-like intermediate observed at hydrogen rich condition on Pt(111) after interaction with oxygen
Janay B. MacNaughton, Lars-Åke Näslund, Toyli Anniyev, Hirohito Ogasawara and Anders Nilsson, *Phys. Chem. Chem. Phys.*, 2010
DOI: 10.1039/b926409b

Influence of additives in defining the active phase of the ethylene oxychlorination catalyst

N. B. Muddada,[a] U. Olsbye,[a] L. Caccialupi,[b] F. Cavani,[b] G. Leofanti,[c] D. Gianolio,[d] S. Bordiga[d] and C. Lamberti*[d]

Received 15th December 2009, Accepted 22nd March 2010
First published as an Advance Article on the web 28th April 2010
DOI: 10.1039/b926502n

The understanding, at the atomic level, of the role played by additives (dopants or promoters) in the chemistry of an industrial catalyst is a very complex and difficult task. We succeeded in this goal for the ethylene oxychlorination catalyst ($CuCl_2/\gamma$-Al_2O_3), used to produce dichloroethane, a key intermediate of the polyvinyl chloride chemistry (PVC). Among the most used additives for both fluid and fixed beds technologies (LiCl, KCl, CsCl, $MgCl_2$, $LaCl_3$, $CeCl_4$) we have been able to highlight that KCl, and CsCl, forming in reaction conditions a mixed phase with $CuCl_2$, strongly modify the catalyst behaviour. In particular, these additives are able to displace the rate determining step from the CuCl oxidation (undoped catalyst) to the $CuCl_2$ reduction. This results from the decrease of the rate of the latter reaction, thus the overall activity of the system. For all remaining additives the rate determining step remains the CuCl oxidation, as for the undoped catalyst. These results have been obtained coupling the catalyst activity monitored with a pulse reactor working in both non-depletive and depletive modes with time resolved XANES spectroscopy performed under in operando conditions (*i.e.* coupled with mass spectrometry). Formation of CuK_xCl_{2+x} and $CuCs_xCl_{2+x}$ mixed phases has been proved monitoring the Cu(II) *d–d* transitions with UV-Vis spectrometer and the CO stretching frequency of carbon monoxide adsorbed on reduced catalyst by *in situ* IR spectroscopy. Finally, of high relevance is the observation that the fully oxidized catalyst is inactive. This unexpected evidence highlight the role of coordinatively unsaturated Cu(I) species in adsorbing ethylene on the catalyst surface indicating that copper, in the working catalyst, exhibits a (I)/(II) mixed valence state.

1. Introduction

Oxychlorination is a key-process in the modern chemical industry, playing a relevant role for chlorine atom incorporation in hydrocarbons, both saturated and unsaturated, *e.g.*, in methane, ethylene and benzene.[1,2] Recently, CO oxychlorination has also been taken into consideration for the synthesis of phosgene in alternative to the traditional process of CO direct chlorination.[3,4] More specifically, almost all the world production of polyvinyl-chloride (PVC) is nowadays obtained by the polymerization of vinyl chloride monomer (VCM), which is produced using ethylene, oxygen and chlorine as reagents following reaction (1). Production of VCM is based on cracking of 1,2-dichloroethane (EDC),

$$C_2H_4Cl_2 \rightarrow C_2H_3Cl + HCl \qquad (1)$$

which in its turn is produced by two parallel processes, *viz.* direct chlorination (2) and oxychlorination (3):

$$C_2H_4 + Cl_2 \rightarrow C_2H_4Cl_2 \qquad (2)$$

$$C_2H_4 + 2HCl + 1/2O_2 \rightarrow C_2H_4Cl_2 + H_2O \qquad (3)$$

The latter reaction, recycling HCl produced by the cracking of 1,2-dichloroethane (1), is particularly important in industrial applications because it was specifically developed to reduce the raw material (Cl_2) consumption and the exit of useless product (HCl) outside the cycle, in agreement with the modern requests of chemical industry.[5–7]

Oxychlorination reaction (3) is performed at 490–530 K and 5–6 atm using both air and oxygen in fluid or fixed bed reactors. Commercial catalysts are produced by impregnation of γ-alumina with $CuCl_2$ (4–8 wt% Cu). Other chlorides, (mainly alkaline or alkaline earth chlorides) in a variable concentration, are also added in order to improve the catalytic performances making the catalyst more suitable for use in industrial reactors.[5–11] In particular, KCl is always present in the catalysts used in fixed bed technologies, sometimes together with other alkali-metal chlorides such as CsCl, NaCl or LiCl.[12–15] Rare-earth-metal chlorides such as $LaCl_3$, added to $CuCl_2$ and KCl, are also claimed in the patent literature.[14] $MgCl_2$ is the base additive (also named dopant) in the catalysts used in fluid bed processes, where alkali-metal (such as LiCl)

[a] *inGAP centre of Research-based Innovation, Department of Chemistry, University of Oslo, Sem Saerlandsvei 26, N-0315 Oslo, Norway*
[b] *Dipartimento di Chimica Industriale e dei Materiali, ALMA MATER STUDIORUM Università di Bologna, Viale Risorgimento 4, 40136 Bologna, Italy*
[c] *Consultant, Via Firenze 43, 20010 Canegrate (Milano), Italy*
[d] *Department of Inorganic, Physical and Materials Chemistry and NIS centre of excellence, University of Torino, Via P. Giuria 7, I-0125 Torino, Italy. E-mail: carlo.lamberti@unito.it; Fax: +390116707855; Tel: +39011-6707841*

or rare-earth-metal chlorides (such as $LaCl_3$) can also be added.[16–18] Of interest is the fact that unsupported, Cu-free, $LaCl_3$ has been found to be active in the methane oxychlorination.[19]

In spite of an abundant literature on the subject,[5–9,15,20–32] a significant improvement of the knowledge of the system has been done only recently,[28–32] even if limited to the base catalyst (containing only $CuCl_2$ without additives). It has been proved[28,29] that two different copper species are present on the activated catalyst (dried at 500 K in N_2 flux): a surface aluminate where the copper ions are hosted in the octahedral vacancies of γ-Al_2O_3, and a highly dispersed copper chloride. The former phase takes place at copper content lower than 0.95 wt% Cu per 100 m^2 support, conversely the latter precipitates directly from the solution once the adsorptive capacity of alumina is exhausted. Successively it has been shown that the overall ethylene oxychlorination reaction (3) is catalyzed only by the $CuCl_2$ phase following a three steps redox mechanism: (i) chlorination of ethylene by reduction of $CuCl_2$ to CuCl; (ii) oxidation of CuCl to an oxychloride; and (iii) re-chlorination with HCl (closure of the catalytic cycle[30,31]):

$$2CuCl_2 + C_2H_4 \rightarrow C_2H_4Cl_2 + 2CuCl, \quad (4)$$

$$2CuCl + 1/2\ O_2 \rightarrow Cu_2OCl_2, \quad (5)$$

$$Cu_2OCl_2 + 2HCl \rightarrow 2CuCl_2 + H_2O. \quad (6)$$

Recently,[33] an *in situ*, time resolved, XANES study has allowed us to determine the Cu(II) $\leftrightarrow$ Cu(I) transformation occurring on the $CuCl_2/\gamma$-Al_2O_3 base catalyst in ethylene oxychlorination environment along the 373–623 K range. These data, together with the simultaneous determination of the catalyst activity, have demonstrated that the rate determining step of the ethylene oxychlorination reaction is the oxidation of CuCl according to eqn (5).

In ref. 33 the key role of potassium chloride dopant, present in the industrial catalysts used in fixed bed technologies, has also been highlighted. It has been shown that the $KCl/CuCl_2/\gamma$-Al_2O_3 catalyst behaves differently from the base one, working in a prevailing oxidized state. Combining operando XANES experiments with catalytic tests of ethylene conversion in pulse reactors and with IR experiments of adsorbed CO, it was concluded that the active phase of the of the $KCl/CuCl_2/\gamma$-Al_2O_3 is a mixed chloride (K_xCuCl_{2+x}) phase,[33] which reduces the ability of the active surface to adsorb ethylene and/or transfer two Cl atoms to each ethylene molecule. The formation of the double compound, although not detectable by XRD owing to too small crystal size,[29] was suggested by IR spectroscopy of adsorbed CO.

In this paper we extend the *in situ* XANES study to $MgCl_2/CuCl_2/\gamma$-Al_2O_3, $CsCl/CuCl_2/\gamma$-Al_2O_3, $LiCl/CuCl_2/\gamma$-Al_2O_3, $LaCl_3/CuCl_2/\gamma$-Al_2O_3, $CeCl_4/CuCl_2/\gamma$-Al_2O_3, samples, representing almost all the dopants claimed or used in the catalysts employed in both fixed and fluid bed technologies. XANES spectra, collected in operando conditions, have been supported by catalyst activity in pulse reactor, IR and UV-Vis spectroscopies.

The aim of the present work is to improve the understanding, on the chemical and atomic levels, of the role that dopant addition has on the chemistry of the ethylene oxychlorination reaction. This means that we will not enter into the engineering advantages related to an improvement of the structural resistance of the catalysts pellets hosted inside the reactors, to the reduction of the chemical and mechanic corrosion of the reactor walls *etc*. Notwithstanding this big limitation, our aim is very ambitious because the effect of additives is potentially extremely complex, and can be summarized in the following four main points. (i) $CuCl_2$ could form with the chloride of the corresponding additive cation a mixed chloride,[3,33–36] thus modifying (on the chemical ground) the active phase of the catalyst. (ii) Additive cations can compete with Cu^{2+} cations in the saturation of cationic vacancies at the alumina surface, thus altering the fraction of Cu^{2+} cations present in the active phase, that has been established for the bare $CuCl_2/\gamma$-Al_2O_3 in ref. 28 and 29 to be a known function of the alumina surface area and of the copper loading. (iii) Additive cations can modify the acidity of the support, which has been proved to be of both Lewis (surface Al^{3+} species) and Brønsted (surface Al–OH species) nature.[30] (iv) Additive cations can modify the Cu dispersion, favoring or inhibiting the clustering of the particles of the active phase on the support. In this work, we focus on the influence of promoters on the active site, improving our knowledge of the role that dopant addition has on the chemistry and redox behaviour of the active phase and on the effect that these chemical modifications has on the increase or decrease of catalytic activity observed as a consequence of catalyst doping.

2. Synthesis, experimental and methods

2.1 Materials

All samples have been prepared by impregnation of a γ-alumina (Condea Puralox SCCa 30/170, surface area: 168 $m^2\ g^{-1}$, pore volume: 0.50 $cm^3\ g^{-1}$) with the aqueous solution of the corresponding chlorides following the incipient wetness method as described elsewhere.[28] After impregnation, the samples were dried at 373 K under a dry air flow for 3 h and then kept at RT. To minimize aging effects,[29] characterizations of samples (also at the synchrotron) were performed 1 h after impregnation. Following the nomenclature already used in the previous papers,[28–33,37,38] samples will be labeled according to wt% content of the different metals (Cu and additive). As an example, sample Cu5.0 represents a 5.0 wt% Cu loaded sample without additives, while sample K3.6Cu5.0 represents a catalyst prepared with 5.0 wt% Cu plus 3.6 wt% K. In all catalysts used for XANES, IR and UV-Vis-NIR DRS spectroscopies the amount of copper has been fixed to 5 wt%, while for the doped samples, an atomic ratio of Cu to dopant metal equal to 1 : 1 has been adopted, resulting to K3.6Cu5.0, Mg1.9Cu5.0, Cs10.4Cu5.0, Li0.5Cu5.0, La10.9Cu5.0 and Ce11.0Cu5.0 catalysts. In all the catalysts used for catalytic tests in pulse reactor the amount of copper was always 5 wt% and the atomic ratio Cu : dopant was equal to 2 : 1, resulting in K1.55Cu5.0, Mg0.95Cu5.0, Li0.26Cu5.0 and Cs5.21Cu5.0 samples.

2.2 Characterization techniques

The XANES experiments in operando conditions have been performed by feeding a cell containing a self supported thin pellet of the catalyst with a diluted mixture of the three reagents (C_2H_4 : HCl : O_2 : N_2 = 100 : 36.1 : 7.6 : 180), representative of the fixed bed process. In the course of the experiment the temperature was increased from 373 to 623 K, was kept constant at 623 K for 10 min, and then decreased again to 373 K. In both ramps a heating (cooling) speed of 12 K min^{-1} has been adopted, while each XANES spectrum has been obtained by integrating for 30 s. Both values resulted in a good compromise between signal/noise ratio of the spectra and temperature resolution of the experiment: one spectrum each 6 K. The gas output was analyzed by a Balzers Quadstar 422 quadrupole mass spectrometer. Details on the X-ray absorption cell allowing measurements in operando conditions to be made have been reported elsewhere.[37]

The quantification from XANES spectroscopy of the average oxidation state of a transition metal hosted inside a given sample, needs the use of appropriate reference compounds with well defined oxidation state and having a local environment of the metal as close as possible to that of the investigated sample. It has been shown that the XANES spectra of the activated undoped catalyst ($CuCl_2/\gamma$-Al_2O_3) before and after reduction in C_2H_4 atmosphere at 500 K resemble that of $CuCl_2$ and CuCl model compounds, respectively, with some differences.[30,32,38] Discrepancies are due to the facts that copper chloride particles are nanosized and to the fact that the catalyst contains a surface Cu–aluminate phase, having O and not Cl as neighbors and not reacting with ethylene. This causes a constant fraction of Cu^{2+} to always be present (which has XANES features different from that of $CuCl_2$). These studies reveals that ($CuCl_2/\gamma$-Al_2O_3) before and after reduction in C_2H_4 atmosphere at 500 K are, in our study, better references than bulk $CuCl_2$ and CuCl model compounds.

XANES spectra have been collected at the ID24 dispersive EXAFS beamline[39] of the ESRF facility. For each experiment the dispersive set-up allows the collection of a large number of XANES spectra. For each spectrum, two independent methods have been used to quantify the fraction of Cu(II) of the active phase on the catalyst in the ith spectrum, y_i. The first one is based on edge position, that we have arbitrarily defined as the energy corresponding to normalised $\mu x = 0.5$ (see horizontal dotted segment in Fig. 1). According to this method, the Cu(II) fraction is defined as: $y_i = (E_i - E_{Red})/(E_{Ox} - E_{Red})$, where E_{Ox} and E_{Red} are the energy of the edge in the oxidized and reduced reference spectra respectively; and E_i the position of the edge in the i-th spectrum.[33,38,40] the second is based on the intensity (I_i) of the first maximum of the Cu(I) component in the derivative of the ith spectrum at 8982 eV: $y_i = 1 - I_i/I_{Red}$, where I_{Red} is the intensity of the maximum in the first derivative spectrum of the reduced reference spectrum (see vertical dotted line in the inset of Fig. 1). These methods allow us to determine the onset temperatures of Cu(II) → Cu(I) reduction during the ramp up experiments (*vide infra*, Fig. 4 and Table 1) as the temperature where the Cu(II) fraction reaches the value $y_i = 0.9$. The onset temperature for the catalytic activity has been obtained from the O_2 consumption

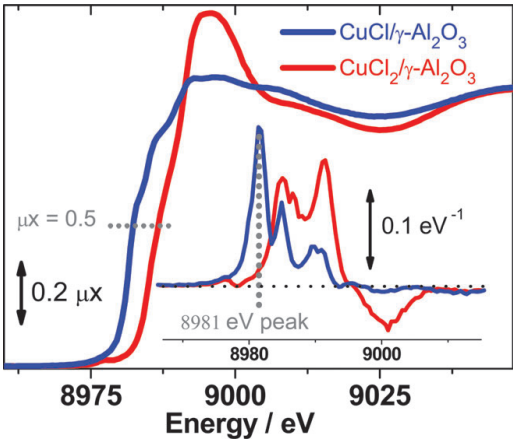

Fig. 1 XANES spectra, collected in transmission mode with the standard step scan acquisition mode, of the activated $CuCl_2/\gamma$-Al_2O_3 catalyst before, red, and after, blue, reduction in C_2H_4 atmosphere at 500 K. These spectra are used as reference for the material containing 100% Cu(I) and Cu(II) in the active phase, respectively in the evaluation of the average oxidation state of the catalysts along the reaction (*vide infra*, Fig. 2 and 3). The horizontal dashed segment indicates position in the spectrum used to evaluate the fraction of Cu(II) from the edge shift. The inset contains the corresponding first derivative: the horizontal doted line represents the zero level. The vertical dotted line evidences the huge peak in the first derivative spectrum of the Cu(I) phase. As the derivative of the spectrum of the Cu(II) phase is negligible at that energy, for any spectrum collected in operando conditions, the intensity of the signal at 8981 eV in its derivative is proportional to the amount of Cu(I) in the sample.

(z) data as the intercept between two lines defined as follows. The former is the best ($z = a$) constant line passing through the low temperature points (where there is zero activity). The latter is the best ($z = bT + c$) line passing through the high temperature points (where the activity is certainly started).

For IR measurements, performed at room temperature, a thin self-supporting wafer of the catalyst has been prepared and activated under dynamic vacuum at 500 K for 2 h, inside an IR cell designed to allow *in situ* temperature treatments, reagents dosage and evacuation. Before CO dosage, the sample was reduced at 500 K in ethylene and then cooled down to RT. The IR spectra have been recorded at 2 cm^{-1} resolution on a BRUKER FTIR 66 spectrometer equipped with a mercury cadmium telluride cryodetector. UV-Vis-NIR spectra have been performed in diffuse reflectance mode on a Cary 5 spectrophotometer, equipped with a reflectance sphere. Before UV-Vis-NIR experiments, samples were activated under a dynamic vacuum at 500 K for 2 h.

Activity tests of the oxychlorination reaction have been made by using a pulse reactor made of glass, placed in an oven. The outlet of the reactor is directly fed to a gas-chromatographic column, packed with 1% SP-1000-carbopack 60/80; the column is maintained at 150 °C. A flame-ionization detector (T 220 °C) is used to determine the concentration of unconverted ethylene and of produced 1,2-DCE. Pulses of reactants are directly injected into the reactor, by means of a

Table 1 Summary of the main results obtained from the analysis of the operando XANES spectra reported in Fig. 4. For the ramp up experiments we report the starting (at 373 K) and the final (at 623 K) fraction of Cu(II) and the temperature when a valuable fraction of Cu(I) and a valuable amount of O_2 consumption have been detected. For the ramp down experiments we just report the starting (at 623 K) an the final (at 373 K) fraction of Cu(II). Typical errors in the determination of the Cu(II) fraction is ±5%, while for the starting temperatures for the Cu(II) reduction and the O_2 conversion processes the errors are ±10 K, note that in a single XANES spectrum the sample temperature increases (decreases) by 6 K.

	Ramp up				Ramp down	
Catalyst	Cu(II) [%] Initial	Cu(II) [%] Final	T start/K Cu(II) reduction	T start/K O_2 conversion	Cu(II) [%] Initial	Cu(II) [%] Final
Cu5.0	100	0	480	480	0	0–20
Li0.5Cu5.0[a]	95	25	550	500	0	0–10
K3.1Cu5.0[a]	100	35	520	480	30	70
Cs10.4Cu5.0[a]	90	45	580	560	35	100
Mg1.9Cu5.0	95	0	490	480	0	10
La10.9Cu5.0[b]	100	0–10	510	520	0–10	0–10
Ce11.0Cu5.0[b]	100	0–10	475	470	0–10	0–10
Cu/α-Al_2O_3[a]	100	50	505	525	30	30

[a] The difference between the fraction of Cu(II) measured at the end of the ramp up experiment (third column) and the beginning of the ramp down (sixth column) testifies the fact that equilibrium conditions have not been reached at the end of the ramp up experiment and that the reduction process still continues during the 10 min isotherm at 623 K that separates the beginning of the ramp down experiment from the end of the ramp up one. [b] For these samples, in the 550–623 K interval of the ramp up experiment, and during the whole ramp down one a systematic difference of 10% in the Cu(II) fraction evaluated from the two methods (edge shift and intensity of the of the first peak in the derivative spectra) has been observed, see parts (e) and (f) in Fig. 4.

gas syringe. In order to better evidence variations of catalytic performance with pulse number, a high catalyst volume/gas volume was used: 0.30 g catalyst, carrier (N_2) 30 mL min^{-1}. Pulse tests were carried out at 493 K in both non-depletive and depletive modes. Non-depletive mode consists in alternating a pulse of air (0.25 mL), with one of HCl (0.20 mL) and one of ethylene (0.10 mL) (corresponding to the stoichiometric ratio for ethylene oxychlorination to dichloroethane), and repeating the sequence until a constant ethylene conversion is asymptotically obtained, which corresponds to a pseudo steady-state situation. At these conditions, the catalyst can be considered as representative of the steady state reached under flow conditions, with the exception of a lower surface coverage by adsorbed reactants. Once the steady state conditions have been reached, the experiment continues under depletive mode, dosing ethylene pulses until the consumption of half of the total chlorine available on the sample, as predicted by eqn (4) is reached. The overall amount of ethylene needed in this step measures the total amount of reactive Cu(II) species available for redox interaction under pseudo-steady-state conditions. The catalyst samples used in these tests had the following composition: K1.55Cu5.0, Mg0.95Cu5.0, Li0.26Cu5.0 and Cs5.21Cu5.0, in which the atomic ratio Cu : dopant is 2 : 1.

2.3 Brief description on the different industrial processes and comparison with the adopted experimental set-up

Before entering into the discussion of the experimental results it is worth spending some time in describing the relevance and limitation of the adopted experimental set-ups in simulating the behaviour of industrial reactors.

The two main issues of the industrial process for $C_2H_4Cl_2$ production are total hydrogen chloride conversion and minimal combustion. In general the higher the HCl/C_2H_4 ratio is, the lower the selectivity to CO_x, and the higher the amount of unconverted HCl. Therefore, it is necessary to search for a compromise in the industrial operation. This is one of the main reason why dopants were introduced, in order to allow operation at lower HCl/C_2H_4 ratio, and to achieve total HCl conversion, at the same time keeping the selectivity to DCE as high as possible. The main difference between an air based and an oxygen based oxychlorination process is that an air based process is a once-through process while in an oxygen based process the gaseous product is recycled back to the reactor after bleeding out a small vent stream to avoid build up of by-products and inerts. The impact of this is: (i) Once-through air based processes operate with a surplus of the cheapest reactant oxygen, 10–30%, and with an HCl/C_2H_4 close to the stoichiometric ratio (1–5% surplus of ethylene). (ii) The reactor feed composition in an oxygen based process depends on the composition of the recycle gas. In a fixed bed process this tends to be ethylene rich while in a fluid bed process it is $CO + CO_2$ rich. In both processes the O_2 content in the recycle gas is kept low, <1 vol%, to avoid combustible gas mixtures. This means that an oxygen based process is operated with a reactor feed close to stoichiometric with respect to O_2 (O_2/HCl feed close to 0.25) while the ethylene surplus is quite high, particularly in fixed bed processes.

Moreover, the oxychlorination reaction (3) is highly exothermic ($\Delta H = -240$ kJ mol^{-1}) and requires heat removal for temperature control, which is essential for efficient production. This is easily achieved in the fluid bed reactors discussed so far, but in fixed bed reactors undesired hot spots have to be minimized as they lead to more by-products, mainly through increased ethylene oxidation to carbon oxides and increased $C_2H_4Cl_2$ cracking. Temperatures higher than 600 K will also progressively deactivate the catalyst through $CuCl_2$ sublimation. The tendency to develop hot spots can be minimized by packing the reactor tubes with catalysts having a progressively different ratio between the active cupric chloride phase and the dopant phase, in order to provide an activity gradient along the length of the reactor. Compared with the fluid bed process, fixed bed oxychlorination generally operates at higher temperatures and gauge pressures.

On the basis of this summary, it is evident that the type of dopant, its concentration, the oxidant source (air or O_2), the steam stoichiometry, the reaction temperature, and pressure are specific of each type of industrial reactor. It is worth underlining that the aim of the present study is to investigate the role of dopant on the redox behavior of Cu chloride based catalysts in the oxychlorination reaction. Consequently we decided not to try to reproduce the exact operation condition of each single different reactor, but to fix the feed composition adopted in the operando XANES experiments (closer to an oxygen-based rather than to an air-based process) for all additives investigated in this work. Thus, it is evident that the numerical values obtained in this work could not be used directly to obtain quantitative data for a given industrial reactor. However, reported results have a general value from the chemical point of view, regardless of the type of reactor (fluid or fixed bed), of the type of oxidant used in the feed (air or oxygen), of the feed composition and of the reaction pressure and they can consequently be used to construct useful qualitative trends.

3. Results and discussion

3.1 *In situ* XANES study in operando conditions

The *in situ* XANES study on Cu5.0 and K3.1Cu5.0, presented in ref. 33 is now extended to the Mg1.9Cu5.0, Cs10.4Cu5.0, Li0.5Cu5.0, La10.9Cu5.0 and Ce11.0Cu5.0 catalysts. In the course of experiments, the catalyst was fed with the flux of C_2H_4, O_2 and HCl mixture and the temperature was increased from 373 to 623 K and then decreased again to 373 K after 10 min in isotherm at 623 K, where XANES spectra were not monitored. This allows us to investigate the wide range of temperatures which can be found in the different zones of the fixed bed reactors at different periods of catalyst lifetime. XANES spectroscopy being very sensitive to the Cu(I) ↔ Cu(II) changes,[30,31,33,37,38,41–50] the oxidation state of the catalyst was investigated by the change of features in the XANES spectra. This is particularly true when appropriate model compounds, with well defined oxidation and coordination states, are available for comparison. In this regard, the reader should refer to the comparison of the XANES spectra done in ref. 30–32 and 38 and to the related discussion. In the quoted papers it has been shown that the XANES spectra either of the fresh catalyst (just thermally activated) or of the catalyst after interaction with HCl [*i.e.* at the end of the step-wise cycle described in eqn (4)–(6)], were very close to that of the $CuCl_2$ model compound.

As far as the XANES spectra obtained on the catalyst after interaction with C_2H_4 in static conditions are concerned, it has been shown that they were in fair agreement with that of CuCl, except for a less pronounced 1s → 4p transition. The difference with the reference compound has been explained in terms of the high dispersion of the CuCl particles formed on the reduced catalyst, showing 50% of surface Cu(I) as determined in a combined IR/CO chemisorption study.[30]

Fig. 2a,b reports the XANES spectra and the corresponding first derivatives obtained during the ramp-up experiment on sample Cu5.0. The corresponding ramp down results are reported in Fig. 2c,d. Fig. 3 reports the results of the same experiment performed on K3.1Cu5.0 catalysts.

A comparison between the XANES spectra reported in Fig. 2a and spectra of model compounds points out that the low temperature spectra are close to that of $CuCl_2$, while the high temperature spectra are close to that of CuCl, see also Fig. 1.[30–32,38] The $CuCl_2$ to CuCl reduction is evidenced by the progressive shift of the edge of Cu5.0 catalyst, which moves from 8988.5 to 8981.5 eV upon increasing temperature from 373 to 623 K, and by the white line shift from 8996.5 to 8988.5 eV accompanied by an intensity decrease of about 25% (compare red and blue curves in Fig. 2a). The derivative spectra (Fig. 2b) shows the typical features of $CuCl_2$ (two resolved maxima at 8986 and 8992 eV and one minimum at 9001.5 eV, see the red curve) and CuCl (strong maximum at 8982 eV, blue curve) in the low and high temperature ranges, respectively.[30–32,38] The presence of two isosbestic points in XANES (8990 and 9005 eV) and derivative spectra (8984 and 8995 eV) is noteworthy because it is the direct proof that only two species are present on the catalyst in a significant amount: $CuCl_2$ and CuCl in

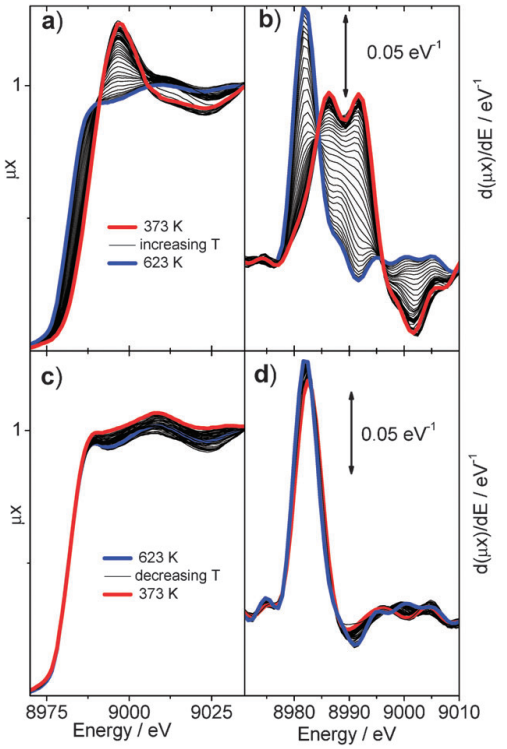

Fig. 2 Part (a): XANES spectra (each collected over 30 s) of Cu5.0 catalyst during the heating part of the experiment: from 373 (red curve) up to 623 K (blue curve) by 12 K min^{-1}. Part (b): corresponding derivative spectra Fourier-filtered to remove the high frequency noise. Parts (c) and (d) as parts (a) and (b) for the cooling part of the experiment from 623 (blue curve) down to 373 K (red curve) by 12 K min^{-1}.

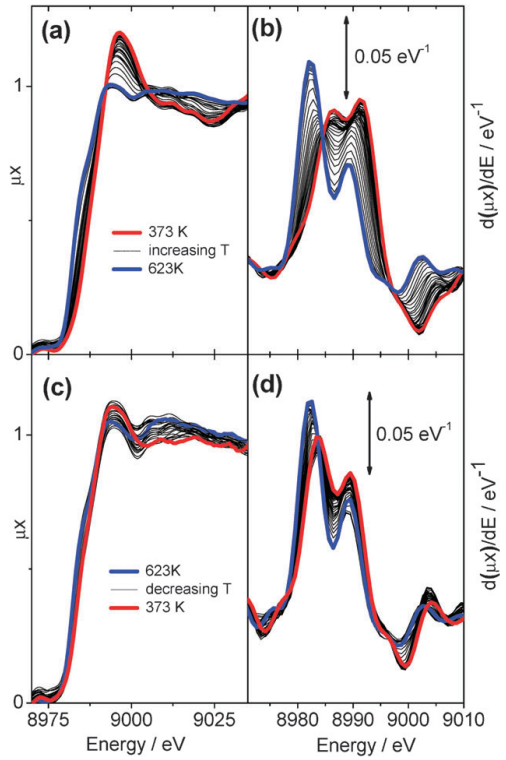

Fig. 3 As Fig. 2 for the K3.1Cu5.0 catalyst.

mutual transformation. The oxychloride species, formed following path (5) is not detected because the re-chlorination step is too fast (*vide infra*). During the ramp-down experiment (Fig. 2c,d) the oxidation state of the copper species present on the catalyst does not undergo any significant changes, being the XANES features nearly unchanged. Basically the small differences observed in the spectra reported in Fig. 2c are due to the error in the normalization of the dispersive XANES spectra. This means that, in the presence of reagent flux, the stable form of the active phase on Cu5.0 catalyst is CuCl.

Fig. 3 reports the data of the above discussed experiment repeated on sample K3.1Cu5.0. In this case it is evident that the quality of the spectra is not as good as that found in the previous experiment. This is simply a consequence of the higher difficulty that we had in finding a sufficiently homogeneous point on the catalyst pellet to perform the dispersive experiment. As dispersive XAFS concentrate the whole polychromatic beam in few μm, the sample homogeneity must be guaranteed at that scale, a point that is much more demanding than in standard XAFS. Notwithstanding these problems, inherent to the technique, we can conclude that for K3.1Cu5.0, the behaviour of the XANES features during the ramp up experiment (parts a and b) is similar to that shown by Cu5.0 catalyst (Fig. 2a,b), although less pronounced (the edge shift stops at 8986 eV). This means that the reduction of Cu(II) species is not complete for the K3.1Cu5.0 catalyst even at 623 K. Conversely, a different behaviour is observed during the ramp down (Fig. 3c,d), where the oxidation state of copper comes back to +2. The remaining catalysts, for which raw XANES spectra (and corresponding derivatives) are not reported for brevity, behave similarly to Cu5.0 (Mg1.9Cu5.0, La10.9Cu5.0) or to K3.1Cu5.0 (Cs10.4Cu5.0), which is the case for the Li0.5Cu5.0 intermediate.

In the present work, see Fig. 1, Cu(II) → Cu(I) reduction was monitored by the decrease of the white line intensity (parts a and c of Fig. 2 and 3) and by the edge blue shift, more evident in the first derivative spectra (parts b and d of Fig. 2 and 3). A quantitative evaluation of Cu(I) and Cu(II) concentration has been obtained from the cross analysis of edge position and first derivative maxima as reported in detail in ref. 38.

In Fig. 4 we report, for the whole set of catalysts, the fraction of Cu(II) (evaluated from the edge shift and from the intensity of the first maximum of the derivative of the XANES spectra, full and dashed lines, respectively) and activity (evaluated by the O_2 consumption, scattered dots) as a function of the temperature during both ramp up (left) and down (right) experiments. For all the samples only Cu(II) is present at the starting point (373 K) and the catalyst is inactive. O_2 conversion and Cu(II) reduction start when a cut off temperature (peculiar of each sample) is reached and then progressively increases. From the huge amount of data reported in Fig. 4, the most relevant values have been extracted and summarized in Table 1. In particular, for each sample we report: (i) the percentage of Cu(II) at the begin and at the end of both ramps; (ii) the temperatures where the Cu(II) reduction process and the oxychlorination reaction start for the ramp-up experiment.

Within the uncertainty of the experiment (±10 K) Cu5.0, Mg1.9Cu5.0, Ce11.0Cu5.0 and La10.9Cu5.0 begin to convert C_2H_4 into $C_2H_4Cl_2$ at the same temperature when Cu(II) begins to be reduced to Cu(I). The phenomenon occurs around 480 ± 10 K for Cu5.0, Mg1.9Cu5.0 and Ce11.0Cu5.0 and at a slightly higher temperature (510 ± 10 K) for La10.9Cu5.0 catalyst. These catalysts exhibit a complete reduction of Cu(II) to Cu(I) at the end of the ramp up experiment. During the ramp down experiment the four catalysts remain in the reduced state, being the final estimated Cu(II) fraction in the 0–10% range. In the following we will refer to Cu5.0, Mg1.9Cu5.0, Ce11.0Cu5.0 and La10.9Cu5.0 catalysts in a comprehensive way as to Family I. In summary, at the typical oxychlorination temperature, Cu(I) dominates and the rate-determining step of the overall oxychlorination reaction (for Family I catalysts) is the oxidation of CuCl, eqn (5).

Catalysts Li0.5Cu5.0, K3.1Cu5.0 and Cs10.4Cu5.0 have a significantly different behaviour. For these samples the start of the reduction process occurs at higher temperature: around 520, 550 and 580 K for K3.1Cu5.0, Li0.5Cu5.0 and Cs10.4Cu5.0, respectively (Table 1). In all cases the catalyst starts to consume O_2 at a temperature 20–50 K lower than the corresponding reduction temperature, meaning that the catalysts is already working when the fraction of Cu(I) is below the XANES detection limit. At the end of the ramp up experiment only a fraction of copper lies in the reduced state 75, 65 and 55% for Li0.5Cu5.0, K3.1Cu5.0 and Cs10.4Cu5.0 respectively

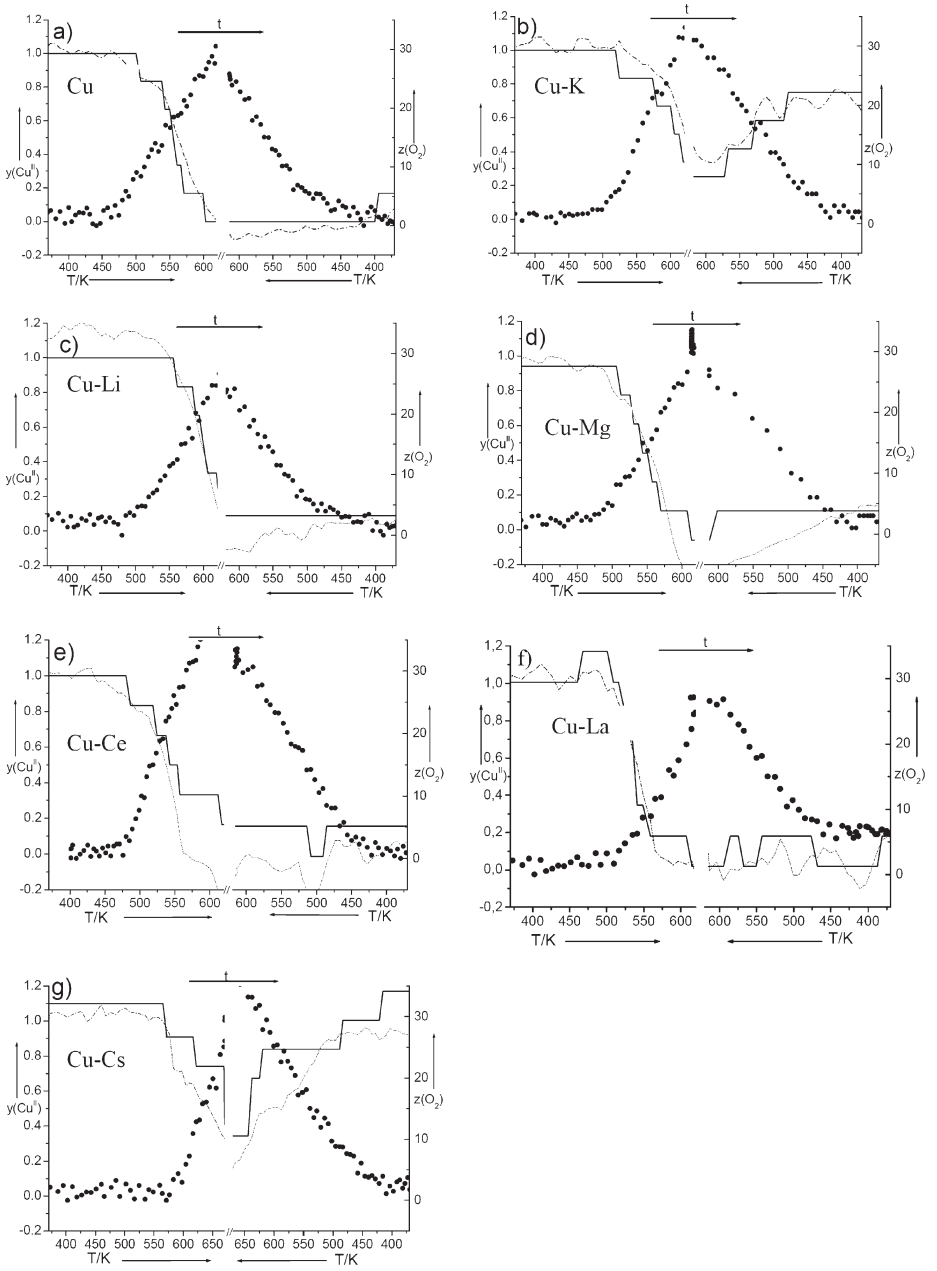

Fig. 4 Summary of the XANES experiments in operando conditions. O_2 conversion (scattered dots right axis: z) and Cu(II) fraction (left axis: y), determined from the edge shift (full line) and from the first maximum of the derivative spectrum (dotted line) during temperature ramp up (left part). Right part as the left part for the temperature ramp down. (a)–(g) parts refers to catalysts Cu5.0, K3.1Cu5.0, Li0.5Cu5.0, Mg1.9Cu5.0, Ce11.0Cu5.0, La10.9Cu5.0 and Cs10.4Cu5.0, respectively.

(Table 1). Only Li0.5Cu5.0 is able to complete the reduction, holding the sample at the maximum temperature for 10 min (see experimental), and to remain in the reduced state during the ramp down. Conversely, K3.1Cu5.0 and Cs10.4Cu5.0

confirm their high affinity towards the oxidized state being the Cu(II) fraction at the end of the ramp down 70 and 100% respectively. The data summarized in Fig. 4 imply that the rate-determining step of the overall oxychlorination reaction (3) catalyzed by K3.6Cu5.0 and Cs10.4Cu5.0 is the reduction of the active phase, eqn (4). In the following we will refer to K3.1Cu5.0 and Cs10.4Cu5.0 catalysts in a comprehensive way as for Family II. For catalyst Li0.5Cu5.0, the situation is not so sharply defined (see also the spectroscopy results reported in section 3.4) and intermediate behaviors between those followed by Families I and II have been observed.

Of interest is the experiment performed supporting 5 wt% on a low surface area α-Al_2O_3 support (see last line in Table 1). Notwithstanding the fact that $CuCl_2$ supported on α-Al_2O_3 exhibits a very low dispersion (owing to the low surface area of the support: 18 $m^2\ g^{-1}$), we surprisingly observe a significant reduction of the copper phase. This implies that the overall oxychlorination reaction is not just a surface reaction but that it is able to propagate inside the $CuCl_2$ bulk.

3.2 *In situ* XANES study in C_2H_4, O_2 and O_2–HCl mixture flows

To understand the different behavior of Family I catalysts, where the reduced state of copper prevails, with respect to Family II, where copper is mainly present as Cu(II), two representative samples of both categories (Cu5.0 and K3.1Cu5.0, respectively) have been subjected to further investigation.

Fig. 5 reports the oxidation state of copper in both Cu5.0 (parts a and b) and K3.1Cu5.0 (parts c and d) catalysts in two subsequent ramp up experiments performed by increasing the temperature from 373 to 623 K in flow of ethylene (parts a and c) and, after cooling down to RT (data not reported), by another heating ramp in oxygen (parts b and d). By comparing the two reduction ramps (Fig. 5a and c), it is evident that at each temperature the fraction of Cu(II) is higher in K3.1Cu5.0 than in Cu5.0 catalysts. At the end of the ramp, the latter is completely reduced, while the former still contain 35% of Cu(II), see data summarized in Table 2. The subsequent ramp up experiment performed in O_2 flux (continuous and dotted lines in Fig. 5b,d) results in an immediate reoxidation for K3.1Cu5.0 sample, while for Cu5.0 sample the first significant Cu(II) increase occur at around 400–420 K (see Table 2). Both samples undergo a complete re-oxidation at the end of the heating ramp in O_2 flux. This result is in apparent conflict with the tendency of Cu5.0 catalyst to remain in the reduced state in reaction condition, *vide supra* section 3.1, Fig. 4a and Table 1. However, when the same experiment is repeated with a O_2–HCl mixture (scattered symbols in Fig. 5b), the oxidation of Cu5.0 catalyst is inhibited: it starts only around 550–580 K, and, even at 623 K, Cu(I) is still the dominant copper species on the catalyst, see Table 2.

The behaviour of Cu5.0 and K3.1Cu5.0 during ramping under O_2 atmosphere is probably a combination of thermodynamic and kinetic effects. Thermodynamics drive the surface state towards Cu(II) at all temperatures, but kinetics are too slow, especially for the Cu5.0 catalyst, to obtain full oxidation at low temperatures. When HCl is added to the O_2 flow, then oxidation is even slower, and this may suggest that HCl and O_2 compete for adsorption sites on the catalyst, further slowing down the oxidation process.

3.3 The dynamics of the Cu species: activity in pulse reactor operating in non-depletive and depletive modes

XANES experiments demonstrate that the effect of dopants is very complex. In order to gain a deeper insight on the role of alkali and alkaline earth metal ions on the catalytic properties, pulse experiments were carried out in both *non-depletive* (in Fig. 6) and *depletive* (Fig. 7) modes.

Pulse experiments, carried out in a *non-depletive* mode, were performed by alternating one pulse of air with one of HCl and one of ethylene. Each cycle of three pulses modifies the characteristics of the active phase, because rates for the reactions reported in eqn (4)–(6) are different. In other words, when the average oxidation state of Cu in the active layer is far from that one in the steady-state reaction conditions, the rates of the incorporation of Cl and O atoms in the active phase are not in balance with the rates for the removal of the Cl and O atoms (the latter occurring when ethylene is pulsed). Asymptotically, the three rates become numerically equivalent, and a pseudo steady state is reached (equilibrated catalyst), for the adopted specific reaction conditions. After that, no further variation of catalytic performance is expected when pulses of reactants are again cyclically fed to the catalyst. On the basis of what learnt from operando XANES experiments reported in Fig. 5b, the fact that in non-depletive conditions we are dosing oxygen alone (without the co-presence of HCl), implies that it will be more efficient in oxidizing the active phase than in a flow reactor where its action will be partially inhibited by HCl. So the equilibrated state reached in these conditions will be more oxidized than that reached in a flow reactor working at the same temperature.

Fig. 6 compares the ethylene conversion at 493 K as a function of the number of three pulses cycle. It is worth noting that similar experiments made at different temperatures (data not reported) showed that at 493 K there is minimal formation of heavy compounds (whereas at lower temperatures the formation of heavy compounds is relevant). Therefore, no phenomena of catalyst deactivation due to heavies' accumulation are present in the data reported in Fig. 6, at least in the course of our experiment.

With all the catalysts the ethylene conversion increased when the number of pulse cycles was increased. It is striking to note that in all cases the fully oxidized fresh catalyst is inactive in ethylene conversion and that the activity progressively increases, with different slopes depending on the additive, till pseudo-steady state is reached. This underlines an unexpected feature of this class of catalysts that need the presence of a fraction of reduced Cu(I) species to convert ethylene. In other words the active phase must be regarded as a $CuCl_2$/CuCl mixed phase. A possible explanation of the presented data is that a coordinatively unsaturated Cu(I) site is needed to fix ethylene at the surface.

Non-depletive pulse tests support XANES experiments, already summarized in Fig. 4: both experiments underline that the composition of the active phase changes upon exposure to

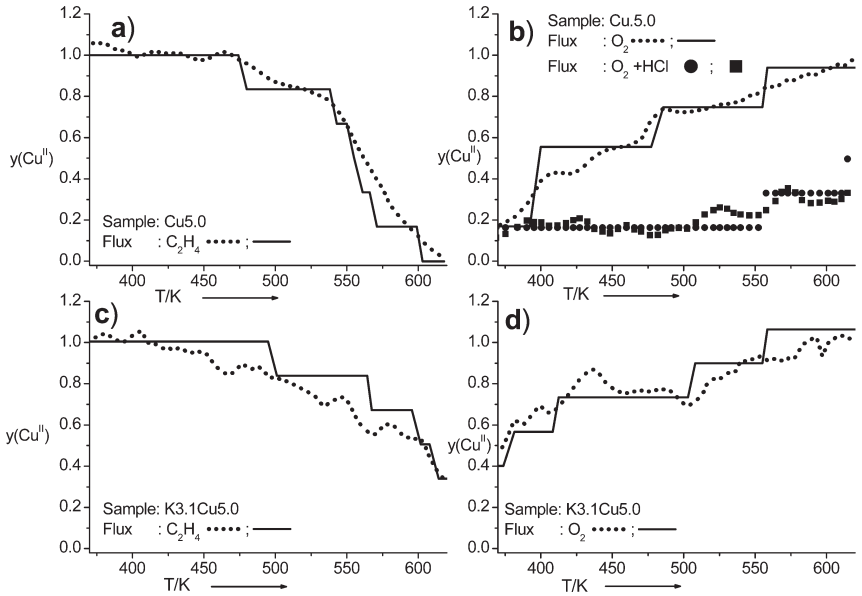

Fig. 5 Cu(II) fraction determined from the edge shift (full line) and from the intensity of the first maximum of the derivative of the XANES spectrum (dotted line) during a ramp up experiment (370–620 K) in flux of a single reagent. Part (a): Cu5.0 sample in ethylene flux. Part (b) Cu5.0 sample in oxygen flux. The experiment reported in part (b) follows temporarily that reported in part (a). Parts (c) and (d) as parts (a) and (b) for the K3.1Cu5.0 sample. The scattered circles and squares also reported in part (b) refer to the Cu(II) fraction of Cu5.0 catalyst (determined from the edge shift and from the intensity of the first maximum of the derivative) during a ramp-up experiment (370–620 K) in O_2-HCl mixed flux.

Table 2 Summary of the main results obtained from the analysis of the XANES spectra collected during the ramp up experiments preformed on Cu5.0 and K3.1Cu5.0 catalysts in different fluxes, and reported in Fig. 5. We report the starting (at 373 K) an the final (at 623 K) fraction of Cu(II) and the temperature when a valuable fraction of Cu(I) has been detected in the reduction runs (in ethylene flux) or when a valuable reoxidation occurs in the oxidation runs (O_2 and O_2 + HCl flux). Typical errors in the determination of the temperature and of the Cu(II) fraction are ± 10 K and ± 5%, respectively

Catalyst	Fluxed Gas	Cu(II) [%] Initial	Cu(II) [%] Final	*T* start/K Cu(II) reduction	*T* start/K Cu(I) oxidation
Cu5.0	C_2H_4	100	0	475	—
K3.1Cu5.0	C_2H_4	100	35	495	—
Cu5.0	O_2	15	100	—	400–420
K3.1Cu5.0	O_2	40	100	—	370–400
Cu5.0	O_2 + HCl	15	35	—	550–580

reactants. The observed behavior is due to the progressive reduction of the active phase, which shifts from $CuCl_2$ to a valence-mixed $CuCl_2$/CuCl phase; this also leads to the generation of a more active layer. The data reported in Fig. 6, highlight unambiguously the need for Cu(I) adsorbing sites on the catalyst surface. This could not be unambiguously affirmed from XANES data, because in that case two variable were simultaneously modified: the catalyst temperature and the Cu(II)/Cu(I) fraction, so that it was not easy from XANES data only to discriminate between them. Moreover a fraction of reduction lower than 5% would easily escape from XANES detection.

Coming to the differences among the different dopants, the results shown in Fig. 6 demonstrate that the catalysts showing the greater activity at pseudo steady state (equilibrated catalysts) were Mg0.95Cu5.0, Cu5.0 and Li0.26Cu5.0, the least active were K1.55Cu5.0 and Cs5.21Cu5.0. Since tests were carried out under *non-depletive* conditions, a correspondence with Cu oxidation state is not possible.

However, the amount of Cu(II) available in the equilibrated catalyst can be determined by carrying out depletive pulse experiments (feeding only ethylene pulses) on the equilibrated catalysts, see Fig. 7. In this case, the Cl atoms are picked up by the ethylene, with the concomitant reduction of Cu(II) to Cu(I), according to reaction (4). Therefore, the initial activity in ethylene conversion is high, and then progressively decreases because of the depletion of Cl. The integration of the area below the experimental curves (see inset) provides a direct estimate of the fraction of Cu(II) sites available for the reduction by ethylene at the pseudo-steady-state condition reached in the previous part of the experiment (Fig. 6). In good agreement with the XANES results, catalysts having the lowest amount

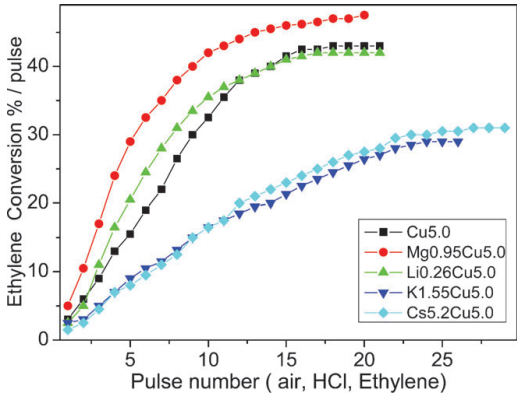

Fig. 6 Percentage of ethylene conversion per pulse in non-depletive mode at the temperature of 493 K. Pulse number refer to the subsequent dosage of three different pulses of air, HCl and ethylene.

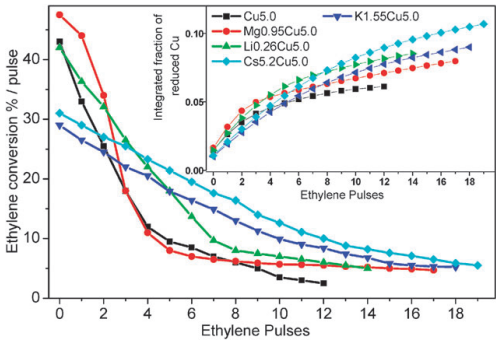

Fig. 7 Percentage of ethylene conversion per pulse in depletive mode at the temperature of 493 K. Pulse number refer to the dosage of one pulse of ethylene. Inset: calculated integral fraction of Cu(II) reduced to Cu(I).

of Cu(II) were Cu5.0 and Mg0.95Cu5.0, those having the greater amount of Cu(II) were Li0.26Cu5.0, K1.55Cu5.0 and Cs5.21Cu5.0.

As far as the reaction rate is concerned (slope of the curves in the first pulses of Fig. 7) it is shown that the more oxidized was the catalyst, the lower was the rate of Cu(II) reduction by ethylene: Mg0.95Cu5.0 $\approx$ Cu5.0 > Li0.26Cu5.0 > K1.55Cu5.0 $\approx$ Cs5.21Cu5.0. This is a clear indication that dopants had an effect on the rates of steps (4–6). The two families of catalysts emerging from the XANES experiments are also differentiated by the successive non-depletive and depletive pulse experiments reported in Fig. 6 and 7. For samples classified in Family II (Cs5.21Cu5.0 and K1.55Cu5.0), the lower activity at pseudo steady state was due to the lower reduction level of Cu in the equilibrated catalyst; the latter was a consequence of the lower reaction rate for reaction (4), as compared to the rates for steps (5) and (6). On the contrary, in catalysts Li0.26Cu5.0 and Mg0.95Cu5.0 the reduction rate was not much different from that of the undoped Cu (defining Family I); with the latter samples, the corresponding equilibrated catalyst was more deeply reduced, and finally it was more active.

Summarizing, notwithstanding the fact that catalytic tests in pulse reactor reaches a pseudo steady state, while operando XANES experiments were completely out of equilibrium (owing to the high temperature gradient) and notwithstanding the different dopant amount present in the two series of samples used in the two investigations, the existence of two families of catalysts is firmly confirmed.

3.4 Spectroscopic evidences on the presence of two different Cu active phases in the two catalysts families

Without entering into the details of neither UV-Vis-NIR spectra of Cu(II) species, nor IR spectroscopy of CO adsorbed on surface Cu(I) sites, in this paragraph we will just report the raw spectroscopic data, discussing only the marked differences between the results obtained on the two families of catalysts. The reader interested on a deeper spectroscopic assignment should refer to the quoted references.

UV-Vis DRS data reported in Fig. 8a clearly shows that catalysts belonging to Family I (Cu5.0, La10.9Cu5.0, Mg1.9Cu5.0, Ce11Cu5.0...) exhibit a single well defined a band with a maximum at about 13000–12000 cm^{-1}, due to a d–d $^2E_g \rightarrow {}^2T_{2g}$ transition characteristic of Cu(II) ions in octahedral complexes.[28,47,50–52] Samples K3.1Cu5.0 and Cs10.4Cu5.0, belonging to Family II, exhibit also a second marked component around 9500–9000 cm^{-1}, clearly indicating that a significant fraction of Cu(II) sites lies in a strongly distorted octahedral geometry induced by a modification of the ligand field. This spectroscopic evidence suggests that, for Family II catalysts, we are no more dealing with a pure copper $CuCl_2$, as seems to be the case for catalysts belonging to Family I.

Further evidence comes from IR spectroscopy of adsorbed CO. CO is an excellent probe molecule for Cu(I) sites,[30,53–60] because its interaction is normally rather strong. The interaction can be separated into an electrostatic, a covalent σ-dative and a π-back donation contributions, the first two causing a blue shift of the $\tilde{\nu}_{CO}$ (with respect to that of the CO molecule in the gas phase $\tilde{\nu}_{CO}$ = 2143 cm^{-1}, see vertical dotted line in Fig. 8b), while the last causes a red shift.[61–64] From a measurement of the $\tilde{\nu}_{CO}$ of a given Cu(I) carbonyl complex, information are so obtained on the nature of the $Cu^+\cdots CO$ bond. On the contrary, the interaction of CO with Cu(II) is very weak and has been only very rarely observed,[65,66] and in the present case it can be considered, in first approximation, negligible at all. This implies that catalysts were reduced in ethylene at 500 K before CO dosage to allow the molecule to probe the surface of the active CuCl phase.[30,31,33] Quoted references proved that, at 300 K, only monocarbonyls are formed on Cu(I) sites and that absorption of CO on the support does not occur.

Before entering in the discussion of the IR spectra collected on dosing CO on the reduced forms of the catalysts, the results obtained by Scarano *et al.*[55] dosing CO on disordered CuCl nano-crystals grown by vapor phase deposition on a

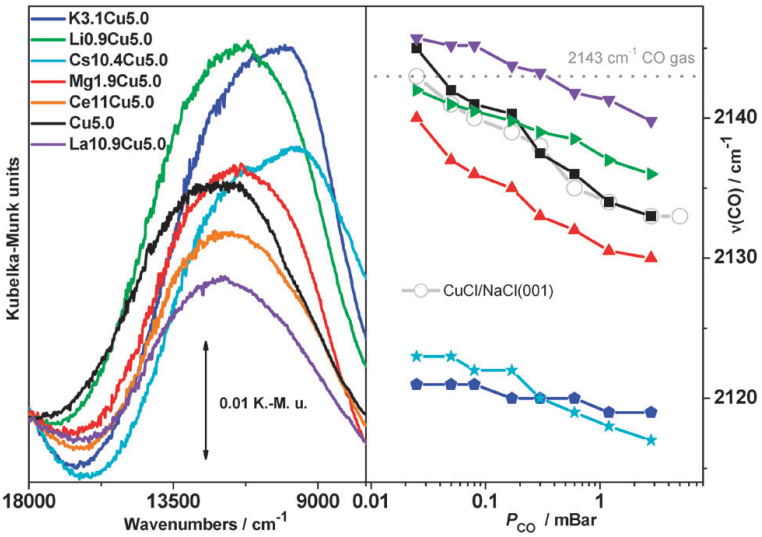

Fig. 8 Part (a) UV-Vis DRS spectra, in the *d–d* transitions region for the different catalysts. K–M u. = Kubelka–Munk units. Part (b) Evolution of the C–O stretching frequency, $\tilde{\nu}_{CO}$, as a function of the CO equilibrium pressure (logarithmic scale) in IR experiments of CO dosed at 300 K on the different catalysts. To observe $Cu^{+}\cdots CO$ complexes catalysts were pre-reduced in ethylene at 500 K before cooling down at RT and CO dosage. The corresponding set of spectra are reported in Fig. 9. The gray open circles refer to the data collected by Scarano *et al.*[55] on CuCl nano-crystals grown by vapor phase deposition on a NaCl(001) and represent a reference for the pure CuCl phase. The horizontal dotted line refer to the stretching frequency of the unperturbed CO molecule: $\tilde{\nu}^{0}_{CO} = 2143\ cm^{-1}$.

NaCl(001) substrate are worth to be recalled. In that surface science study, authors observed that the $\tilde{\nu}_{CO}$ of the $Cu^{+}\cdots CO$ adducts formed on disordered CuCl nano-crystals evolved from 2143 to 2133 cm^{-1} upon increasing the CO equilibrium pressure (P_{CO}). Such shifts have been reported in Fig. 8a (gray scattered curve), to be compared with similar results obtained on pure and doped catalysts. Note that the frequency shift of a vibrational mode of an adsorbate upon changing its equilibrium pressure (*i.e.* upon changing the surface coverage) is a phenomenon that is well known in surface science and is due to the mutual perturbation of adjacent carbonyls[67–70] and can be used to gain additional information on the phase probed by CO because not only the frequencies but also the frequency shifts as a function of P_{CO} becomes informative.[30]

Fig. 9 reports the evolution of the IR bands due to $Cu^{+}\cdots CO$ adducts formed at 300 K at the surface of the ethylene reduced catalysts (parts a–f) as a function of CO equilibrium pressure (P_{CO}). Also in this case, Cu5.0, La10.9Cu5.0, Mg1.9Cu5.0 and Li0.9Cu5.0 (Fig. 9a–d, Family I) behaves in a marked differently way with respect to K3.1Cu5.0 and Cs10.4Cu5.0 samples (Fig. 9e–f, Family II).

For the undoped catalyst (Fig. 9a), the $Cu^{+}\cdots CO$ band exhibits a progressive red-shift, upon increasing P_{CO}, from 2145 down to 2131 cm^{-1} that is very similar to what observed by Scarano *et al.*[55] for CuCl/NaCl(001), compare black and gray lines in Fig. 8b. This means that, in the present experiment, the CO molecules are probing the surface of small CuCl particles previously reduced by ethylene. Very similar spectra, in both $\tilde{\nu}_{CO}$ positions and shifts have been obtained on Mg1.9Cu5.0, Li0.9Cu5.0 and La10.9Cu5.0 (Fig. 9b–d). Note that for these four catalysts the low P_{CO} spectra exhibit a very small $\Delta\tilde{\nu}_{CO} = \tilde{\nu}_{CO} - \tilde{\nu}^{0}_{CO}$, indicating that electrostatic and σ-donation effects are almost equivalent to the π-back donation ones (see dotted vertical line in Fig. 8b). The IR results reported in Fig. 9a–d, indicates that for all catalysts, ascribed to Family I, the probed Cu^{+} sites are hosted in small CuCl nanoparticles, where Cu^{+} adsorbing sites are adjacent to each other[30] and that additives are not present in the copper chloride phase, as they are only barely able to perturb the $\tilde{\nu}_{CO}$ values and their shifts *vs.* P_{CO}. Similar small variations of the C–O stretching frequency have been observed on the pure $CuCl_2/Al_2O_3$ system (*i.e.* without additives) just by changing the copper loading or the degree of reduction.[30]

Before entering into the discussion of the IR spectra obtained on Family II catalysts, it is worth recalling that after the treatment with C_2H_4 at 500 K, both K3.1Cu5.0 and Cs10.4Cu5.0 catalysts are not fully reduced (see XANES results summarized in Fig. 4), so that CO will probe only the reduced fraction of surface copper species. For both K3.1Cu5.0 and Cs10.4Cu5.0 catalysts (Fig. 9e and f), $Cu^{+}\cdots CO$ adducts are characterized by IR bands appearing in a different region with respect to what's observed in the case of Family I catalysts. In the case of Family II, $\tilde{\nu}_{CO}$ values are significantly below that of the unperturbed CO molecule (see dotted vertical line in Fig. 8b), resulting in $\Delta\tilde{\nu}_{CO}$ values that go from −20 to −27 cm^{-1}. This indicates that the $Cu^{+}\cdots CO$ interaction is dominated by the π-back donation and that we are dealing with classical carbonyls[61–64] Moreover, for

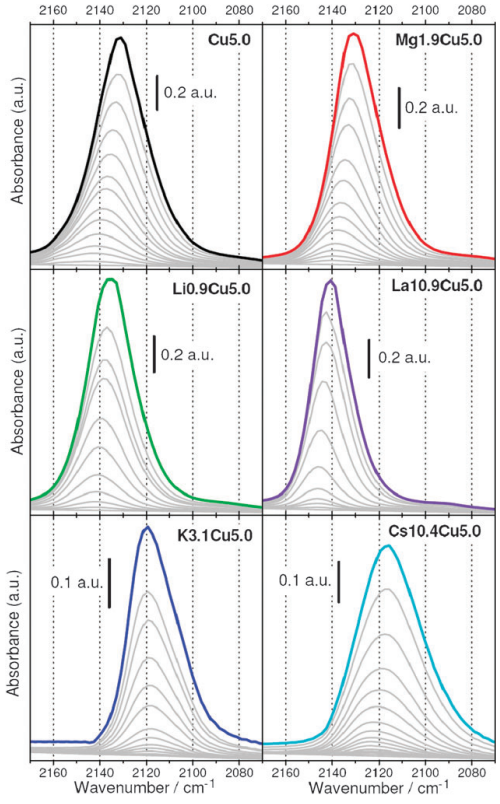

Fig. 9 Evolution of the IR spectra in the C–O stretching region, as a function of the CO equilibrium pressure in IR experiments of CO dosed at 300 K on the different catalysts. To observe $Cu^{+}\cdots CO$ complexes catalysts were pre-reduced in ethylene at 500 K before cooling down at RT and CO dosage. For each set of spectra, the position of the maximum of the $Cu^{+}\cdots CO$ band has been reported *vs.* P_{CO} in Fig. 8b.

K3.1Cu5.0 sample the $\tilde{\nu}_{CO}$ value is almost pressure independent, while, for the Cs10.4Cu5.0 case only a small red-shift is observed upon increasing P_{CO}, suggesting that in these cases Cu(I) adsorbing sites are sufficiently isolated from each other that the interaction between two $Cu^{+}\cdots CO$ adducts is negligible (or less important).

Summarizing, Cu5.0, La10.9Cu5.0, Mg1.9Cu5.0 and Li0.9Cu5.0 samples behaves similarly to what is observed for highly dispersed CuCl nanoparticles,[55] where surface Cu^{+} sites are separated just by one Cl^{-} anion, while a much larger distance must be inferred for copper species hosted on K3.1Cu5.0 and Cs10.4Cu5.0 samples because Cu^{+} sites are separated also by dopant cations and by unreduced Cu^{2+} cations. For Family II catalysts, reported spectroscopies show that the local environment of copper species, in both oxidized (UV-Vis-NIR) and reduced (IR) forms, is different from that experienced in pure copper chloride and are in favour of the development of a cation mixed (or melt) CuM_xCl_{2+x} phase (M = K or Cs).[3,33–36]

4. Summary and conclusions

Pulse tests demonstrate that the average oxidation state of Cu at the pseudo steady state is affected by the presence of the promoters. Moreover, it has been shown that a fully oxidized catalyst is not active for the oxychlorination reaction. This implies that, for all samples, the active phase is a valence mixed $CuCl_2$/CuCl phase, in agreement with XANES measurements in operando conditions. The relevance of Cu(I) ions can be justified by its ability to coordinate ethylene molecules.

Reactions (4)–(6), combining $CuCl_2$ and CuCl phases, are able to explain the behaviour of Family I catalysts, that is similar to that of the undoped catalyst.[30,31] The case of Family II catalysts is clearly more complex and a deep discussion is required. We infer the development of a cation mixed (or melt) CuM_xCl_{2+x} phase (M = K or Cs),[3,33–36] in which a decrease of the rate for step (4) with respect to steps (5) and (6) makes relatively more efficient the incorporation of depleted Cl and the re-oxidation of the reduced Cu. It is evident that in a cation mixed CuM_xCl_{2+x} phase it is more difficult for ethylene to find two adjacent Cu sites and that this difficulty increases with the M/Cu ratio. Both UV-Vis and IR spectroscopies support this hypothesis showing that the local environment of copper species is different from that experienced in pure copper chloride. Therefore, in the case of Family II catalysts, eqn (4)–(6) should be rewritten as follows:

$$2CuM_xCl_{2+x} + C_2H_4 \rightarrow C_2H_4Cl_2 + 2CuM_xCl_{1+x}, \quad (M = K \text{ and/or } Cs) \qquad (7)$$

$$2CuM_xCl_{1+x} + 1/2\ O_2 \rightarrow Cu_2O\ M_{2x}Cl_{2+2x}, \qquad (8)$$

$$Cu_2OM_{2x}Cl_{2+2x} + 2HCl \rightarrow 2CuM_xCl_{2+x} + H_2O. \qquad (9)$$

The case of Li makes exception, as it has been found to behave as an intermediate between Family I and II. The peculiar behaviour of Li can be tentatively explained by considering that while it is possible to precipitate $KCuCl_3$ at temperatures above 350 K, it is not possible to precipitate $LiCuCl_3$ directly from a solution.[71]

The experimental evidence here reported highlight the important role of alkali dopants in redox catalysis. As also pointed out in the case of o-xylene oxidation to phthalic anhydride,[72] selected alkali dopants, specifically Cs and K, do not simply play the role of tuning surface acidic properties but have a profound effect on redox properties of the catalyst and hence on catalytic performance. This implies a long-range effect which corresponds to a modification of the electronic properties of the active phase, rather than a localized interaction between the active site and the dopant atom.

The data reported in Fig. 6 unambiguously show that K or Cs addition causes a decrease of the overall catalyst activity. As the overall ethylene oxychlorination reaction (3) is highly exothermic ($\Delta H = -240$ kJ mol^{-1}), it is difficult to control the bed temperature for a too-active catalyst. Therefore, at an industrial level, the modulation of the intrinsic activity achieved by means of the addition of controlled amounts of selected dopants allows the reactor to be more easily managed, lowering the formation of hot-spots and hence hindering the formation of over oxidation and over chlorinated by-products.

This model explains why fixed bed reactors have catalysts with different M/Cu ratio along the reactants/product feed direction. Moreover, K and Cs additives, favoring the oxidized state (II) of Cu minimizes the Cu loss caused by the volatility of Cu(I) species. These combined aspects allow to improve the catalyst performance for fixed bed technology.

Acknowledgements

This collaborative work has been developed in the frame of the Network of Excellence Idecat (FP6 of the EU). C. Prestipino, G. Spoto, L. Capello, G. Casali, E. Groppo, A. Zecchina, B. Cremaschi, and M. Garilli, are gratefully acknowledged for the stimulating discussions that we had on this subject along years. We are indebted to S. Diaz Moreno and to R. Weigel for their fundamental support during XAS data acquisition and to M. Sanchez Del Rio for his important support on the complex data handling. N. Muddada thanks the Erasmus Mundus MaMaSELF program (http://etudes.univ-rennes1.fr/mamaself) that allowed him to come to Europe for his Masters and the Norwegian Research Council for his PhD.

References

1 F. Cavani and J. H. Teles, *ChemSusChem*, 2009, **2**, 508.
2 F. Cavani, G. Centi, S. Perathoner and F. Trifiro, *Sustainable Industrial Chemistry*, Wiley-VCH, Wenheim, 2009.
3 T. Z. Zhang, C. Troll, B. Rieger, J. Kintrup, O. F. K. Schluter and R. Weber, *Appl. Catal., A*, 2009, **365**, 20.
4 T. Z. Zhang, C. Troll, B. Rieger, J. Kintrup, O. F. K. Schluter and R. Weber, *Appl. Catal., A*, 2009, **357**, 51.
5 J. S. Naworski and E. S. Evil, in *Applied Industrial Catalysis*, ed. B. E. Leach, Academic Press, New York, 1983, vol. 1, p. 239.
6 M. N. Newmann, *Encyclopedia of Polymer Science and Engineering*, Wiley, New York, 1985, vol. 17.
7 M. Garilli, P. L. Fatutto and F. Piga, *Chim. Ind.*, 1998, **80**, 333.
8 A. Arcoya, A. Cortes and X. L. Seoane, *Can. J. Chem. Eng.*, 1982, **60**, 55.
9 W. D. Mross, *Catal. Rev. Sci. Eng.*, 1983, **25**, 591.
10 X. J. Lu, J. Liu, G. D. Zhou, Y. N. Li, K. J. Xhen, W. X. Li and T. X. Cheng, *Chin. J. Catal.*, 2005, **26**, 587.
11 L. Xueju, L. Jie, Z. Guangdong, Z. Kaiji, L. Wenxing and C. Tiexin, *Catal. Lett.*, 2005, **100**, 153.
12 P. R. Laurer, G. Krome, L. Cordemans, R. Seifert and E. Danz, Eur. Pat. 54674, 1981.
13 K. Shiozaki and A. Onischi, Eur. Pat. 62320, 1982.
14 I. Fatutto, D. Carmello and A. Marsella, Eur. Pat. 1053789, 2000.
15 P. S. S. Prasad, K. B. S. Prasad, P. K. Rao and V. K. Kaushik, *J. Mater. Sci.*, 1997, **32**, 1479.
16 H. Derieth, R. Walter, G. Weidenbach and M. Strebbele, Eur. Pat. 255156, 1988.
17 J. S. Eden and J. A. Cowfer, US Pat. 4849393, 1989.
18 D. Carmello, M. Grilli, P. Fatutto and L. Caccialupi, Eur. Pat. 1045731, 1999.
19 E. Peringer, S. G. Podkolzin, M. E. Jones, R. Olindo and J. A. Lercher, *Top. Catal.*, 2006, **38**, 211.
20 A. Baiker and W. L. Holstein, *J. Catal.*, 1983, **84**, 178.
21 K. Rollins and P. A. Sermon, *J. Chem. Soc., Chem. Commun.*, 1986, 1171.
22 E. M. Fortini, C. L. Garcia and D. E. Resasco, *J. Catal.*, 1986, **99**, 12.
23 P. A. Sermon, K. Rollins, P. N. Reyes, S. A. Lawrence, M. A. Martin Luengo and M. J. Davies, *J. Chem. Soc., Faraday Trans. 1*, 1987, **83**, 1347.
24 P. S. Sai Prasad and P. Kanta Rao, *J. Chem. Soc., Chem. Commun.*, 1987, 951.
25 C. L. Garcia and D. E. Resasco, *J. Catal.*, 1990, **122**, 151.
26 A. J. Rouco, *Appl. Catal., A*, 1994, **117**, 139.
27 S. Wachi and Y. Asai, *Ind. Eng. Chem. Res.*, 1994, **33**, 259.
28 G. Leofanti, M. Padovan, M. Garilli, D. Carmello, A. Zecchina, G. Spoto, S. Bordiga, G. T. Palomino and C. Lamberti, *J. Catal.*, 2000, **189**, 91.
29 G. Leofanti, M. Padovan, M. Garilli, D. Carmello, G. L. Marra, A. Zecchina, G. Spoto, S. Bordiga and C. Lamberti, *J. Catal.*, 2000, **189**, 105.
30 G. Leofanti, A. Marsella, B. Cremaschi, M. Garilli, A. Zecchina, G. Spoto, S. Bordiga, P. Fisicaro, G. Berlier, C. Prestipino, G. Casali and C. Lamberti, *J. Catal.*, 2001, **202**, 279.
31 G. Leofanti, A. Marsella, B. Cremaschi, M. Garilli, A. Zecchina, G. Spoto, S. Bordiga, P. Fisicaro, C. Prestipino, F. Villain and C. Lamberti, *J. Catal.*, 2002, **205**, 375.
32 C. Prestipino, S. Bordiga, C. Lamberti, S. Vidotto, M. Garilli, B. Cremaschi, A. Marsella, G. Leofanti, P. Fisicaro, G. Spoto and A. Zecchina, *J. Phys. Chem. B*, 2003, **107**, 5022.
33 C. Lamberti, C. Prestipino, F. Bonino, L. Capello, S. Bordiga, G. Spoto, A. Zecchina, S. D. Moreno, B. Cremaschi, M. Garilli, A. Marsella, D. Carmello, S. Vidotto and G. Leofanti, *Angew. Chem., Int. Ed.*, 2002, **41**, 2341.
34 C. M. Fontana, E. Gorin, G. A. Kidder and C. S. Meredith, *Ind. Eng. Chem.*, 1952, **44**, 363–368.
35 C. M. Fontana, E. Gorin, G. A. Kidder and R. E. Kinney, *Ind. Eng. Chem.*, 1952, **44**, 369–373.
36 C. M. Fontana, E. Gorin and C. S. Meredith, *Ind. Eng. Chem.*, 1952, **44**, 373–378.
37 C. Lamberti, C. Prestipino, S. Bordiga, G. Berlier, G. Spoto, A. Zecchina, A. Laloni, F. La Manna, F. D'Anca, R. Felici, F. D'Acapito and P. Roy, *Nucl. Instrum. Methods Phys. Res., Sect. B*, 2003, **200**, 196.
38 C. Lamberti, S. Bordiga, F. Bonino, C. Prestipino, G. Berlier, L. Capello, F. D'Acapito, F. X. Llabres i Xamena and A. Zecchina, *Phys. Chem. Chem. Phys.*, 2003, **5**, 4502.
39 M. Hagelstein, A. San Miguel, A. Ressler, A. Fontaine and J. Goulon, *J. Phys. IV*, 1997, **7**, C2-303.
40 R. Le Toquin, W. Paulus, A. Cousson, C. Prestipino and C. Lamberti, *J. Am. Chem. Soc.*, 2006, **128**, 13161.
41 Y. Kuroda, A. Kotani, H. Maeda, H. Moriwaki, T. Morimato and M. Nagao, *J. Chem. Soc., Faraday Trans.*, 1992, **88**, 1583.
42 Y. Kuroda, T. Mori, Y. Yoshikawa, S. Kittaka, R. Kumashiro and M. Nagao, *Phys. Chem. Chem. Phys.*, 1999, **1**, 3807.
43 L. S. Kau, D. J. Spira-Solomon, J. E. Penner-Hahn, K. O. Hodgson and E. I. Solomon, *J. Am. Chem. Soc.*, 1987, **109**, 6433.
44 N. J. Blackburn, R. W. Strange, J. Reedijk, A. Volbeda, A. Farooq, A. Karlin and J. Zubieta, *Inorg. Chem.*, 1989, **28**, 1349.
45 M. Fernández-García, I. Rodríguez-Ramos, P. Ferreira-Aparicio and A. Guerrero-Ruiz, *J. Catal.*, 1998, **178**, 253.
46 P. Kappen, J.-D. Grunwaldt, B. S. Hammershøi, L. Tröger and B. S. Clausen, *J. Catal.*, 2001, **198**, 56.
47 G. Turnes Palomino, P. Fisicaro, S. Bordiga, A. Zecchina, E. Giamello and C. Lamberti, *J. Phys. Chem. B*, 2000, **104**, 4064.
48 V. Bolis, S. Maggiorini, L. Meda, F. D'Acapito, G. Turnes Palomino, S. Bordiga and C. Lamberti, *J. Chem. Phys.*, 2000, **113**, 9248.
49 C. Prestipino, G. Berlier, F. X. Llabres i Xamena, G. Spoto, S. Bordiga, A. Zecchina, G. Turnes Palomino, T. Yamamoto and C. Lamberti, *Chem. Phys. Lett.*, 2002, **363**, 389.
50 F. X. Llabres i Xamena, P. Fisicaro, G. Berlier, A. Zecchina, G. Turnes Palomino, C. Prestipino, S. Bordiga, E. Giamello and C. Lamberti, *J. Phys. Chem. B*, 2003, **107**, 7036.
51 C. K. Jorgensen, *Prog. Inorg. Chem.*, 1970, **12**, 101.
52 A. Delabie, K. Pierloot, M. H. Groothaert, R. A. Schoonheydt and L. G. Vanquickenborne, *Eur. J. Inorg. Chem.*, 2002, 515.
53 E. Giamello, D. Murphy, G. Magnacca, C. Morterra, Y. Shioya, T. Nomura and M. Anpo, *J. Catal.*, 1992, **136**, 510.
54 C. Lamberti, S. Bordiga, M. Salvalaggio, G. Spoto, A. Zecchina, F. Geobaldo, G. Vlaic and M. Bellatreccia, *J. Phys. Chem. B*, 1997, **101**, 344.
55 D. Scarano, P. Galletto, C. Lamberti, R. DeFranceschi and A. Zecchina, *Surf. Sci.*, 1997, **387**, 236.
56 A. Zecchina, S. Bordiga, M. Salvalaggio, G. Spoto, D. Scarano and C. Lamberti, *J. Catal.*, 1998, **173**, 540.

57 D. Scarano, S. Bordiga, C. Lamberti, G. Spoto, G. Ricchiardi, A. Zecchina and C. O. Arean, *Surf. Sci.*, 1998, **411**, 272.
58 A. Zecchina, S. Bordiga, G. T. Palomino, D. Scarano, C. Lamberti and M. Salvalaggio, *J. Phys. Chem. B*, 1999, **103**, 3833.
59 C. Lamberti, G. T. Palomino, S. Bordiga, G. Berlier, F. D'Acapito and A. Zecchina, *Angew. Chem., Int. Ed.*, 2000, **39**, 2138.
60 C. Prestipino, L. Capello, F. D'Acapito and C. Lamberti, *Phys. Chem. Chem. Phys.*, 2005, **7**, 1743.
61 S. H. Strauss, *J. Chem. Soc.-Dalton Trans.*, 2000, 1.
62 A. J. Lupinetti, S. H. Strauss and G. Frenking, *Prog. Inorg. Chem.*, 2001, **49**, 1.
63 V. Bolis, A. Barbaglia, S. Bordiga, C. Lamberti and A. Zecchina, *J. Phys. Chem. B*, 2004, **108**, 9970.
64 D. Gianolio, E. Groppo, J. G. Vitillo, A. Damin, S. Bordiga, A. Zecchina and C. Lamberti, *Chem. Commun.*, 2009, **46**, 976.
65 K. Hadjiivanov and H. Knozinger, *J. Catal.*, 2000, **191**, 480.
66 C. Prestipino, L. Regli, J. G. Vitillo, F. Bonino, A. Damin, C. Lamberti, A. Zecchina, P. L. Solari, K. O. Kongshaug and S. Bordiga, *Chem. Mater.*, 2006, **18**, 1337.
67 D. Scarano, G. Spoto, S. Bordiga, A. Zecchina and C. Lamberti, *Surf. Sci.*, 1992, **276**, 281.
68 A. Zecchina, D. Scarano, S. Bordiga, G. Spoto and C. Lamberti, *Adv. Catal.*, 2001, **46**, 265.
69 E. Ozensoy and D. W. Goodman, *Phys. Chem. Chem. Phys.*, 2004, **6**, 3765.
70 E. Groppo, S. Bertarione, F. Rotunno, G. Agostini, D. Scarano, R. Pellegrini, G. Leofanti, A. Zecchina and C. Lamberti, *J. Phys. Chem. C*, 2007, **111**, 7021.
71 W. G. Palmer, *Experimental Inorganic Chemistry*, Cambridge University Press, London, 1952.
72 S. Anniballi, F. Cavani, A. Guerrini, B. Panzacchi, F. Trifiro, C. Fumagalli, R. Leanza and G. Mazzoni, *Catal. Today*, 2003, **78**, 117.

Publication III

Nuclear Instruments Methods
Phys. Research B 2012

"Doped-$CuCl_2/Al_2O_3$ catalysts for ethylene oxychlorination: influence of additives on the nature of active phase and reducibility"

D. Gianolio, N. B. Muddada, U.Olsbye and C. Lamberti

Publication IV

Journal of Catalysis 2011

"The role of chlorine and additives on the density and strength of Lewis and Brønsted acidic sites of gamma-Al_2O_3 support used in oxychlorination catalysis: a FTIR study"

N. B. Muddada , U. Olsbye, T. Fuglerud, S. Vidotto, A. Marsella, S. Bordiga, D. Gianolio, G. Leofanti and C. Lamberti

Unpublished Manuscript

2012

“Influence of dopants in controlling the by-products formation in ethylene oxychlorination reaction: site selective mechanistic details”

N. B. Muddada , T. Fuglerud, U. Olsbye, and C. Lamberti